Occurrence and fate of endocrine disrupting chemicals and other hydrophobic organic compounds in a tropical river in Kenya

Von der Fakultät für Chemie und Physik
der Technischen Universität Bergakademie Freiberg

genehmigte

Dissertation

zur Erlangung des akademischen Grades
doctor rerum naturalium
(Dr. rer. nat.)

vorgelegt

von M.Phil.-Umweltgesundheit, Bilha Chepchirchir

Gutachter: Prof. Dr. Gerrit Schüürmann, TU Bergakademie Freiberg
Prof. Dr. Ralf Ebinghaus, Helmholtz-Zentrum Geesthacht

Tag der Verleihung: 14. Dezember 2017

Statement on published work

Some of the data presented in this dissertation has been published in a journal article:

Chepchirchir B. S., Paschke A., and Schüürmann G., 2017. Passive sampling for spatial and temporal monitoring of organic pollutants in surface water of a rural-urban river in Kenya. Science of the Total Environment 601–602:453–460. http://dx.doi.org/10.1016/j.scitotenv.2017.05.143.

The published work that is included in this dissertation concerns the preparation, field-deployment and extraction of silicone rubber, analysis of extracts, and also some of the discussions on research findings.

Declaration

I hereby declare that I completed this work without any improper help from a third party and without using any aids other than those cited. All ideas derived directly or indirectly from other sources are identified as such. In the selection and use of materials and in the writing of the manuscript I received support from Prof. Gerrit Schüürmann and Dr. Albrecht Paschke.

The calibration experiment (section 3.1) was done in conjunction with Xiaolong Zhou's masters thesis titled "Untersuchung der Aufnahmekinetik und Sorptionskapazität ausgwählter Umweltchemikalien in Polyethersulfon-Membranen". He did the following steps under my supervision: preparation of working solutions, method development in the GC, cleaning of twisters®, extraction of water samples using twisters®, analysis by thermal desorption-GC-MS, and data acquisition and analysis. We did the following sections together: preparation and pre–cleaning of PES strips, preparation of standards and extraction of membranes. We did the following steps interchangeably: refilling of the water tank and changing of membranes. I did the following steps: organisation of materials and procedures to be used in the experiment, preparation of the experimental set-up together with Dr. Paschke and Uwe Schröter, GC–MS analysis of PES extracts, and data acquisition. The raw data as given in section K of the appendix is common to both theses. However, final data analysis was done individually and results may be unique to each thesis.

Persons other than those above did not contribute to the writing of this thesis. I did not seek the help of a professional doctorate-consultant. Only those persons identified as having done so received any financial payment from me for any work done for me. This thesis has not previously been published in the same or a similar form in Germany or abroad.

December 18, 2018 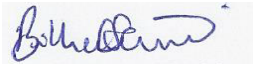

Date Signature

Acknowledgements

This research was supported by the Ministry of Higher Education Science and Technology (MOHEST), Kenya and the German Academic Exchange Service (DAAD). I am grateful to them for providing financial and administrative support that enabled me to relax and concentrate on my studies.

I would like to express my sincere gratitude to my advisor Prof. Gerrit Schüürmann for giving me a chance to study in Germany. This has given me a lot of exposure that has helped me to grow professionally. I also thank him for the academic and administrative support which led to the smooth running of my doctoral studies. I thank him for his advice/education on matters science that helped me to build my knowledge base, and for positive criticism of my work that helped me to be both an analytical and also a critical thinker.

I also sincerely thank Dr. Albrecht Paschke for introducing me into passive sampling and for mentoring me. Dr. Paschke provided me with literature that I needed to understand this field, and also provided technical support whenever I needed, including acquisition of the passive samplers that I used in this study. He and Uwe helped to set up the apparatus for pre–cleaning and extracting silicone rubber strips, and for sediment extraction, and also the apparatus for the calibration experiment. He assisted me in the acquisition of SEM images for the passive samplers from another department. Additionally, he organised for conference/workshop attendance and field visits in Germany and accompanied me to these events that gave me a lot of exposure in passive sampling. Aside from the scientific work, Dr. Paschke organised for tours and other events that made me conversant with the social–cultural side of Germany and helped me integrate so that the working environment would be conducive.

I also thank Uwe Schröter for the valuable support and assistance in the laboratory. Uwe introduced to me the operation of instruments and other general laboratory procedures. He assisted a lot in maintaining the instruments and ensured they were in good working condition before, during and after analysis, and he also placed orders for spare parts whenever needed. He also assisted in method development in the GC, preparation of standards, and in analysis of data. He assisted me to set up the calibration experiment, and he carried out the entire elimination experiment in conjuction with Dr. Paschke. Whenever I needed assistance from another laboratory in terms of chemicals or instrumental analysis, Uwe was readily available to fetch the required chemicals/apparatus, or to introduce me to the members of other laboratories. Besides, Uwe was always there to ensure my social welfare was taken care of. I am very grateful to him.

I would also like to thank Dr. Monika Möder for allowing me to work in her laboratories in sediment extraction. In conjunction, I would like to thank Petra Keil for her assistance in setting up and operating the accelerated solvent extractor used in sediment extraction.

The laboratory experiment was done in conjunction with Xiaolong Zhou's master thesis. I thank him for his assistance with establishment of water concentrations, preparation of standards, and instrumental analysis in the GC.

I thank the National Environmental Management Authority, Eldoret office for providing the means of transport and field assistants during fieldwork. Additionally, I thank the Department of Biotechnology, University of Eldoret for letting me use their deep freezers to store field samples.

Finally, I thank my colleagues and everyone else for lending a hand/idea to me here and there, and for their contribution in making Germany a home away from home.

Zusammenfassung

Diese Arbeit untersucht die Anwendung der passiven Probenahme als neue Monitoring–Technik, die in der Lage ist, Gewässerschadstoffe bei niedrigen Umweltkonzentrationen zu bestimmen und direkt zur Risikobewertung genutzt werden kann. Im Freiwasser und im Sediment eines tropischen Flusses in Kenia kamen zwei Passivsammler, Polyethersulfon (PES) und Silikongummi (SR), zum Einsatz, um endokrin wirksame Substanzen (EDCs) und hydrophobe organische Verbindungen (HOCs) zu erfassen. PES wurde dabei erstmalig für die zeitintegrierte Beprobung eingesetzt und war in der Lage, die Zielsubstanzen in niedrigen Konzentrationen zu erfassen. Diese unterschieden sich nicht signifikant von den auf Basis der bereits gut etablierten SR ermittelten Werte, ungeachtet der Differenzen in den Aufnahmemechanismen der beiden Sammlermaterialien. SR hat sich als robuster Sammler erwiesen, dessen *in situ* Sammelraten man über Referenzsubstanzen (PRCs) ermitteln kann. Diese Sammelraten korrelieren linear mit den SR-Wasser- und Oktanol-Wasser-Verteilungskoeffizienten der Substanzen und sind vergleichbar mit Literaturbefunden, die nahelegen, dass die Substanzaufnahme durch die wässrige Grenzschicht als geschwindigkeitsbestimmende Barriere kontrolliert wird. Die vorliegende Arbeit demonstriert, dass Passivsammler in abgelegenen Gebieten eingesetzt und bei richtiger Aufbewahrung während Transport und Lagerung auch weit entfernt vom Ausbringungsort sowie zeitlich verzögert analysiert werden können. Die Aufnahme- und Eliminierungskinetik der Zielsubstanzgruppen sowie wichtige diesbezügliche PES-Eigenschaften wurden in Labor-Kalibrierexperimenten untersucht. Für das poröse PES konnte eine Intrapartikel-Diffusion bestätigt werden, die als langsamer Prozess, gekoppelt mit der vermuteten hohen Sorptionskapazität des PES, eine Linearität der Aufnahmekurven bewirkt. Dies lässt wiederum darauf schließen, dass PES während kürzerer Expositionszeiträume im kinetischen Aufnahmemodus arbeitet. Die Aufnahme- und Eliminierungskurven der einzelnen Substanzen zeigen eine Anisotropie, die auf mechanistische Unterschiede bei der Adsorption und Des-

orption aufgrund der porösen und glasartigen Natur des PES beruhen könnten. Aus diesem Grund werden PRCs nur ungenügend aus dem PES eliminiert, so dass man sie anders als beim SR nicht nutzen kann, um *in situ* Sammelraten zu ermitteln. Zur Beurteilung des Sediment-Wasser-Austausches der Zielsubstanzen wurde ein fugazitätsbasiertes Sedimentmodell eingesetzt. Die berechneten Fugazitätsverhältnisse sind jeweils größer als eins, was darauf hinweist, dass die Sedimente eine Kontaminationsquelle für das Oberflächenwasser darstellen.

Abstract

This thesis explores the application of passive sampling as a novel monitoring technique capable of quantifying aquatic pollutants at low environmental concentrations, and in a form that is directly applicable to risk assessment. Two passive samplers, namely polyethersulfone (PES) and silicone rubber (SR), were used to monitor some endocrine disruptors (EDCs) and hydrophobic organic chemicals (HOCs) in freshwater and sediments of a tropical river in Kenya. PES was applied for the first time for time-integrative sampling of these compound classes and was able to quantify the target coumponds at low concentrations that were not significantly different to those obtained using the well established SR, despite differences in uptake mechanisms with both sampler materials. SR was found to be a robust sampler given that *in situ* sampling rates derived using performance reference compounds (PRCs) yielded linear correlations to both SR-water and octanol-water partition coefficients that were comparable to those reported in literature, for substance uptake that is controlled by the water boundary layer as rate-limiting barrier. This study demonstrated that passive samplers can be applied in remote locations, and with proper storage, they can be transported and analyzed far afield. Uptake and elimination kinetics and key properties of PES for the compound classes were also determined in laboratory calibration experiments. Intraparticle diffusion in the porous PES was confirmed, and this being a slow process coupled with the possibly high sorption capacity of PES, resulted in linearity of uptake curves so that PES was concluded to operate in the kinetic mode within a short-term exposure duration. Uptake and elimination curves of individual compounds in PES displayed anisotropy attributed to different mechanistic pathways for adsorption and desorption due to its porous and glassy nature. For these reasons also, PRCs were not sufficiently dissipated from PES implying they cannot be used to determine *in situ* sampling rates, unlike in SR. Lastly, to assess the sediment–water exchange of target compounds, fugacity ratios were calculated using a fugacity-based sediment model, where the ratios were

found to be greater than unity implying that sediments act as a source of pollutants to surface water.

List of Symbols and Abbreviations

A	surface area of polymer
B	proportionality constant
BBP	butylbenzyl phthalate
C_{p}	concentration in polymer
C_{pw}	concentration in porewater
C_{s}	concentration in sediments
C_{w}	concentration in water
DBP	di-n-butyl phthalate
DDT	dichlorodiphenyltrichloroethane
DDXs	metabolites of dichlorodiphenyltrichloroethane
DEHP	bis(2-ethylhexyl) phthalate
δ_{P}	solubility parameter
D_{p}	diffusivity in polymer
D_{w}	diffusivity in water
EDCs	endocrine disrupting chemicals
f	fraction of remaining PRC
f_{oc}	fraction of organic carbon
f_{s}	fugacity in sediments
f_{w}	fugacity in water
H	Henry's law constant
HOCs	hydrophobic organic contaminants
k_{e}	elimination rate
k_{ex}	exchange rate coefficient
k_{id}	intraparticle diffusion coefficient
k_{o}	overall mass transfer coefficient
k_{u}	uptake rate
K_{hdw}	hexadecane-water partition coefficient

K_{oc}	organic carbon-water partition coefficient
K_{om}	organic matter-water partition coefficient
K_{ow}	octanol-water partition coefficient
K_{pw}	polymer-water partition coefficient
m	function of the adsorption mechanism
M	molar mass
N_o	initial mass of PRC before exposure
N_t	mass of chemical sorbed onto a polymer
n_t	amount of chemical adsorbed
$N_{t,PRC}$	mass of PRC remaining after exposure
OCPs	organochlorine pesticides
PAHs	polycyclic aromatic hydrocarbons
PES	polyethersulfone
PCBs	polychlorinated biphenyls
POCIS	polar organic chemical integrative sampler
PRCs	performance reference compounds
PSDs	passive sampling devices
Q_s	quantity of chemical in sediments
R_s	sampling rate
SEM	scanning electron microscope
SR	silicone rubber
t	time
T_g	glass transition temperature
TOC	total organic carbon
TWA	time weighted average concentrations
WBL	water boundary layer
Z_s	fugacity capacity in sediment
Z_w	fugacity capacity in water

Contents

Chapter 1

Introduction

1.1 Research scope of this thesis

Several endocrine disruptors (EDCs) and hydrophobic organic chemicals (HOCs) have been found to adversely affect humans and/or wildlife. EDCs are an emerging class of compounds that are known or suspected to affect the endocrine system resulting in a wide range of health effects. In reality, the term EDCs is a relatively new term used for chemicals that are not so new in terms of environmental monitoring. Consider dichlorodiphenyltrichloroethane (DDT) for instance, a known endocrine disruptor that has been monitored for more than half a century, given its environmental persistence. Other HOCs that are not generally categorized as EDCs but are also widely monitored due to their known health effects include the polynuclear aromatic hydrocarbons (PAHs). It was outside the scope of this thesis to investigate the health effects of organic compounds. Rather, the focus was on monitoring EDCs and other hydrophobic organic chemicals (HOCs) in the aquatic environment and specifically targeting PAHs, polychlorinated biphenyls (PCBs), organochlorine pesticides (OCPs) [DDT and its metabolites, hexachlorobenzene and methoxychlor] and

three phthalates [butylbenzylphthalate (BBP), di-n-butylphthalate (DBP) and di-(2-ethylhexyl)phthalate (DEHP)]. These compounds/compound groups were monitored in freshwater and sediments and at concentrations that are relevant for risk assessment, that is, freely dissolved concentrations. In doing so, silicone rubber (SR)– and polyethersulfone (PES)–based passive sampling techniques were employed. SR–based passive sampling technologies are already developed and the purpose of this thesis was to further their applicability to a wider range of compounds and environments. PES–based passive sampling techniques are still at the development stage, and this thesis aims to investigate the uptake kinetics of PES in laboratory experiments and then apply it in the field. PES and SR strips were exposed *in situ* in a tropical river in Kenya. In addition, sediments were collected and used for *ex situ* analysis of total organic carbon (TOC) content, total concentrations of the organic compounds and also freely dissolved concentrations in porewater. Lastly, the fate of the organic compounds in the river system, specifically the sediment–water exchange was modelled using a fugacity–based sediment model.

1.2 Passive sampling: a versatile monitoring tool

Anthropogenic activities have led to pollution of water resources by xenobiotics, including HOCs like PAHs, PCBs, OCPs and phthalates. Some of these HOCs are suspected endocrine disruptors. HOCs lower the water quality and negatively impact on the aquatic ecosystem and dependent human populations either directly or indirectly. Accordingly, novel monitoring strategies that are capable of sensing the pollutants at their low environmental concentrations are required.

HOCs are generally hydrophobic and partition preferably to lipids and organic components of sediments and particulate matter in air where some HOCs may remain for long durations due to their environmental persistence [41]. In a river/stream micro–

environment with minimal point-source pollution, and depending on the weather and hydrodynamics, physical and chemical processes involving but not limited to volatilization, deposition, decomposition and upwelling from sediments can cause exchanges to occur between the solid, lipid and air phases and the water phase. As such, the HOCs are among commonly detected pollutants in the water phase of rivers and as a result of their known negative health impacts, concerted efforts have been made to regulate their use and to regularly monitor inland surface waters [38, 67].

Monitoring of surface water has conventionally been carried out by grab sampling to yield total concentrations (C_{total}) that are not directly applicable in ecological fate and risk assessment [47]. This process requires freely dissolved aqueous concentrations (C_{free}) that can effectively be measured directly using passive sampling devices (PSDs). Besides, this novel monitoring strategy offers several other advantages over the conventional grab sampling. For instance, PSDs are relatively inexpensive and easy to deploy and this makes their use particularly attractive in remote locations. In addition, the time-integrative character and low sensitivity of PSDs gives a 'big picture' about the true field situation that can be both informative and also act as an early warning system. In this context, a recent report by the United Nations Environmental Programme (UNEP) highlights the urgency in expanding water monitoring stations in Africa as a means to identifying hot spots that can be used to set up priorities for data collection, with the overall goal of curbing pollution and enhancing water security [160]. The use of grab sampling as a monitoring tool in such regions is operationally difficult given the low fiscal and physical infrastructure. Passive sampling would therefore offer a more versatile monitoring approach especially when cheap polymeric materials are used as sorbents.

In this research, PES and SR, were applied in monitoring for PAHs, PCBs, OCPs and the phthalates: BBP, DBP and DEHP in a tropical river in Kenya. SR is a

well developed passive sampler, and has been widely applied to monitor HOCs. Its uptake of HOCs is known to be an absorption process since the flexible polymer chains accommodate and allow the mobility of solutes within the polymer network. In addition, experimental partition coefficients (K_{pw}) for a number of HOCs are also available. Sampling rates of HOCs can also be determined *in situ* using performance reference compounds (PRCs). PES has only recently emerged as a sorbent for organic chemicals and several data gaps exist regarding, for instance, its K_{pw}, uptake kinetics, sampling rates (R_{s}), and whether PRCs can be applied to determine *in situ* R_{s}. Though it has been found to be a good sorbent [122, 165], rarely has it been applied in the field [119, 120] and never has it been used as a sorbent for the compounds like PAHs and PCBs. On the other hand, these compounds have been well studied using other PSDs including SR [124, 132]. Hence, SR was deployed as a reference alongside PES. PES was also applied to determine porewater concentrations.

1.3 Fugacity–based environmental models: simple yet powerful

In the environment, chemicals are not static but rather move from one compartment to another depending on environmental conditions and physicochemical properties. Chemical flows are driven by their fugacity gradients and generally move from regions of high to low fugacities. Actually, the process is much more intricate but the use of fugacities simplifies the process while generating all the relevant information. Thus, fugacity–based models have been widely applied when considering the transfer of chemicals between environmental compartments [90]. In sediment–water compartments, understanding chemical fluxes is useful in for instance, assessing the potential for accumulation or release from the compartment, estimating bioavailability and bioconcentration in biota, estimating the residence time or recovery, and in

planning for or assessing the effectiveness of remediation measures. In this research, a fugacity–based sediment model was used to assess fluxes of HOCs between sediments and water.

1.4 Objectives and outline

The overall objective of this research was to assess the occurrence and fate of HOCs in a tropical river system. This was achieved through a defined set of specific objectives which were to:

1) determine the sampling rates and partition coefficients of PCBs, PAHs, OCPs, and phthalates in PES.

2) investigate the uptake and elimination kinetics of HOCs and PRCs so as to assess the feasibility of using PRCs to measure *in situ* sampling rates of PES.

3) deploy PES in a tropical river in parallel to SR as sorbents for the HOCs and compare their performance,

4) collect sediments and determine total organic carbon (TOC) content and total chemical concentrations (C_{s})

5) use passive sampling to determine freely dissolved concentrations (C_{pw}) of HOCs in sediment porewater, and

6) determine the sediment–water fluxes of the HOCs using a fugacity–based sediment model

This dissertation organizes the research work in chapters. The definitions and examples of EDCs are discussed in *Chapter 2*. Also in this chapter, the environmental

occurrence of the target groups of compounds that may or may not be classified as EDCs and the monitoring strategies used in environmental matrices are highlighted. Finally, the theoretical basis of passive sampling and the fugacity approach to estimate sediment-water exchange of the organic compounds is discussed. *Chapter 3* which broadly describes the materials and methods used is organized into four main sections: 1) the laboratory calibration experiment that was used to determine key properties of PES, 2) field application of PES and SR, 3) determination of concentrations in whole sediments and sediment porewater, and 4) the setup and input data for the fugacity–based sediment model. The research outcome is discussed in *Chapter 4*. Experimental R_s for PES from the calibration experiment are given and are also correlated with compound properties. The sorption mechanism is explained using uptake and elimination curves, and this is also used to assess the (un)suitability of PRCs use to determine *in situ* R_s of PES. The outcome of field deployment of PES and SR in a tropical river is also discussed. Next, concentrations of the HOCs in sediments and sediment porewater are explored. Lastly, the application of the sediment model is elaborated. *Chapter 5* gives a synopsis of the research by highlighting the key findings and also draws conclusions, outlining considerations for further research.

Chapter 2

A review of literature

2.1 Endocrine disrupting chemicals

2.1.1 Definition

The term endocrine disruptor first came up in 1991 at the Wingspread conference. Endocrine disruptors are also known as hormonally active agents [75] or endocrine disrupting chemicals (EDCs) [33] and are defined as exogenous substances or respective mixtures that alter the function(s) of the endocrine system and consequently causes adverse health effects in an intact organism, or its progeny, or in (sub)populations [63].

EDCs comprise a broad, highly heterogeneous group of chemicals, for example some natural compounds (e.g. phytoestrogens), industrial chemicals and by–products, pesticides, drugs, metals and some compounds considered as persistent organic pollutants (POPs). In reality, endocrine disruptors is a 'relatively new' term applied to not so new chemicals in the field of environmental monitoring. It is considered new

in terms of the mechanisms of action elicited in causing health effects. Upon exposure to relevant doses, EDCs can block, mimic, or alter the activity of hormones, thus disrupting normal growth, development and physiological maintainance.

2.1.2 Examples of EDCs and their endocrine–related effects

Exposure to EDCs has been suspected to be linked to the growing evidence of increase in endocrine–related disorders which include endometriosis, cryptorchidism, decrease in sperm quality, obesity, thyroid disruption and diabetes [33, 175]. Initially, EDCs were thought to exert their effects on the endocrine system by influencing the actions of three groups of hormones: estrogens, androgens and thyroid hormones. These changes could cause alteration in normal hormone levels, inhibition or stimulation of hormone production and an alteration in body distribution, thereby affecting the functions that these hormones control [137]. In addition to the aforementioned mechanisms of action, EDCs can also act through membrane receptors, non–steroid receptors (e.g. neurotransmitter receptors), orphan receptors (e.g. aryl hydrocarbon receptor, AhR), transcriptional coactivators, and enzymatic pathways involved in steroid biosynthesis and/or metabolism [33, 137, 156]. In most cases however, the causal evidence is by no means universally conclusive and still requires elaborate and standardized inter–laboratory studies. Some published health effects of EDCs are described below and others summarized in table 2.1.

Polychlorinated biphenyls (PCBs) are chlorinated organic compounds that were once widely applied in the manufacture of carbonless copy paper and as dielectric and coolant fluids in electrical apparatus. Despite a worldwide ban in their production and use, PCBs are still detected in environmental matrices owing to their high hydrophobicity and environmental persistence. The ban was occasioned by the observation of adverse effects in humans and wildlife following exposure, notably the development and progression of cancer through, for instance, oxidative damage

to DNA [104]. In addition, PCBs have been implicated in some endocrine–related disorders, for instance the increased incidences of rheumatic diseases through disturbance of metabolism and balance of adipokines [1]. Recent studies have also linked PCBs to thyroid–related disorders occasioned by a disruption in the distribution and metabolism of thyroid hormones [20], notably a reduction in serum thyroxine (T4) levels through binding to the AhR or because PCB and its hydroxylated metabolites act as T4 antagonists by binding to transthyretin [70, 95]. Some studies indicated that PCBs were associated with reduced thyroid hormone levels and/or positive associations with thyroid–stimulating hormone (TSH) in pregnant women [20]. Furthermore, hydroxylated PCBs have been shown to have weak estrogenic and anti–estrogenic activities by agonizing or antagonizing estrogen receptors (ER) [76, 157].

Phthalates are a group of chemicals that are commonly used as plasticizers in various industrial and consumer products. Concern over phthalates stems from associated health effects and the fact that they are ubiquitous high production volume chemicals which implies that although they are easily metabolized, body burdens do not decrease due to continued exposure [73, 153]. Phthalate toxicity targets mainly the reproductive and respiratory systems, but may also be involved in the carcinogenesis processes and autism [163]. Bis(2-ethylhexyl) phthalate (DEHP) and its metabolite, mono(2-ethylhexyl)phthalate (MEHP) are the most studied phthalates, and DEHP is classified a as priority pollutant in water monitoring by environmental protection agencies [38]. Prenatal exposure to DEHP increased the prevalence of cryptorchidism and hypospadias which are symptoms of testicular dysgenesis syndrome (TDS) and also lead to shortening of the anogenital distance (AGD) in male rodents due to an induction in abnormal Leydig cells function and a decrease in testosterone synthesis [143, 155, 163]. DEHP and MEHP have been associated with suppression of estradiol levels, prolonged estrous cycles and the absence of ovulation in female rats [94]. Exposure to DEHP from hatching to adulthood accelerated the

start of spawning and decreased egg production of exposed female marine medaka while exposure to both DEHP and MEHP resulted in a significant increase in plasma 17β-estradiol (E2) and a decrease in testosterone (T)/E2 ratios in males [181]. Butyl benzyl phthalate (BBP) was found to elicit anti–androgenic activities in an in vitro study employing yeast–based assays [148]. Phthalates may activate the AhR that plays a significant role in cell proliferation and differentiation and in tumorigenesis [135, 163]. Phthalates have also been associated with the increased risk of asthma development in children possibly through alterations in DNA methylation [172].

Dichlorodiphenyltrichloroethane (DDT) is a synthetic chemical that was once widely used as an insecticide until it was banned and its use restricted to vector control, such as mosquitoes, under the Stockholm convention on persistent organic pollutants [161]. DDT is classified as a possible human carcinogen and an endocrine disruptor [161]. DDT and its metabolites have been associated with endocrine-related diseases such as testicular tumors, type 2 diabetes and endometrial, breast and pancreatic cancers [44]. For instance, high testicular mass and abnormal histology in male Sprague-Dawley rats were observed after exposure in utero, during lactation and directly to DDT [113]. An in vivo study demonstrated the potential of o,p'-DDT as a xenostrogen by binding to ER and therefore induced vitellogenesis in mature male tilapia [78]. Recent studies using rats indicated that ancestral exposure to DDT can promote obesity and associated disease transgenerationally [144].

Polycyclic aromatic hydrocarbons (PAHs) are a group of more than 100 different chemicals that are released to the environment mainly as a result of incomplete combustion of fossil fuels but can also emanate naturally from coal tar and crude oil. Evidence supporting PAHs as endocrine disruptors is rather weak [133]. Nevertheless, a few studies have shown disruptive activities of parent PAHs or their metabolites. 7,12-Dimethylbenz(a)anthracene was shown in vitro to decrease the number of membrane dopamine receptors and stimulate prolactin release by direct

Table 2.1: Some EDCs, their modes of action and health effects

Chemical	Mode(s) of action	Some health effects	References
Methoxychlor	estrogenic, antiestrogenic, antiandrogenic	DNA methylation changes in the ovary	[74, 80, 105, 182]
4-t-OP[a]	estrogenic, antiandrogenic	induces vitellogenin, gonadal alteration	[76, 110, 174]
4-NP[b]	estrogenic	induces vitellogenin, endometriosis, gonadal alteration	[174]
Vinclozolin	estrogenic, antiandrogenic	disease states or tissue abnormalities (prostate disease, kidney disease, immune system abnormalities, testis abnormalities, and tumor development) in adult rats from F1-F4 generations	[10, 80]
BPA[c]	estrogenic, antiandrogenic	prostate hyperplasia, increased anogenital distance, early puberty	[110]
PBDEs[d]	estrogenic, antiestrogenic, thyroid	eggshell thinning	[51, 98, 136]
EE2[e]	estrogenic	induces vitellogenin	[77, 114]

[a]4-tert-Octylphenol; [b]4-Nonylphenol; [c]bisphenol A; [d]polybrominated diphenyl ethers; [e]17α-Ethinylestradiol.

estrogen-like actions on the anterior pituitary [112]. Using whole-cell ER binding and E2 metabolism assays, PAHs from environmental samples were found to induce antiestrogenic responses in metabolically intact human breast cancer cells [12]. PAHs can also act as EDCs by impacting ER signaling indirectly through interactions with AhR [141]. PAHs have shown the potential to disrupt the reproductive cycle of fish living in polluted environments, due to impairment of steroid biosynthesis [100].

The discussions above exemplify health effects resulting from exposure to a single EDC. However, EDCs rarely occur as single compounds in the environment and resultant effects may therefore be due to exposure to mixtures of EDCs that may

act synergistically or antagonistically. For instance, one study demonstrated that in utero exposure to a mixture of genistein (a phytoestrogen) and DEHP induced short– and long–term alterations in testicular gene and protein expression different from individual exposures [68].

It was outside the scope of this thesis to investigate the health effects of EDCs and other HOCs. However, it was necessary to highlight reported health effects to demonstrate the need for monitoring these compounds in the environment. This thesis therefore mainly investigates the occurrence of EDCs and other EDCs in the environment.

2.1.3 Occurrence of EDCs and HOCs in the environment

EDCs and other HOCs enter the freshwater environment through a variety of ways that can be broadly classified as point and non–point sources. Point sources include direct discharge of effluent from wastewater treatment plants. In developed nations, this type of discharge dominates the sources of EDCs and HOCs in surface water. Non–point sources encompass all diffuse sources including overland flow during snowmelt or a rainfall event, wet and/or dry atmospheric deposition, urban runoff and spray drifts during pesticide application. Non-point sources dominate the entry mode of EDCs and HOCs to surface water in developing nations.

Once in the aquatic environment, the compounds can undergo further processes such as partitioning between the environmental compartments comprising water, sediments, air and biota and respective subcompartments, degradation and transportation. Phase transfer of a compound largely depends on its physicochemical properties namely, water solubility and three partition coefficients: air–water (K_{aw}) that defines volatility, octanol–water (K_{ow}) that defines hydrophobicity and organic carbon (K_{oc}) that defines the preference of a compound for the organic phase. Es-

sentially, K_{ow} and K_{oc} are correlated. As a general rule, hydrophobic compounds ($\log K_{ow} > 3.0$) partition preferably to lipids and the organic phase in sediments and suspended matter. Thus, assuming that surface water comprises mainly the water and sediment phases, measured concentrations of EDCs and HOCs can be described in three ways: sorbed concentration (C_{sorbed}) for EDCs sorbed to bottom and suspended sediments, freely dissolved concentrations (C_{free}) for those in aqueous phase only without including solid phases and total concentrations (C_{total}) that include both aqueous and solid phases. EDCs and HOCs have been detected in the different environmental compartments. Some occurrences of EDCs and HOCs in water, sediments, biota and air are listed in table 2.2.

DDT and its metabolites are hydrophobic and persistent in the environment, with half-lifes for microbial degradation ranging from 3 to 20 years [83]. This implies that DDT and its degradation products are susceptible to long–range transport and bioaccumulation and may still be detected years after its ban. For instance, dated sediment/soil cores in the floodplains of river Elbe gave a trend analysis of DDT use in Germany with peaks in the 1940–1950s [46]. In Kenya, DDTs have been detected in air, water, soil, sediments and fish lipids (table 2.2). In addition to slow release from environmental reservoirs, occurrence of DDT in Kenya as a typical example of many African countries can emanate from continued application during vector control and release from old stock piles [72, 154]. It is expected that concentration levels will decrease with the full implementation of the Africa stockpiles programme that was initiated to clear all obsolete pesticide stocks in Africa [177].

Similar to DDTs, PCBs and PAHs are also ubiquitous in the environment due to a tendency to bioaccumulate. They are therefore often detected in most environmental matrices worldwide including sediments/soil [46], biota [150], water [37] and air [72]. PAHs are often accidental byproducts of combustion processes while PCBs are intentionally produced. Global PCBs production between 1930 and 1993 was

Table 2.2: Occurrence of PAHs, PCBs and DDTs in environmental matrices in Kenya and Germany

Chemical group	Matrix	Location	Method of analysis	Concentration	Reference
dl-PCBs[a]	fish	lake Victoria	GC-MS	0.2-19.0 pg/g	[150]
dl-PCBs	surface sediments	lake Victoria	GC-MS	136 pg/g dw	[151]
dl-PCBs	fish	Germany	GC-MS	1.2-59 pg/g ww[c]	[152]
PCBs	soil	Kenya	GC-MS	n.d.-55.49 µg/kg dw	[154]
PCBs	sediments	Germany	GC-MS	0.02-0.906 µg/g dw	[107]
PCBs	air, passive air sampler	Kenya	GC-MS	0.7-71.3 ng/sample	[72]
OCPs	air, passive air sampler	Kenya	GC-MS/MS, GC-MS	<0.2-2.3 ng/sample	[72]
OCPs	streams	Germany	GC-MS	0.4-22 µg/SPMD	[170]
OCPs	soil	Kenya	GC-ECD, GC-MS	n.d.-49.74 µg/kg dw	[154]
OCPs	seawater	Kenya	GC-ECD	0.503-9.025 ng/g	[171]
OCPs	sediments	Kenya	GC-ECD	0.584-59.00 ng/g	[171]
DDT, DDD[b]	fish lipid	Kenya	GC-ECD	1011 ng/g, 418 ng/g	[171]
DDT	air, passive air sampler	Kenya	GC-MS	1.3-8970 ng/sample	[72]
PAHs	river water	Kenya	GC-MS	2.69-14.22 ng/L	[37]
PAHs	air, passive air sampler	Kenya	GC-MS	145-9680 ng/sample	[72]
PAHs	floodplain soil	Germany	GC-MS	0-81.5 mg/kg	[117]

[a]dioxin–like PCBs; [b]DDT metabolite; [c]concentrations are given in reference as pgWHO-TEQ/g where TEQ is toxic equivalency.

estimated at 1325810 tonnes [25]. Despite the ban in 2001 under the Stockholm convention on persistent organic pollutants (POPs), PCBs are continually released from environmental reservoirs and undergo long–range transport. In developing countries, additional sources include leakages from obsolete transformer oil and e–waste that originate from illegal transboundary movement of electronic material [43].

Pollution from plastics is a growing worldwide concern. Plastics are major sources of phthalates, like DEHP, that are usually added to improve flexibility. Worldwide production of phthalates increased from 2 to 5.5 million tons from the 1980s to 2000 but the trend has now decreased, for instance to 221000 tons of DEHP in 2004 in western Europe [184]. Owing to its extensive usage, DEHP has been detected worldwide in surface waters (0.013–18.5 mg/L), wastewater (0.716–122 mg/L), landfill leachate (88–460 mg/L), sludge (12–1250 mg/kg), soil (2–10 mg/kg) [184].

2.2 Monitoring for EDCs and HOCs in the environment

Research into EDCs and other HOCs is growing tremendously due to the existence of large data and knowledge gaps. Research fields can be categorized as follows: development and/or improvement of chemical and bioanalytical methods, development and application of novel sampling techniques to determine concentrations (C_{total}, C_{sorbed}, C_{free}) in environmental matrices and modification of treatment/remediation technologies.

Several treatment/remediation technologies have been developed and applied for the removal of EDCs and HOCs from water despite inconsistencies in efficiency due to heterogeneity in properties of matrices and the compounds [28]. Some technolo-

gies include chlorination, ozonation, supercritical fluid extraction, adsorption using granular activated carbon and separation using micro–, ultra– and nano–filtration membranes such as PES.

Bioanalytical methods encompass the use of biosensors or biological assays to provide qualitative or quantitative information. Biosensors combine biological material (e.g. cell receptors, enzymes, antibodies) with a physicochemical detector. The detector operates for instance by optical or electrochemical means to transform the signal resulting from interaction of the analyte with the biological material into another easily readable and quantifiable signal. An example is an amperometric biosensor containing antibodies as biorecognition element for the detection of estradiol and atrazine [127]. On the other hand, correlation of exposure to EDCs and resultant health effects in humans and wildlife is still debatable. Attempts at establishing cause–effect relationships have therefore been made using different types of biological assays. The mechanisms involved in the biological assays to determine EDCs include cell proliferation, ligand binding, vitellogenin induction, and antigen–antibody interactions [28]. Examples of biological assays are whole organism assays e.g. transgenic zebrafish, cellular bioassays such as luciferase and non–cellular bioassays, e.g. the enzyme-linked immunosorbent assays.

Chemical methods relying on mass–based analytical devices, namely mass spectrometry (MS), have widely been used to quantify EDCs and HOCs in environmental matrices. Depending on the analyte properties, various combinations of instruments can be used such as high performance liquid chromatography coupled with mass spectrometry (HPLC–MS) and gas or liquid chromatography coupled with mass spectrometry (LC-MS, GC–MS) or tandem mass spectrometry (LC–MS/MS, GC–MS/MS).

Although the chemical methods are unequivocal in terms of sensitivity and precision,

their performance is heavily dependent on reliable sample extraction and pretreatment given that EDCs and HOCs occur in the environment at low concentrations. Grab sampling has conventionally been used as a sample preparation technique. However, the inherent artefacts associated with grab sampling that may lead to false negatives has led to the development of a novel monitoring technique termed passive sampling. In this research, passive sampling was applied to monitor EDCs and HOCs in water and sediments in a tropical river system and also in determining their fate. The principles of operation and applications of passive sampling are discussed in the following sections.

2.3 Application of passive sampling in environmental monitoring of EDCs and HOCs

2.3.1 Passive versus grab sampling

Grab sampling involves the capture and removal of an aliquot of water from the environmental, usually 1 L, for *ex situ* analysis. This implies that large volumes of water need to be collected, transported and analyzed. The analysis yields total concentrations in the aliquot that comprises both freely dissolved and sorbed concentrations. The information generated represents that of a single point in time, which may over-represent true environmental concentrations if the aliquot was captured during an episodic event and vice versa.

Passive sampling involves the free flow of compounds from the water phase to an engineered phase as a function of the differences in chemical potential or fugacity between the two phases. No mechanical work is involved in the movement of the compound between the phases. Passive samplers pre-concentrate the compounds *in situ* by acting as the preferred partitioning phase and generate information about

freely dissolved concentrations over an extended period. In most cases, low detection limits are achieved since large volumes of water are sampled.

Environmental quality standards (EQS) are developed from concentrations of whole water samples as generated by grab sampling [39]. Thus passive sampling cannot at the moment be used to generate EQS but is recommended by regulatory frameworks as a complementary monitoring tool [40]. Nevertheless, passive sampling is a valuable monitoring procedure as it yields information over a longer duration than grab sampling and can therefore be used as a screening tool to identify pollutants at low environmental concentrations or when the pollution source is intermittent, or in trend monitoring where it can serve as an early warning tool [99]. In addition, passive samplers are attractive for monitoring in remote regions or those with minimal infrastructure as they are easier to deploy and can be stored for longer durations prior to analysis as compared to grab samples.

2.3.2 Uptake process during passive sampling

Passive sampling is based on diffusive mass transfer of an organic compound to and from an ambient fluid (environmental phase) to a passive sampling device (PSD) (an engineered sampling or receiving phase) that is in contact with it. As such, only freely dissolved compounds are accumulated by the PSD. The PSD is exposed to the environmental medium for a user-defined period, and accumulates compounds from the medium in a non-depletive mode until thermodynamic equilibrium is achieved or until the PSD is removed. Mass transfer is based on the differences in chemical potential between two phases. Diffusive mass transfer into the PSD follows Fick's law that relates the flux [j_{x}, (ng/d)] in the x–direction of a given phase (i), to the concentration gradient between the end points of that phase [23]. The flux across the phase is proportional to the chemical diffusivity, D_{i} (m^2/d), and the concentration gradient, $\delta C/\delta x$, where C (ng/m^3) is the concentration, and x (m) is the distance

in the direction of flux. The relation is given as:

$$j_{\mathrm{x}} = -D \cdot \frac{\delta C}{\delta x} \tag{2.1}$$

For a given phase (i), equation 2.1 can also be written as:

$$j_{\mathrm{i}} = \frac{-D_{\mathrm{i}}}{\delta_{\mathrm{i}}} \cdot \Delta C_{\mathrm{i}} = k_{\mathrm{i}} \Delta C_{\mathrm{i}} \tag{2.2}$$

where δ_{i} (m) is the effective phase thickness, and ΔC_{i} (ng/m^3) is the concentration difference across the phase and represents the driving force for the flux process. $k_{\mathrm{i}} = \frac{-D_{\mathrm{i}}}{\delta_{\mathrm{i}}}$ (m/d), and represents the mass transfer coefficient (MTC) for the phase.

For illustration, consider a single–phased PSD that is exposed to the water phase on both sides. In this case, mass transfer is a stepwise process involving movement through three layers as shown in figure 2.1, that is, from the bulk water phase through the water boundary (WBL) and biofilm layers and finally through half the thickness of the PSD. The rate of mass transfer is controlled by resistances in the WBL and the PSD that are attributed to the inherent properties of the compound and PSD, hydrodynamics and environmental conditions [166]. This is attributed to the average distance the chemical must diffuse through the water phase to reach the PSD [δ_{w}, (m)], the diffusivity in water [D_{w}, (m^2/d)], the diffusivity in the PSD [D_{p}, (m^2/d)], and the capacity of the PSD for the chemical [11]. It is assumed that the fluxes through the successive regions (WBL, biofilm, and finally the PSD) are linearly proportional to the concentration difference between the end points of the phases [61]. Using equation 2.2, fluxes across the WBL (j_{w}), the biofilm layer (j_{b}), and the PSD (j_{p}) can be written as:

$$\begin{aligned} j_{\mathrm{w}} &= k_{\mathrm{w}} (C_{\mathrm{w}} - C_{\mathrm{w}-}) \\ j_{\mathrm{b}} &= k_{\mathrm{b}} (C_{\mathrm{b}+} - C_{\mathrm{b}-}) \\ j_{\mathrm{p}} &= k_{\mathrm{p}} (C_{\mathrm{p}+} - C_{\mathrm{p}-}) \end{aligned} \tag{2.3}$$

where k_w, k_b and k_p are the MTCs for the WBL, biofilm, and PSD phases respectively. C_w and C_{w-} are concentrations (e.g. in ng/L) in bulk water and the water side of the biofilm-water interface respectively. Similarly, C_{b+} and C_{b-} are concentrations (e.g. in ng/L) at the biofilm–water and the biofilm–PSD interfaces respectively, and C_{p+} and C_{p-} are concentrations (e.g. in ng/L) in the PSD side and the PSD–biofilm interfaces respectively. Assuming that the influence of the biofilm layer to overall flux is insignificant, that the fluxes through the various phases are equal ($j_w = j_b = j_p$), and that sorption equilibrium exists at all interfaces [61], equation 2.3 reduces to:

$$j = k_o (C_w - C_{p+}) \tag{2.4}$$

where k_o (m/d) is the overall MTC.

Assuming that concentrations in the bulk water phase [C_w, (ng/L)] and the PSD [C_p, (ng/kg)] are at equilibrium, C_w can be related to C_p using the PSD–water partition coefficient [K_{pw}, (L/kg)] as:

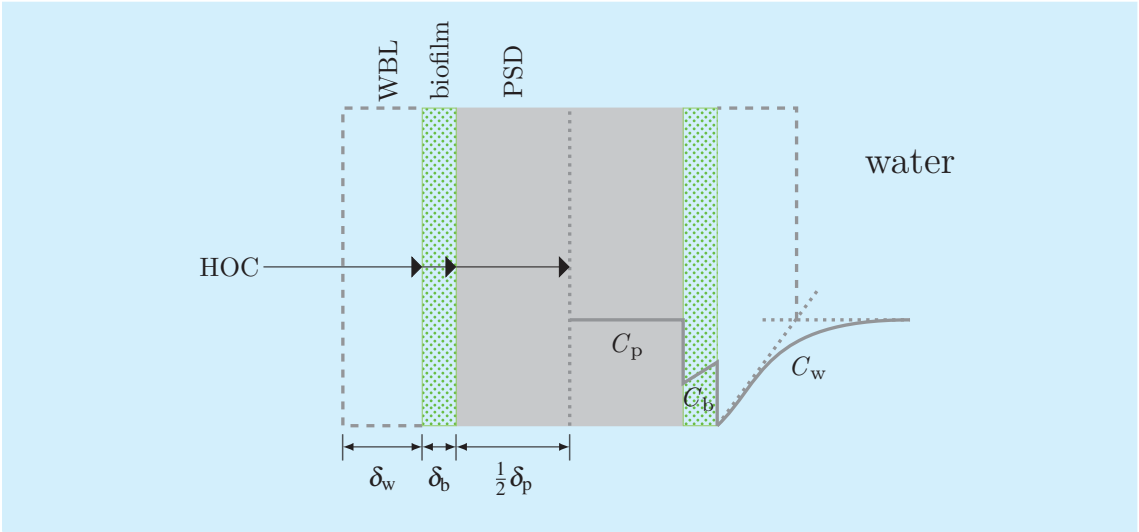

Figure 2.1: Schematic diagram showing the uptake process of a HOC from the water phase to a PSD. The movement of the HOC is from the water phase through to half the thickness of the PSD, and the same process is mirrored in the other half. δ_p, δ_b and δ_w are the thicknesses of the PSD, biofilm layer and WBL respectively. C_w, C_b and C_p are concentrations in water, biofilm and PSD respectively.

$$C_{\mathrm{w}} = \frac{C_{\mathrm{p}}}{K_{\mathrm{pw}}} \tag{2.5}$$

Then the term $C_{\mathrm{p+}}$ in equation 2.4 that represents concentrations on the PSD side can be substituted by C_{w} given in equation 2.5 to yield:

$$j = k_{\mathrm{o}} \left(C_{\mathrm{w}} - \frac{C_{\mathrm{p}}}{K_{\mathrm{pw}}} \right) \tag{2.6}$$

The reciprocal of k_{o} is the overall transport resistance and is a summation of the individual resistances in the three phases as shown in figure 2.1. That is:

$$\frac{1}{k_{\mathrm{o}}} = \frac{1}{k_{\mathrm{w}}} + \frac{1}{k_{\mathrm{b}} K_{\mathrm{bw}}} + \frac{1}{k_{\mathrm{p}} K_{\mathrm{pw}}} \tag{2.7}$$

where the terms on the right–hand side of the equation are respectively, the transport resistances in the WBL, biofilm and PSD and K_{bw} (L/kg) is the biofilm–water partition coefficient. Assuming that resistance in the biofilm layer is insignificant, equation 2.7 reduces to:

$$\frac{1}{k_{\mathrm{o}}} = \frac{1}{k_{\mathrm{w}}} + \frac{1}{k_{\mathrm{p}} K_{\mathrm{pw}}} \tag{2.8}$$

and the overall mass transfer resistance is therefore controlled by resistances in the water and PSD phases. As already mentioned, for a given phase (i), $k_{\mathrm{i}} = \frac{-D_{\mathrm{i}}}{\delta_{\mathrm{i}}}$. Substituting this relation into equation 2.8 gives:

$$\frac{1}{k_{\mathrm{o}}} = \frac{\delta_{\mathrm{w}}}{D_{\mathrm{w}}} + \frac{\delta_{\mathrm{p}}}{D_{\mathrm{p}} K_{\mathrm{pw}}} \tag{2.9}$$

The phase thicknesses are described in figure 2.1. The rate limiting barrier is the step with the greatest resistance [61]. From equation 2.9, a thin PSD with high K_{pw} and diffusion coefficients effectively reduces the contribution of the PSD to the overall transport resistance. The thickness of the WBL is fictitious as it is controlled by complex hydrodynamics [61]. However, the contribution of the WBL to transport resistance can be controlled by deployment of the PSD in locations with sufficiently high flow rates. The hydrodynamic theory postulates that resistance in the water

phase is proportional to ${D_w}^{2/3}$, therefore $k_w = F{D_w}^{2/3}$, where F is a proportionality constant [23, 61, 132]. Using this relation, equation 2.9 is re-written as:

$$\frac{1}{k_o} = \frac{1}{F{D_w}^{2/3}} + \frac{\delta_p}{D_p K_{pw}} \tag{2.10}$$

Generally, at low flow rates (<1 cm/s), moderately to highly hydrophobic compounds are under WBL control while the less hydrophobic (log $K_{ow} < 4.5$) are under membrane control [61]. On the other hand, compounds with high diffusion coefficients in the PSD experience low resistance [131]. Diffusive mass transfer is therefore optimal at low resistances, that is, with a thin WBL and high diffusivity in the PSD and can be controlled by selecting a PSD with sufficiently high diffusivity of the compounds of interest and by deploying the PSD in locations with high flow rates ($\gg$1 cm/s).

Given water as the medium of interest, the uptake of an analyte from water onto a PSD occurs by fluxes through the three interphases shown in figure 2.1, and is a three-phased process that follows first order kinetics (figure 2.2) [23]. As shown in figure 2.2, the accumulation of a chemical in the PSD until equilibrium follows a curvilinear approach [23]. At the initial stage, termed the linear or kinetic phase, mass transfer proceeds unidirectionally to the PSD which is considered to be in zero-sink condition and acts as the preferred partitioning phase [21]. As the accumulated amounts in the PSD increase, both sorption and desorption start to occur (curvilinear phase in figure 2.2) and this process proceeds until thermodynamic equilibrium is achieved at which point sorption and desorption processes are approximately equally fast.

Equilibration times differ with the sampler characteristics, partition coefficients and hydrodynamics and can range from hours to years. Short equilibration times of hours to days reflect high water flow rates, low partition coefficients, and high surface area to volume ratios of the sampler [21]. By contrast, equilibrium attainment can take

months to years for highly hydrophobic compounds and for thick nonpolar PSDs or low flow rates, in which case the samplers yield a time weighted average C_w over the exposure period [85].

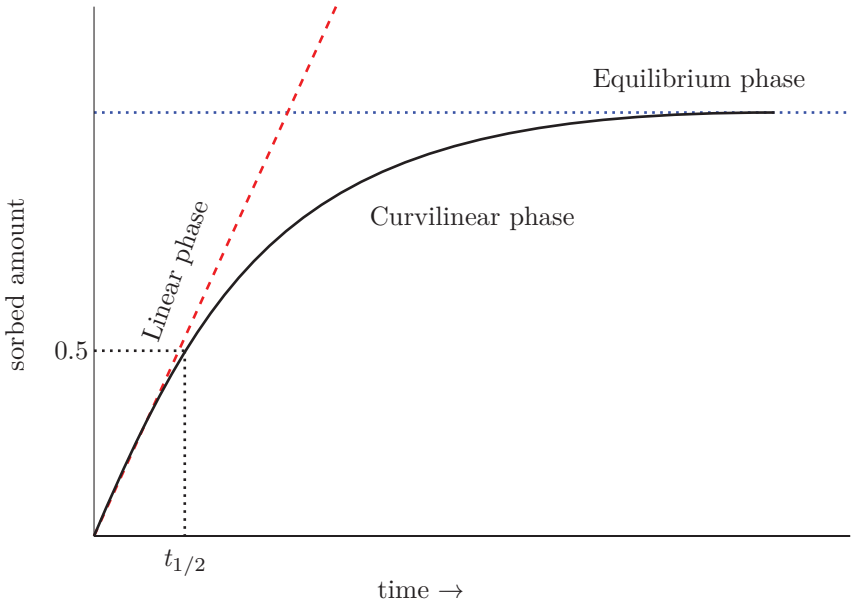

Figure 2.2: An illustration of the phases involved during the uptake of an organic compound from the aqueous phase onto a PSD.

2.3.3 First–order model for estimating the uptake of an organic compound from the aqueous phase to a PSD

The rate of change of solute concentration in the PSD (dC_p/dt) is inversely proportional to its thickness, $1/\delta_p = A/V$. Using this relation and equation 2.6, the rate of change of solute concentration in the PSD is given as:

$$\frac{dC_p}{dt} = \frac{A \cdot j}{V} = \frac{k_o A}{V}\left(C_w - \frac{C_p}{K_{pw}}\right) \tag{2.11}$$

where and A (m^2) and V (m^3) are the PSD surface area and volume respectively. Since the PSD mass [m, (kg)] and volume are proportional, mass can be used in

place of volume in equation 2.11 [132] as:

$$\frac{dC_{\mathrm{p}}}{dt} = \frac{k_{\mathrm{o}}A}{m}\left(C_{\mathrm{w}} - \frac{C_{\mathrm{p}}}{K_{\mathrm{pw}}}\right) \tag{2.12}$$

Assuming constant C_{w} and zero initial concentration, the evolution of analyte amounts accumulated in the polymeric sorbent is determined by a solution to equation 2.12 [55] (see section B in the appendix) given as:

$$C_{\mathrm{p}} = K_{\mathrm{pw}}C_{\mathrm{w}}\left[1 - e^{-k_{\mathrm{ex}}t}\right] \tag{2.13}$$

where t (d) is the time and k_{ex} is the exchange rate of an organic chemical between the water phase and the polymer and is given by:

$$k_{\mathrm{ex}} = \frac{k_{\mathrm{o}}A}{K_{\mathrm{pw}}m} = \frac{R_{\mathrm{s}}}{K_{\mathrm{pw}}m} \tag{2.14}$$

where R_{s} (L/d) is the sampling rate, that is, the volume of water cleared per day. From equation 2.14, $R_{\mathrm{s}} = k_{\mathrm{o}}A$. Accordingly, R_{s} can be determined theoretically by substituting k_{o} in this relation with equation 2.10 to give:

$$R_{\mathrm{s}} = \frac{A}{\frac{1}{FD_{\mathrm{w}}{}^{2/3}} + \frac{\delta_p}{D_{\mathrm{p}}K_{\mathrm{pw}}}} \tag{2.15}$$

D_{p} for some PSDs have been developed and values are available in literature [132]. D_{w} is difficult to determine experimentally but there are models used for its estimation [140]. Substituting equation 2.14 into equation 2.13 yields:

$$C_{\mathrm{p}} = K_{\mathrm{pw}}C_{\mathrm{w}}\left[1 - e^{-\frac{R_{\mathrm{s}}t}{K_{\mathrm{pw}}m}}\right] \tag{2.16}$$

Given $N_{\mathrm{t}} = C_{\mathrm{p}}m$ where N_{t} (µg/kg) is the amount of analyte sorbed onto the polymer at time t, equation 2.16 can be rearranged and used to calculate C_{w} as:

$$C_{\mathrm{w}} = \frac{N_{\mathrm{t}}}{K_{\mathrm{pw}}m\left[1 - e^{-\frac{R_{\mathrm{s}}t}{K_{\mathrm{pw}}m}}\right]} \tag{2.17}$$

2.3.4 Kinetic and equilibrium sampling

For highly hydrophobic compounds or at short exposure times ($k_{ex} \ll 1$), $\left[1 - e^{-\frac{R_s t}{K_{pw} m}}\right]$ in equation 2.17 approximates $\frac{R_s}{K_{pw} m} t$, and on substitution and rearranging, the equation reduces to:

$$N_t \approx C_w R_s t \tag{2.18}$$

In this case, the sorption process is operating in the kinetic regime since $N_t \propto t$, and therefore uptake is linear and time-integrative. At long exposure duration ($k_{ex} \gg 1$) or for compounds that reach equilibrium within a short interval of time, the uptake phase is in the equilibrium regime and $\left[1 - e^{-\frac{R_s t}{K_{pw} m}}\right] \approx 1$. Hence equation 2.17 reduces to:

$$N_t = C_w K_{pw} m \tag{2.19}$$

2.3.5 Determination of K_{pw} and R_s

Passive sampling attempts to determine C_w by solving equation 2.17 using sorbed analyte amounts, R_s and K_{pw}. The latter two parameters are usually determined in a calibration process that involves equilibration of PSDs with contaminated water in one out of three possible laboratory experimental designs: static exposure, static renewal and continuous flow-through. While producing valid results, each of these methods has its advantages and disadvantages, and the choice of a particular method will depend on time and instrumental availability.

K_{pw} is then calculated by employing equation 2.5 using the amounts sorbed onto the PSD at equilibrium (C_p) and aqueous concentrations (C_w). This equation assumes that equilibrium between the water and sampler phases has been attained. Alternatively, K_{pw} can also be empirically determined using uptake (k_u) and elimination

(k_e) rates as given by the kinetic equation:

$$K_{pw} = \frac{k_u}{k_e} \tag{2.20}$$

The initial phase of the sampling process termed the kinetic phase (Figure 2.2) approaches linearity and occurs in the duration when $t < t_{\frac{1}{2}}$, where $t_{\frac{1}{2}}$ is the time at which the sorbent reaches 50% of its equilibrium concentration [115]. Using plots of C_p against C_w, uptake rates in this phase can then be estimated by linear regression. Theoretically, the upper-bound time limit within which the linear regression model can be applied is determined by [61]:

$$t_{\frac{1}{2}} = \frac{\ln 2}{k_{ex}} \tag{2.21}$$

Alternatively, R_s can be determined by calibrating the PSDs *in situ* using performance reference compounds (PRCs) [48, 146]. The uptake of a compound by a PSD is affected by environmental factors including temperature, flow velocities and biofouling [48], hence generally, there are variabilities between laboratory and field situations. Therefore PRCs have been used to correct the inconsistency to improve the validity of estimated C_w. PRCs are either chemicals that are usually not found in the field or isotopically labeled compounds and are spiked onto the PSDs prior to deployment. The PRCs amounts before (N_o) and after ($N_{t,PRC}$) exposure are then used to estimate the dissipation rate constant for the PRCs as [146] (see section B of the appendix for derivation):

$$f = \frac{N_{t,PRC}}{N_o} = \exp\left(-R_s.\frac{t}{K_{pw}m}\right) = \exp\left(-\frac{B}{M^{0.47}}.\frac{t}{K_{pw}m}\right) \tag{2.22}$$

where f represents the fraction of remaining PRCs, M the molar mass and B the proportionality constant that is dependent on the hydrodynamics. Assuming that the dissipation of a PRC and the uptake of an analogous analyte is isotopic, equation 2.22 is solved for the dissipation rate of the PRCs by non-linear least squares

regression and used to infer the R_s of an analyte [146]. The calculated R_s are then substituted in equation 2.17 to determine C_w.

2.3.6 Estimation of K_{pw} and R_s

It is impractical for a calibration experiment to include all the possible compounds that can be found in the environment due to prohibitive time and cost implications. However, known K_{pw} or R_s values of some compounds can be correlated to their physicochemical properties and the correlations can then be used to calculate the values for other compounds within the same group. Octanol–water partition coefficients ($\log K_{ow}$) have typically been used although they may have an uncertainty of about 0.2 log units except those that have been optimized for thermodynamic consistency [85]. Molar masses have also been used in correlation [132]. In addition, K_{pw} can be estimated using polyparameter linear free energy relationships [36].

2.3.7 Properties of PES in relation to its uptake of HOCs

PES is a hydrophobic synthetic polymer whose structure consists of diaryl sulfone groups linked through an ether in a repeating sequence (figure 2.3a). The aromatic groups limit the chain mobility and determine the membrane properties for which it is widely used, namely mechanical, thermal, hydrolytic and chemical stability as evidenced by a high glass transition temperature (T_g) of 225 °C [26]. However, the hydrophobic nature of PES makes it prone to biofouling, hence the membrane is commonly modified by different technologies using hydrophilic additives. Modified PES has a large capacity for hydrogen bonding with water [138], wets out quickly and is less prone to biofouling [183]. The basic PES has a density of $1.37\,g/cm^3$ [14], a fractional free volume of 0.151 [138] and a solubility parameter, δ_P of 10.8 $(cal/cm^3)^{1/2}$ [52].

PES membranes used in this study (Supor®-200) were flat sheets sold as a roll (3 m × 0.254 m × 145 µm) and supplied by Pall Corporation (Pensacola, USA). They are hydrophilic, and polyethylene glycol (PEG) (figure 2.3b) is used to improve the wetting properties [49]. The membranes are porous (0.2 µm average pore size) as shown in figure 2.4.

Uptake of compounds from the aqueous phase into porous PSDs may follow different pathways/mechanisms than those in classical PSDs such that the first–order uptake model described above (equation 2.17) may not be applicable. First, the influence of the porous structure of these PSDs on their uptake processes for HOCs will be described alongside the classical PSDs. Thereafter, suitable models for describing the uptake mechanisms into the porous membranes will be highlighted. PES will be discussed as an example of a porous membrane, and reference is drawn to its

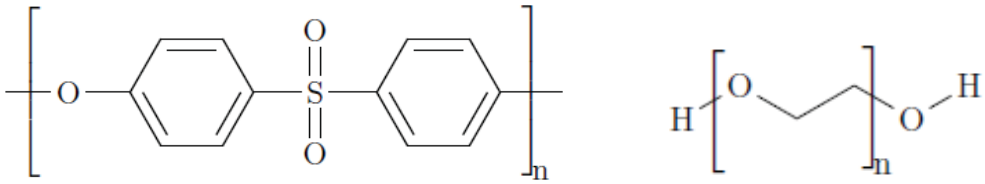

(a) (b)

Figure 2.3: General structures of (a) polyethersulfone and (b) polyethylene glycol.

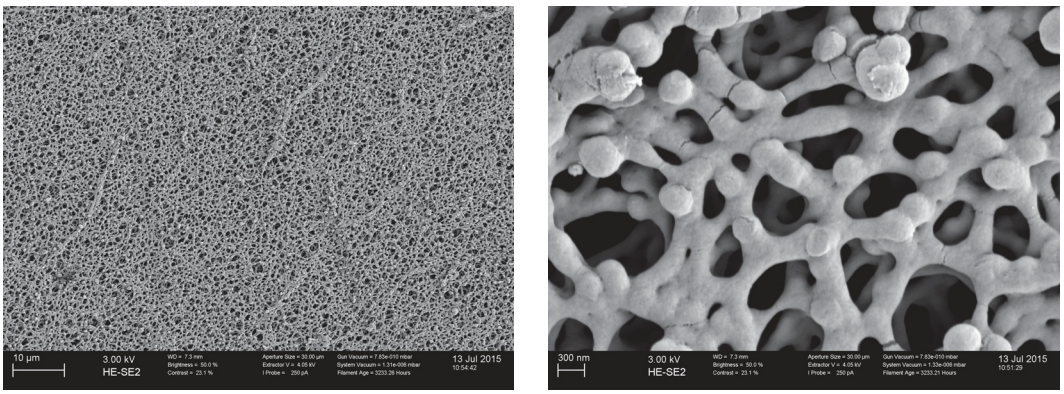

(a) (b)

Figure 2.4: SEM micrographs of plane faces of unused PES membranes at (a) 10 µm and (b) 300 nm. The micrographs were produced courtesy of ProVIS, UFZ Leipzig.

structure as shown in figure 2.4.

Polymeric sorbents generally consist of crystalline and amorphous regions. The amorphous region is characterized on the basis of its internal structure as either glassy or rubbery, and this also forms the basis for classification of a polymer in either of the two categories [158]. Whether a polymer is glassy or rubbery can be gauged by considering the glass transition temperature, where a rubbery polymer is one that exists above its T_g at room temperature (e.g silicone rubber, $T_g = -125\,°C$), and a glassy polymer exists below its T_g (e.g PES, $T_g = 225\,°C$). Rubbery polymers have an abundance of amorphous regions that are loose and flexible due to randomly arranged molecules and can expand to accommodate a sorbate. The amorphous regions are the main sorption sites for HOCs in rubbery polymers. Glassy polymers are an amalgam of amorphous and condensed glassy phases that contain holes/pores. Thus, sorption sites in glassy polymers additionally involve holes/pores.

In essence, silicone rubber contains an abundance of amorphous regions that readily undergo rearrangement in the presence of a sorbate by spontaneous expansion and relaxation, and can therefore be viewed thermodynamically as a suitable liquid phase that allows a chemical to diffuse through it, in a partitioning process. On the other hand, the high T_g of PES implies stiffer chains and stronger intermolecular interactions in addition to steric hindrance to bond rotations resulting from the occurrence of phenyl rings in its backbone [134]. This means that unlike silicone rubber, whose polymer chains are flexible, PES is characterised by a rigid condensed structure, whereby the segmental mobility of polymer chains is limited and are therefore not readily amenable for rearrangement in the presence of a sorbate. In addition, the rigid structure of PES results in the existence of pores, that are limited in number, are not uniform in size (consists of meso– and micro–pores), and span a range of steric and electronic characteristics (figure 2.4) [179]. This implies that sorption of HOCs to PES may be through a combination of sorption to the amorphous regions

(partitioning) and pore–filling (non-linear adsorption) mechanisms, and considering the well connected pores and that the PES membrane is wettable, it is possible that the pores fill up easily [158, 179].

Diffusion processes through which compounds move from the aqueous phase into PES involve bulk liquid diffusion, diffusion through the water–boundary layer, pore diffusion, and matrix diffusion (figure 2.5) [17]. The thickness of the water boundary layer is usually reduced through agitation of the experimental set–up and by field deployment in suitable locations with sufficient flow rates. This leaves matrix (membrane) diffusion and pore diffusion as the rate limiting processes [118]. Matrix diffusion occurs in penetrable solid phases (amorphous domains) while pore diffusion occurs at the surface of the pore and/or in "pore or vicinal" water [118]. The numerous pores (figure 2.4) result in abundant sorption sites. The pores and/or unrelaxed free volume regions (fractional free volume of 0.151) enhance the sorption of HOCs since the narrow pores offer multiple contact points within the PES matrix for the sorbate, leading to heightened sorption energies [134, 138]. At low-phase concentrations (<1–1.5% of aqueous solubility), HOCs sorb favourably to these high energy sites since they have the strongest affinity for the compounds, and as the high–affinity regions become saturated, sorption is then limited to less strongly sorbing (amorphous) regions [158]. The presence of additional high–energy sorption sites in glassy polymers gives them a higher sorptive capacity for HOCs than rubbery polymers. Indeed, in an assessment of various plastics, Saquing et al. [134] found that at low aqueous-phase concentrations (<10 µg/L), glassy plastics (polyvinyl chloride, PVC, K_{pw}=809.2 L/µg) exhibited higher partition coefficients for toluene than the rubbery plastics (polyethylenes, PEs, K_{pw}=70.7–123.1 L/µg). This indicates that glassy polymers have higher capacities than rubbery ones, such that uptake of compounds into the glassy polymers within the short–term laboratory experiment or field campaign will generally remain in the linear phase (see figure 2.2). Therefore, owing to the additional sorption sites, uptake of HOCs in PES may

not follow the same first–order sorption kinetics as in silicone rubber. An example of the uptake process for a PES blend is described below.

In an assessment of water sorption and transport in PES/polyethyloxazoline blends, Schult and Paul [139] made the following observations: i) sorption/desorption kinetics for PES were generally Fickian, but a two-stage sorption mode was observed in blends containing polyethyloxazoline, a polar additive used to improve PES wettability, ii) diffusion coefficients decreased with increasing polyethyloxazoline content, due to a decrease in the fractional free volume, and iii) the diffusion coefficient was dependant on water vapour activity due to plasticization induced by high levels of sorbed water, and the dependency increased with increase in the composition of polyethyloxazoline. The two-stage sorption process was characterized by rapid initial water uptake that was controlled by Fickian kinetics, followed by a slower

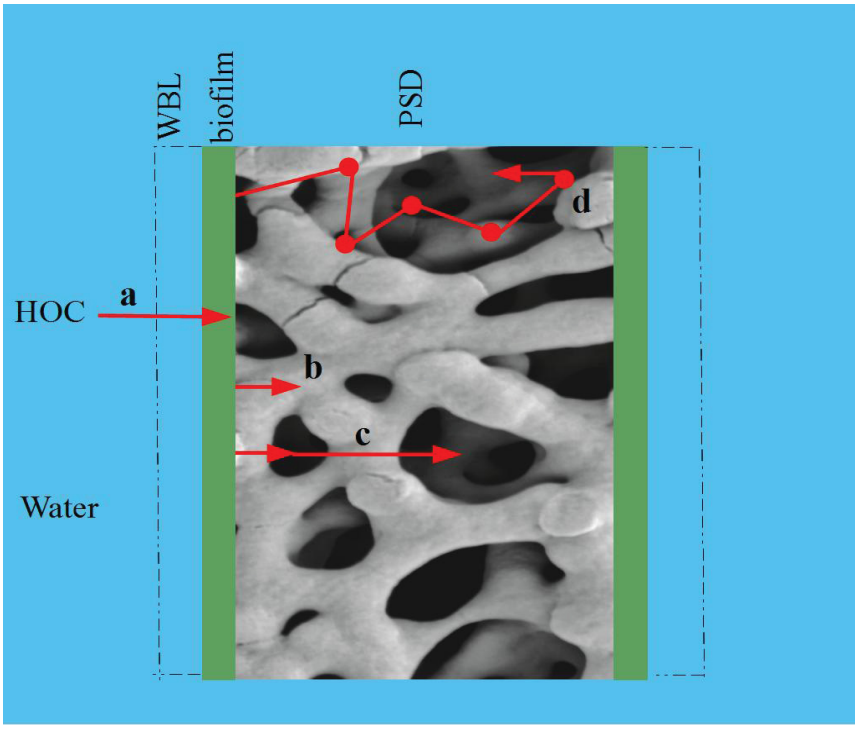

Figure 2.5: Uptake processes for a HOC from the water phase into a porous PSD like PES membrane. a) diffusion through the bulk water phase, WBL, and biofilm, b) PES matrix diffusion, c) water–filled pore diffusion, and d) surface pore diffusion.

approach to equilibrium. The reduction in uptake rates was attributed to time-dependent relaxations of the polymer that controlled further sorption, and which were driven by stresses created as a result of the gradient of water in the film and facilitated by plasticization at high water concentrations. Given that polyethylene glycol serves the same function as polyethyloxazoline, it is possible that water uptake in the PES–polyethylene glycol blend used in this study follows similar kinetics and rate–limiting processes.

The overall law governing chemical accumulation in a passive sampler is usually developed by considering only the rate–limiting process [17]. Considering first–order uptake equations 2.17 and 2.18 that are used for calculations involving most passive samplers including silicone rubber, the limiting processes considered are membrane or boundary layer diffusion that are dependent on their thickness. As already discussed, uptake mechanisms for HOCs in the glassy PES are more intricate than those in rubbery polymers like silicone rubber, and additionally involve pore diffusion as a rate–limiting step. As also discussed, when the membrane is deployed in experimental or field conditions that substantially reduce the thickness of the boundary layer, then this leaves membrane (essentially pore) diffusion as the rate limiting process. Therefore, equations 2.17 and 2.18 could perhaps be inadequate for describing the uptake kinetics in PES.

When the rate–limiting process is diffusion into pores (intraparticle diffusion), then this has to be accounted for and considered when modelling the uptake of chemicals. Variants of an intraparticle diffusion model originally developed by Weber and Morris [173] have been applied to model adsorption in cyclodextrin–polysulfone [16] and POCIS–nylon [17] samplers, and are respectively given as:

$$n_{\mathrm{t}} = k_{\mathrm{id}} \cdot t^{1/2} + \mathbf{C} \tag{2.23}$$

$$n_t = k_{id} \cdot t^m \tag{2.24}$$

where n_t (ng/g) the amount of chemical adsorbed, k_{id} (ng/g·d$^{1/2}$) or (ng/g·d^m) is the intraparticle diffusion coefficient, t (d) is the time, m is a function of the adsorption mechanism, and C is a constant that defines the boundary effect. The C value has been postulated to reflect the extent of the boundary layer thickness and its influence in the uptake process, where the larger the value of C, the greater the boundary layer effect [178]. Negative C values imply a retardation of intraparticle diffusion, positive values imply a rapid sorption process in the short–term duration, and zero values connote intraparticle diffusion as the only rate–limiting process [178]. m defines the factor that controls chemical accumulation in the membrane. First-order accumulation kinetics occur when $m = 1$, and $m = 0.5$ implies intraparticle diffusion process is the only factor controlling accumulation, while $0.5 < m < 1$ implies both intraparticle and first-order processes occur concurrently and each partially controls the accumulation process [17]. Equations 2.23 and 2.24 are useful in elucidating the uptake mechanisms, that is, the limiting processes, and can be used to gauge whether or not first–order uptake mechanisms hold.

2.3.8 Types of PSDs

PSDs are broadly categorized in various ways depending on the sampling principle, the sampled medium and the sampler design.

In terms of the main uptake phase involved, PSDs can be classified as equilibrium or integrative samplers. Equilibrium samplers generally have low capacities and short equilibration times and operate in the equilibrium regime of the uptake curve (figure 2.2). They are intended for the determination of the environmental concentration of a compound as a function of the equilibrium concentration of the PSD, and equation

2.19 applies [97, 128, 166]. An example of an equilibrium sampler is the solid phase microextraction (SPME) [108]. Integrative samplers provide a time-integrated average concentration over the complete sampling period which covers the whole uptake curve in figure 2.2 [128]. Environmental concentrations determined using these integrative samplers, also called kinetic samplers, are referred to as time-weighted average (TWA) concentrations and are determined using equation 2.17 [166]. TWA concentrations are attractive since episodic events that may be missed out during grab sampling are captured, and low detection limits are achieved due to sampling of large water volumes [32, 128, 166]. Examples of integrative samplers include the semipermeable membrane device (SPMD) [61], the polar organic chemical integrative sampler (POCIS) [7], and silicone rubber (SR) [146].

Considering the sampler design and the type of barrier between the sampler and the sampled medium, PSDs can be regarded as diffusion– or permeation–based samplers [45, 166]. The uptake principle in both types is the same, that is, passive diffusion as a result of differences in chemical potential, and they only differ in their formats. Uptake in diffusion–based PSDs involve diffusion of a compound through a stagnant layer of the environmental medium with defined dimensions and is located between the opening of a tube and the receiving phase that is inside the tube. The permeation–based PSDs utilize diffusion through a membrane that can be porous or nonporous [166]. This latter type of samplers are mostly used in water monitoring. They can be single–phased if the membrane acts as the receiving phase or dual–phased if the membrane is located between the environmental medium and the receiving phase.

2.3.9 Application of PSDs in surface water monitoring

Research into PSDs has increased in the recent past with a focus being on field applications and the development of working principles of new and existing PSDs

[48]. Several PSDs have been and are still being developed to monitor pollutants of different hydrophobicity (log K_{ow}) ranges with some overlapping in the type of pollutants they can accumulate and only differing innately and/or operationally. Thus depending on the end goal and the defined monitoring strategy, one or more out of several PSDs can be applied. The following few paragraphs describe some PSDs and highlight their field applications.

The semipermeable membrane device (SPMD) was the first to be used on a wide scale [60, 61]. It is biphasic consisting of 1 mL synthetic triolein enclosed in a 70–95 µm thick lay-flat low density polyethylene (LDPE) membrane in tubular format. The LDPE membrane mimics a biological membrane and allows selective diffusion of compounds into the synthetic triolein that mimics biological fluid. It has been used to monitor hexachlorobenzene (HCB), polycyclic aromatic hydrocarbons (PAHs), polychlorinated biphenyls (PCBs) [4], polychlorinated dibenzodioxins [79] and organochlorine contaminants [34].

The membrane-enclosed sorptive coating (MESCO) sampler is a combination of passive sampling and stir bar sorptive extraction (SBSE) [111]. SBSE is a solventless extraction method using the novel polydimethylsiloxane (PDMS)-coated Twister® (Gerstel) or silicone rod. The silicone rod or Twister® is enclosed in a LDPE membrane or dialysis membrane bag made from regenerated cellulose and filled with bi-distilled water. The membranes allow diffusion of only dissolved substances to the bi-distilled water from which organic compounds are extracted. MESCO has been applied to monitor organic pollutants like HCB, PAHs, PCBs [4, 168].

Other biphasic samplers are the polar organic chemical integrative sampler (POCIS) [7] and Chemcatcher® [71]. POCIS consists of a sorbent material sandwiched between two membranes, usually polyethersulfone (PES). Chemcatcher® on the other hand has one open face which may or may not be covered with a membrane, for ex-

ample LDPE or PES, depending on the goal of the sampling process. In both cases, the membrane acts as the sorbent protector and uptake rate limiter. The sorbent is selected to suit the contaminants of interest but mostly, polar organic compounds are monitored. For instance, the Chemcatcher® version designed to monitor hydrophobic organic contaminants consists of a C_{18} Empore® disk saturated with n-octanol and enclosed using a LDPE membrane [30, 115]. Uptake kinetics are similar to that of the SPMD and involve diffusion of the compound through the membrane to the sorbent and measured concentrations usually reflect only those measured in the sorbent material. Some applications of POCIS include monitoring of endocrine disrupting compounds [162] and pesticides [121] in surface water. Chemcatcher® has been applied to monitor hydrophobic organic contaminants (HOCs) [5, 167], pesticides [102] and pharmaceuticals and biocides [164].

Mono-phased PSDs consisting of a single membrane as the receiving phase have also emerged. Examples include LDPE [84] and SR [132, 146]. Uptake process of organic compounds by these PSDs is more simplified than that of biphasic membranes and modeling of the uptake is commonly done as outlined in section 2.3.3. These samplers have been applied to monitor for PAHs, PCBs and organochlorine pesticides (OCPs) in surface water [6, 4, 15, 124].

As already highlighted, PES membrane has been applied in passive sampling mostly as a sorbent retainer and sampling rate limiter in Chemcatcher® and POCIS. However, when applying a PES-covered Chemcatcher® in a simulated river environment, Vermeirssen et al. [165] observed that diazinon and diuron appeared in the sorbent material after a lag phase and that the concentrations of the two compounds were respectively, 3– and 6–fold higher than in the sorbent material. This observation was attributed to strong sorption of the compounds to the PES membrane that was used to cover the disk. A similar observation was also made for diuron though with lower PES/sorbent ratios [159]. In addition, Harman et al. [54] observed the uptake

of PAHs and carbazoles in a POCIS sorbent at very low ng/POCIS levels characterized by high variability and poor linear fit and hypothesized the phenomenon to be due to stronger sorption to the PES membrane during the initial sampling stages. These experiments suggest a possible role of PES as a sorbent material.

Indeed, a few studies have confirmed the uptake of compounds from a wide hydrophobicity range by PES, albeit in tubular format. PES tubes have successfully been applied in laboratory experiments for sorptive extraction of a range of polar and non-polar chemicals (log K_{ow} = -0.07–6.88) from water samples [19, 122, 123] and endocrine disrupting chemicals from fish bile [129]. Thus PES has been suggested as a potential sorptive extractor of pollutants from water owing to its versatility during use and good sorption ability for a range of chemicals [122, 123].

Given the varied physicochemical properties of PES –sorbed analytes from the aforementioned studies, there is a possibility of applying PES for sorption of other pollutants including those that are usually out of range of the target analytes for POCIS and Chemcatcher. Nevertheless, most of these studies have been conducted in a simulated environment, and PES has seldom been applied in the field as a sorbent. Hitherto, only two studies report field application of PES to sample galaxolide, tonalide, 4-tert-octylphenol, organochlorine compounds, pesticides, phthalates, musk fragrances and triclosan [119, 120].

Clearly, PES shows potential as a sampler for a wide range of compounds. Yet, both laboratory and field studies to investigate this potential or the suitability of PES as a passive sampler are still very few. Consequently, its key properties (e.g sampling rate) and uptake mechanisms for HOCs from the aqueous phase are still lacking. Thus, this study aimed to bridge the knowledge gap by investigating these properties/processes for PAHs, PCBs, OCPs and phthalates, in order to suggest the suitability of PES as a PSD. In addition its field application was tested using SR as

a reference.

Apart from its application in passive sampling as highlighted above, PES is commonly used in hemodialysis, electromotive and electronics industries, water filtration, gas separation and in passive sampling as a sorbent retainer and sampling rate limiter in the polar organic chemical integrative sampler (POCIS) [8].

SR and other silicones including PDMS are robust and generally have the advantage of high diffusion coefficients for HOCs which implies that resistance in the membrane is negligible as compared to that in the WBL [96, 131]. Thus, deployment conditions can be controlled to reduce WBL resistance and therefore maximize the uptake of chemicals from an environmental matrix. In addition, SR can sorb a wide range of chemicals and has indeed been applied to monitor pesticides, herbicides, PAHs, PCBs and OCPs [35, 124]. This thesis demonstrates the applicability of SR for these HOCs and also for the phthalates DEHP, BBP and dibutylphthalate (DBP) in a tropical environment.

2.3.10 Application of PSDs in sediments monitoring

Freely dissolved concentrations of HOCs in sediment porewater ($C_{\text{free,pw}}$) are more closely associated to risks of adverse effects for biota than total sediment concentrations ($C_{\text{total,pw}}$) [88]. In addition, it is the $C_{\text{free,pw}}$ that is amenable for biodegradation and consequently, it is necessary to determine $C_{\text{free,pw}}$. This has conventionally been done using equilibrium partitioning models that recalculate $C_{\text{free,pw}}$ from $C_{\text{total,pw}}$. However, theoretical prediction using models introduce considerable inaccuracy and uncertainty in risk assessment of contaminated sediments since the predicted concentrations do not generally match the experimentally determined values [96]. Techniques that directly measure $C_{\text{free,pw}}$ are therefore more attractive in risk assessment and to this end, passive samplers have been developed and applied

to monitor HOCs in sediment porewater. Examples are SPME, SPMD, polyethylene, polyoxymethylene and silicone–coated jars [88]. PES was applied in this study to monitor compounds in sediments similar to those in the water column.

As opposed to other mediums such as water, passive sampling methods in heterogeneous sediment matrices operate in the equilibrium regime since at equilibrium, chemical activity and fugacity are the same in the sampler as in the sediment, and therefore $C_{\text{free,pw}}$ can be determined from the concentration in the sampler using a simple partition ratio [96]. Equilibrium attainment is confirmed using three methods [96, 97]: a) conducting a time–series experiment until measured concentrations in the samplers are constant, b) simultaneous extraction using two samplers having different surface area to volume ratios (A/V) with the thinner sampler always having higher concentration until equilibrium, which is confirmed by convergence of concentrations in the two samplers, and c) use of PRCs. Apart from confirmation of equilibrium attainment, sample depletion should be avoided by keeping the extracted amount in the passive sampler far below the dissolved concentration. This is done through correct choice of the sampler volume (V_{p}) for given volumes of sediment (V_{s}) and porewater (V_{pw}) and can be estimated by $\frac{V_{\text{p}}K_{\text{pw}}}{V_{\text{w}}+V_{\text{s}}K_{\text{sw}}} <<< 1$ [97]. Alternatively, non-depletion criteria can be checked by keeping the phase ratio between water and polymer well above the polymer–water partition coefficient [96].

2.4 Estimation methods of sediment–water partition coefficient

In a river system, HOCs partition preferably to the organic phase of sediments and suspended solids. The partitioning process is actually a two–way process that depends on environmental conditions such as temperature, hydrodynamics and properties of both the chemical and sediments, namely, hydrophobicity and organic matter

content respectively. The equilibrium partitioning of a chemical between water and sediment is described by the sediment–water partition coefficient (K_{d}) as:

$$K_{\mathrm{d}} = \frac{Q_{\mathrm{s}}}{C_{\mathrm{w}}} \tag{2.25}$$

where Q_{s} (mol/kg) is chemical concentration in sediments and C_{w} (mol/L) in this context can imply freely dissolved water or porewater concentrations depending on which parameter is under consideration. Given that chemical sorption to sediments occurs mainly by partitioning into organic matter (organic carbon), it is more appropriate to express K_{d} in terms of the organic carbon content. Therefore, K_{d} can be estimated from the organic carbon–water partition coefficient (K_{oc}) and the fraction of organic carbon (f_{oc}) as:

$$K_{\mathrm{d}} = K_{\mathrm{oc}} f_{\mathrm{oc}} \tag{2.26}$$

Using octanol as a surrogate for organic carbon, K_{oc} has been correlated to hydrophobicity (K_{ow}) to obtain linear log–log relationships that can be used to estimate K_{oc} (mol/kg) in the absence of experimental values. One such linear model is the Karickhoff relation [69] given as:

$$\log K_{\mathrm{oc}} = 0.41 \times \log K_{\mathrm{ow}} \tag{2.27}$$

However, the linear models have been deemed insufficient for general prediction since experimentally determined K_{oc} have been found to far exceed those predicted by the models [13]. Empirical K_{oc} can be determined from f_{oc} and concentrations of the HOCs in sediments and water as:

$$K_{\mathrm{oc}} = \frac{Q_{\mathrm{s}}}{C_{\mathrm{w}} f_{\mathrm{oc}}} \tag{2.28}$$

Q_{s} and f_{oc} are based on the sediment dry weight. Equation 2.28 can also be used in risk assessment to predict, for example the partitioning of a HOC from sediments to

water given the other parameters and assuming a uniform desorption process. However, some authors have pointed out that organic carbon, consists of sub–fractions mainly amorphous organic carbon and black carbon that have different affinities for HOCs implying that desorption processes are non-uniform and consist of both fast and slow modes [13, 118]. Models accounting for these subfractions of organic carbon have been developed although it has also been suggested that they do not significantly improve the K_{oc} model for the general prediction of the sediment-porewater distribution [56]. Theoretical models for predicting K_{oc} have also been developed. For instance, in comparing the predictive power of three theoretical models versus experimentally determined K_{oc}, Arp et al. [13] found that a model relating K_{oc} to the subcooled saturated molar water solubility and coal tar–based linear free energy relationships (LFER) models were able to predict experimental K_{oc} within reasonable accuracy. These models are respectively given as [13]:

$$K_{oc} = \frac{1}{C_w^{sat} MW_{oc}} \tag{2.29}$$

$$\text{Log}\, K_{oc} = eE + vV + aA + bB + sS + c \tag{2.30}$$

where C_w^{sat} (mol/L) is the subcooled saturated molar water solubility and MW_{oc} is the molar weight of the sediment's organic phase, equivalent to 0.223 kg/mol. E, V, A, B, and S are the compound–specific parameters describing the excess molar refraction, molar volume, electron acceptor capability, electron donor capability, and the polarizability/dipolarizability, respectively. e, v, a, b, and s are the complementary sorbent–specific parameters.

K_d can also be expressed in fugacity terms as a ratio of the fugacity capacities of sediments (Z_s) and water (Z_w). Fugacity capacity (Z in mol m^3/Pa) is a proportionality constant that links fugacity to chemical concentration (C in mol/m^3) as $C = Zf$. Fugacity (f in Pa) is defined as the escaping tendency of a molecule into

the ideal gas phase and can be regarded as the partial pressure of a chemical [89]. The underlying concept in the fugacity approach is that the fugacities of a chemical in two phases are equal if the multiphase system is at equilibrium. This implies that if the fugacity in one phase can be empirically determined, the resultant value can be used to infer fugacity in the other phase. At disequilibrium, a molecule would essentially 'escape' from one environmental phase to another, and the process would go on until equilibrium. Thus, fugacity-based models employing fugacity ratios elucidate the status of a chemical in a multi–phasic environmental media and can therefore be used to screen for the dominant fate processes and assess bioavailability [169]. Assessment of bioavailability is the objective of equilibrium partitioning and fugacity–based modeling since sediments sequester contaminants from the water phase and can therefore act as reservoirs depending on their organic matter content. Using fugacity capacities, K_{d} is expressed as:

$$K_{\mathrm{d}} = \frac{Z_{\mathrm{s}}}{Z_{\mathrm{w}}} \tag{2.31}$$

where

$$Z_{\mathrm{w}} = \frac{1}{H}; \quad Z_{\mathrm{s}} = \frac{K_{\mathrm{oc}} f_{\mathrm{oc}} \rho_{\mathrm{s}}}{H} \tag{2.32}$$

where H is the Henry's law constant and ρ_{s} (kg/m^3) is the sediment density. See section B for derivation of Z values.

2.5 Fugacity approach to estimate sediment-water exchange of EDCs

The distribution of HOCs between sediment and water phases is an important phenomenon since it influences bioavailability. Owing to their hydrophobicity, HOCs partition preferably to the sediment phase depending on the quantity and availability of sorption phases in the sediments. However, sediment–water exchanges termed

fluxes occur due to a number of complex environmental processes that may be site–specific and include ebulation, bioturbation, groundwater discharge, sediment settling or resuspension and molecular diffusion [82]. The latter process occurs universally and plays the key role in the transfer of contaminants between the two phases and may therefore be used as a baseline for total flux [42]. Molecular diffusion is driven by a concentration or fugacity gradient between the sediment and water phases.

Several fate and transport models have been developed and are available in literature. These models can be categorized into two groups: a) those that use chemical concentrations in calculations and b) those that use the multimedia fugacity approach. Fugacity is a multimedia parameter that describes the escaping tendency of a chemical into the ideal gas phase and therefore directly indicates the potential for spontaneous processes including diffusion and partitioning [96]. The use of fugacity in lieu of concentration simplifies the understanding of fluxes from one environmental phase to another, for example sediment–water, as it provides a parsimonious yet powerful explanation of chemical fluxes. Therefore, when seeking to elucidate chemical behavior profiles and to determine dominant fate processes, fugacity–based models are well suited [125]. Multimedia fugacity models also called Mackay models have four levels that vary progressively in complexity. These are: a) level I that assumes steady state and equilibrium conditions between phases, b) level II that in addition to assumptions made in level I also considers advection and the chemical transformation, c) level III that assumes steady-state, but non-equilibrium conditions between environmental phases and considers transformation, d) level IV that considers non-equilibrium and non-steady-state conditions between phases [89]. Level IV models are the most realistic but are rarely applied due to their complexity and enormous data requirements. Hence, Level III models are the most widely used. Examples of fugacity–based models are the EUSES, EQC and SimpleBOX.

Multimedia fugacity models use fugacity fractions between environmental phases, for example water and sediment, both as a pointer to the direction of movement of a chemical and a basis for other relevant calculations. Even without the use of a complete model, fugacity fractions have been applied to estimate sediment–water fluxes given concentrations in the two phases [169]. However, a full model is better placed to elucidate the relative relevance of various environmental fate processes.

One such model is the Sediment Model developed by the Centre for Environmental Modelling and Chemistry [27]. This model calculates the sediment–water exchange characteristics of a chemical within a defined unit area based on the chemical's physicochemical properties and the total water and sediment concentrations. In principle, the model uses measured concentrations in sediment and overlying water to calculate fugacities in the two phases as:

$$f = \frac{C}{Z} \tag{2.33}$$

where C is chemical concentration and Z the fugacity capacity in the given phase. Each of the phases is divided into three sub-compartments comprising the bulk phase, (pore)water and solid phases. The solid sub-compartments comprise total suspended solids and total sediment solids in the water and sediment phases respectively, and both incorporate organic and mineral matter fractions. The model calculates the fugacity for each sub–compartment which is then used to calculate the overall fugacity capacity for the bulk phase. In water, Z_{w}, is calculated as:

$$Z_{\mathrm{w}} = (Z_{\mathrm{pw}} \times V \cdot f_{\mathrm{pw}}) + (Z_{\mathrm{ow,w}} \times V \cdot f_{\mathrm{ow,w}}) + (Z_{\mathrm{mm,w}} \times V \cdot f_{\mathrm{mm,w}}) \tag{2.34}$$

where Z_{pw}, $Z_{\mathrm{om,w}}$, $Z_{\mathrm{mm,w}}$ are respectively, the fugacity capacities in pure water (operationally defined as water without suspended solids), organic matter and mineral matter in the bulk water phase. Vf_{pw}, $Vf_{\mathrm{om,w}}$ and $Vf_{\mathrm{mm,w}}$ are the volume fractions of pure water, organic matter and mineral matter in the bulk water phase. Z_{pw} is

derived as a reciprocal of the Henry's law constant, then the value obtained is multiplied by the partition coefficients of organic and mineral matter to obtain $Z_{\mathrm{om,w}}$ and $Z_{\mathrm{mm,w}}$ respectively. $Vf_{\mathrm{om,w}}$ and $Vf_{\mathrm{mm,w}}$ are calculated using the fraction of organic matter, the densities of organic and mineral matter and the concentration of total suspended solids. Equations used in the calculations are given in section L.2 of the appendix. When using equation 2.34 for sediments, C_{s} is the measured concentration in dry sediments. Z_{s} is derived from the fugacity capacities and volumes of organic and mineral matter in dry sediment as:

$$Z_{\mathrm{s}} = \frac{(Z_{\mathrm{om,s}} \times V_{\mathrm{om,s}}) + (Z_{\mathrm{mm,s}} \times V_{\mathrm{mm,s}})}{V_{\mathrm{om,s}} + V_{\mathrm{mm,s}}} \tag{2.35}$$

$Z_{\mathrm{om,s}}$ and $Z_{\mathrm{mm,s}}$ are respectively derived by multiplying the partition coefficients of organic and mineral matter by the Z value for porewater, which is a reciprocal of the Henry's law constant.

The model then calculates the ratio of fugacity in sediments (f_{s}) to that in water (f_{w}). This ratio is used to assess the equilibrium status of a chemical between the two phases at unsteady state. Predictions of fugacity ratios at steady state are also made using transport and advection parameters, that is, D– and G–values. These values are also used in calculating sediment–water fluxes that define the relative importance of each environmental fate process and therefore half–lives. In addition, the model uses Z, f_{s} and f_{w} values for the respective (sub)phases to calculate concentrations of chemicals in these phases on a mass balance basis.

On the other hand, the sediment–water fugacity ratio can be calculated from chemical concentrations in the two phases and K_{oc} values as:

$$\frac{f_{\mathrm{s}}}{f_{\mathrm{w}}} = \frac{C_{\mathrm{s}}}{K_{\mathrm{oc}} f_{\mathrm{oc}} \rho_{\mathrm{s}} C_{\mathrm{w}}} \tag{2.36}$$

Refer to section B for derivation of the equation.

The fugacity ratio determined using the Sediment Model or equation 2.36 can serve as an indicator of the sediment–water equilibrium status. Generally, $f = 1$ indicates equilibrium, $f < 1$ a net flux from water to sediment and $f > 1$ a net flux from sediment to water [169].

Chapter 3

Materials and Methods

3.1 Investigation of key properties of PES

3.1.1 Reagents

Reagents used were the following: chromatographic analysis grade cyclohexane, isopropanol, ethyl acetate, methanol and acetone (Merck, Darmstadt), anhydrous sodium sulphate (Merck, Darmstadt), PAHs mix 9 (100 ng/µL in cyclohexane) and pesticide mix 13 (10 µg/mL in toluene) (Dr. Ehrenstorfer, Augsburg), PRCs (d_{10}-acenaphthene, d_{10}-fluorene, d_{10}-phenanthrene, d_{10}-anthracene, d_{10}-pyrene, d_{12}-chrysene, d_{12}-perylene, PCB 29, PCB 54, PCB 77 and PCB 81) (Dr. Ehrenstorfer, Augsburg), d_{10}-fluoranthene internal standard (Dr. Ehrenstorfer, Augsburg) and pure forms of the analytes listed in table C.1 of the appendix. Standard solutions of individual analytes were prepared in methanol at concentrations ranging from 2–3 mg/mL. From these standard solutions, working mixtures (100 ng/mL and 25 ng/mL) of all the analytes were prepared in methanol and stored at 4 °C . A mixture of the PRCs (1.5 mg/mL) were prepared in methanol.

3.1.2 Calibration experiment for investigating uptake kinetics and PRC elimination

Laboratory calibration experiments for passive samplers are generally carried out in one of three possible setups: batch equilibration, static renewal and continuous flow-through designs [23]. A stable flow-through system ensures a continuous supply of freshly contaminated water with minimal disturbance throughout the experimental period that mimics environmental conditions and thus circumvents the depletion of analytes from the water phase and other experimental artifacts inherent in the former two designs. Therefore, calibration of PES was done in this study using a flow-through design. The apparatus was set up as shown in figure 3.1a. Initially, the apparatus was contaminated during five days by completely filling the glass containers with contaminated tap water containing all the analytes at a concentration

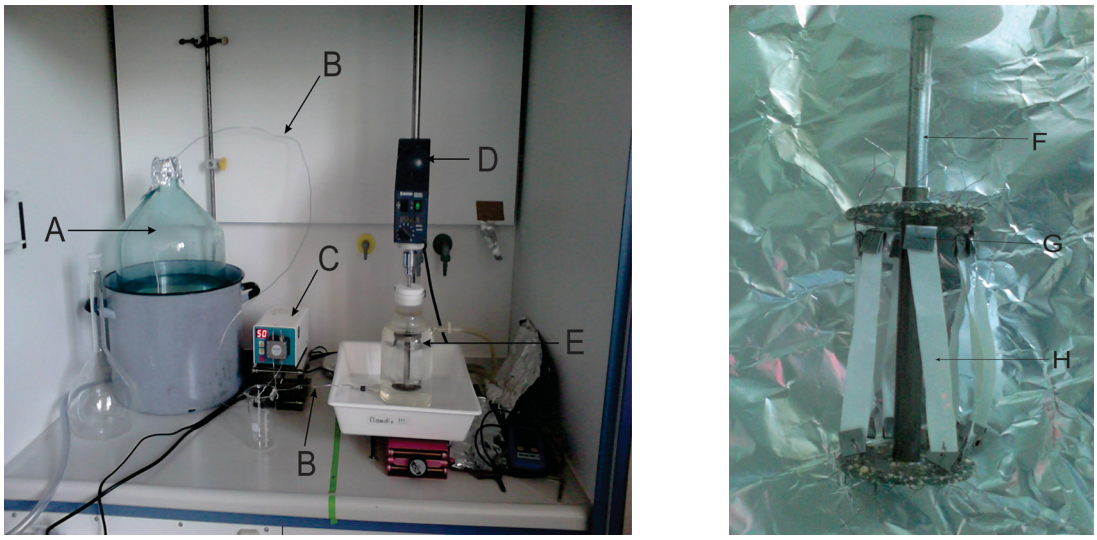

(a) (b)

Figure 3.1: (a) Setup of the flow-through calibration experiment and (b) Clamp used to hold PES membranes. A- 22.4 L glass storage tank; B- connecting hollow wires made of steel; C- pump used for controlling flow rate; D- mortar that controlled the rotation speed of the clamp holding PES membranes; E- 1.4 L experimental glass vessel that housed the membranes; F-rotatable steel clamp; G- steel clips used to hold PES membranes in position; H- PES membrane strips.

of 100 ng/L, which was four-fold the experimental nominal concentration (25 ng/L). Prior to disposal, the pumping system was activated to let contaminated water flow through the system, to ensure no or minimal depletion of analytes from the water phase during the experimental duration by sorption to the apparatus walls.

PES strips measuring 1.0 cm × 9.0 cm (exposure surface area ≈ 14 cm^2) were cut out and pre-cleaned in ethyl acetate and methanol in that order according to the procedure that will be outlined in subsection 3.2.1, then they were spiked with PRCs during three days in 400 mL methanol-water (1:1, v/v) mixture. The PRC-loaded PES strips were stored dry at 4 ℃ until use. All other apparatus and the aluminium foil working surface were pre-cleaned in acetone.

At the start of the experiment, the storage tank and experimental vessel were filled with contaminated tap water at a nominal concentration of 25 ng/L. Eight PRC-loaded PES strips were then fixed using pre-cleaned stainless steel clips and nichrome wires onto a rotatable clamp as shown in figure 3.1b. Rotating speed was set at 130 rpm translating to a river flow velocity of 0.34 m/s under field conditions as will be described in subsection 3.2.2. Flow velocity through the experimental vessel was 5 mL/min to allow enough contact time of the analytes with PES strips without causing depletion from the water phase. Average room temperature during the experimental duration was 23.5 °C. The experiment proceeded continuously for 14 d with short interruptions during membrane removal and replacement which was done intermittently at 2, 4, 7 (in duplicate), 10, 12 and 14 days to ensure continual presence of eight membranes at any point in time during the experimental process. Except the 14^{th} day, at each time interval, two membranes were removed and replaced by an equal number. The used membranes were patted dry with lint-free tissue and stored at 4 °C until extraction. The membranes were extracted in ethyl acetate, concentrated to 1 mL and analyzed as will be described in subsection 3.2.3.

The intent of a calibration process is to determine key PSD properties such as the polymer-water partition coefficient (see equation 2.5) that influence the uptake of analytes from the aqueous phase. Thus while quantifying sorbed concentrations onto PES , aqueous concentrations have also to be determined in parallel. Therefore, 200 mL of water were taken daily from the experimental vessel using a 250 mL Erlenmeyer flask then 17 % methanol and a 24 µL pre-cleaned PDMS-coated twister® (Gerstel) was added. Methanol was used to reduce analyte losses by sorption to the glass wall. Twisters® were pre-cleaned by combustion at 250 ℃ overnight. The flask was then covered with aluminium foil to prevent photolysis and extraction proceeded for 24 h. Then the twister was removed using forceps, gently patted dry with lint-free tissue and stored at -20 ℃ until analysis. Analysis was done by thermal desorption on a gas chromatograph (GC) coupled to a mass spectrometer (MS).

3.1.3 Calibration experiment for the elimination process

Pre-cleaned PES strips were placed in a 500 mL glass bottle containing 400 mL of methanol-water mixture (1:1, v/v) spiked with a standard solution containing 150 µg each of the analytes, then the strips were left to equilibrate during 5 d. Thereafter, the strips were removed and patted dry with lint-free tissue and stored at 4 °C until use. The experiment was carried out using the set up described in section 3.1.2 with the following modifications. Fresh tap water (unspiked) was used, rotation speed was 128 rpm, and the water pump was set at 10 mL/min. Spiked PES strips were fixed onto the rotatable clamp, then the experiment proceeded for 15 d during which membranes were removed and replaced over time ranging from a few hours to days, yielding 19 sampling durations, thrice during which two strips were removed and the rest involved removal of single strips (refer to section E of the appendix). The PES strips were patted dry with lint-free tissue and stored at 4 °C until extraction and analysis, which proceeded as described in sections 3.2.3 and E, respectively.

3.1.4 Calculation of key parameters for PES

Calculation of aqueous concentrations according to equation 2.17 requires the determination of key parameters, namely K_{pw} and R_s. These two parameters were determined from data obtained in the calibration experiment described in section 3.1.2. Apparent K_{pw} was calculated according to equation 2.5 using maximum C_p and average C_w obtained during the 14 d experimental duration. Since PRCs could not be applied to determine *in situ* R_s as will be discussed in subsection 4.1.5, it was estimated by solving equation 2.18 by linear regression using at least five data points that approached linearity. Then k_{ex} was determined using equation 2.13 by nonlinear least squares regression and was then used to calculate 'half-life', $t_{1/2}$. k_o was calculated using the estimated R_s and surface area according to equation 2.14.

3.1.5 Quality assurance

Duplicate PES strips were collected at each sampling time to check for variability in the sorption process during the specified period. In addition, variability in sorption throughout the whole experimental duration was checked by leaving two PES strips to each sample during the first half and the last half of the total experimental duration. These strips were collected at 7 d and 14 d respectively and analyzed. Repeatability was examined by calculating the coefficients of variation (CV) from data of the duplicate samples. Blanks were also used to check for contamination.

3.2 Field application of PES and SR

3.2.1 Pre-deployment preparation

PES sheets were cut into 6.5 cm×10.0 cm pieces giving an exposure surface area of ≈130 cm^2 per membrane. Prior to deployment, the membranes were pre-cleaned in appropriate solvents to remove impurities. Initially, several solvents were tested based on solubility and swelling of PES in the solvent to determine their appropriateness for use in cleaning and extraction. The results (table 3.1) indicate the inappropriateness of chlorinated and some aprotic solvents which resulted in membrane solubility probably due to stress-induced cracking or solvent-induced crystallization [18, 53]. Toluene effected no change in mass while a slight increase was observed in cyclohexane likely due to retention of trapped solvent. The membrane became brittle in toluene and acetonitrile. Thus ethyl acetate and methanol were selected as pre-cleaning solvents in that order.

The pre-cleaning process proceeded as follows: all the sheets were immersed in ethyl acetate in a wide-mouthed 200 mL glass bottle. The bottle was placed on an orbital shaker and the membranes were extracted during 48 h at 90 rpm, then all the solvent was replaced with methanol and the membranes were further extracted during 24 h at 90 rpm followed by air drying in a fume hood to constant weight. The clean membranes were wrapped in pre-cleaned aluminium foil and stored at 4 °C until field deployment. Wire meshes used in deployment of membranes were also cleaned in acetone and stored.

SR membranes were prepared according to the procedure outlined in Smedes and Booij [146] with a few modifications as follows: A SR sheet was cut into 5.5 cm × 9.0 cm pieces and two mounting holes were made at ≈10 mm from the edges, thus the exposure area was ≈100 cm^2 per membrane. The membranes were then pre-

Table 3.1: Performance of PES membrane in various solvents

Solvent	Solubility[a]	Swelling[b] (%)		Change in mass[c]
		24 h	48 h	(%)
Acetonitrile	-	61	61	-0.2
Dimethyl sulfoxide	+	n.d.	n.d.	n.d.
Dichloromethane	+	n.d.	n.d.	n.d.
Ethyl acetate	-	53	58	-0.4
Tetrahydrofuran	+	n.d.	n.d.	n.d.
Toluene	-	71	77	0.0
Cyclohexane	-	37	40	0.4

[a]Solubility of PES membrane in the solvent at room temperature (+, soluble; -, insoluble);
[b,c]Calculated as a percentage relative to the initial value; n.d., not determined.

cleaned by soxhlet extraction in ethylacetate during five days to remove impurities and oligomers, and thereafter soaked twice in methanol for 8 h each to remove ethyl acetate. PRCs were then spiked onto the membranes by equilibrating in a 400 mL methanol-water mixture (1:1, v/v) during seven days. Finally, the membranes were dried with lint free tissue and stored at 4 °C until use.

3.2.2 Field deployment and retrieval

Field performance of PES in comparison to SR was tested by deploying both sorbents in parallel at two stations along Sosiani river, Kenya (0°3′S and 0°55′N, 34°55′E and 35°31′E; see appendix I.2). As its name suggests, the river is rocky and turbulent, and can be considered to be well mixed especially during low flows from December to February. This period marks the dry season with 25.4 mm average rainfall and mean temperature highs of 24.7 °C and lows of 10.7 °C. River flow velocities averaged 0.34 m/s. The two sampling stations were points along the river as it meanders through the town. The sampling campaign was carried out from December 2014 to January 2015.

Given that the average water depth along the river during the sampling period was 0.8 m, the samplers could not be deployed in standard cages, thus a homemade approach was designed as follows. Three PES membranes were secured onto a wire mesh for protection against abrasion. The mesh was then tied on both ends onto a polypropylene rope, onto which nine SR sheets were also fixed. The rope was then first anchored onto boulders that were readily available at the river bed to ensure that the samplers remained immersed in water at approximately two-thirds depth from the water surface, and then further fastened onto wooden pegs at the river banks. Field exposure duration was 30 d. During retrieval, PES membranes were carefully removed from the wire mesh, then both PES and SR samplers were rinsed in river water to remove excess biofouling and debris, patted dry with lint free tissue, wrapped in pre-cleaned aluminium foil and transported in a cooler box at 4 °C. The samplers were stored at −20 °C until analysis.

3.2.3 Extraction and analysis

A PES sampler consisted of one membrane implying three samplers per sampling station. The samplers were patted dry with lint-free tissue and placed in a 100 mL Erlenmeyer flask into which 15 mL ethyl acetate was added, then the membranes were extracted on an orbital shaker during 20 min at 90 rpm. The extract was transferred to a 40 mL evaporation tube, then the extraction process was repeated once using fresh solvent. All the extracts and rinsing amounting to approximately 40 mL were then concentrated to 2 mL on a Turbovap concentration workstation. The extract was cleaned and dried by passing through a glass column packed with anhydrous sodium sulphate into a 40 mL evaporation tube. The column was rinsed twice each with 5 mL ethyl acetate, then the cleaned extract was further concentrated to 1 mL under a cold gentle stream of nitrogen. The extract was transferred into a PTFE-capped glass vial and analyzed by liquid injection on a GC–MS.

A SR sampler consisted of three membranes, yielding triplicate samplers each per sampling station. The samplers were also first patted dry with lint-free tissue, then extracted twice each in 100 mL methanol at room temperature during 12 h and 8 h respectively. The extracts were concentrated to 2 mL on a Turbovap concentration workstation, then 20 mL of ethyl acetate were added and further concentrated to 2 mL. The rest of the procedure then proceeded as with the PES samplers.

3.2.4 Determination of aqueous concentrations

Environmental factors that affect the accumulation of organic chemicals from the aqueous phase onto a passive sampler include temperature and water turbulence [48]. Thus, assuming that the PES calibration experiment was carried out at approximately the field conditions, that is, at a temperature of 23.5 °C and flow velocity of 0.34 m/s, aqueous concentrations were computed by invoking equation 2.18 and using sorbed amounts of the analytes in PES (N_{t}) and R_{s} as discussed in subsection 3.1.4. Aqueous concentrations obtained using SR were calculated from sorbed amounts using equation 2.17. K_{pw} values were obtained from literature [147]. R_{s} were calculated using the non-linear least squares regression and the fractions of remaining PRCs using equation 2.22.

3.2.5 Quality assurance

During all the preparation processes, field deployment and retrieval, duplicate samplers were exposed to air in the vicinity of the working surface. These blanks were extracted and analyzed analogous to the field-exposed samplers. In addition, procedural blanks were also processed similarly but without the samplers. Measured concentrations were blank-corrected where analytes were quantified in blanks.

3.3 Determining HOCs in sediment/porewater

3.3.1 Sediment sampling

At each of the sampling stations, sediments were collected from five points along a transect that was parallel to the deployed passive samplers, by grab sampling using a pre-cleaned stainless steel shovel and container (figure J.1 in appendix). Following the removal of large debris, the sediments were thoroughly mixed to a homogeneous blend from which sub-samples were collected and stored in pre-cleaned brown glass bottles and capped with teflon lids that were lined with aluminium foil. The bottles were transported in ice boxes at 4 °C to the laboratory in Kenya and stored at −20 °C. The sediments were also transported at 4 °C to the laboratory in Germany, and likewise stored at −20 °C until extraction. Before storage, a portion of the wet sediments were air-dried in a fume cupboard to constant weight.

3.3.2 Determining sediment characteristics

Debris was removed from air–dried sediments using a 2 mm sieve, and then the sieved sediments were divided to 10 g portions. Dry matter content was determined by drying sediment portions at 105 °C in a moisture analyzer. Organic carbon was determined semi-quantitatively, in triplicate, through destruction of a sediment portion with hydrogen peroxide followed by drying at 105 °C to constant weight, cooling in a desiccator and measurement of the weight. Weight loss defined the percentage organic carbon content. Soil texture, namely, fractions of silt, clay and sand was determined by sieving method. Details of these procedures are given in appendix J.1.

3.3.3 Extraction of sediment samples for analysis of HOCs

Extractions of sediment samples was done by accelerated solvent extraction (ASE) (Dionex, Sunnyvale, CA). 2 g and 1 g respectively of pre-cleaned florisil and copper were placed in a cellulose thimble that was inside a 22 mL stainless steel extraction cell in that order. 10 g of air–dried sediments were mixed with hydromatrix and added to the thimble, then 1 mL of a solution containing phenanthrene–d10 and PCB 104 (1 µg/L in isopropanol) was added to the mixture and left to dry. Any extra space was filled up with hydromatrix to capacity, then the cell was covered with a cellulose filter before closing with the stainless steel cap. The samples were prepared in duplicate per sampling station. In addition, blanks without sediments were also prepared as controls. The sample cells were then placed on the carousel of an ASE 200 system. Extractions were done using hexane–acetone (1:1, v/v) mixture. The extraction conditions were as follows: 2 extraction cycles at 1500 psi system pressure, 100 °C oven temperature, 5 min preheat time and a static period of 5 min. The extracts were flushed out at 60% cell volume for 120 s using pressurized nitrogen to yield ≈ 30 mL solution. The extracts were concentrated to 1 mL under a cold stream of nitrogen, then they were analyzed by GC–MS.

3.3.4 Determining porewater concentrations using PES

Then 10 g each of homogenized wet and air-dried sediments were weighed out into 30 mL glass bottles. 20 mL of bidistilled water containing sodium azide (0.2 g/L) and a clean PES strip (1.6 cm by 5 cm) were added to each bottle. This dimension of PES strips was chosen to ensure that sorbed amounts were quantifiable and also to ensure non–depletion of compounds from porewater medium (see appendix J.2). The bottles were capped with teflon lids lined on the inside with aluminium foil and shaken at 90 rpm on a horizontal shaker, at room temperature in the dark. Duplicate

samples each were used for air-dried and wet sediments. In addition, blank samples without sediments were also prepared. The experiment was set up in a two-step time series mode lasting 30 d and 54 d. These time steps were chosen to reflect the normal field sampling duration in surface water and approximately double this time to ensure attainment of equilibrium. At the elapse of each experiment duration, the strips were taken out and dried with lint-free tissue. The strips were extracted and analyzed following the procedure outlined in section 3.2.3 and appendix section C.

3.4 Input data for the sediment model

The code for the Sediment Model version 2.00 (see section L.2 of the appendix) was obtained and re-written in Excel to enable adjustments where applicable [27]. Water and sediment concentrations and total organic carbon (TOC) were determined as described in sections 3.3.4, 3.3.3 and 3.3.2 respectively, then the values were used to calculate organic carbon partition coefficients (K_{oc}). Organic matter partition coefficient, K_{om} was calculated as a product of K_{oc} and the mass fraction of organic matter in sediments (TOM). TOM was estimated from TOC values as $\mathbf{TOM}\,(\%) = 1.803\,\mathbf{TOC} + 1.135$ [66]. Total suspended solids (TSS) in water were determined gravimetrically by sieving 500 mL water sample through a pre–cleaned and weighed 0.45 µm glass fiber filter (Pall Corporation). The filter was dried overnight at 105 °C and thereafter cooled and weighed again. The concentration of TSS in water was calculated in mg/L as a quotient of the differences in filter weight measurements and the water volume. Chemical concentration in TSS was estimated using equation 2.28 and freely dissolved C_{w} determined using SR, and experimental K_{oc} and TOC. Total water concentrations were a sum of freely dissolved and TSS concentrations. Other input data were determined in the field or using estimation models/equations or obtained from literature. A summary of the specific parameters and data sources are given in table L.1 of the appendix.

Chapter 4

Results and Discussion

4.1 Laboratory determined key properties of PES

4.1.1 Uptake of HOCs from the aqueous phase into PES

Sorption potential of PES for HOCs is demonstrated in the uptake curves as shown in figure 4.1. Further data is available in section D of the appendix. The uptake of BBP and most PAHs (figure 4.1, left) remained in the linear range up to 10–12 d. Maximum sorbed concentrations were recorded at these sampling times before they slightly reduced or remained fairly constant in subsequent days. For the rest of the compounds, uptake generally remained in the linear range for the complete experimental duration (figure 4.1, right). Hence, it seems that in PES, some compounds attain apparent equilibrium faster than others. Vermeirssen et al. [165] established similar linear plots for diazinon and diuron during a 32–day experimental duration but other compounds (deisopropylatrazine and benzotriazole) reached equilibrium within 5–8 days. The term apparent equilibrium is used here since true equilibrium may not necessarily have been achieved. Non–achievement of equilibrium for most

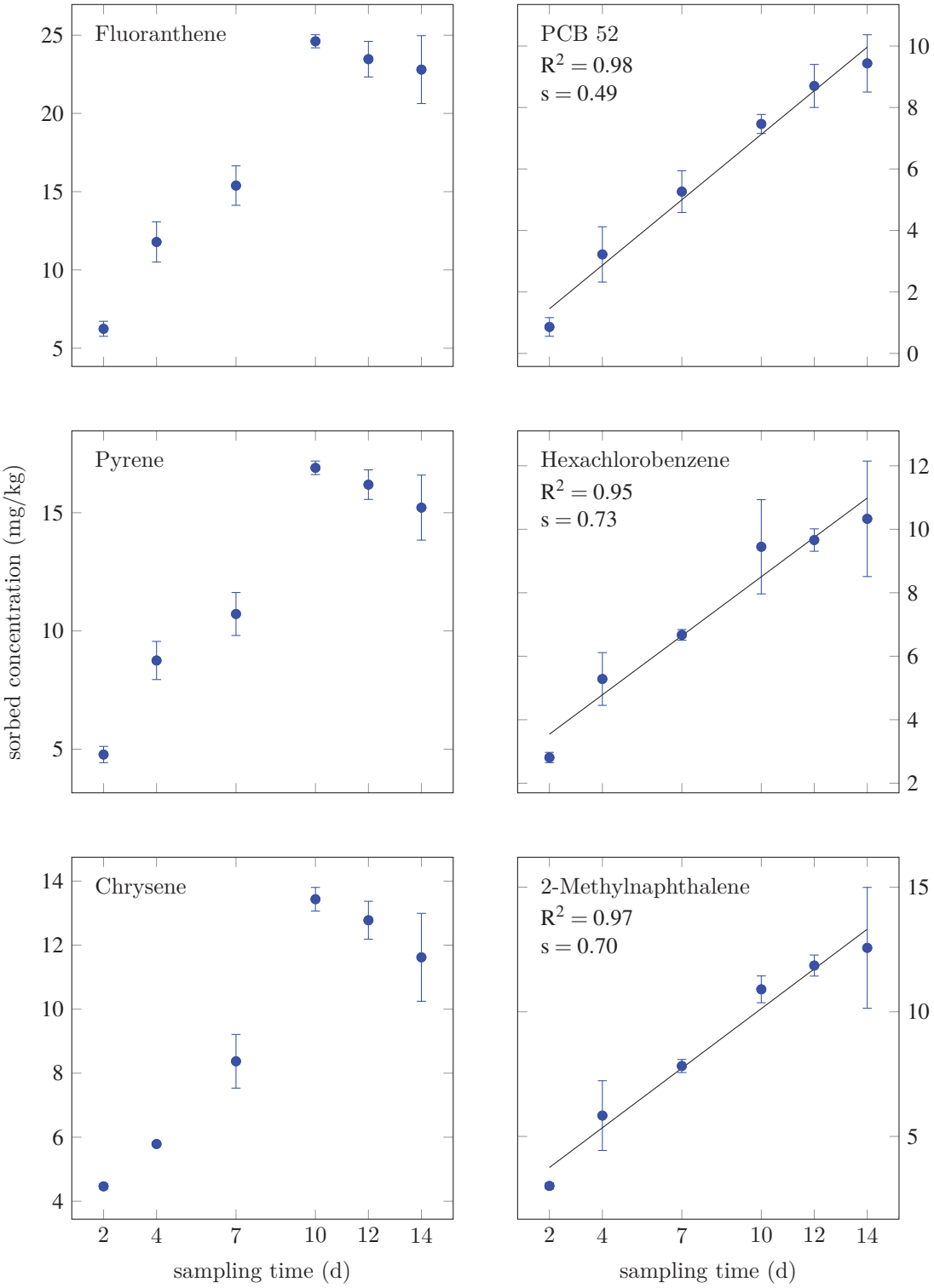

Figure 4.1: Uptake curves for some HOCs that attained apparent equilibrium (left) and those that remained in the linear phase for the whole experimental duration (right). • represents the mean of measured concentrations, and error bars represent the standard deviation from the mean (n=2, n=4 at day 7).

compounds can be explained by the diffusion process in the porous membrane. Considering the structure of PES (figure 2.4) and its sorption mechanisms as highlighted in section 2.3.7, it is possible that for some compounds, uptake during the first few days is a simultaneous sorption to dissolution sites (amorphous regions) and the condensed glassy phases (hole–filling process). Sorption to dissolution sites is faster owing to the higher diffusion coefficients, but as these regions fill up, sorption is slowed down in the condensed phases due to lower diffusivities in these regions, and this phenomenon may give an impression of equilibrium attainment. Glassy polymers generally have lower diffusion coefficients than rubbery polymers with the ratio $D_{\text{rubbery}}/D_{\text{glassy}}$ ranging from 10^2 to 10^8 and increases with penetrant diameter [134]. Indeed, nuclear magnetic resonance (NMR) studies of $^{13}CO_2$ sorption in glassy polystyrene and polycarbonate polymers showed that jumps between dissolution sites had 1000-fold greater diffusion coefficients and 2-fold lower activation energies than jumps between holes/pores [179]. This means that jumps/diffusion through condensed regions/pores is a slower process. The occurrence of diffusion in the condensed regions (intraparticle diffusion) of PES membrane will be demonstrated further on, and since it is a slow process, this explains the linearity of uptake curves (figure 4.1) and the delay in establishment of equilibrium. Thus, uptake of HOCs to PES within the experimental duration that also falls within the range of a typical field deployment will generally be kinetic (see figure 2.2).

Given the heterogeneity of pore sizes (figure 2.4), movement of the compounds from the filled–up surface sorption sites to the mesopores or micropores may be slower due to steric hindrance at the void opening [179]. If this is true, then is seems to affect mainly the PAHs (figure 4.1, left) and not the PCBs, chlorinated HOCs and substituted PAHs (figure 4.1, right). For instance, the uptake curves for PCBs 28 and 52 (LeBas molar volumes = 247.3 and 268.2 cm^3/mol, respectively) were linear while those of benzo[a]anthracene and benzo[a]pyrene (LeBas molar volumes = 248.0 and 263.0 cm^3/mol, respectively) showed an initial linear phase followed

by a reduction in the uptake as shown in figure 4.1 (left). It is possible that the molecular length and shape determines the presence/absence of steric hindrance at the pore openings, so that PAHs with bended structures consisting of three or more fused rings experience difficulty penetrating the pores (see structures in section A of the appendix). Thus, sorption of PAHs, especially the high molecular weight, may be limited to the surface and as the sorption sites get filled, then uptake is reduced. This observation is supported by the fact that sorbed amounts of PAHs generally decreased with increase in molecular weight (see data in section D of the appendix), which is attributable to steric exclusion. In principle, the rates of chemical uptake (k_{u}) and release (k_{e}) should be fairly equivalent at equilibrium so that the uptake curve at this stage is generally flattened as shown in figure 2.2. The downward curvature of the uptake curves at apparent equilibrium (figure 4.1, left) can be explained by slowed uptake due to intraparticle diffusion, in addition to the non–uniform uptake and elimination rates as will be discussed in section 4.1.2.

As also observed by Vermeirssen et al. [165], uptake of most compounds remained in the linear phase (figure 4.1, right). These observations indicate that PES probably has a high sorptive capacity for the HOCs resulting in high partition coefficients, in which case true equilibrium may not be attained within the practical time scale of an experimental set–up [21]. The sorption capacity of PES was not investigated in this study and remains an open question for further research. However, a high sorption capacity is plausible considering the occurrence of both dissolution and high–energy hole/pore sorption sites, unlike rubbery polymers that mostly comprise only the dissolution sites. This observation has been demonstrated in other glassy polymers, for instance, where PVC had a higher partition coefficient for toluene (K_{pw}=809.2 L/µg) than the rubbery PE (K_{pw}=70.7–123.1 L/µg) [134]. High sorptive capacity of PES implies equilibration may take longer than two weeks, probably months or years. This is possible given that equilibration of HOCs in rubbery (absorptive) polymers like SR and LDPE that have higher diffusion coefficients than

glassy polymers, may take several weeks to years depending on the hydrophobicity of the HOCs [23, 130].

The PES membrane used in this study is considered polar due to the presence of a polar additive (polyethylene glycol) and O–containing moieties in PES structure. In line with the general principle "like dissolves like", it is expected that hydrophobic compounds will preferably not sorb to the PES–polyethylene glycol blend. However, the results of this study (figure 4.1) show the contrary, which further shows that for sorption to polymers, the concept "like dissolves like" is not always mechanistically operative [50]. This observation can be attributed to the spatial arrangement of sorption domains in PES membrane, and the degree of cross–linking [50]. Given that PES backbone is essentially hydrophobic (contact angle = 56°), it is possible that the polar moieties are masked in the interior, leaving the non–polar groups (benzene rings) exposed outside to water, to act as sorption sites for the HOCs [50, 65]. If these O–containing groups were exposed outside, they would interact with water molecules through hydrogen bonding leading to the formation of water clusters that would reduce the accessibility of HOCs to the sorption domains and compete with them for sorption sites, thereby reducing their sorption [50].

If the spatial arrangement of sorption domains holds as discussed above, then uptake may also be favoured by a compatible sorbate/sorbent system due to similarity in solubility parameters. For example, the dispersion (δ_d), polar (δ_p), and hydrogen–bonding (δ_h) terms of the Hansen solubility parameters (δ_{Ha} in $MPa^{1/2}$) for PES are 19.6, 10.8, and 9.2, respectively. These parameters are similar to those of DDT (20.0, 5.5, 3.1), BBP (19.0, 11.2, 3.1), naphthalene (19.2, 2.0, 5.9), phenanthrene (20.8, 2.6, 5.4), and hexachlorobenzene (21.9, 2.1, 0.0), and the HOC/PES interaction is expected to be dominated by dispersion forces [52].

Additionally, the rigid cross–linked structure of PES creates a large surface area

and abundant pores and sorption sites (figure 2.4). The narrow pores offer multiple contact points within the PES matrix for the sorbate, leading to heightened sorption energies such that at low-phase concentrations, HOCs sorb favourably to these high energy sites since they have strong affinity for the compounds [134, 138].

To elucidate the mechanisms that control the uptake process for HOCs in PES, further uptake curves were drawn using the intraparticle diffusion model equations 2.23 (figure 4.2a) and 2.24 (figure 4.2b). Generally, the logarithmic form of equation 2.24 yielded better linear fits ($R^2 = 0.81 - 1.00$) than equation 2.23 ($R^2 = 0.70 - 1.00$). Table 4.1 shows other regression parameters. At the first instance, the general linearity of the uptake curves indicates that accumulation of the compounds in PES is intraparticle diffusion controlled. Whether this is the only limiting process or not can be elucidated by considering the values of the y–intercept (C) in equation 2.23 and slopes (m) in equation 2.24. As already mentioned in section 2.3.7, the following conclusions can be made from the value of C: positive values imply rapid sorption in the short–term, negative values a retardation in the intraparticle diffusion, and $C = 0$ implies that sorption is controlled by intraparticle diffusion. On the other hand, $m = 1.0$ implies first–order kinetics control the sorption process, $0.5 < m < 0.8$ implies both first–order kinetics and intraparticle diffusion are involved, and $m = 0.5$ implies intraparticle diffusion is the only rate–limiting process [17].

None of the linear plots drawn using equation 2.23 passed through the origin and C values ranged from 3.23 to -5.24 (table 4.1). Using equation 2.24, the slope of the regression line (m values) had a mean value of 0.64 ± 0.24 and were in the range $0.5 < m < 0.8$ for most compounds with their C values being significantly different from zero ($p < 0.002$). This shows that for these compounds, both intraparticle diffusion and first order uptake kinetics control sorption to PES. The extent to which either of the processes controls the accumulation of a chemical is not known.

Table 4.1: Regression parameters for uptake curves drawn using the intraparticle diffusion equations 2.23 and 2.24

Compound name	Regression parameters							
	Equation 2.23 [16]				Equation 2.24 [17]			
	k_{id}	C	R^2	s	m	log k_{id}	R^2	s
Naphthalene	2.08	1.12	0.79	1.08	0.48	3.41	0.83	0.08
Acenaphthylene	3.87	-1.85	0.99	0.42	0.66	3.36	0.99	0.03
Acenaphthene	3.07	-0.96	0.98	0.49	0.62	3.33	0.97	0.04
Phenanthrene	9.18	-5.24	0.95	2.04	0.68	3.69	0.98	0.04
Anthracene	3.08	-0.65	0.96	0.62	0.54	3.42	0.97	0.03
Fluoranthene	7.96	-4.41	0.92	2.43	0.70	3.61	0.96	0.05
Pyrene	5.08	-1.82	0.89	1.76	0.64	3.52	0.94	0.06
Benz[a]anthracene	3.55	3.23	0.72	2.23	0.37	3.79	0.81	0.06
Chrysene	3.90	-1.27	0.86	1.57	0.59	3.45	0.92	0.06
Benzo[b]fluoranthene	7.63	-0.54	0.70	5.02	0.53	3.83	0.82	0.09
Benzo[k]fluoranthene	3.85	-0.15	0.81	1.85	0.50	3.58	0.86	0.07
Benzo[a]pyrene	1.34	0.88	0.75	0.76	0.39	3.31	0.84	0.06
Indeno[1,2,3-cd]pyrene	1.95	0.58	0.75	1.14	0.46	3.37	0.85	0.07
Benzo[ghi]perylene	1.61	-2.26	0.90	0.54	1.63	1.79	0.96	0.13
2-Methylnaphthalene	4.19	-2.79	0.99	0.39	0.73	3.28	0.99	0.03
2,7-Dimethylnaphthalene	4.13	-3.25	0.99	0.44	0.78	3.21	0.99	0.02
Hexachlorobenzene	3.27	-1.59	0.98	0.48	0.66	3.28	0.98	0.04
Methoxychlor	3.51	0.70	0.86	1.42	0.50	3.58	0.89	0.06
PCB 28	4.85	-2.64	0.99	0.53	0.64	3.46	0.99	0.02
PCB 52	3.72	-4.36	1.00	0.17	1.19	2.67	0.96	0.09
PCB 101	4.63	-2.17	1.00	0.25	0.63	3.46	1.00	0.01
PCB 138	3.87	-1.78	0.95	0.90	0.63	3.39	0.97	0.04
PCB 153	3.64	-1.75	0.99	0.43	0.65	3.34	0.99	0.02
PCB 180	3.65	-1.72	0.94	0.91	0.65	3.34	0.95	0.05
o,p´-DDE	4.47	-1.98	0.99	0.33	0.63	3.45	1.00	0.01
p,p´-DDE	5.29	-2.63	1.00	0.36	0.65	3.50	1.00	0.01
o,p´-DDD	4.29	-1.48	0.98	0.54	0.60	3.48	0.99	0.02
p,p´-DDD	2.56	-1.30	0.95	0.59	0.65	3.18	0.98	0.04
o,p´-DDT	2.78	-1.08	0.96	0.53	0.61	3.28	0.98	0.03
p,p´-DDT	5.73	-3.10	0.95	1.31	0.67	3.50	0.98	0.04
BBP	0.99	0.81	0.79	0.51	0.44	3.17	0.84	0.07

k_{id} is in $\mu g/g \cdot d^{1/2}$ in equation 2.23 or $ng/g \cdot d^{m}$ in equation 2.24, s= standard error.

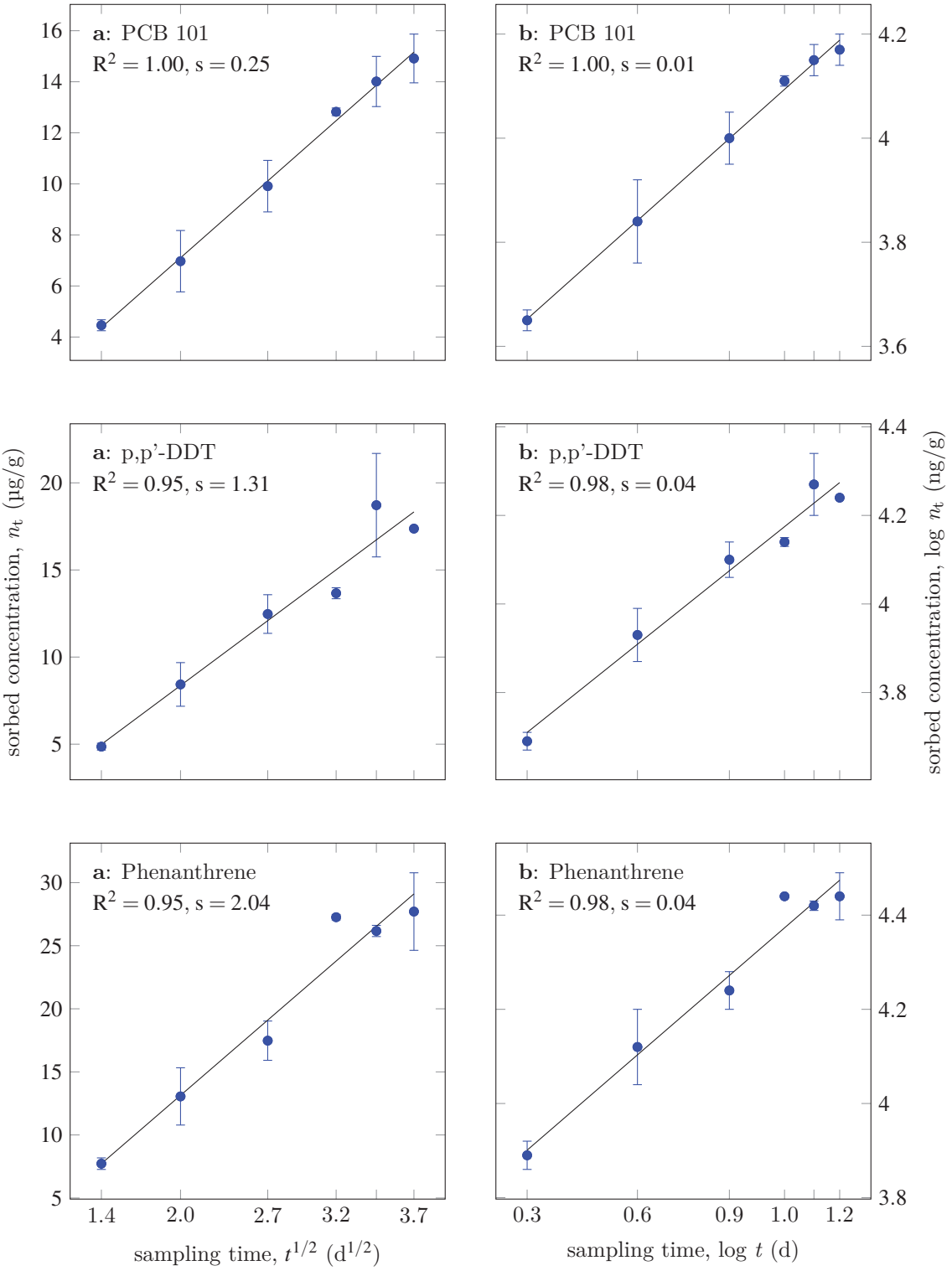

Figure 4.2: Uptake curves for some HOCs drawn using the intraparticle diffusion equations 2.23 (figure **a**) and 2.24 (figure **b**). • represents the mean of measured concentrations, and error bars represent the standard deviation from the mean (n=2).

For a few compounds however, $m \leq 0.5$ and their C values were not significantly different from zero ($p > 0.002$) indicating that for these compounds, intraparticle diffusion step is the limiting process.

Besides intraparticle diffusion, other factors such as molecular weight, shape and size, and chemical interaction with the membrane may also be involved in the uptake process. Using equation 2.24, k_{id} values for PCBs showed a slight progressive decrease down the homologous series (mean $k_{id} = 2.52 \pm 0.35\,\mu g/g \cdot d^m$, $m = 0.64 \pm 0.01$), with the exception of PCB 52 ($k_{id} = 0.47\,\mu g/g \cdot d^m$, $m = 1.19$). Thus, intraparticle diffusion of PCBs decreases slightly with molecular weight and degree of chlorination. The anomaly with PCB 52 is not yet clear as it cannot be linked to planarity or degree of chlorine substitution, given the pattern in k_{id} values for the other members of the homologous series. Given that $m \approx 1$ for PCB 52, it can be concluded that its uptake follows first–order kinetics, and may be limited to the amorphous regions.

For PAHs, k_{id} values showed greater variation (mean $k_{id} = 3.09 \pm 1.72\,\mu g/g \cdot d^m$, $m = 0.64 \pm 0.29$), especially for isomers, for instance phenanthrene ($k_{id} = 4.90\,\mu g/g \cdot d^m$, $m = 0.68$) versus anthracene ($k_{id} = 2.63\,\mu g/g \cdot d^m$, $m = 0.54$). and benz[a]anthracene ($k_{id} = 6.17\,\mu g/g \cdot d^m$, $m = 0.37$) versus chrysene ($k_{id} = 2.82\,\mu g/g \cdot d^m$, $m = 0.59$). This observation shows a possible role of the molecular shape and size in uptake process contributing to a phenomenon like steric hindrance, such that sorption is limited to the surface for larger molecular weight PAHs.

Generally, k_{id} values for all compounds were in the range $0.87 < k_{id} < 9.18\,\mu g/g \cdot d^{1/2}$ (equation 2.23) and $0.06 < k_{id} < 6.76\,\mu g/g \cdot d^m$ (equation 2.24) and showed no specific pattern down homologous series. Furthermore, excluding two outliers on the basis of their m values (benzo[ghi]perylene and PCB 52), no correlation ($R^2 = 0.01$) was found between log k_{id} values and logs of K_{ow} (slope=0.02) or molar masses (slope=-

0.04) (figure 4.3). No correlation ($R^2 = 0.00$) was also found between log k_{id} and log LeBas molar volume (slope=-0.03). This indicates that chemical uptake in PES is generally non-specific and may only be limited by the modes of interaction of the specific chemical with the membrane.

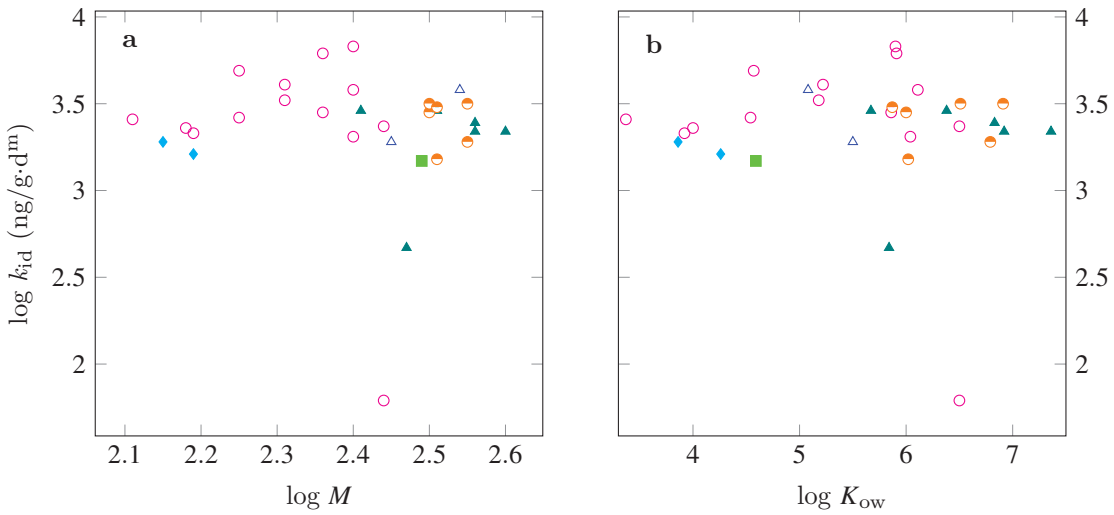

Figure 4.3: Relationship between k_{id} and (a) molar masses, and (b) K_{ow} for PAHs (○), methylated naphthalenes (♦), PCBs (▲), DDXs (◓), pesticides (△), and BBP (■).

4.1.2 The anisotropy of uptake and elimination curves

Elimination curves were plotted using the amount of analytes remaining in spiked PES strips following desorption over time. As shown in figure 4.4 below and table E.2 in the appendix, PES shows a greater affinity for the compounds since the amounts desorbed were insignificant ($p > 0.05$). Between 3–19% of initial amounts (C_0) were desorbed for all compounds except alpha–HCH and heptachlor at 31% and 30%, respectively. The possible causes of this observation are discussed below.

Figure 4.5 shows typical examples of sorption and desorption curves for individual compounds in PES membrane (figures 4.5a–d), and sorption of a compound against the desorption of an analogous PRC (figure 4.5e). The sorption and desorption

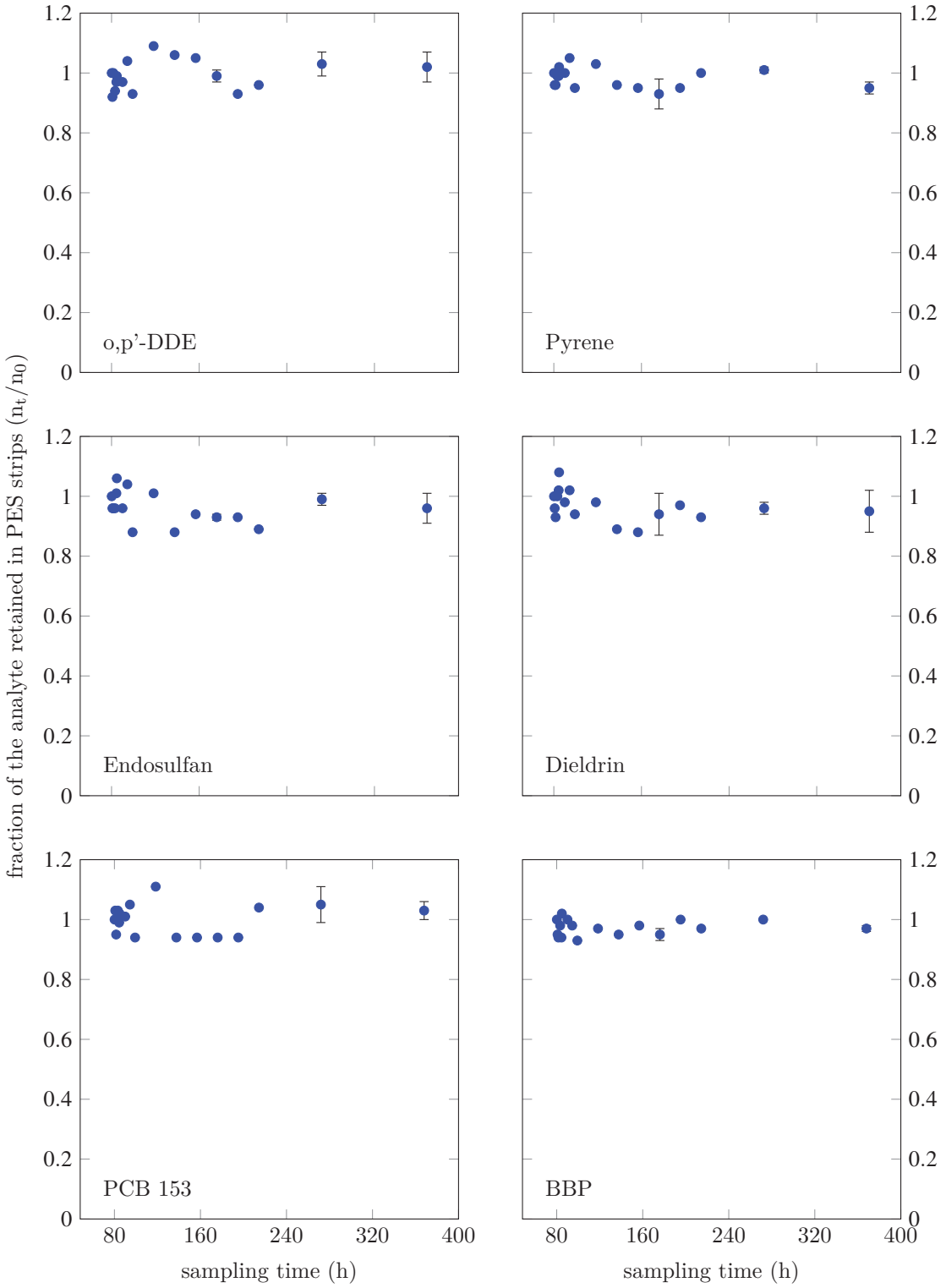

Figure 4.4: Elimination curves for some compounds. • represents measured amounts, and error bars represent the standard deviation from the mean (n=2). n_t is the remaining amount at time t, and n_0 is the amount in spiked PES at time t=0.

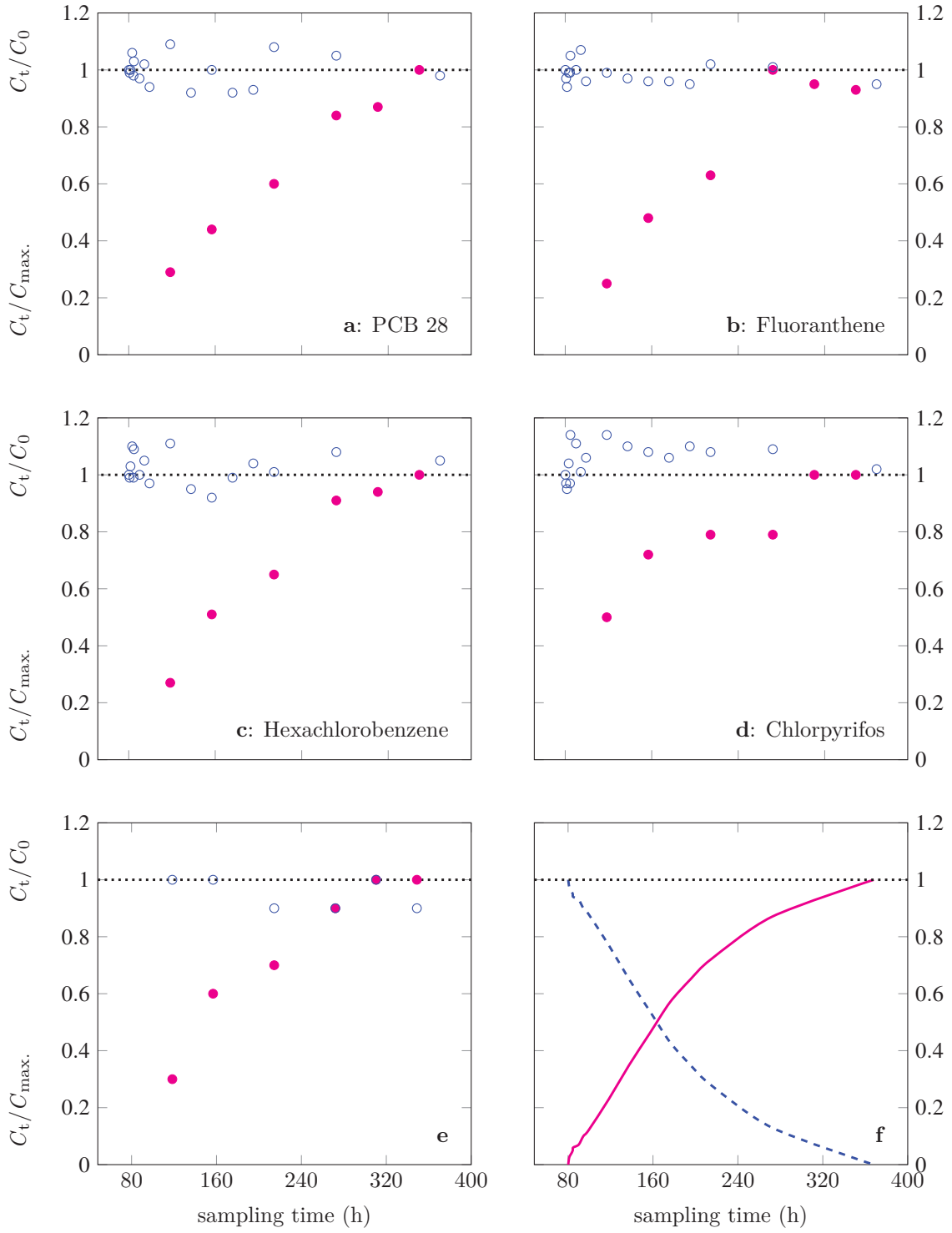

Figure 4.5: Plots of uptake (•) versus release (○) of compounds against time. The plot **e** shows the uptake of acenaphthene versus release of acenaphthene-d_{10}. The plot **f** is the expected uptake (——) and release (- - -) curves for an isotropic exchange. C_o and $C_{max.}$ are the initial and maximum measured concentrations respectively, and C_t is the concentration at time t.

curves clearly demonstrate anisotropy. That is, under the experimental conditions, the sorption curve does not mirror the desorption one as would be expected in an isotropic exchange (figure 4.5f). Figure 4.5f shows sorption reversibility that is a typical for rubbery polymers, for instance silicone rubber [132]. Sorption/desorption reversibility occurs because of the flexible amorphous domains, which together with their spatial arrangement and the degree of cross–linking, gives silicones a suitable configuration that allows high diffusivity of hydrophobic organic compounds [130]. This allows a chemical to diffuse through it, in a partitioning process, yielding sorption/desorption isotropy as shown in figure 4.5f.

The sorption/desorption anisotropy displayed by PES membrane (figures 4.5a–e) suggests a departure from the partitioning process for organic compounds exhibited by rubbery polymers. Indeed, intraparticle diffusion of HOCs in PES was demonstrated in the previous section 4.1.1 that is attributed to its porous nature. As previously discussed, the structure of PES creates conditions that favour its uptake of compounds from the aqueous phase (figures 4.1). However, these same conditions may be unfavourable for their release (figure 4.4), at least within the experimental duration, leading to anisotropic sorption/desorption curves (figure 4.5). This observation suggests that the mechanistic pathways for sorption and desorption are different, that is, these processes may occur to/from different microenvironments [3]. This situation may be due to a much reduced relaxation speed of polymer chains owing to the rigidity of the polymer structure, in contrast to the flexible chains of silicone rubber, resulting in slow diffusion of the HOCs [134].

In view of the porous nature of PES, the differences in the uptake and elimination curves (figure 4.5) could also be attributed to, among other factors, i) capillary condensation in the nanovoids where the sorbing molecules become entrapped within the pores such that desorption from these sites is generally unfavourable and therefore slow, and/or ii) pore deformation/reorganization by the sorbates that leads to

different physical pathways for sorption and desorption [59, 86, 158]. The different pathways occur when sorbate molecules force the expansion of pores creating a new internal surface area within the PES matrix such that on desorption, a lag can exist between sorbate molecules leaving the pores and relaxation of the surrounding matrix to its original state [86]. Lu and Pignatello [86] also attributed pore deformation in soil organic matter and a resultant upward shift in the sorption isotherm to a conditioning effect caused by a chemical agent other than the test compound. The conditioning effect has also been demonstrated in glassy polymers, whose uptake mechanisms for HOCs have been found to be similar to those of SOM [24, 64]. In this case, the conditioning agent can be solvents that are used for pre–cleaning to remove impurities. The conditioning effect results when sorption of the agent causes plasticization (an induced change in the thermal and mechanical properties of the glassy polymer making it more flexible) of the glassy polymer causing it to change to rubbery state such that the holes disappear. This leads to an increase in the diffusion coefficient and enhanced sorption due to increasing segmental mobility of polymer chains. Following removal of the conditioning agent, additional high–energy sorption sites are created which also enhances the sorption capacity.

In their experiment, Lu and Pignatello [86] noted that in addition to an upward shift in the sorption isotherm for the conditioned SOM relative to the non–conditioned, non–linearity was also enhanced, which was attributed to the increase in porosity. In the current study, PES was pre–cleaned using ethylacetate and methanol. Whether this process resulted in plasticization is not reflected in the results, given the linearity of uptake curves for most compounds (figures 4.1, right, and 4.2).

Plasticization by water is also possible, especially for hydrophilic polymers, where the process is a function of temperature [52]. Schult and Paul [138] observed hysteresis between the sorption and desorption of water (at 40 °C) by PES and attributed it to plasticization of the polymer by water molecules. However, the extent of the

plasticization, and for the different PES blends has not yet been well researched.

4.1.3 Experimental sampling rates

R_s was estimated by linear regression using all or part of N_t data that approached linearity in the uptake curve and equation 2.18, where C_w was the average water concentration during the experimental duration. Estimated R_s values given in table 4.2 ranged from 1.15 L/d (methoxychlor) to 12.88 L/d (chrysene). Figure 4.6 is a plot of log R_s against logs of K_{ow} and molar masses. Estimated R_s had poor correlation to both K_{ow} ($\log R_s = 0.02 \log K_{ow} + 0.54$, $R^2 = 0.00$) and molar mass ($\log R_s = -0.26 \log M + 1.25$, $R^2 = 0.02$). Thus, K_{ow} and molar masses are unsuitable for predicting sampling rates.

Except for the hydrophilic additives that are grafted in to improve wetting properties and reduce membrane biofouling, PES backbone is essentially hydrophobic (contact angle 56°) [65, 183]. Consequently, it is expected that hydrophobic interactions would primarily contribute to its uptake of HOCs from the aqueous phase. However, given the poor correlation between K_{ow} and sampling rates, it can be concluded that hydrophobicity does not play a significant role in the uptake process. The poor correlation between R_s for the HOCs and their K_{ow} indicates that hydrophobic interactions are not the primal mechanism governing the uptake of HOCs from the aqueous phase onto PES and can therefore not fully explain the uptake mechanisms. It is possible that besides the hydrophobic effect and intraparticle diffusion, other interactive mechanisms such as $\pi - \pi$ interactions between the aromatic rings of the HOCs and PES and hydrogen bonding through the polar sulfonyl groups are involved in the uptake process.

Chen et al. [31] proposed that non–hydrophobic interactions can be elucidated by first normalizing aqueous concentrations using n-hexadecane–water partition

Table 4.2: Sampling rates of HOCs and other chemical properties

Compound name	Molar mass (g/mol)	log K_{ow}	V_{LeBas} (cm^3/mol)	R_s (L/d)
Naphthalene	128.8	3.37	147.6	2.23 ± 0.88
Acenaphthylene	151.4	4.00	165.7	2.72 ± 0.49
Acenaphthene	154.9	3.92	173.0	2.48 ± 0.54
Phenanthrene	177.8	4.57	199.0	5.36 ± 1.12
Anthracene	177.8	4.54	197.0	6.12 ± 1.14
Fluoranthene	204.2	5.22	217.0	8.14 ± 1.66
Pyrene	204.2	5.18	214.0	6.23 ± 1.34
Benz[a]anthracene	229.1	5.91	248.0	8.45 ± 2.90
Chrysene	229.1	5.86	251.0	12.79 ± 2.73
Benzo[b]fluoranthene	251.2	5.90	268.9	11.58 ± 2.80
Benzo[k]fluoranthene	251.2	6.11	268.9	4.10 ± 1.04
Benzo[a]pyrene	251.2	6.04	263.0	4.94 ± 1.26
Indeno[1,2,3-cd]pyrene	275.4	6.50	283.5	4.26 ± 1.11
Benzo[ghi]perylene	275.4	6.50	277.0	1.61 ± 0.48
2-Methylnaphthalene	141.3	3.86	169.8	4.66 ± 0.88
2,7-Dimethylnaphthalene	154.9	4.26	192.0	6.17 ± 1.03
PCB 28	257.0	5.67	247.3	5.56 ± 0.81
PCB 52	295.1	5.84	268.2	3.54 ± 0.51
PCB 101	323.6	6.38	289.1	4.42 ± 0.67
PCB 138	363.1	6.83	310.0	5.23 ± 1.05
PCB 153	363.1	6.92	310.0	5.00 ± 0.84
PCB180	398.1	7.36	330.9	4.30 ± 0.89
o,p'-DDE	316.2	6.00	305.2	4.93 ± 0.89
p,p'-DDE	316.2	6.51	305.2	6.52 ± 1.07
o,p'-DDD	323.6	5.87	312.6	3.90 ± 0.79
p,p'-DDD	323.6	6.02	312.6	2.42 ± 0.66
o,p-DDT	354.8	6.79	333.5	1.66 ± 0.38
p,p'-DDT	354.8	6.91	333.5	3.07 ± 0.72
Hexachlorobenzene	281.8	5.50	221.4	3.47 ± 0.78
Methoxychlor	346.7	5.08	354.3	1.15 ± 0.46
Butyl benzyl phthalate	312.4	4.59	384.2	0.24 ± 0.11

Errors represent the standard deviation from the mean. R_s values are for 14 cm^2.

coefficients as:

$$C_{\mathrm{hd}} = C_{\mathrm{w}} K_{\mathrm{hdw}} \tag{4.1}$$

where K_{hdw} is the n-hexadecane–water partition coefficient, and is selected because as an inert reference phase, it has a methylene structure that cannot take part in other interactions such as hydrogen bonding and electron donor–acceptor interactions. K_{hdw} values were estimated using linear free energy relationships (LFER) and are available in section G of the appendix. C_{hd} represents the concentration of a compound in n-hexadecane that would be in equilibrium with the observed aqueous concentration (C_{w}). Such normalization enables the free energy contribution of the solvent to the sorption process to be eliminated so that the direct interactions between sorbates and PES can be elucidated. Equation 4.1 was substituted into equation 2.18 to yield an equation for normalized sampling rates as:

$$N_{\mathrm{t}} = \frac{R_{\mathrm{s}}}{K_{\mathrm{hdw}}} \cdot C_{\mathrm{hd}} \cdot t \tag{4.2}$$

Plots of normalized sampling rates ($R_{\mathrm{s,norm.}}$) against molar masses and diffusivity in water are given in figure 4.7. In figure 4.7a, plots of normalized uptake rates for

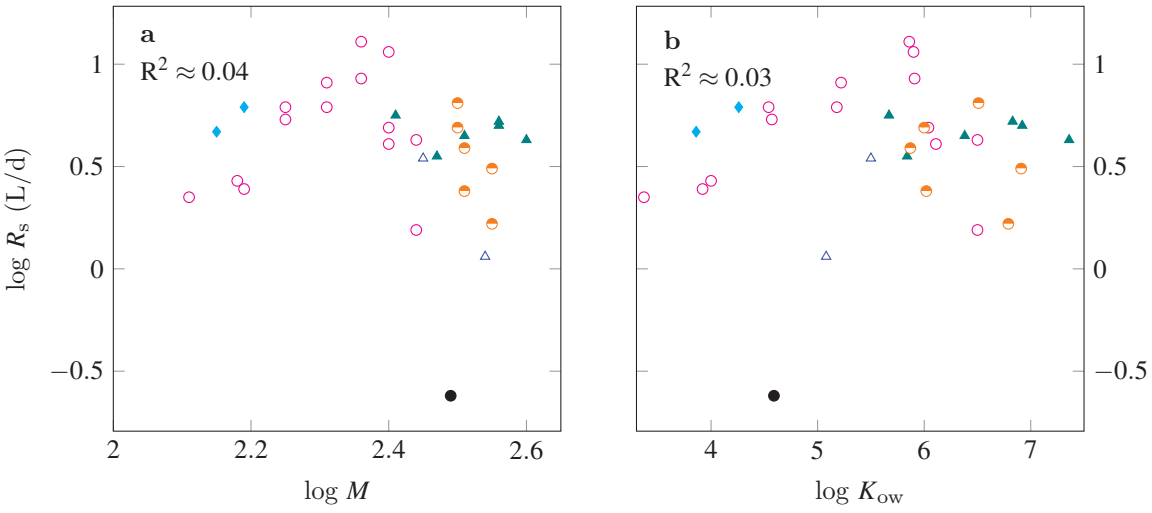

Figure 4.6: Log-log relationship between R_{s} of HOCs onto PES and their (a) molar mass and (b) K_{ow} for PAHs (○), methylated naphthalenes (♦), PCBs (▲), DDXs (◓), pesticides (△) and BBP (⊗).

29 compounds were indistinguishable, implying that their uptake mechanisms are broadly similar. Generally, $R_{\text{s,norm.}}$ correlated linearly with logs of molar masses ($y = -9.04x + 16.43$, $\mathrm{R}^2 = 0.93$, $\mathrm{s} = 0.35$, $\mathrm{n} = 29$). Specifically, uptake for PAHs was best fitted using a second order polynomial ($y = -29.63x^2 + 126.11x - 137.38$, $\mathrm{R}^2 = 0.95$, $\mathrm{n} = 16$). The downward curvature in plots for PAHs at higher molar mass suggests the occurrence of resistance to sorption in PES due to the size and shape of the molecule. This observation further suggests the role of pores and pore diffusion in the uptake process so that large molecules probably undergo steric hindrance, and their sorption is effectively restricted to surface. This observation was also made when considering intraparticle diffusion as discussed in section 4.1.1. The issue of possible steric hindrance does not occur with PCBs since $R_{\text{s,norm.}}$ decreased strictly with increasing mass ($y = -10.44x + 20.06$, $\mathrm{R}^2 = 0.99$, $\mathrm{n} = 6$). It was also observed in section 4.1.1 that their intraparticle diffusion coefficients generally decreased with increasing molar mass. Uptake curves for DDXs had a poorer linear fit ($y = -15.46x + 32.53$, $\mathrm{R}^2 = 0.48$, $\mathrm{n} = 6$). Two compounds (methoxychlor and BBP) had log $R_{\text{s,norm.}}$–log M fits that were distinguishable from the rest, implying their

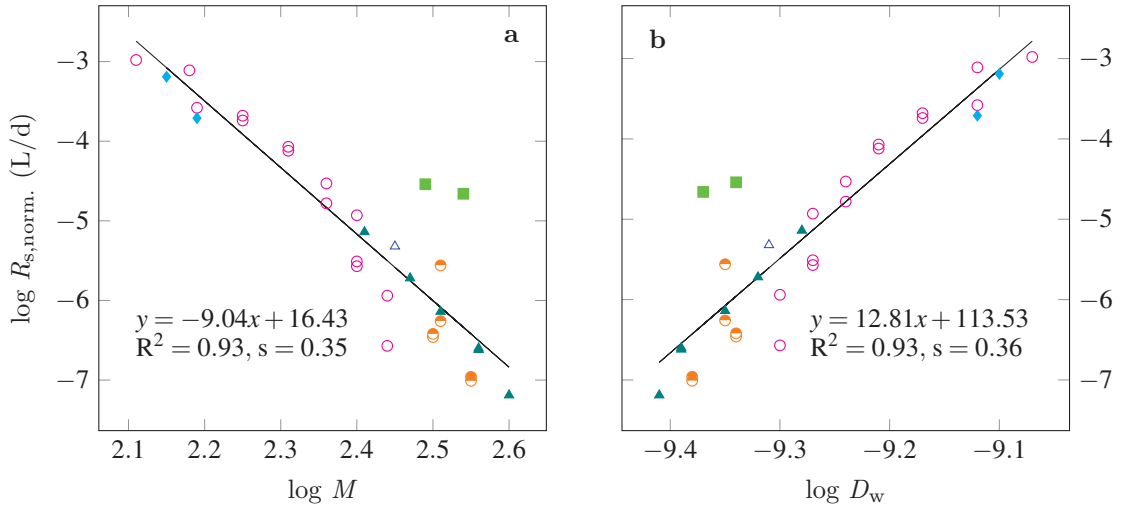

Figure 4.7: Log-log relationship between $R_{\text{s,norm.}}$ and (a) molar mass, and (b) diffusivity for PAHs (○), methylated naphthalenes (♦), PCBs (▲), DDXs (◓), hexachlorobenzene (△), and outliers (methoxychlor and BBP) (■). D_{w} was calculated using the equation by Schwarzenbach et al. [140] (see appendix I.5).

uptake mechanisms differ from that of the other compounds. This is possible since unlike the other compounds, they have O–containing moieties in their structures (see section A in the appendix) that may participate in hydrogen bonding with PES. Figure 4.7b shows plots of log $R_{s,norm.}$ against log D_w, and this plot mirrors that of log $R_{s,norm.}$–log M in figure 4.7a. This observation is plausible since diffusivity in water varies inversely with molar mass, so a lower diffusivity is expected at higher molar mass, and vice versa.

Similarity in scatter plots in figures 4.7a and 4.7b portrays a general pattern in the uptake mechanisms for the compounds. With reference to figure 4.7, $R_{s,norm.}$ decreases with increase in molar mass, which shows the role of mass/size in the uptake process. The uptake mechanism for most compounds may involve an initial (ad)sorption on PES surface through $\pi - \pi$–bonding followed by intraparticle diffusion as already discussed in section 4.1.1, where the latter process is rate limiting [118].

4.1.4 Apparent PES–water partition coefficients

Vermeirssen et al. [165] carried out a 7.5 d equilibration experiment to determine partition coefficients of some organic compounds to PES, and also a 32 d flow through experiment using Chemcatcher and POCIS to estimate K_{pw} in PES that was used to cover these PSDs. In the latter experiment, K_{pw} was estimated by modelling data from the PES membranes that were removed at 6 d and 32 d, where K_{pw} was determined using uptake and elimination rates. Uptake of most compounds in PES remained fairly in the linear range for the complete 32 d experimental duration. Empirical K_{pw} values from the equilibration experiment (calculated using equation 2.5) and those modeled from the 6 d and 32 d flow–through experiment fitted fairly well onto the 1:1 line indicating that data from the equilibrium experiment and those modelled from the 6 d flow–through experiment, though still in the linear

uptake range, did not yield significant differences in K_{pw} values.

Thus in this study, apparent K_{pw} for the analytes were similarly calculated using equation 2.5, where C_p and C_w represented the maximum sorbed concentrations and average water concentrations recorded during the experimental period, respectively. K_{pw} could not be calculated using uptake and elimination rates as described by equation 2.20, since release of spiked compounds or PRCs was slow as already discussed in section 4.1.2. The calculated apparent log K_{pw} values are shown in table 4.3, and ranged from 5.55 L/kg for BBP to 7.03 L/kg for chrysene. Average log K_{pw} for these 31 compounds was 6.58 L/kg with an average standard deviation of 0.29 log units. Excluding BBP, average log K_{pw} values for the remaining 30 compounds was 6.62 L/kg $\pm$ 0.23 log units. These observations indicate that log K_{pw} values of the compounds were not significantly different from each other. Given the low standard deviation in log K_{pw} for all compounds, it can be concluded that PES is a non–selective sampler for these compounds. Generally, PES yielded apparent partition coefficients that are higher than those recorded for LDPE and SR [147]. This finding is valid since glassy polymers have higher sorptive capacity than rubbery polymers as already discussed. Saquing et al. [134] also made a similar finding, where glassy PVC had a higher partition coefficient for toluene (K_{pw}=809.2 L/µg) than the rubbery PE (K_{pw}=70.7–123.1 L/µg).

In the absence of experimental values, predictive models are often formulated by empirical correlation of K_{pw} for the analytes to their K_{ow}, assuming that hydrophobic interactions and therefore a partitioning process dominates the uptake process from the aqueous phase. In such a case and assuming equilibrium, K_{pw} can be predicted from K_{ow} or sometimes the molar mass (M) of the HOCs by plotting the parameters on a 2–dimensional logarithmic scale. Accordingly, strong linear correlations have been established between K_{pw} of HOCs to various PSDs and their K_{ow}, for instance, SR ($\mathbf{R^2 = 0.97, 0.94}$) [147, 180] and polyethylene ($\mathbf{R^2 = 0.89}$) [2].

Table 4.3: Apparent K_{pw} values, k_o, k_{ex} and R_s for HOCs.

Compound name	Molar mass (g/mol)	log K_{ow}	log K_{pw} (L/kg)	k_{ex} (1/d)	R_s (L/d)	$1/k_o$ (m^2 d/L)
Naphthalene	128.8	3.37	6.37 ± 0.02	0.2275	2.23 ± 0.88	6.27E-04
Acenaphthylene	151.4	4.00	6.43 ± 0.06	0.1873	2.72 ± 0.49	5.14E-04
Acenaphthene	154.9	3.92	6.41 ± 0.07	0.2070	2.48 ± 0.54	5.65E-04
Phenanthrene	177.8	4.57	6.71 ± 0.05	0.1878	5.36 ± 1.12	2.61E-04
Anthracene	177.8	4.54	6.82 ± 0.04	0.1965	6.12 ± 1.14	2.29E-04
Fluoranthene	204.2	5.22	6.81 ± 0.01	0.1835	8.14 ± 1.66	1.72E-04
Pyrene	204.2	5.18	6.72 ± 0.01	0.1906	6.23 ± 1.34	2.25E-04
Benz[a]anthracene	229.1	5.91	6.98 ± 0.02	0.2070	8.45 ± 2.90	1.66E-04
Chrysene	229.1	5.86	7.03 ± 0.01	0.1800	12.79 ± 2.73	1.09E-04
Benzo[b]fluoranthene	251.2	5.90	6.99 ± 0.02	0.1702	11.58 ± 2.80	1.21E-04
Benzo[k]fluoranthene	251.2	6.11	6.56 ± 0.08	0.1847	4.10 ± 1.04	3.41E-04
Benzo[a]pyrene	251.2	6.04	6.69 ± 0.06	0.2150	4.94 ± 1.26	2.84E-04
Indeno[1,2,3-cd]pyrene	275.4	6.50	6.60 ± 0.09	0.1849	4.26 ± 1.11	3.29E-04
Benzo[ghi]perylene	275.4	6.50	6.09 ± 0.09	0.1167	1.61 ± 0.48	8.98E-04
2-Methylnaphthalene	141.3	3.86	6.64 ± 0.08	0.1722	4.66 ± 0.88	3.01E-04
2,7-Dimethylnaphthalene	154.9	4.26	6.75 ± 0.08	0.1632	6.17 ± 1.03	2.27E-04
PCB 28	257.0	5.67	6.75 ± 0.05	0.1616	5.56 ± 0.81	2.52E-04
PCB 52	295.1	5.84	6.45 ± 0.04	0.1402	3.54 ± 0.51	3.95E-04
PCB 101	323.6	6.38	6.65 ± 0.03	0.1807	4.42 ± 0.67	3.17E-04
PCB 138	363.1	6.83	6.73 ± 0.02	0.1735	5.23 ± 1.05	2.68E-04

Continued on next page

Table 4.3 Continued from previous page

Compound name	Molar mass (g/mol)	log K_{ow}	log K_{pw} (L/kg)	k_{ex} (1/d)	R_s (L/d)	$1/k_o$ (m^2 d/L)
PCB 153	363.1	6.92	6.69 ± 0.03	0.1927	5.00 ± 0.84	2.80E-04
PCB180	398.1	7.36	6.65 ± 0.03	0.1708	4.30 ± 0.89	3.26E-04
o,p'-DDE	316.2	6.00	6.70 ± 0.02	0.1887	4.93 ± 0.89	2.84E-04
p,p'-DDE	316.2	6.51	6.81 ± 0.02	0.1829	6.52 ± 1.07	2.15E-04
o,p'-DDD	323.6	5.87	6.61 ± 0.06	0.1910	3.90 ± 0.79	3.59E-04
p,p'-DDD	323.6	6.02	6.40 ± 0.09	0.1625	2.42 ± 0.66	5.80E-04
o,p-DDT	354.8	6.79	6.25 ± 0.06	0.1755	1.66 ± 0.38	8.41E-04
p,p'-DDT	354.8	6.91	6.50 ± 0.07	0.1639	3.07 ± 0.72	4.57E-04
Hexachlorobenzene	281.8	5.50	6.54 ± 0.08	0.1864	3.47 ± 0.78	4.04E-04
Methoxychlor	346.7	5.08	6.17 ± 0.05	0.2107	1.15 ± 0.46	1.21E-03
Butyl benzyl phthalate	312.4	4.59	5.55 ± 0.02	0.2552	0.24 ± 0.11	5.93E-03

Log K_{ow} values were obtained from the references [147], [149] and [153]; R_s values were calculated using 14 cm^2 PES strip. Errors represent the standard deviation from the mean.

Given the hydrophobic nature of PES backbone (contact angle 56°), it is expected that hydrophobic interactions would primarily contribute to its uptake of HOCs from the aqueous phase [65, 183]. However, this study could not verify an explicit correlation between K_{pw} for HOCs and their respective K_{ow} and molar masses as depicted in figure 4.8 and as a result, the relation is deemed not sufficiently for use in prediction.

The poor correlation between K_{pw} for the HOCs and their K_{ow} indicates that hydrophobic interactions are not the primal mechanism governing the uptake of HOCs from the aqueous phase onto PES and can therefore not fully explain the uptake mechanisms. Hitherto comparative literature values for the compounds are non-existent. However, literature K_{pw} values for other compounds yielded a similarly poor correlation (figure 4.9) to log K_{ow} and molar mass. As with sampling rates, the poor correlation can be attributed to other interactive mechanisms such as $\pi - \pi$ interactions and hydrogen bonding.

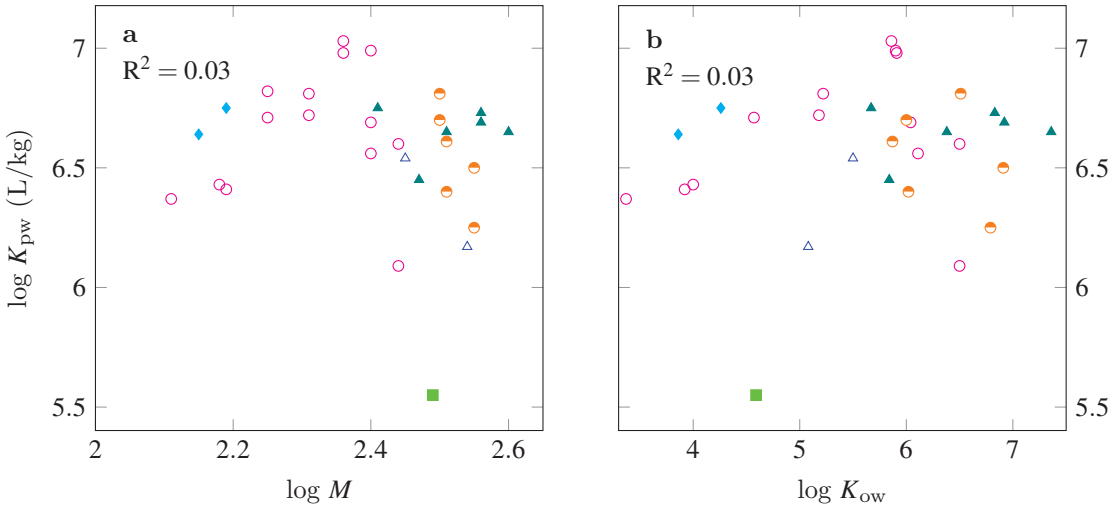

Figure 4.8: Log-log relationship between K_{pw} of HOCs and their (a) molar masses and (b) K_{ow} for PAHs (○), methylated naphthalenes (♦), PCBs (▲), DDTs (◓), pesticides (△), and BBP (■).

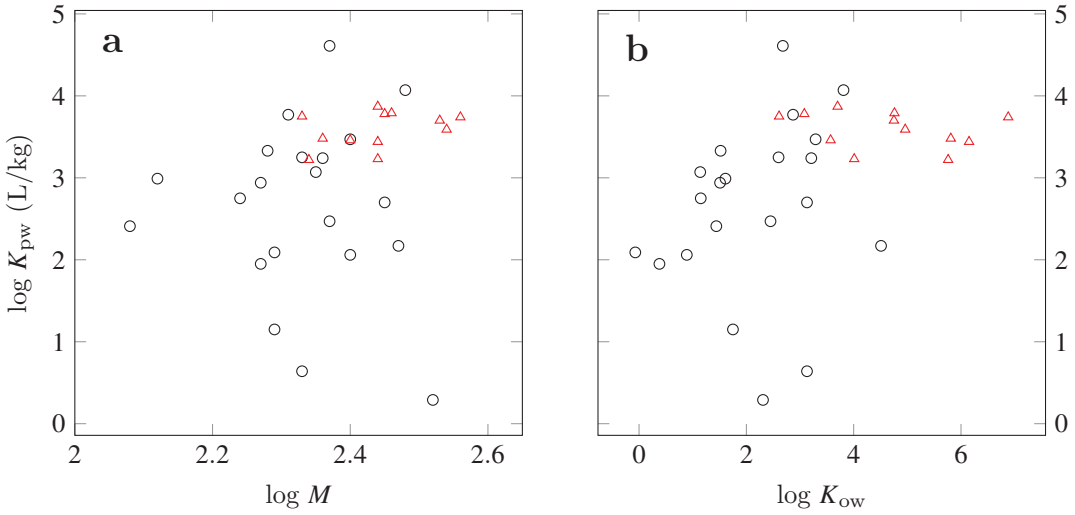

Figure 4.9: Relationship between K_{pw} of some compounds and their (a) molar masses and (b) K_{ow} on a log scale. Data was taken from Vermeirssen et al. [165] (○) and Prieto et al. [123] (△).

4.1.5 Insufficent PRC release from PES

Application of PRCs to determine *in situ* sampling rates of compounds is only possible when the uptake rates of compounds and the dissipation rates of analogous PRCs exhibit isotropy [168]. In this case, plotting the accumulation of a compound on a PSD and the dissipation of an analogous PRC should result in a symmetrical uptake-release curve as shown in figure 4.5f [132]. PRCs desorption data was taken during the respective sampling days of the calibration experiment and an example of a typical plot of the uptake of compounds and PRCs dissipation from PES is given in figure 4.5e. Only 8% of spiked acenaphthene-d10 was dissipated. In general, 0–20% of all the PRCs were dissipated during the 14 d experimental duration (see section H of the appendix). Desorption of PRCs from the same PES sampler used in the calibration experiment was also tested under field conditions in the Saale river, Germany for a duration of 30 d. Results showed that $< 20\%$ of the original amounts dissipated in 64% of the spiked PRCs. The range of amounts desorbed for all the PRCs was 6–35% of the original. As already discussed in previous sections, a

number of intrinsic PES properties may favour its uptake of compounds, for example, possible plasticization in the presence of water, orientation of the O–containing moieties, and presence of nanovoids and/or unrelaxed free volume regions. Indeed PES was shown to contain voids in its structure at an average diameter of 200 nm (see figures 2.4 and 4.16). While some of the aforementioned PES properties may favour its uptake of compounds from the aqueous phase, they might also hinder its release of the compounds. The anisotropy observed with PRCs can be explained by drawing analogy from sorption–desorption hysteresis reported in natural organic matter and other glassy polymers [87, 118].

Pignatello and Xing [118] attributed the phenomenon to the activation energy of sorptive bonds and mass transfer limitations. These authors attribute the hysteresis to three factors: differences in the kinetic energy for sorption and desorption especially for large molecules that may interact simultaneously at multiple points and become difficult to desorb, steric hindrance to desorption owing to the shape of pores, and a cooperative change in the polymer material induced by the sorbing compound. Pre–existence of cavities (pores) that can accommodate incoming sorbates may endear the pores as preferred sorption sites [87]. Inside the pores, sorbates may bind to multiple sites causing constriction that causes a lag in desorption or they may cause an irreversible pore deformation [109]. It is also possible that pores expand by the thermal motion of incoming sorbates, creating new internal surface area in the solid so that on desorption, a lag can exist between the exit of sorbates from pores and relaxation of the surrounding matrix to its original state [86]. Furthermore, it is possible that adsorption is involved in the uptake process, and this involving strong bonds, is difficult to dissociate.

Hence, it can be concluded that the exchange kinetics between compounds and analogous PRCs in PES exhibits anisotropy. The anisotropy observed in this study implies PRCs are generally unsuitable for determination of *in situ* sampling rates of

PES and alternative procedures have to be employed.

4.1.6 Quality assurance

Sampling using PES was found to be repeatable since the CV of 95% of all analysis from duplicate samples ranged from 0–19% which can be considered acceptable. The rest had CV of 20–35% but this represented only 5% of the total samples and cannot significantly influence the whole outcome. In addition, there was no significant variation in the sorption process and therefore in the aqueous concentrations during the complete experiment given that the CV of all compounds from the 7 d sampling time of the first and last halves of the experiment was 2–15%.

Only a few compounds were detected in blanks but at concentrations below the limits of quantitation except for naphthalene (99 ng/PES) and 2-methylnaphthalene (32 ng/PES). Given that uptake remained largely in the linear phase and that sorption and desorption may not occur simultaneously as seen in the case of PRCs, the blank values for these compounds were subtracted from measured concentrations.

4.2 Field application of PES and SR

4.2.1 Brief overview

Triplicate PES and SR strips were prepared and deployed in parallel at two stations along Sosiani river, Kenya for a duration of 30 d after which the PSDs were retrieved and extracted. The extracts were analysed by GC-MS for OCPs, PAHs, PCBs and phthalates (DBP, DEHP, BBP). The aim was to assess the field applicability of the two samplers under tropical conditions and also to compare their performance in sorption of HOCs.

4.2.2 Range of compounds sorbed by the samplers

Of the target compound groups, only PAHs and phthalates were detected. Specifically, the 2–4–ringed members and benzo[b+k]fluoranthene were detected in quantifiable amounts by PES, benzo[a]pyrene was below the limit of quantitation, and the 6–ringed members were not detected. 2 to 5–ringed PAHs were detected by SR while the 6–ringed members were not quantifiable. Dibenz[a,h]anthracene, PCBs, DDXs, methoxychlor and hexachlorobenzene were not detected at all by both PSDs. Lack of detection of these compounds is possibly due to their absence in the water phase since they could be sampled by PES as described in the calibration experiment (section 4.1.1) and have been sampled in other fresh water environments using silicone rubber [124]. All the target phthalates were detected by both samplers.

Noteworthy is that non-target screening using the Agilent deconvolution reporting software of PES extracts positively identified (AMDIS match factor > 85) other compounds including pesticides (diazinon, chlorpyrifos and pirimiphos-methyl) encompassing a log K_{ow} range of 3.8–5.0, implying PES can be applied to other compounds with different physicochemical properties. Indeed PES has been found to sorb the pesticides atrazine, diazinon and diuron (log K_{ow} = 2.60–3.81) [159, 165], herbicides (log K_{ow} = 2.21–3.45) [122] and several polar and non-polar chemicals ranging from caffeine to octocrylene (log K_{ow} = -0.07–6.88) [123].

However, the aforementioned studies were carried out in either laboratory or simulated environments. PES is usually applied in the POCIS as a sorbent retainer and diffusion rate limiter [8]. Field deployments of PES as an independent sorbent are rare, and one such application established its uptake of galaxolide, tonalide and 4-tert-octylphenol from wastewater effluent [120]. Passive sampling is mainly a field application technique, hence this research further added to the field applicability of PES and for compounds that have not been investigated before by this sorbent.

On the other hand, silicone rubber has been used to monitor OCPs, PAHs and PCBs in surface water [9, 35]. Wide applications of SR in environmental monitoring stems from its robustness and also because key properties determining uptake of the aforementioned HOCs are well established [132, 147]. The range of chemicals that can be sampled by SR are not limited to the mentioned HOCs, but can be extended to other compounds such as phthalates and alkylated PAHs as was done in this study. However, there are no literature values of uptake rates and partition coefficients of phthalates to SR. Determination of these parameters was outside the scope of this study and therefore environmental concentrations, as will be discussed in the next sections, are reported as sorbed and not freely dissolved values.

4.2.3 Freely dissolved concentrations determined using SR

Solving equation 2.17 for the determination of aqueous concentrations requires knowledge of sorbed amounts, K_{pw} and R_{s} values. Field-determined R_{s} are more reliable as this parameter is affected by environmental factors including temperature, flow rates and biofouling [23]. Where applicable, PRCs have been recommended for correction of the environmental variabilities and to allow for the determination of *in situ* R_{s} [4, 62]. Accordingly, PRCs have been used during field deployment of SR [6, 101] and were likewise used in this study. Visual inspection of the membranes upon retrieval did not reveal any damages or excess biofouling (see figure I.1 in the appendix). The PRC data were used to calculate R_{s} and C_{w} of analytes in an excel spreadsheet using the procedure described by Smedes and Booij [146]. An example of the spreadsheet calculation for one sampler is given in section I.1 of the appendix.

Following exposure of SR membranes, even the PRC with the lowest molecular weight or K_{ow} (acenaphthene-d10) could be quantified (see table I.1 as an example) suggesting low transfer kinetics during the exposure duration. PRC recoveries ranged from 5.5% (acenaphthene-d10) to 88.1% (PCB 54) in station 1 and 3.3%

(acenaphthene-d10) to 100% (perylene-d12) in station 2. In the latter case however, fractions were slightly above one and were therefore fixed to unity.

The parameter B in equation 2.22 was obtained by fitting all the fractions of remaining PRCs as a function of $\log(K_{pw}M^{0.47})$ by unweighted non-linear least squares estimation [146]. This approximation procedure is insensitive to outliers and therefore all data can be used regardless of the level of dissipation. Examples of the outcome are given in figure 4.10, and an example of the auxiliary data supporting these figures is shown in table I.2 of the appendix. B was then used to calculate the $R_{s,300}$ of a hypothetical compound with molar mass 300 g/mol. The relative standard deviation of PRC–derived $R_{s,300}$ for the hypothetical compound was 1.2% and 5.9% ($n = 3$ each) in sampling stations 1 and 2, respectively. The calculated $R_{s,300}$ of the hypothetical compound was then used to estimate R_s of target analytes, and the results are given in table 4.5. R_s values of all compounds from station 1 were approximately 2.3–fold higher than those from station 2. This constant ratio in sampling rates for all compounds originated from a similar ratio of the associated B values, namely 692 and 306 in stations 1 and 2, respectively. Sampling rates for

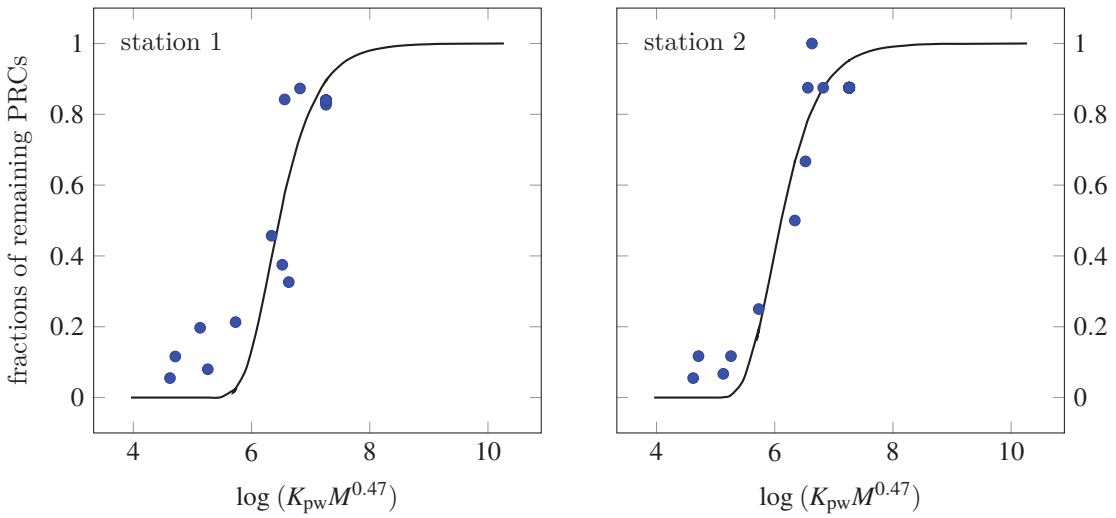

Figure 4.10: Plots of fractions of remaining PRCs in SR against $\log(K_{pw}M^{0.47})$. — represents the model fit and • the measured fractions of retained PRCs.

compounds were calculated as:

$$R_{\mathrm{s,\,analyte}} = R_{\mathrm{s,300}} \times \left(\frac{300}{M}\right)^{0.47} \tag{4.3}$$

Where

$$R_{\mathrm{s,300}} = \frac{B}{300^{0.47}} \tag{4.4}$$

Hence, given that the value in brackets in equation 4.3 is always constant for a particular compound regardless of the sampling site, sampling rates will therefore only differ with the value of $R_{\mathrm{s,300}}$ for the hypothetical compound and therefore B. B is a proportionality constant that combines all factors associated with hydrodynamic conditions and sampler geometry [132]. Using samplers of uniform geometry in all sampling sites implies that differences in sampling rates between sites would be proportional to the differences in hydrodynamic conditions, mainly the flow rates. Higher flow rates decreases the thickness of the water boundary layer and therefore the mass transfer resistance implying higher sampling rates.

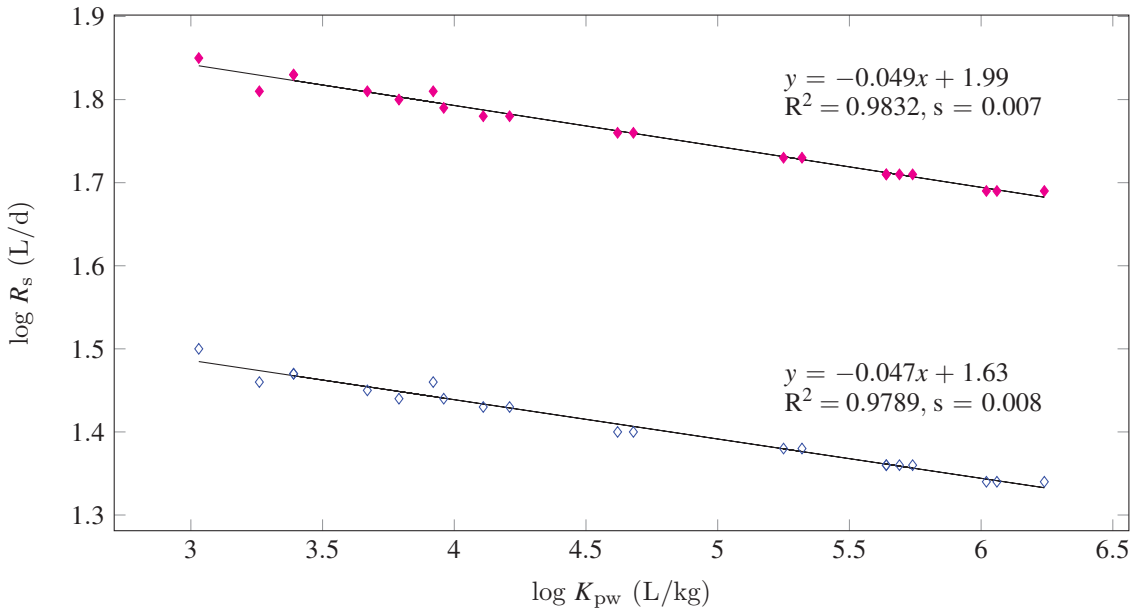

Figure 4.11: A plot of PRC–derived log R_s for PAHs against literature values of log K_{pw} from Smedes et al. [147]. (♦) and (◇) represent data from stations 1 and 2 respectively along Sosiani river.

Figure 4.11 is a plot of log R_s derived from field–dissipated PRCs against log K_{pw} values obtained from literature [147]. Strong linear correlations ($R^2 = 0.98$) were obtained using data from both sampling stations. Slopes of the regression lines were not significantly different from each other ($p > 0.05$) and could therefore be averaged to -0.048. The y–intercept collectively describes the influence of environmental variables such as flow rates and temperature. Given that temperature was fairly constant throughout the sampling period, it is likely that the slightly higher y–intercept value in station 1 (1.99) is attributable to a higher flow rate than in station 2 (1.63). Therefore, representing the y–intercept by $b_\circ$ and using the average slope, R_s could be related to K_{pw} as:

$$R_s = K_{pw}^{-0.048} b_\circ \tag{4.5}$$

Figure 4.12 shows a linear correlation between PRC–derived R_s for PAHs and log K_{ow}. R_s decreased linearly with increasing log K_{ow}. Strong linear correlations

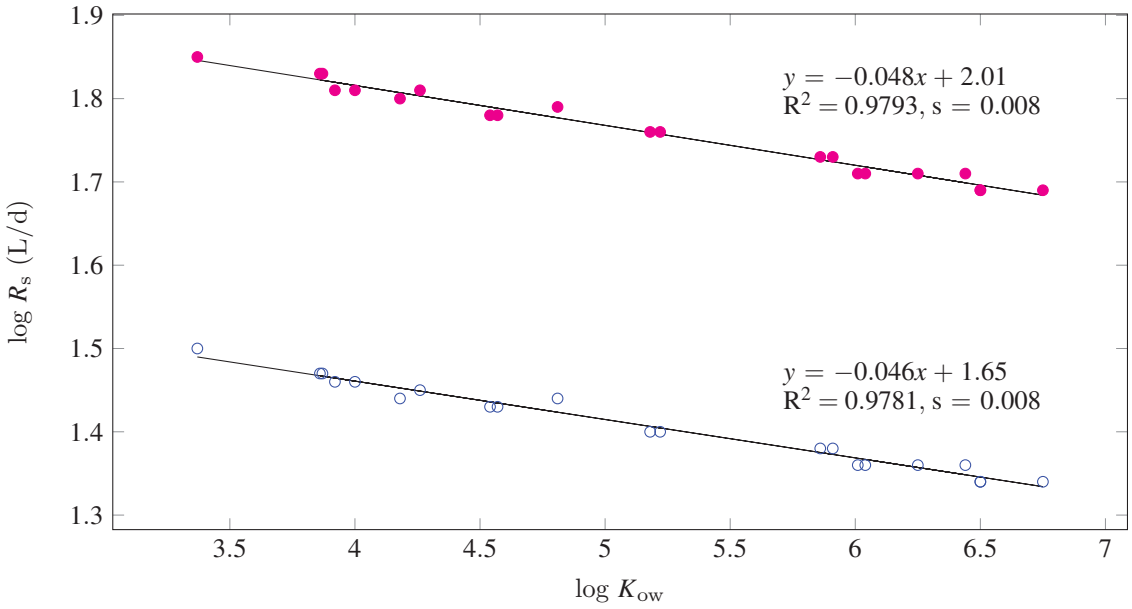

Figure 4.12: A plot of PRC–derived log R_s for PAHs against their log K_{ow} from stations 1 (•) and 2 (○) along Sosiani river. Log K_{ow} values of parent PAHs were obtained from Smedes et al. [147] and those of methylated naphthalenes from the SRC website [149].

($R^2 = 0.98$) were found between log R_s and log K_{ow} from the two sampling stations with no significant difference between slopes ($p > 0.05$). Using an average slope and a representative y–intercept, R_s could be related to K_{ow} as:

$$R_s = K_{ow}^{-0.047} b_\circ \tag{4.6}$$

This relation is similar to that described in equation 4.5 above when relating R_s to K_{pw}. Therefore, for these groups of compounds and in the particular field situation, K_{ow} could serve as a predictor of sampling rates in lieu of K_{pw}. The value -0.047 in equation 4.6 falls in the range of reported literature values ($R_s \approx K_{ow}^{-0.02} - K_{ow}^{-0.08}$) for uptake that is controlled by the water boundary layer [124, 132].

In an assessment of several polymers used in passive sampling, Rusina et al. [131] reported that the transport resistance in silicone membrane, particularly AlteSil, was far less than that in water. That is, from equation 2.10, $\frac{\delta_p}{D_p K_{pw}} << \frac{1}{F {D_w}^{2/3}}$ where $\frac{1}{F {D_w}^{2/3}}$ is the mass transfer resistance in water. This implies that uptake of compounds by silicone rubber is mainly affected by diffusion through the water boundary layer and R_s would therefore vary with D_w, that is:

$$R_s = A F D_w^{2/3} \tag{4.7}$$

where F is a proportionality constant that explains the contribution of hydrodynamic conditions [132]. Experimental D_w values are rare but a number of existing predictive equations can be used. These equations relate D_w to one or more of the following parameters: molecular volume (V), temperature (T), molecular weight (M) and viscosity (μ). Some of the equations are given in section I.5 of the appendix, and figure 4.13 shows plots of log R_s from station 1 against logs of D_ws.

From figure 4.13, the models yielded varied predictions of slopes and only the slope predicted using the equation for D_w provided by Schwarzenbach et al. [140] (page

809) approached the exponent 2/3 in equation 4.7 as stipulated by the hydrodynamic theory. Calculated D_w values varied by a factor of 1.19 to 1.61 between models and decreased from naphthalene to dibenzo[a,h]anthracene by a factor of 1.51 to 2.05. R_s values predicted using equation 4.7 with D_w values from the various models were fitted to field R_s with the unknown parameter F as an adjustable variable. The predicted R_s were plotted against field values, and results of the calculated statistical parameters are given in table 4.4. The best fit was obtained using the equation for D_w by Schwarzenbach et al. [140]. The equation by Worch [176] also performed well. Logs of predicted R_s using D_w values from these two equations were plotted against log K_{ow} and are shown in figure 4.14.

Slopes of the regression lines from the Schwarzenbach et al. [140] relation matched those from field R_s values as already shown in figure 4.12. Slopes produced using

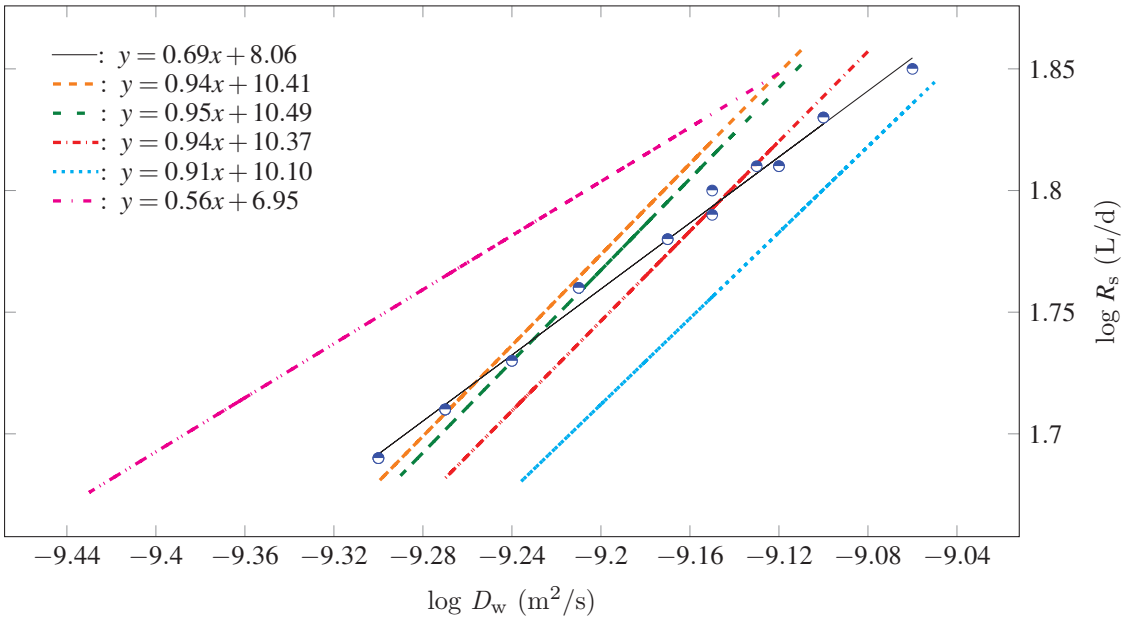

Figure 4.13: A plot of log R_s for station 1 against log D_w determined using various equations: (——) Schwarzenbach et al. [140], (- - -) Othmer and Thakar [106], (- -) Hayduk and Laudie [58], (-·-·-) Chang and Wilke [29], (·····) Worch [176] and (-·-·) Hayduk and Minhas [57]. For illustration, the data points shown were plotted against log D_w determined using the Schwarzenbach equation.

Table 4.4: Statistical parameters resulting from plotting predicted R_s using equation 4.7 against field values

Equation for predicting D_w	slope	intercept	R^2	s
Station 1				
Othmer and Thakar	0.69	17.94	0.9667	0.92
Hayduk and Laudie	0.68	18.62	0.9670	0.90
Chang and Wilke	0.69	17.93	0.9665	0.92
Schwarzenbach et al.	1.01	-0.35	0.9999	0.04
Worch	0.75	14.54	0.9999	0.06
Hayduk and Minhas	1.16	-9.35	0.9677	1.51
Station 2				
Othmer and Thakar	0.70	7.87	0.9677	0.40
Hayduk and Laudie	0.69	8.17	0.9679	0.39
Chang and Wilke	0.70	7.87	0.9675	0.40
Schwarzenbach et al.	1.01	-0.25	0.9999	0.03
Worch	0.76	6.37	0.9999	0.03
Hayduk and Minhas	1.16	-4.26	0.9688	0.66

D_w values from Worch [176] also fell within the range described in literature [124, 132].

Equation 2.17 that takes into account all the uptake phases including linear, equilibrium and pseudo-equilibrium (figure 2.2) was used to calculate C_w using field–determined R_s, sorbed amounts and K_{pw} obtained from literature [147]. This equation is useful in determining aqueous concentrations of compounds that may not reach equilibrium within the sampling duration. Equilibrium status of a PSD can be inferred from the residence time τ (d), that is, the mean length of time that a chemical spends in a PSD, where solute exchange follows first-order kinetics [61]. τ is determined as:

$$\tau = \frac{1}{k_e} \tag{4.8}$$

where k_e (1/d) is the elimination rate. Given that in SR, elimination and uptake

rates are isotropic, τ can also be calculated from R_s and K_{pw} values [61, 132]. Thus, it would take a few hours to years for establishment of equilibrium under the field conditions (see table 4.5).

Calculated C_w values are given in table 4.5. Freely dissolved concentrations ranged from 0.02–25.95 ng/L and were dominated by lower molecular weight members.

4.2.4 Freely dissolved concentrations determined using PES

As described in subsection 4.1.5, PRCs could not be applied to PES. Therefore to minimize the errors introduced when using laboratory results to estimate field values, the calibration experiment as described in subsection 3.1.2 was conducted at field conditions, that is, ≈24.0 °C temperature and 0.34 m/s flow velocity. In addition, field-exposed PES underwent minimal biofouling (see appendix I.2) and

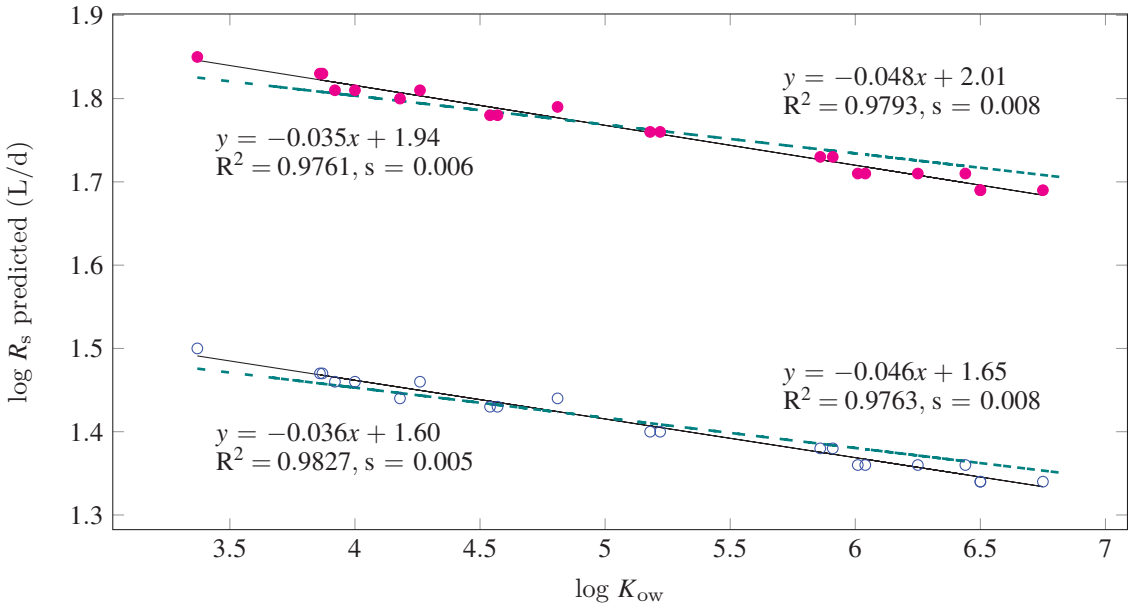

Figure 4.14: Plots of log R_s predicted using equation 4.7 and D_w values derived from (——) Schwarzenbach et al. [140] (equations on the right) and (- -) Worch [176] (equations on the left) against log K_{ow}. • and ○ represent values from stations 1 and 2 respectively.

could not be expected to significantly affect the uptake process. R_s obtained in the calibration experiment, as given in table 4.6, were normalized to the surface area of field-exposed PES strips and then used to calculate C_w at the two sampling stations assuming constant flow velocities. C_w was calculated using the kinetic model (equation 2.18, and the values are given in table 4.6. Similar to C_w determined using SR, detected PAHs were dominated by the lower molecular weight compounds with freely dissolved concentrations ranging from 0.01–1.28 ng/L.

4.2.5 Comparison of sorbed PAHs determined using PES and SR in relation to their properties

Figure 4.15 shows the total sorbed amounts of PAHs from the two sampling stations grouped by the number of rings and normalized to 100 cm^2 of sorbent material. The accumulated 4– and 5–ringed PAHs in the two sorbents were at an approximately 1:1 ratio. The amounts of sorbed 3–ringed, methylated naphthalenes and 2–ringed PAHs in PES were, respectively, 2–, 3– and 4–fold higher than in SR. Hence, PES showed greater sorption for the lower molecular weight PAHs than SR.

PES and SR are structurally different (see figure 4.16) implying the uptake process of HOCs from the aqueous phase into these sorbents may follow different pathways. SR exhibits a uniform non-porous structure that is considered rubbery (T_g = −125 °C) with a flexible and expandable structure [131]. The flexible rubbery chains can move/restructure to create free volume and accommodate compounds during sorption at dilute concentrations. The cavities created on swelling are not permanent, rather they are 'fleeting' and can also relax when releasing the chemical upon desorption. This property, in addition to the non-polar character makes SR have high accessibility and diffusivities for HOCs [22, 126, 131].

In view of this, SR would be the better sorbent for PAHs but the opposite was

Table 4.5: Freely dissolved concentrations of PAHs measured using SR at sampling stations 1 and 2 along Sosiani river

Compound name/parameter	Log K_{pw} [a] (L/kg)	R_s (L/d)		τ (d)		C_w (ng/L)[c]	
		Station 1	Station 2	Station 1	Station 2	Station 1	Station 2
B	-	692	306	-	-	-	-
$R_{s,\ (300)}$ [b]	-	47.4(1.2)	21.0(5.9)	-	-	-	-
Naphthalene	3.37	70.7	31.3	0.3	0.8	16.13 ± 4.30	25.95 ± 9.38
Acenaphtylene	4.00	65.2	28.9	1.6	3.5	6.03 ± 0.32	8.09 ± 1.94
Acenaphthene	3.92	64.8	28.7	1.3	2.9	0.84 ± 0.11	0.92 ± 0.27
Fluorene	4.18	62.6	27.7	2.5	5.6	6.32 ± 0.18	7.84 ± 0.96
Phenanthrene	4.57	60.6	26.8	6.2	14.1	8.60 ± 0.29	10.80 ± 0.41
Anthracene	4.54	60.6	26.8	5.8	13.1	0.65 ± 0.13	0.91 ± 0.01
Fluoranthene	5.22	57.1	25.3	29.5	66.6	1.89 ± 0.07	3.51 ± 0.14
Pyrene	5.18	57.1	25.3	26.9	60.8	1.77 ± 0.06	3.92 ± 0.16
Benzo[a]anthracene	5.91	53.9	23.9	153.2	345.5	0.09 ± 0.01	0.30 ± 0.02
Chrysene	5.86	53.9	23.9	136.6	308.0	0.20 ± 0.01	0.62 ± 0.04
Benzo[b+k]fluoranthene	6.01	51.4	22.8	202.3	456.0	0.07 ± 0.01	0.21 ± 0.02
Benzo[e]pyrene	6.44	51.4	22.8	544.4	1227.3	0.05 ± 0.01	0.13 ± 0.01
Benz[a]pyrene	6.04	51.4	22.8	216.7	488.6	0.02 ± 0.00	0.06 ± 0.01
Perylene	6.25	51.4	22.8	351.5	792.4	< SL	< SL
Indeno[1,2,3-cd]pyrene	6.50	49.3	21.8	651.7	1473.8	< SL	< SL
Dibenzo[a,h]anthracene	6.75	49.1	21.7	1163.6	2632.9	n.d	n.d
Benzo[g,h,i]perylene	6.50	49.3	21.8	651.7	1473.8	< SL	< SL
1-Methylnaphthalene	3.87	67.4	29.8	1.1	2.5	3.50 ± 0.79	5.35 ± 2.88

Continued on next page

Table 4.5 Continued from previous page

Compound name/parameter	Log K_{pw} [a] (L/kg)	R_s (L/d)		τ (d)		C_w (ng/L)[c]	
		Station 1	Station 2	Station 1	Station 2	Station 1	Station 2
2-Methylnaphthalene	3.86	67.4	29.8	1.1	2.5	4.07 ± 0.88	6.20 ± 3.36
2,7-Dimethylnaphthalene	4.26	64.4	28.5	2.9	6.5	3.08 ± 0.38	3.33 ± 1.47
1,6,7-Trimethylnaphthalene	4.81	61.9	27.4	10.6	23.9	4.09 ± 0.27	5.45 ± 1.71

[a]values were obtained from Smedes et al. [147] except for the alkyl naphthalenes which were estimated using the model provided therein; [b]values in brackets represents CV (%, $n = 3$); [c]errors represent the standard deviation from the mean ($n = 3$); n.d, not detected; SL is the TWA sampling limit (see section I.4 of the appendix for details).

Table 4.6: Freely dissolved concentrations of PAHs measured using PES at sampling stations (ST) 1 and 2 along Sosiani river

Compound name	R_s (130 cm^2) (L/d)	C_w (ng/L)[f]	
		ST 1	ST 2
Naphthalene	20.7	0.36 ± 0.10	1.28 ± 0.16
Acenaphthylene	25.3	0.2 ± 0.01	0.44 ± 0.05
Acenaphthene	23.0	0.06 ± 0.00	0.10 ± 0.01
Fluorene[a]	38.7	0.22 ± 0.01	0.42 ± 0.05
Phenanthrene	49.8	0.41 ± 0.02	0.84 ± 0.11
Anthracene	56.9	0.03 ± 0.00	0.05 ± 0.00
Fluoranthene	75.6	0.14 ± 0.01	0.23 ± 0.03
Pyrene	57.8	0.21 ± 0.01	0.31 ± 0.03

Continued on next page

Table 4.6 Continued from previous page

Compound name	R_s (130 cm^2) (L/d)	C_w (ng/L)[f] ST 1	ST 2
Benz[a]anthracene	78.4	0.02 ± 0.00	0.02 ± 0.00
Chrysene	118.7	0.02 ± 0.00	0.03 ± 0.00
Benzo[b+k]fluoranthene	107.6	0.01 ± 0.00	0.01 ± 0.00
Benzo[e]pyrene[b]	45.8	< SL	< SL
Benzo[a]pyrene	45.8	< SL	< SL
Perylene[b]	45.8	< SL	< SL
Indeno[1,2,3-cd]pyrene	39.5	< SL	< SL
Dibenz[a,h]anthracene[c]	27.2	n.d.	n.d.
Benzo[ghi]perylene	15.0	n.d.	n.d.
1-Methylnaphthalene[d]	43.3	0.13 ± 0.00	0.25 ± 0.03
2-Methylnaphthalene	43.3	0.16 ± 0.01	0.25 ± 0.04
2,7-Dimethylnaphthalene	57.3	0.13 ± 0.00	0.16 ± 0.02
1,6,7-Trimethylnaphthalene[e]	50.3	0.10 ± 0.00	0.13 ± 0.02

n.d., not detected; R_s for some compounds were estimated as follows: [a & c]average of values from 3– and 6–ringed members respectively, [b & d]equivalent to that of the isomers benzo[a]pyrene and 2-Methylnaphthalene respectively, [e]average of values of all alkyl naphthalenes; [f]errors represent standard deviations ($n = 3$), concentrations were calculated using the kinetic model (equation 2.18).

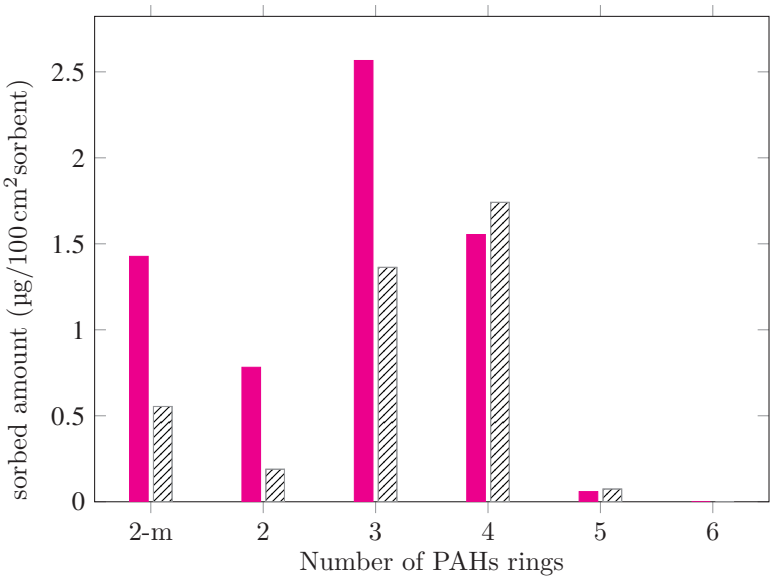

Figure 4.15: A comparison of sorbed concentrations of PAHs sampled at the two stations using PES ( ) and SR ( ). Bars represent the total sum of sorbed concentrations from the two stations grouped by the number of PAH rings. 2-m represents methyl naphthalenes.

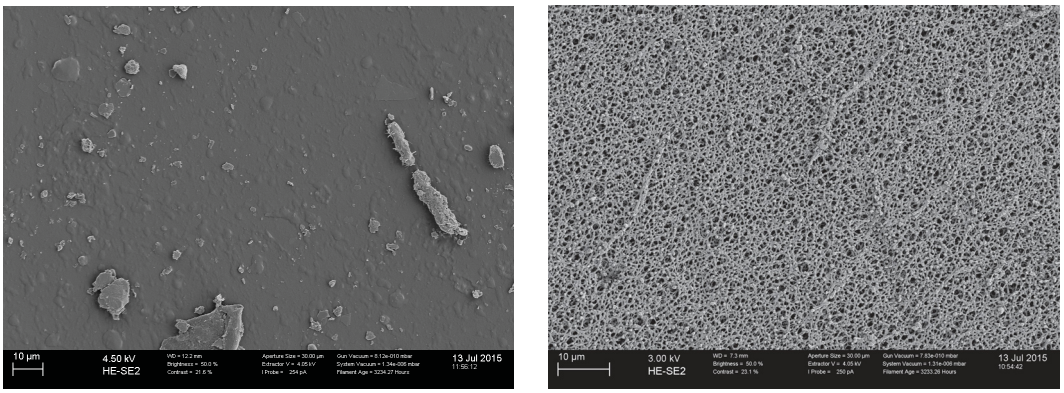

(a) (b)

Figure 4.16: SEM micrographs of plane faces of unused (a) SR and (b) PES membranes. The micrographs were produced at ProVIS, UFZ Leipzig.

generally observed in this study as shown in figure 4.15. Some explanations for the better sorption of PES can be put forth. As discussed previously, PES is porous and has a comparatively rigid structure ($T_g = 225\,°C$), and it is unlikely that rubbery chains dominate its structure. Hence PES has higher sorption capacity resulting from the occurrence of both dissolution and adsorption sites in pores, so that despite

the resultant lower diffusivity than in SR, sorbed concentrations would still exceed or compare to those accumulated in SR. Additionally, given its hydrophilic (due to additives) and porous nature, it is possible that PES-water interactions through hydrogen bonding causes PES to undergo plasticization in the presence of water [81]. Plasticization leads to a depression in T_g causing an increased mobility in the dynamically–constrained amorphous solid and also an increased free volume which causes diffusivity and therefore sorption to be favourably enhanced [81, 134].

4.2.6 Comparison of PES and SR regarding PRCs use

Rusina et al. [132] demonstrated that the uptake of a compound (e.g. PAH) by SR versus the release of an analogous deuterated compound (PRC) exhibited isotropy as shown in figure 4.5f. This observation can be explained by the rubbery nature of SR that makes it amenable for swelling and relaxation during sorption and desorption processes, respectively, without causing significant structural changes in the polymer material. Simply, SR can be viewed as a provider of temporary shelter to a compound which can be released given favourable conditions. This shows the suitability of PRCs in determining *in situ* sampling rates for SR. Accordingly, PRCs were successfully used in this study to determine *in situ* sampling rates, and the release of spiked PRCs was concomitant with their molar masses as shown in figure 4.10. PRC–derived *in situ* sampling rates also varied linearly with K_{pw} and K_{ow} as shown in figures 4.11 and 4.12, respectively, and the resulting correlations matched literature values for uptake that is controlled by the water boundary layer [124, 132].

On the other hand, PES showed anisotropy in its uptake of compounds versus release of analogous PRCs as shown in figure 4.5e, thus PRCs could not be used to determine *in situ* sampling rates. Possible causes of the anisotropy has already been discussed in section 4.1.5.

4.2.7 Quality assurance

The coefficients of variation of sorbed concentrations of PAHs derived from triplicate PES strips deployed at each of the two sampling stations ranged from 0–16% except for naphthalene (29%). Given that these errors represent the total sum of errors from all the processes including preparation, deployment, storage, extraction and analysis, the use of PES for field sampling was therefore considered to be repeatable.

The higher CV for naphthalene was attributed to cross-contamination during handling given that naphthalene exists plentifully in air. Blanks were used during membrane preparation, deployment and retrieval to check for contamination. Only naphthalene, 2-Methylnaphthalene and phenanthrene were detected in sufficient quantities and were subtracted from measured concentrations.

4.2.8 Concentrations of phthalates in Sosiani river as determined using PES and SR

Concentrations of phthalates sorbed onto PES and SR are given in tables 4.7 and 4.8, respectively. All the three target phthalates were detected in both sampling stations and were dominated by bis(2-ethylhexyl)phthalate (DEHP), most probably due to its widespread use [93].

Concentrations shown in the tables have been blank-corrected given that phthalates were quantifiable in blanks. For instance, the amount in blanks for DBP exceeded those measured in station 1 by SR hence the zero value. SR was comparatively more prone to background interference. Benzyl butyl phthalate (BBP) had the least blank value and dibutyl phthalate (DBP) the highest. Therefore, although the two samplers can be used to monitor phthalates as demonstrated by this study, quality

control and assurance remains the key challenge and must always be ensured. This is because phthalates are high production volume chemicals that are widely used and are therefore ubiquitous in the laboratory environment, occurring in organic solvents, ambient air, instruments and apparatus [103]. Nevertheless, background interference can be reduced by using phthalate–free solvent and water where possible and glass apparatus. In addition, preparation and analysis can be carried out in a dedicated phthalate–free room with a purified air filter [103]. All these steps can reduce background interference but cannot totally eliminate it, hence blanks must always be used during all sampler handling steps.

Coefficients of variation of DBP from triplicate SR samplers was 147% and can be attributed to background interference. Otherwise, the rest of the CVs ranged from 3–21% and therefore sampling for phthalates using the two samplers was considered repeatable.

Sorbed amounts were normalized to $100\,\mathrm{cm}^2$ sampler material for purposes of comparison. There was no significant difference in measured amounts between the two samplers ($p > 0.05$). While considering the susceptibility to background interference, PES was more suitable for the assessment of phthalates in surface water. It should be noted that the sorbed amounts were not recalculated to aqueous concentrations due to absence of experimental K_{pw} values for SR. Determination of these K_{pw} was outside the scope of this study but can be performed if background interference is checked.

The sampling rate for BBP in PES was determined in this study and have already been reported in table 4.2. Using these values for calculation yielded C_{w} values for BBP of 0.78 ng/L and 1.18 ng/L in stations 1 and 2 respectively.

Table 4.7: Concentrations of phthalates sorbed onto PES from Sosiani river

Compound name	Calibration data			Average (n=3) concentrations of phthalates[a] (ng/100 cm^2 PES)				
	Cal. range (ng)	Cal. levels	R^2	Blanks	Station 1	CV (%)	Station 2	CV (%)
Dibutyl phthalate	0.15-4.00	8	0.9986	506.4	95.3	21	274.4	21
Benzyl butyl phthalate	0.10-2.50	7	0.9997	0.0	23.9	6	36.0	9
Bis(2-ethylhexyl) phthalate	0.20-4.00	7	0.9980	146.1	1335.8	11	1545.3	9

[a] the concentrations at the two stations shown have been blank–corrected where applicable; Cal., calibration.

Table 4.8: Concentrations of phthalates sorbed onto SR from Sosiani river

Compound name	Calibration data			Average (n=3) concentrations of phthalates[a] (ng/100 cm^2 SR)				
	Cal. range (ng)	Cal. levels	R^2	Blanks	Station 1	CV (%)	Station 2	CV (%)
Dibutyl phthalate	0.15-4.00	8	0.9986	3395.5	0.0	0	361.5	147
Benzyl butyl phthalate	0.10-2.50	7	0.9997	44.9	16.7	14	45.3	3
Bis(2-ethylhexyl) phthalate	0.20-4.00	7	0.9980	970.3	1391.8	7	1970.9	12

[a] the concentrations at the two stations shown have been blank–corrected.

4.2.9 Performance of PES in comparison to SR

Generally, PES was easier to handle than SR and offered several advantages. It was less prone to biofouling than SR probably due to its hydrophilic nature that reduces hydrophobic interactions with biofouling [142]. PES therefore yielded cleaner extracts. Preparation and extraction procedures for PES consumed less time and solvent. For instance, the duration of the extraction procedure and the amount of solvent used per sampler was 50 min, 40 mL and 20 h, 200 mL, respectively, for PES and SR. Furthermore, less membrane material was used in making a PES sampler than SR. The results reported in section 4.2.5 are averages from three samplers consisting of, respectively, one and three PES and SR strips. That is, 300 cm^2 of SR were required to achieve the same concentration sampled by 130 cm^2 of PES. However, PES was quite delicate, and field deployment was therefore carried out in a protective environment made of wire meshes to prevent losses due to abrasion.

Nevertheless, both samplers performed equally well in terms of sorption of the HOCs. On the other hand, SR is a well developed PSD with known working principles for some HOCs and has already been applied in the field [124, 146].

4.3 PAHs in porewater and sediments

Concentrations of PAHs in porewater of air–dried and wet sediments were determined by equilibrating PES strips with porewater during 30 d and 54 d. Coefficients of variation of data from each sampling station were calculated and are given in tables J.1 and J.2 in the appendix. CVs for all duplicate experiments were $\leq 26\%$ indicating repeatability. CVs from both the air–dried and wet sediments for the 30 d and 54 d experiments were $\leq 18\%$ and $\leq 20\%$, respectively, and this verified that concentrations in PES did not change much over time.

Overall CVs calculated using all data from each sampling station, that is, all the raw data from air-dried and wet sediments are also listed in tables J.1 and J.2. Naphthalene and its alkylated derivatives recorded poor values ($53\% \leq \mathrm{CV} \leq 94\%$) since concentrations from air-dried sediments were much higher than those from wet sediments probably due to contamination from air during the drying process. CVs for the other compounds were $\leq 38\%$. This implies that under controlled conditions, the use of air-dried sediments in lieu of wet ones does not lead to a significant difference in measured concentrations.

Freely dissolved porewater concentrations (C_{pw}) were calculated using equation 2.18 and data from the 54 d experiment using wet sediments. Calculated C_{pw} are given in table 4.10. PAHs up to benzo[b+k]fluoranthene were detected. Although the higher molecular weight PAHs were quantifiable in sediment extracts as shown in the table, these compounds were not detected in PES extracts. Since sorption of higher molecular weight PAHs may experience steric hindrance so that the process is restricted to the membrane surface as earlier discussed, the sorbed concentrations from sediment porewater may be too low for quantification. On the other hand, these higher molecular weight PAHs may also experience slowed desorption from sediments through the processes discussed in section 4.1.2, so that their concentrations in porewater are very low as is often observed in sediments [118].

Equation J.4 was used to determine if non-depletion criteria were met. For the compounds detected in PES exctacts, the calculated values were all in the order $10^{-3} - 10^{-4}$ confirming non–depletion.

Sediment characteristics are given in table 4.9. The sediments were considered sandy given that the percentages of sand at both sampling stations were higher than those of silt and clay. Total organic carbon (TOC) was 1.09% and 1.49% in stations 1 and 2, respectively. TOC data were converted to fraction form, yielding fractions of

Table 4.9: Characteristics of sediments from sampling stations along Sosiani river

Sampling site	Surrounding land use	Sediment texture (% d.w[a])			TOC[b] (% d.w) (SD[c])
		Silt	Clay	Sand	
Station 1	urban, commercial	13.26	17.87	68.87	1.09 (0.11)
Station 2	urban, commercial	17.01	22.41	60.58	1.49 (0.15)

[a] dry weight; [b] total organic carbon; [c] standard deviation.

Table 4.10: Porewater and organic carbon normalized total sediment concentrations of PAHs in Sosiani river

Compound name	C_{pw} (ng/L)		C_s[a] (µg/kg$_{TOC,\ d.w.}$)	
	Station 1	Station 2	Station 1	Station 2
Naphthalene	15.5 ± 4.1	14.0 ± 3.0	9.6 ± 3.6	7.7 ± 0.6
Acenaphthylene	6.3 ± 0.0	5.6 ± 0.0	0.5 ± 0.0	0.1 ± 0.0
Acenaphthene	12.0 ± 0.0	12.0 ± 0.0	0.6 ± 0.1	0.2 ± 0.0
Fluorene	10.7 ± 0.2	9.2 ± 0.0	2.3 ± 0.3	1.0 ± 0.1
Phenanthrene	6.3 ± 0.1	3.7 ± 0.1	6.6 ± 0.9	1.4 ± 0.7
Anthracene	5.9 ± 0.2	5.6 ± 0.0	1.0 ± 0.1	0.4 ± 0.2
Fluoranthene	5.6 ± 0.1	4.1 ± 0.1	0.8 ± 0.1	0.3 ± 0.1
Pyrene	6.8 ± 0.2	4.5 ± 0.0	5.9 ± 0.3	1.6 ± 0.3
Benz[a]anthracene	5.4 ± 0.1	5.2 ± 0.0	1.9 ± 0.0	0.6 ± 0.1
Chrysene	2.5 ± 0.0	2.3 ± 0.0	2.9 ± 0.0	0.8 ± 0.5
Benzo[b+k]fluoranthene	5.5 ± 0.0	5.4 ± 0.0	2.6 ± 0.3	0.9 ± 0.7
Benzo[e]pyrene	<LOQ	<LOQ	1.5 ± 0.1	0.5 ± 0.4
Benzo[a]pyrene	<LOQ	<LOQ	1.2 ± 0.6	0.5 ± 0.3
Perylene	n.d.	n.d.	0.5 ± 0.1	0.2 ± 0.3
Indeno[1,2,3-cd]pyrene	n.d.	n.d.	< LOQ	< LOQ
Dibenz[a,h]anthracene	n.d.	n.d.	n.d	n.d
Benzo[ghi]perylene	n.d.	n.d.	< LOQ	< LOQ
1-Methylnaphthalene	4.3 ± 0.1	3.7 ± 0.3	4.3 ± 0.2	2.7 ± 0.1
2-Methylnaphthalene	5.2 ± 0.1	4.7 ± 0.4	2.2 ± 0.2	1.4 ± 0.0
2,7-Dimethylnaphthalene	4.8 ± 0.2	4.1 ± 0.0	2.0 ± 0.2	0.8 ± 0.1
1,6,7-Trimethylnaphthalene	9.3 ± 0.1	8.6 ± 0.0	1.3 ± 0.2	0.2 ± 0.3

d.w., dry weight; n.d., not detected; LOQ, limit of quantitation; [a] C_s values are a quotient of average total concentrations from duplicate measurements using dry sediments, and f_{oc}.

organic carbon (f_{oc}) which were then used to normalize the measured total sediment concentrations. Results are given in table 4.10.

Sediment concentrations were markedly higher than porewater concentrations probably since C_s were determined by depletive methods and represent both bioavailable and bound fractions. On the other hand, C_{pw} represents only the bioavailable fraction, and essentially represents chemical activity, the driving force for all chemical interactions with sediment–associated contaminants such as partitioning to organisms, diffusive exchange, and environmental reactivity [88].

4.4 Fugacity modeling of sediment–water exchange

4.4.1 Fugacity fractions and sediment–water fluxes

Sediment–overlying water exchange of compounds was estimated using the Sediment Model [27]. The model's code was re-written in Excel to enable adjustments where applicable. The model was applied to simulate sediment–water fluxes of PAHs using phenanthrene, fluoranthene and pyrene as examples. Table L.1 gives the model input parameters and the outputs are given in tables 4.11, L.2 and L.3.

Fugacity fractions at the assumed non-steady state were 5.31, 5.24 and 11.51 for phenanthrene, fluoranthene and pyrene, respectively. Since the fugacity fractions were greater than one, the sediments act as a repository for these organic compounds and probably for others within the same K_{ow} range or greater. Therefore, chemical fluxes should be from sediments to the water phase for these PAHs. Thus, in addition to other non–point source inputs, the historically contaminated sediments could act as a source to the water phase.

The model apportions the sediment–water movement of a chemical to resuspension,

deposition, burial, reaction and diffusion [89]. Actually, the transfer pathways are much broader, and in addition, may involve other site–specific processes such as ebullition, bioturbation and groundwater discharge [82]. The model seems to lump these processes and model them together as diffusive flux. The influence of the aforementioned transfer pathways are described by D–values. $D_{\text{diffusion}}$ was calculated as a product of the sediment–water mass transfer coefficient, the unit area and Z values for water. All these parameters were constant since Z–values for overlying water and porewater were both calculated using the Henry's law constant as the only parameter. Thus, sediment–water and water–sediment $D_{\text{diffusion}}$ values were equal for a single compound but differed between compounds. $D_{\text{deposition}}$ was calculated as a product of the respective G–value and the Z–value for total suspended solids. $D_{\text{resuspension}}$ and D_{burial} were both calculated as a product of the Z–value for total sediment solids and their respective G–values. D_{reaction} was calculated from the volume and Z–value for sediments, and the degradation half–life for the compound.

Fluxes were calculated as a product of D–values and fugacities, then they were also expressed as a percentage of net water–sediment transfer for better understanding of the relative contribution of each pathway to the overall flux. For all the compounds, sediment–water fluxes exceeded the water–sediment movement implying that sediments act as a source of PAHs to overlying water (see tables 4.11, L.2 andL.3). For phenanthrene and pyrene, deposition ($\approx 100\%$) was predicted to be the main pathway for losses from the water phase since the compounds have low aqueous solubilities and high hydrophobicity and therefore partition preferably to suspended solids. For fluoranthene, losses from the water phase involved deposition (66%) and water–sediment diffusion (34%). Thus, deposition was the main pathway of PAH losses from water but this process depends on the concentration of suspended solids, deposition rates and hydrodynamics. The combined reaction and burial contributed the greatest to losses from sediments since their values were more than 24–fold greater than the net water–sediment transfer.

Table 4.11: Model output for fluoranthene: Z values, concentrations, fugacities, transfer rates and half–life

Water	Z values	Concentration		Amount		
	(mol/(m^3 Pa))	(mol/m^3)	(µg/g)	(mol)	(g)	(% in system)
Bulk water	2.01E+00	1.89E-08	3.82E-06	1.51E-05	3.05E-03	3.67E+00
Water	1.05E+00	9.79E-09	1.98E-06	7.83E-06	1.58E-03	1.90E+00
Total suspended particles	1.83E+03	1.71E-05	3.23E-03	7.27E-06	1.47E-03	1.77E+00
Organic matter	1.92E+03	1.80E-05	3.64E-03	7.27E-06	1.47E-03	1.77E+00
Mineral matter	2.06E+00	1.93E-08	1.56E-06	3.90E-10	7.88E-08	9.47E-05

Sediment	Z values	Concentration		Amount		
	(mol/(m^3 Pa))	(mol/m^3)	(µg/g)	(mol)	(g)	(% in system)
Bulk sediment	2.69E+02	1.32E-05	2.45E-03	3.96E-04	8.02E-02	9.63E+01
Porewater	1.05E+00	5.13E-08	1.04E-05	1.23E-06	2.49E-04	2.99E-01
Total sediment solids	1.34E+03	6.59E-05	9.18E-03	3.95E-04	7.99E-02	9.60E+01
Organic matter	1.92E+03	9.42E-05	1.90E-02	3.95E-04	7.99E-02	9.60E+01
Mineral matter	2.06E+00	1.01E-07	8.17E-06	1.82E-07	3.69E-05	4.43E-02

Fugacity	(Pa)	Half life	(h)	(yr)
F_w	9.37E-03	Water-sediment transfer	3436	0.39
F_s	4.91E-02	Sediment-water transfer	3.73E+04	4.3
Sediment to water ratio	5.24	Sediment burial and reaction	3.70E+03	0.4
Fugacity predictions at steady state		Sediment losses and transfer	337	0.38
Sediment to water ratio at steady state	1.96E-01			
Water fugacity (given sediment fugacity as above)	2.51E-07			

Continued on next page

Table 4.11 Continued from previous page

Sediment fugacity (given water fugacity as above)		1.83E-09			
Transfer rates	D value (mol/(Pa h))	G value (m^3/h)	Flux (mol/h)	Flux (kg/yr)	(%)[a]
Diffusion (water-sediment)	1.12E-01		1.05E-09	1.85E-06	34
Diffusion (sediment-water)	1.12E-01		5.48E-09	9.70E-06	180
Deposition	2.13E-01	1.17E-04	2.00E-09	3.54E-06	66
Resuspension	3.85E-02	2.87E-05	1.89E-09	3.35E-06	62
Burial	5.78E-02	4.31E-05	2.84E-09	5.02E-06	93
Reaction	1.4538		7.13E-08	1.26E-04	2342
Water-sediment transfer	3.25E-01		3.05E-09	5.40E-06	100
Sediment-water transfer	1.50E-01		7.37E-09	1.31E-05	242
Sediment burial and reaction	1.51E+00		7.42E-08	1.31E-04	2435

[a] % of net water–sediment transfer; F_w and F_s are fugacities in water and sediments, respectively.

The model predicted the half–life for sediment losses and transfer to be approximately 0.16, 0.38 and 0.01 yr for phenanthrene, fluoranthene and pyrene, respectively. This observation can be attributed to the short degradation half-life for these PAHs as compared to more persistent chemicals, for instance DDT. For all the PAHs, half-lives for water–sediment and sediment–water transfers under steady state conditions were predicted to be 0.39–1.67 yr and 4–17 yr, respectively. Therefore, under continuous non–point source discharge to the river, the PAHs would quickly accumulate in the sediment phase where they would dwell for a longer time.

4.4.2 Predicted and experimental C_{pw} and C_w

The model also calculates freely dissolved concentrations in overlying water and porewater using their Z–values and respective fugacities. Table 4.12 shows measured and predicted concentrations in the two sub–compartments.

The model predicted C_{pw} which were 2–70 greater than measured concentrations. It should be noted, however, that the reliability of the predictions depends on the accuracy of measured total concentrations in sediments and the K_{oc} value used. Taking pyrene as an example, predicted C_{pw} (ng/L) were 79.53, 13.51 and 18.23 when using K_{oc} values estimated from the Karickhoff's equation, equation 2.29, and the coal tar–LFER, respectively. Predictions for phenanthrene and fluoranthene using the aforementioned K_{oc} sources also followed a similar pattern. On the other hand, experimental C_{pw} were lower probably due to slowed desorption as discussed in section 4.1.2. It is expected that for the same sediment and experimental conditions, C_{pw} may vary when using different PSDs due to differences in partitioning properties between different types and sources of polymers used as PSDs [96].

The model calculates C_w using water fugacity that is determined from Z–values and concentration of the bulk water phase. Z–values are calculated using volume

Table 4.12: Experimental and predicted freely dissolved concentrations in overlying water and porewater

Compound name	Predicted (ng/L)		Measured (ng/L)	
	C_w	C_{pw}	C_w [a]	C_{pw} [b]
Phenanthrene	68.37	363.09	9.70	5.00
Fluoranthene	1.98	10.37	2.70	4.85
Pyrene	6.91	79.53	2.85	5.65

[a] represents an average from the two sampling stations measured using SR; [b] also represents an average from the two sampling stations measured using PES.

fractions of water and suspended solids and associated sub–components.

The bulk phase comprises water and suspended solids and the concentration of the latter is an input to the model that is used to determine volume fractions. Reliability of suspended solids measurement is therefore important when using the model to predict C_w. In this study, the concentration of suspended solids was an average from measurements of water samples collected twice over a 30 d duration. This value may have been higher than the average for daily measurements over the 30 d duration, hence the lower predicted C_w. On the other hand, experimental C_w represents time-weighted average concentrations measured *in situ* continuously during the 30 d duration using SR. Thus, experimental C_w were considered a more authentic representation of aqueous concentrations.

4.4.3 Model sensitivity regarding the input parameters

A. Effect of K_{oc} values on predicted fugacity fractions

K_{oc} is an important parameter when considering the fate of a HOC in a river system since the HOC preferably partitions to the organic phase of sediment solids. K_{oc}

is an input parameter in fate models and can be determined experimentally or estimated using existing equations. In this study, K_{oc} values were estimated using the Karickhoff's equation, yielding fugacity fractions of 5.31, 5.24 and 11.51 for phenanthrene, fluoranthene and pyrene, respectively. K_{oc} estimated from equation 2.29 and the coal tar–LFER were also used in calculations. K_{oc} values from both equations caused under–prediction of fugacity fractions, that is, 1.75, 2.97 and 6.34 for phenanthrene, fluoranthene and pyrene, respectively, when using equation 2.29, and 2.24, 2.91 and 5.71 for phenanthrene, fluoranthene and pyrene, respectively, when using the coal tar–LFER. This also caused an under–prediction in predicted sediment–water fluxes.

B. Effect of variation of other parameters on predicted fugacity fractions

Model input parameters that were susceptible to changes were tested theoretically, one–at–a–time, to check their influence on model outputs, specifically the fugacity fraction. Of the input parameters listed in table L.1, only five parameters, namely, concentration of suspended solids, total concentrations in water and sediments and mass fraction of organic carbon in suspended solids and sediments significantly affected the fugacity fraction.

Input parameters were varied over a range relative to the given quantities then the values were plotted against resultant fugacity fractions. For example, the influence of variations in organic carbon content of suspended and sediment solids on the predicted *ff* was tested by varying the mass fraction of organic carbon over a 46–point range from 0.5% to 5.0% TOC. The results were that fugacity fractions increased linearly with increase in the fraction of organic carbon in suspended solids, and *ff* decreased exponentially with increase in the TOC fraction in sediment solids. The influence of parameter variations on *ff* were analyzed by regression methods [116]. Results are given in table 4.13.

Three parameters varied linearly with *ff*: concentration of suspended solids, mass fraction of TOC in suspended solids and total concentration in water with sensitivity, considered as the slope of the regression line, increasing in that order. The variation of concentration in sediment and fraction of organic carbon in sediment solids were fitted with a fifth order polynomial.

4.4.4 Concluding remarks

The model was useful in predicting sediment–water exchange of PAHs. It is simple and easy to understand, use and interpret since the use of fugacity directly indicates how close the system is to equilibrium, and which are the directions of the diverse diffusive transfer processes without requiring partition coefficients in the various flux equations [90]. In addition, the model was able to explain all the major processes while requiring little input which makes it relatively convenient. However, its performance relies on accurate inputs and where applicable, the input parameters should be determined experimentally.

Field measurements represent the environmental situation in real time and cannot

Table 4.13: Regression equations produced when predicted fugacity fractions were plotted against varying values of the input parameters

Input parameter	Regression equation	R^2
Concentration of TSS[a]	$y = 0.004x + 0.095$	1.0000
Total concentration in water	$y = 222x - 21$	0.9856
Fraction of organic carbon in TSS	$y = 105x + 0.095$	1.0000
Fraction of organic carbon in SS[b]	$y = (-8E+09)x^5 + (7E+08)x^4 - (2E+07)x^3 + (4E+05)x^2 - (4E+03)x + 18.7$	0.9999
Concentration in sediment	$y = (-4E+06)x^5 + (2E+05)x^4 - (2E+03)x^3 + (15.36)x^2 - 0.05x + 0.09$	0.9974

[a] total suspended solids; [b] sediment solids.

therefore be wholly replaced by theoretical predictions. However, the model can be used for instance, when planning a field campaign, to better explain experimental values or when planning management strategies such as remediation measures. Its use in tandem with passive sampling would be particularly attractive since both procedures use fugacity as the measurement/prediction endpoint.

Chapter 5

Summary and Conclusion

5.1 Summary

5.1.1 Development of PES as a passive sampler

A polymeric material, PES, was investigated as a possible sorbent for PAHs, PCBs and OCPs. Its uptake and elimination kinetics were determined in flow–through calibration experiments. The experiments were carried out at a temperature and flow rate that was similar to field values. The following key findings were made:

1. Though the PES membrane used was hydrophilic, hydrophobic compounds could sorb into it with low limits of quantitation. This observation was attributed to partitioning to the non-polar moieties in PES and/or favourable non-linear sorption to nanovoids and unrelaxed free volume regions.

2. For most compounds, uptake remained in the linear range for the complete experimental duration. This observation was attributed to the possible high

sorption capacity of PES due to the occurrence of both dissolution sites (amorphous regions) and condensed glassy phases (pores) resulting in a higher free volume than rubbery polymers, and a slower intraparticle diffusion process. It was also postulated that flexibility of the polymer chains in the presence of a sorbate could also be induced by possible plasticization by water owing to the wettability of the polymer.

3. Uptake curves for PAHs were linear for 10–12 d before concentrations became fairly constant or decreased slightly. In addition, sorbed amounts of PAHs decreased with increase in molecular mass. The observations were attributed to the slow process of intraparticle diffusion coupled with steric hindrance at the pore openings resulting from the size and shape of molecules, so that sorption may have limited to the surface.

4. Intraparticle diffusion in PES was confirmed. Using equations 2.23 and 2.24, the function for intraparticle diffusion, m, ranged from $0.5 < \mathrm{m} < 0.8$ for most compounds and their C values were significantly different from zero ($p < 0.002$), implying that sorption was controlled by both first–order kinetics and intraparticle diffusion. For some compounds, $\mathrm{m} \leq 0.5$ and their C values were not significantly different from zero ($p > 0.002$), showing that intraparticle diffusion is the only rate–limiting process. For PCB 52, $\mathrm{m} \approx 1.0$ suggesting that sorption was controlled by first order kinetics. For DDXs, m values did not vary much between compounds ($\mathrm{m} = 0.64 \pm 0.03$) but were slightly lower for the *ortho–para* substituted members than the *para–para* substituted.

5. No correlation ($\mathrm{R}^2 = 0.01$) was found between the intraparticle diffusion coefficient, log k_{id}, and log K_{ow}s (slope=0.02) or molar masses (slope=-0.04), showing that generally, sorption was independent of hydrophobicity or molar mass. Values of k_{id} for PAHs showed greater variation attributed to steric hin-

drance. Those of PCBs reduced slightly with increase in molar mass, except for PCB 52, whose anomalous behaviour could not be attributed to planarity or molecular weight. Those of DDXs did not vary much and showed no specific pattern between the compounds. It was concluded that chemical uptake in PES is generally non-specific and may only be limited by the modes of interaction of a given chemical with the membrane.

6. Given the porous and glassy nature of PES, the occurrence of the slow process of intraparticle diffusion, and the generally linear uptake curves, it was concluded that PES probably has a high capacity for the HOCs, in which case true equilibrium may not be attained within the practical time scale of an experimental set–up or short–term field deployment. Aqueous concentrations may therefore be estimated using equation 2.18.

7. Anisotropy was observed between uptake and elimination curves of individual compounds or a compound and an analogous PRC. This was attributed to different mechanistic pathways for sorption and desorption such that the processes may occur to/from different microenvironments. Additionally, anisotropy was attributed to possible capillary condensation in voids, pore deformation/reorganization by the sorbates, a conditioning effect, a reduced relaxation speed of polymer chains owing to the rigidity of the polymer structure, and differences in kinetic energy for sorption and desorption.

8. Anisotropy in uptake of a compound versus the release of an analogous PRC demonstrated the unsuitability of PRCs for determination of *in situ* sampling rates. Sampling rates have to determined using kinetic experiments at field conditions or sampling at short time intervals in the field.

Estimated sampling rates were correlated to compound properties by linear regression of the logarithmic values. The following key findings were made:

1. Generally, sampling rates had poor correlation to both hydrophobicity ($\log R_s = 0.02 \log K_{ow} + 0.54$, $R^2 = 0.00$) and molar mass ($\log R_s = -0.26 \log M + 1.25$, $R^2 = 0.02$). This indicates that hydrophobic interactions are not the primal mechanism governing the uptake of HOCs from the aqueous phase onto PES, and it is possible that other mechanisms such as $\pi - \pi$ interactions between the aromatic rings of the HOCs and PES and hydrogen bonding through the polar sulfonyl groups are involved in the uptake process.

2. Average apparent log K_{pw} for the 31 compounds under investigation was $6.58\,L/kg \pm 0.29$ log units. The small variation in log K_{pw} implies that uptake in PES is generally non–specific. The apparent K_{pw} values also had no correlation to hydrophobicity and molar mass.

3. The role of mechanisms other than hydrophobicity in the uptake process was determined by normalizing R_s values with n-hexadecane–water partition coefficients. Generally, normalized R_s correlated linearly with logs of molar masses ($y = -9.04x + 16.43$, $R^2 = 0.93$, $s = 0.35$, $n = 29$). Normalized R_s for PAHs were best fitted using a second order polynomial, and showed a downward curvature at higher molar mass, suggesting the occurrence of resistance to sorption in PES due to steric hindrance. Those of PCBs decreased strictly with increasing mass ($y = -10.44x + 20.06$, $R^2 = 0.99$, $n = 6$) while those of DDTs had a poorer linear fit ($y = -15.46x + 32.53$, $R^2 = 0.48$, $n = 6$). $\pi - \pi$–interaction was suggested as a mechanism for chemical (ad)sorption to PES surface, and pore and matrix diffusion for penetration into the polymer. Normalized R_s for two compounds (methoxychlor and BBP) had log $R_{s,norm.}$–log M fits that were distinguishable from the rest, implying their uptake mechanisms differ from that of the other compounds, possibly due to the O–containing moieties in their structure that could participate in hydrogen bonding.

5.1.2 Field application of PES and SR

PES was also deployed in a tropical river in parallel to SR to monitor for PAHs, PCBs and OCPs on a comparative basis. For PES, freely dissolved concentrations were calculated using sorbed amounts and experimental R_s values. Freely dissolved concentrations measured using SR were determined using sorbed amounts, K_{pw} values obtained from literature [147], and R_s that were determined *in situ* using PRCs. The major outcomes of the field deployment can be summarized as follows:

1. Only PAHs were detected by both sorbents. Additionally, other compounds from a log K_{ow} range of 3.8–5.0 (e.g. diazinon, chlorpyrifos) were identified in a non-target screening of PES extracts.

2. PRC–derived sampling rates for SR correlated linearly to partition coefficients ($R_s = K_{pw}^{-0.048} b_\circ$, $R^2 = 0.98$), and hydrophobicity ($R_s = K_{ow}^{-0.047} b_\circ$, $R^2 = 0.98$) as reported in literature for uptake that is controlled by the water boundary layer [124, 132].

3. R_s for SR varies with D_w as described by the hydrodynamic theory given as: $R_s = AFD_w^{2/3}$. Different equations were used to predict molecular diffusivity in water and the calculated values were correlated to PRC–derived sampling rates using the aforementioned equation. Resultant slopes ranged from 0.56 to 0.95. The best fit (slope = 0.69) was obtained using D_w values derived from the equation by Schwarzenbach et al. [140]. Field–determined sampling rates were best fitted to predicted R_s values that were estimated using equation 4.7 and water diffusivities that were calculated using the equation proposed by Schwarzenbach et al. [140].

4. By normalization of the sorbed amounts to 100 cm^2, PES showed greater sorption for the lower molecular weight PAHs than SR. This observation was at-

tributed to the higher sorption capacity of PES due to larger free volume owing to the presence of both amorphous and condensed (pores) regions. As a result, sorbed amounts in PES may exceed or equate to those in SR despite lower diffusivity in PES due to intraparticle diffusion.

5. PRCs could be applied in determining *in situ* sampling rates for SR due to the isotropic exchange in sorption of a compound and the desorption of an analogous PRC. As already mentioned, this exchange was anisotropic for PES, thus PRCs were unsuitable for determination of *in situ* sampling rates.

6. BBP, DBP and DEHP in river water were determined using PES and SR and reported as sorbed concentrations. The use of field and laboratory blanks was necessary due to the high tendency for cross–contamination during processing given that phthalates are ubiquitous in the environment. In some cases, concentrations in blanks were higher than that in samplers, especially with DBP as evidenced by poor coefficients of correlation (147%) between replicate measurements. BBP had the least tendency for cross–contamination. Reported concentrations represent blank–corrected values and ranged from 23.9–1545.3 ng/100 cm^2 PES and 0.0–1970.9 ng/100 cm^2 SR.

7. PES required significantly less time and solvent during preparation and extraction than SR. However, SR was more resilient and could withstand abrasion. PES was delicate and had to be deployed in wire meshes.

5.1.3 Concentrations of PAHs in sediments and porewater

1. TOC and sediment characteristics were determined experimentally. TOC (% d.w) were 1.09 and 1.49 in the two stations respectively. Sediments were extracted by accelerated solvent extraction and analyzed for PAHs. The con-

centrations were normalized with TOC. Concentrations ranged from below detection limit for the higher molecular weight members to 9.6 µg/kg($_{\text{TOC, d.w}}$) for naphthalene.

2. PES strips were equilibrated with porewater in contaminated sediments. The PES strips were extracted and analyzed to yield porewater concentrations ranging from below detection limit for the higher molecular weight members to 15.5 ng/L for naphthalene. Alkyl naphthalenes and parent PAHs upto benzo[b+k]fluoranthene were detected.

5.1.4 Fugacity modeling of sediment–water fluxes

1. A sediment model [27] was used to estimate the sediment–water transfer of PAHs. Fugacity ratios were greater than unity and sediment–water fluxes exceeded water–sediment fluxes implying that sediments act as a source of PAHs to surface water. Deposition of suspended solids was found to be the main pathway for PAH losses from the water phase. On the other hand, reaction and burial of sediment solids were found to be the major loss pathways from sediments. It was concluded that the model is a useful tool in predicting sediment–water fluxes especially when the input parameters are determined experimentally where possible.

2. Predicted C_{pw} which were 2–70 greater than measured concentrations and were found to be sensitive to the K_{oc} value used in calculation. Predicted C_{w} was seven and two times higher than measured concentrations for phenanthrene and pyrene, respectively. There was no significant difference in measured and predicted C_{w} for fluoranthene.

5.2 Conclusion

Passive sampling is a useful tool that can effectively assess the pollution status of surface waters at trace concentration levels and therefore serves as an early warning system. In view of global environmental assessment, this research demonstrated that passive sampling as a surface water monitoring and assessment tool is applicable even in remote regions with poor infrastructure and varied climatic and hydraulic conditions. Passive sampling offers many advantages over conventional monitoring approaches. Specifically in these regions, this monitoring approach is easier to implement as it reduces the implied costs especially when cheap polymeric sorbents are used. Two key attractions are the drastic reduction in transport costs that would be high when using conventional monitoring procedures, and the possibility to store the used sorbent materials for a longer duration which implies that in the absence of a laboratory in the vicinity of the sampling location, these sorbents can be transported elsewhere for analysis.

Some passive sampling devices are well developed and applied while some are still under development in terms of their working principles and/or applications. Silicone rubber is an example of a well developed sampler and was applied in this study with success and reproducibility equalling that reported in literature on its application in various parts of the world. Its advantages are versatility and robustness. The greatest disadvantage lies in the pre–cleaning step that is time– and solvent–consuming. This step can be circumvented by availability of commercialised pre–cleaned sheets.

There are few literature reports on application of PES as a sampler. However, its uptake kinetics are still not clear. This research attempted to close the knowledge gap by assessing the uptake kinetics and key properties of PES for PAHs, PCBs and OCPs. PES was found to be a non-selective sorbent for these compounds and performed equally to the well to SR when applied in the field. Nevertheless, the

findings from this study, in addition to literature reports, cannot endear PES as a well developed sampler at the moment, given that its uptake kinetics differ from those of most well developed samplers like SPMD and SR. Knowledge gaps still exist which can be subject for further research. These include:

- Determination of the sorption capacity of PES given that it is a non–specific sorbent for both polar and nonpolar compounds. Besides passive sampling, PES also finds use in filtration membranes and it is interesting to investigate the sorption capacity and breakthrough points so that both its efficiency in purifying water and the duration within which it can perform these functions fully can be known.

- Further investigation into the uptake mechanisms, especially the membrane–compound properties that drives uptake so that a general sorption model can be drawn. Given that PES is usually used as a uptake rate–limiter in POCIS, determination of membrane–compound interactions will also be useful in elucidating burst and lag effects, and the suitability PES–enclosed POCIS for sampling various compounds.

- Further investigation into the causes of anisotropy between uptake and desorption curves by focussing on chemical interaction with PES using other methods like spectroscopy.

- Determination of diffusion coefficients of compounds in wet PES and partition coefficients between PES and water.

In addition, passive samplers can be used to monitor HOCs in porewater. The measured concentrations represent bioavailable fractions that are amenable for diffusion, uptake by benthic organisms and degradation. PES was used in this study to measure concentrations of PAHs. The use of passive samplers to determine porewa-

ter concentrations is still at infancy and this opens avenues for further development. Most of the studies are carried out *ex situ* due to long equilibration times in the field. It would be interesting to develop versatile passive samplers with short equilibration times to measure the concentrations *in situ*.

Environmental fate models are useful tools in predicting the behaviour of chemicals in the environment. Particularly, fugacity–based models are parsimonious and calculate fugacity fractions as a direct tool for assessing the likely direction of movement of a chemical in the environment. Their application in tandem with passive sampling technologies can be a powerful strategy in environmental management.

References

[1] Abella, V., Pérez, T., Scotece, M., Conde, J., Pirozzi, C., Pino, J., Lago, F., González-Gay, M. Á., Mera, A., Gómez, R., and Gualillo, O. "Pollutants make rheumatic diseases worse: Facts on polychlorinated biphenyls (PCBs) exposure and rheumatic diseases". Life Sciences 157 (2016), pp. 140–144.

[2] Adams, R. G., Lohmann, R., Fernandez, L. A., MacFarlane, J. K., and Gschwend, P. M. "Polyethylene devices: Passive samplers for measuring dissolved hydrophobic organic compounds in aquatic environments". Environmental Science & Technology 41 (2007), pp. 1317–1323.

[3] Ahn, W.-Y., Kalinichev, A. G., and Clark, M. M. "Effects of background cations on the fouling of polyethersulfone membranes by natural organic matter: Experimental and molecular modeling study". Journal of Membrane Science 309 (2008), pp. 128–140.

[4] Allan, I. J., Booij, K., Paschke, A., Vrana, B., Mills, G. A., and Greenwood, R. "Field performance of seven passive sampling devices for monitoring of hydrophobic substances". Environmental Science & Technology 43 (2009), pp. 5383–5390.

[5] Allan, I. J., Booij, K., Paschke, A., Vrana, B., Mills, G. A., and Greenwood, R. "Short-term exposure testing of six different passive samplers for the monitoring of hydrophobic contaminants in water". Journal of Environmental Monitoring 12 (2010), pp. 696–703.

[6] Allan, I. J., Harman, C., Ranneklev, S. B., Thomas, K. V., and Grung, M. "Passive sampling for target and nontarget analyses of moderately polar and nonpolar substances in water". Environmental Toxicology and Chemistry 32 (2013), pp. 1718–1726.

[7] Alvarez, D. A., Huckins, J. N., Petty, J. D., Jones-Lepp, T., Stuer-Lauridsen, F., Getting, D. T., Goddard, J. P., and Gravell, A. "Tool for monitoring hydrophilic contaminants in water: Polar organic chemical integrative sampler (POCIS)". In: Passive Sampling Techniques in Environmental Monitoring. Ed. by Greenwood, R., Mills, G., and Vrana, B. Vol. 48. Amsterdam: Elsevier, 2007. Chap. 9, pp. 199–227.

[8] Alvarez, D. A., Petty, J. D., Huckins, J. N., Jones-Lepp, T. L., Getting, D. T., Goddard, J. P., and Manahan, S. E. "Development of a passive, in situ, integrative sampler for hydrophilic organic contaminants in aquatic environments". Environmental Toxicology and Chemistry 23 (2004), pp. 1640–1648.

[9] Amdany, R., Chimuka, L., Cukrowska, E., Kukučka, P., Kohoutek, J., Tölgyessy, P., and Vrana, B. "Assessment of bioavailable fraction of POPS in surface water bodies in Johannesburg City, South Africa, using passive samplers: An initial assessment". Environmental Monitoring and Assessment 186 (2014), pp. 5639–5653.

[10] Anway, M. D., Leathers, C., and Skinner, M. K. "Endocrine disruptor vinclozolin induced epigenetic transgenerational adult-onset disease". Endocrinology 147 (2006), pp. 5515–5523.

[11] Apell, J. N., Tcaciuc, A. P., and Gschwend, P. M. "Understanding the rates of nonpolar organic chemical accumulation into passive samplers deployed in the environment: Guidance for passive sampler deployments". Integrated Environmental Assessment and Management 12 (2016), pp. 486–492.

[12] Arcaro, K. F., O'Keefe, P. W., Yang, Y. I., Clayton, W., and Gierthy, J. F. "Antiestrogenicity of environmental polycyclic aromatic hydrocarbons in human breast cancer cells". Toxicology 133 (1999), pp. 115–127.

[13] Arp, H. P. H., Breedveld, G. D., and Cornelissen, G. "Estimating the *in situ* sediment−porewater distribution of PAHs and chlorinated aromatic hydrocarbons in anthropogenic impacted sediments". Environmental Science & Technology 43 (2009), pp. 5576–5585.

[14] Astakhov, E. Y., Kolganov, I. M., Klinshpont, E. R., Tsarin, P. G., and Kalacheva, A. A. "Influence of polyvinylpyrrolidone on morphology, hydrophilicity, and performance of polyethersulfone microfiltration membranes". Petroleum Chemistry 52 (2012), pp. 557–564.

[15] Bao, L.-J., Xu, S.-P., Liang, Y., and Zeng, E. Y. "Development of a low-density polyethylene-containing passive sampler for measuring dissolved hydrophobic organic compounds in open waters". Environmental Toxicology and Chemistry 31 (2012), pp. 1012–1018.

[16] Baruah, K., Bhattacharyya, P. K., and Hazarika, S. "Adsorption of dilute alcohols onto cyclodextrin–polysulfone membrane: Experimental and theoretical analysis". Journal of Chemical & Engineering Data 60 (2015), pp. 2549–2558.

[17] Belles, A., Pardon, P., and Budzinski, H. "Development of an adapted version of polar organic chemical integrative samplers (POCIS-Nylon)". Analytical and Bioanalytical Chemistry 406 (2014), pp. 1099–1110.

[18] Benhalima, A., Hudon, F., Koulibaly, F., Tessier, C., and Brisson, J. "Polyethersulfone polymers and oligomers — Morphology and crystallization". Canadian Journal of Chemistry 90 (2012), pp. 880–890.

[19] Blanco-Zubiaguirre, L., Delgado, A., Ros, O., Posada-Ureta, O., Vallejo, A., Prieto, A., Olivares, M., and Etxebarria, N. "Assessment of commercially available polymeric materials for sorptive microextraction of priority and

emerging nonpolar organic pollutants in environmental water samples". Environmental Science and Pollution Research 21 (2014), pp. 11867–11883.

[20] Boas, M., Feldt-Rasmussen, U., and Main, K. M. "Thyroid effects of endocrine disrupting chemicals". Molecular and Cellular Endocrinology 355 (2012), pp. 240–248.

[21] Booij, K., Robinson, C. D., Burgess, R. M., Mayer, P., Roberts, C. A., Ahrens, L., Allan, I. J., Brant, J., Jones, L., Kraus, U. R., Larsen, M. M., Lepom, P., Petersen, J., Pröfrock, D., Roose, P., Schäfer, S., Smedes, F., Tixier, C., Vorkamp, K., and Whitehouse, P. "Passive sampling in regulatory chemical monitoring of nonpolar organic compounds in the aquatic environment". Environmental Science & Technology 50 (2016), pp. 3–17.

[22] Booij, K. and Smedes, F. "An improved method for estimating *in situ* sampling rates of nonpolar passive samplers". Environmental Science & Technology 44 (2010), pp. 6789–6794.

[23] Booij, K., Vrana, B., and Huckins, J. N. "Theory, modelling and calibration of passive samplers used in water monitoring". In: Passive Sampling Techniques in Environmental Monitoring. Ed. by Greenwood, R., Mills, G., and Vrana, B. Vol. 48. Amsterdam: Elsevier, 2007. Chap. 7, pp. 141–169.

[24] Bos, A., Pünt, I. G. M., Wessling, M., and Strathmann, H. "CO_2-induced plasticization phenomena in glassy polymers". Journal of Membrane Science 155 (1999), pp. 67–78.

[25] Breivik, K., Sweetman, A., Pacyna, J. M., and Jones, K. C. "Towards a global historical emission inventory for selected PCB congeners—a mass balance approach: 3. An update". Science of the Total Environment 377 (2007), pp. 296–307.

[26] van der Bruggen, B. "Chemical modification of polyethersulfone nanofiltration membranes: A review". Journal of Applied Polymer Science 114 (2009), pp. 630–642.

[27] Centre for Environmental Modelling and Chemistry. Sediment Model. (2016). URL: http://www.trentu.ca/academic/aminss/envmodel/models/Sedt2.html (visited on 04/01/2016).

[28] Chang, H.-S., Choo, K.-H., Lee, B., and Choi, S.-J. "The methods of identification, analysis, and removal of endocrine disrupting compounds (EDCs) in water". Journal of Hazardous Materials 172 (2009), pp. 1–12.

[29] Chang, P. and Wilke, C. "Some measurements of diffusion in liquids". The Journal of Physical Chemistry 59 (1955), pp. 592–596.

[30] Charriau, A., Lissalde, S., Poulier, G., Mazzella, N., Buzier, R., and Guibaud, G. "Overview of the Chemcatcher® for the passive sampling of various pollutants in aquatic environments Part A: Principles, calibration, preparation and analysis of the sampler". Talanta 148 (2016), pp. 556–571.

[31] Chen, W., Duan, L., and Zhu, D. "Adsorption of polar and nonpolar organic chemicals to carbon nanotubes". Environmental Science & Technology 41 (2007), pp. 8295–8300.

[32] Coes, A. L., Paretti, N. V., Foreman, W. T., Iverson, J. L., and Alvarez, D. A. "Sampling trace organic compounds in water: A comparison of a continuous active sampler to continuous passive and discrete sampling methods". Science of the Total Environment 473 (2014), pp. 731–741.

[33] Diamanti-Kandarakis, E., Bourguignon, J.-P., Giudice, L. C., Hauser, R., Prins, G. S., Soto, A. M., Zoeller, R. T., and Gore, A. C. "Endocrine-disrupting chemicals: An Endocrine Society scientific statement". Endocrine Reviews 30.4 (2009), pp. 293–342.

[34] Ellis, G. S., Rostad, C. E., Huckins, J. N., Schmitt, C. J., Petty, J. D., and MacCarthy, P. "Evaluation of lipid-containing semipermeable membrane devices for monitoring organochlorine contaminants in the Upper Mississippi river". Environmental Toxicology and Chemistry 14 (1995), pp. 1875–1884.

[35] Emelogu, E. S., Pollard, P., Robinson, C. D., Webster, L., McKenzie, C., Napier, F., Steven, L., and Moffat, C. F. "Identification of selected organic

contaminants in streams associated with agricultural activities and comparison between autosampling and silicone rubber passive sampling". Science of the Total Environment 445 (2013), pp. 261–272.

[36] Endo, S. and Goss, K.-U. "Applications of polyparameter linear free energy relationships in environmental chemistry". Environmental Science & Technology 48 (2014), pp. 12477–12491.

[37] Erick, K. M., Hudson, N. N., and Mildred, P. N. "Physico-chemical characteristics and levels of polycyclic aromatic hydrocarbons in untreated water from Ngong river, Kenya". Journal of Pollution Effects & Control 4 (2016), p. 2.

[38] European Commission. Directive 2008/105/EC of the European Parliament and of the Council of 16 December 2008 on environmental quality standards in the field of water policy. (2008). URL: http://eur-lex.europa.eu/legal-content/EN/TXT/?uri=celex:32008L0105 (visited on 04/12/2016).

[39] European Commission. Directive 2013/39/EU of the European Parliament and of the Council amending Directives 2000/60/EC and 2008/105/EC as regards priority substances in the field of water policy. (2013). URL: http://eur-lex.europa.eu/eli/dir/2013/39/oj (visited on 06/12/2016).

[40] European Commission. Guidance Document no. 19 – Common Implementation Strategy for the Water Framework Directive (2000/60/EC). Guidance on surface water chemical monitoring under the Water Framework Directive. Technical Report - 2009 - 025. (2009), p. 132.

[41] European Commission. Polychlorinated biphenyls and polychlorinated terphenyls (PCBs / PCTs). (2016). URL: http://ec.europa.eu/environment/waste/pcbs/ (visited on 04/12/2016).

[42] Fernandez, L. A., Lao, W., Maruya, K. A., and Burgess, R. M. "Calculating the diffusive flux of persistent organic pollutants between sediments and the water column on the Palos Verdes Shelf Superfund site using polymeric

passive samplers". Environmental Science & Technology 48 (2014), pp. 3925–3934.

[43] Gioia, R., Akindele, A. J., Adebusoye, S. A., Asante, K. A., Tanabe, S., Buekens, A., and Sasco, A. J. "Polychlorinated biphenyls (PCBs) in Africa: A review of environmental levels". Environmental Science and Pollution Research 21 (2014), pp. 6278–6289.

[44] Gore, A. C., Chappell, V. A., Fenton, S., Flaws, J. A., Nadal, A., Prins, G. S., Toppari, J., and Zoeller, R. T. "EDC-2: The endocrine society's second scientific statement on endocrine-disrupting chemicals". Endocrine Reviews 36 (2015), E1–E150.

[45] Górecki, T. and Namieśnik, J. "Passive sampling". Trends in Analytical Chemistry 21 (2002), pp. 276–291.

[46] Götz, R., Bauer, O.-H., Friesel, P., Herrmann, T., Jantzen, E., Kutzke, M., Lauer, R., Paepke, O., Roch, K., Rohweder, U., Schwartz, R., Sievers, S., and Stachel, B. "Vertical profile of PCDD/Fs, dioxin-like PCBs, other PCBs, PAHs, chlorobenzenes, DDX, HCHs, organotin compounds and chlorinated ethers in dated sediment/ soil cores from flood-plains of the river Elbe, Germany". Chemosphere 67 (2007), pp. 592–603.

[47] Greenberg, M. S., Chapman, P. M., Allan, I. J., Anderson, K. A., Apitz, S. E., Beegan, C., Bridges, T. S., Brown, S. S., Cargill, J. G., McCulloch, M. C., Menzie, C. A., Shine, J. P., and Parkerton, T. F. "Passive sampling methods for contaminated sediments: Risk assessment and management". Integrated Environmental Assessment and Management 10 (2014), pp. 224–236.

[48] Greenwood, R., Mills, G., and Vrana, B. "Passive Sampling Techniques in Environmental Monitoring". In: Wilson & Wilson´s Comprehensive Analytical Chemistry. Ed. by Barceló, D. Vol. 48. Amsterdam, The Netherlands: Elsevier, 2007. Chap. 7, pp. 141–169.

[49] Guibal, R., Lissalde, S., Charriau, A., and Guibaud, G. "Improvement of POCIS ability to quantify pesticides in natural water by reducing polyethy-

lene glycol matrix effects from polyethersulfone membranes". Talanta 144 (2015), pp. 1316–1323.

[50] Guo, X., Wang, X., Zhou, X., Kong, X., Tao, S., and Xing, B. "Sorption of four hydrophobic organic compounds by three chemically distinct polymers: Role of chemical and physical composition". Environmental Science & Technology 46 (2012), pp. 7252–7259.

[51] Hamers, T., Kamstra, J. H., Sonneveld, E., Murk, A. J., Kester, M. H. A., Andersson, P. L., Legler, J., and Brouwer, A. "In vitro profiling of the endocrine-disrupting potency of brominated flame retardants". Toxicological Sciences 92 (2006), pp. 157–173.

[52] Hansen, C. M. Hansen solubility parameters: A user's handbook. CRC press, 2007.

[53] Hansen, C. M. "On predicting environmental stress cracking in polymers". Polymer Degradation and Stability 77 (2002), pp. 43–53.

[54] Harman, C., Tollefsen, K.-E., Bøyum, O., Thomas, K., and Grung, M. "Uptake rates of alkylphenols, PAHs and carbazoles in semipermeable membrane devices (SPMDs) and polar organic chemical integrative samplers (POCIS)". Chemosphere 72 (2008), pp. 1510–1516.

[55] Hawker, D. W. "Modeling the response of passive samplers to varying ambient fluid concentrations of organic contaminants". Environmental Toxicology and Chemistry 29 (2010), pp. 591–596.

[56] Hawthorne, S. B., Grabanski, C. B., and Miller, D. J. "Measured partition coefficients for parent and alkyl polycyclic aromatic hydrocarbons in 114 historically contaminated sediments: Part 2. Testing the $K_{OC}K_{BC}$ two carbon–type model". Environmental Toxicology and Chemistry 26 (2007), pp. 2505–2516.

[57] Hayduk, W. and Minhas, B. S. "Correlations for prediction of molecular diffusivities in liquids". The Canadian Journal of Chemical Engineering 60 (1982), pp. 295–299.

[58] Hayduk, W. and Laudie, H. “Prediction of diffusion coefficients for nonelectrolytes in dilute aqueous solutions”. AIChE Journal 20 (1974), pp. 611–615.

[59] Huang, W. and Weber Jr., W. “A distributed reactivity model for sorption by soils and sediments. 10. Relationships between desorption, hysteresis, and the chemical characteristics of organic domains”. Environmental Science & Technology 31 (1997), pp. 2562–2569.

[60] Huckins, J. N., Manuweera, G. K., Petty, J. D., Mackay, D., and Lebo, J. A. “Lipid-containing semipermeable membrane devices for monitoring organic contaminants in water”. Environmental Science & Technology 27 (1993), pp. 2489–2496.

[61] Huckins, J. N., Petty, J. D., and Booij, K. Monitors of organic chemicals in the environment: Semipermeable membrane devices. Springer Science & Business Media, 2006.

[62] Huckins, J. N., Petty, J. D., Lebo, J. A., Almeida, F. V., Booij, K., Alvarez, D. A., Cranor, W. L., Clark, R. C., and Mogensen, B. B. “Development of the permeability/performance reference compound approach for in situ calibration of semipermeable membrane devices”. Environmental Science & Technology 36 (2002), pp. 85–91.

[63] IPCS. Global assessment of the state-of-the-science of endocrine disruptors. Report. Geneva, Switzerland, (2002), p. 180.

[64] Ismail, A. F. and Lorna, W. “Penetrant-induced plasticization phenomenon in glassy polymers for gas separation membrane”. Separation and Purification Technology 27 (2002), pp. 173–194.

[65] Jermann, D., Pronk, W., Boller, M., and Schäfer, A. I. “The role of NOM fouling for the retention of estradiol and ibuprofen during ultrafiltration”. Journal of Membrane Science 329 (2009), pp. 75–84.

[66] Jiménez, E. I. and García, V. P. “Relationships between organic carbon and total organic matter in municipal solid wastes and city refuse composts”. Bioresource Technology 41 (1992), pp. 265–272.

[67] Jones, K. C. and De Voogt, P. “Persistent organic pollutants (POPs): State of the science”. Environmental Pollution 100 (1999), pp. 209–221.

[68] Jones, S., Boisvert, A., Naghi, A., Hullin-Matsuda, F., Greimel, P., Kobayashi, T., Papadopoulos, V., and Culty, M. “Stimulatory effects of combined endocrine disruptors on MA-10 Leydig cell steroid production and lipid homeostasis”. Toxicology 355 (2016), pp. 21–30.

[69] Karickhoff, S. W. “Semi-empirical estimation of sorption of hydrophobic pollutants on natural sediments and soils”. Chemosphere 10 (1981), pp. 833–846.

[70] Kato, Y., Haraguchi, K., Ito, Y., Fujii, A., Yamazaki, T., Endo, T., Koga, N., Yamada, S., and Degawa, M. “Polychlorinated biphenyl-mediated decrease in serum thyroxine level in rodents”. Drug Metabolism and Disposition 38 (2010), pp. 697–704.

[71] Kingston, J. K., Greenwood, R., Mills, G. A., Morrison, G. M., and Persson, L. B. “Development of a novel passive sampling system for the time-averaged measurement of a range of organic pollutants in aquatic environments”. Journal of Environmental Monitoring 2 (2000), pp. 487–495.

[72] Klánová, J., Čupr, P., Holoubek, I., Borůvková, J., Přibylová, P., Kareš, R., Tomšej, T., and Ocelka, T. “Monitoring of persistent organic pollutants in Africa. Part 1: Passive air sampling across the continent in 2008”. Journal of Environmental Monitoring 11 (2009), pp. 1952–1963.

[73] Koch, H. M., Lorber, M., Christensen, K. L., Pälmke, C., Koslitz, S., and Brüning, T. “Identifying sources of phthalate exposure with human biomonitoring: Results of a 48h fasting study with urine collection and personal activity patterns”. International Journal of Hygiene and Environmental Health 216 (2013), pp. 672–681.

[74] Kojima, H., Katsura, E., Takeuchi, S., Niiyama, K., and Kobayashi, K. “Screening for estrogen and androgen receptor activities in 200 pesticides by in

vitro reporter gene assays using Chinese hamster ovary cells". Environmental Health Perspectives 112 (2004), p. 524.

[75] Krimsky, S. "An epistemological inquiry into the endocrine disruptor thesis". Annals of the New York Academy of Sciences 948 (2001), pp. 130–142.

[76] Kuiper, G. G. J. M., Lemmen, J. G., Carlsson, B., Corton, J. C., Safe, S. H., van der Saag, P. T., van der Burg, B., and Gustafsson, J.-Å. "Interaction of estrogenic chemicals and phytoestrogens with estrogen receptor ". Endocrinology 139 (1998), pp. 4252–4263.

[77] Länge, R., Hutchinson, T. H., Croudace, C. P., Siegmund, F., Schweinfurth, H., Hampe, P., Panter, G. H., and Sumpter, J. P. "Effects of the synthetic estrogen 17α-ethinylestradiol on the life-cycle of the fathead minnow (Pimephales promelas)". Environmental Toxicology and Chemistry 20 (2001), pp. 1216–1227.

[78] Leaños-Castañeda, O., Van Der Kraak, G., Rodríguez-Canul, R., and Gold, G. "Endocrine disruption mechanism of o, p -DDT in mature male tilapia (Oreochromis niloticus)". Toxicology and Applied Pharmacology 221 (2007), pp. 158–167.

[79] Lebo, J. A., Gale, R. W., Petty, J. D., Tillitt, D. E., Huckins, J. N., Meadows, J. C., Orazio, C. E., Echols, K. R., Schroeder, D. J., and Inmon, L. E. "Use of the semipermeable membrane device as an in situ sampler of waterborne bioavailable PCDD and PCDF residues at sub-parts-per-quadrillion concentrations". Environmental Science & Technology 29 (1995), pp. 2886–2892.

[80] Lemaire, G., Mnif, W., Mauvais, P., Balaguer, P., and Rahmani, R. "Activation of α-and β-estrogen receptors by persistent pesticides in reporter cell lines". Life Sciences 79 (2006), pp. 1160–1169.

[81] Levine, H. and Slade, L. "Water as a plasticizer: Physico-chemical aspects of low-moisture polymeric systems". Water Science Reviews 3 (1988), pp. 79–185.

[82] Lick, W. “The sediment-water flux of HOCs due to “diffusion” or is there a well-mixed layer? If there is, does it matter?” Environmental Science & Technology 40 (2006), pp. 5610–5617.

[83] Lintelmann, J., Katayama, A., Kurihara, N., Shore, L., and Wenzel, A. “Endocrine disruptors in the environment (IUPAC Technical Report)”. Pure and Applied Chemistry 75 (2003), pp. 631–681.

[84] Lohmann, R. “Critical review of low-density polyethylene’s partitioning and diffusion coefficients for trace organic contaminants and implications for its use as a passive sampler”. Environmental Science & Technology 46 (2011), pp. 606–618.

[85] Lohmann, R., Booij, K., Smedes, F., and Vrana, B. “Use of passive sampling devices for monitoring and compliance checking of POP concentrations in water”. Environmental Science and Pollution Research 19 (2012), pp. 1885–1895.

[86] Lu, Y. and Pignatello, J. J. “Demonstration of the “conditioning effect” in soil organic matter in support of a pore deformation mechanism for sorption hysteresis”. Environmental Science & Technology 36 (2002), pp. 4553–4561.

[87] Lu, Y. and Pignatello, J. J. “History-dependent sorption in humic acids and a lignite in the context of a polymer model for natural organic matter”. Environmental Science & Technology 38 (2004), pp. 5853–5862.

[88] Lydy, M. J., Landrum, P. F., Oen, A. M., Allinson, M., Smedes, F., Harwood, A. D., Li, H., Maruya, K. A., and Liu, J. “Passive sampling methods for contaminated sediments: State of the science for organic contaminants”. Integrated Environmental Assessment and Management 10 (2014), pp. 167–178.

[89] Mackay, D. Multimedia environmental models: The fugacity approach. CRC press, 2001, p. 272.

[90] Mackay, D., Arnot, J. A., Webster, E., and Reid, L. "The evolution and future of environmental fugacity models". In: Ecotoxicology Modeling. Springer, 2009, pp. 355–375.

[91] Mackay, D., Shiu, W.-Y., Ma, K.-C., and Lee, S. C. Handbook of physical-chemical properties and environmental fate for organic chemicals. CRC press, 2006.

[92] Mader, B. T., Uwe-Goss, K., and Eisenreich, S. J. "Sorption of nonionic, hydrophobic organic chemicals to mineral surfaces". Environmental Science & Technology 31 (1997), pp. 1079–1086.

[93] Magdouli, S., Daghrir, R., Brar, S. K., Drogui, P., and Tyagi, R. D. "Di 2-ethylhexylphtalate in the aquatic and terrestrial environment: A critical review". Journal of Environmental Management 127 (2013), pp. 36–49.

[94] Mariana, M., Feiteiro, J., Verde, I., and Cairrao, E. "The effects of phthalates in the cardiovascular and reproductive systems: A review". Environment International 94 (2016), pp. 758–776.

[95] Martin, L. and Klaassen, C. D. "Differential effects of polychlorinated biphenyl congeners on serum thyroid hormone levels in rats". Toxicological Sciences 117 (2010), pp. 36–44.

[96] Mayer, P., Parkerton, T. F., Adams, R. G., Cargill, J. G., Gan, J., Gouin, T., Gschwend, P. M., Hawthorne, S. B., Helm, P., Witt, G., You, J., and Escher, B. I. "Passive sampling methods for contaminated sediments: Scientific rationale supporting use of freely dissolved concentrations". Integrated Environmental Assessment and Management 10 (2014), pp. 197–209.

[97] Mayer, P., Tolls, J., Hermens, J. L., and Mackay, D. "Peer reviewed: Equilibrium sampling devices". Environmental Science & Technology 37 (2003), 184A–191A.

[98] Meerts, I., Letcher, R. J., Hoving, S., Marsh, G., Bergman, A., Lemmen, J. G., Burg, B. van der, and Brouwer, A. "In vitro estrogenicity of polybromi-

nated diphenyl ethers, hydroxylated PDBEs, and polybrominated bisphenol A compounds." Environmental Health Perspectives 109 (2001), p. 399.

[99] Miège, C., Mazzella, N., Allan, I., Dulio, V., Smedes, F., Tixier, C., Vermeirssen, E., Brant, J., O'Toole, S., Budzinski, H., Ghestem, J.-P., Staub, P.-F., Lardy-Fontan, S., Gonzalez, J.-. L., Coquery, M., and Vrana, B. "Position paper on passive sampling techniques for the monitoring of contaminants in the aquatic environment–Achievements to date and perspectives". Trends in Environmental Analytical Chemistry 8 (2015), pp. 20–26.

[100] Monteiro, P. R. R., Reis-Henriques, M. A., and Coimbra, J. "Polycyclic aromatic hydrocarbons inhibit in vitro ovarian steroidogenesis in the flounder (Platichthys flesus L.)" Aquatic Toxicology 48 (2000), pp. 549–559.

[101] Monteyne, E., Roose, P., and Janssen, C. R. "Application of a silicone rubber passive sampling technique for monitoring PAHs and PCBs at three Belgian coastal harbours". Chemosphere 91 (2013), pp. 390–398.

[102] Münze, R., Orlinskiy, P., Gunold, R., Paschke, A., Kaske, O., Beketov, M. A., Hundt, M., Bauer, C., Schüürmann, G., Möder, M., and Liess, M. "Pesticide impact on aquatic invertebrates identified with Chemcatcher® passive samplers and the {SPEARpesticides} index". Science of The Total Environment 537 (2015), pp. 69–80.

[103] Net, S., Delmont, A., Sempéré, R., Paluselli, A., and Ouddane, B. "Reliable quantification of phthalates in environmental matrices (air, water, sludge, sediment and soil): A review". Science of The Total Environment 515–516 (2015), pp. 162–180.

[104] Oakley, G. G., Devanaboyina, U.-s., Robertson, L. W., and Gupta, R. C. "Oxidative DNA damage induced by activation of polychlorinated biphenyls (PCBs): Implications for PCB-induced oxidative stress in breast cancer". Chemical Research in Toxicology 9 (1996), pp. 1285–1292.

[105] Orton, F., Rosivatz, E., Scholze, M., and Kortenkamp, A. "Widely used pesticides with previously unknown endocrine activity revealed as in vitro antiandrogens". Environmental Health Perspectives 119 (2011), p. 794.

[106] Othmer, D. F. and Thakar, M. S. "Correlating diffusion coefficient in liquids". Industrial & Engineering Chemistry 45 (1953), pp. 589–593.

[107] Otte, J. C., Keiter, S., Faßbender, C., Higley, E. B., Rocha, P. S., Brinkmann, M., Wahrendorf, D.-. S., Manz, W., Wetzel, M. A., Braunbeck, T., Giesy, J. P., Hecker, M., and Hollert, H. "Contribution of priority PAHs and POPs to Ah receptor-mediated activities in sediment samples from the River Elbe Estuary, Germany". PloS one 8 (2013), e75596.

[108] Ouyang, G. and Pawliszyn, J. "SPME in environmental analysis". Analytical and Bioanalytical Chemistry 386 (2006), pp. 1059–1073.

[109] Pan, B., Lin, D., Mashayekhi, H., and Xing, B. "Adsorption and hysteresis of bisphenol A and 17α-ethinyl estradiol on carbon nanomaterials". Environmental Science & Technology 42 (2008), pp. 5480–5485.

[110] Paris, F., Balaguer, P., Térouanne, B., Servant, N., Lacoste, C., Cravedi, J.-P., Nicolas, J.-C., and Sultan, C. "Phenylphenols, biphenols, bisphenol-A and 4-tert-octylphenol exhibit α and β estrogen activities and antiandrogen activity in reporter cell lines". Molecular and Cellular Endocrinology 193 (2002), pp. 43–49.

[111] Paschke, A., Vrana, B., Popp, P., Wennrich, L., Paschke, H., and Schüürmann, G. "Membrane-enclosed sorptive coating for the monitoring of organic compounds in water". Comprehensive Analytical Chemistry 48 (2007), pp. 231–249.

[112] Pasqualini, C., Sarrieau, A., Dussaillant, M., Corbani, M., Bojda-Diolez, F., Rostène, W., and Kerdelhué, B. "Estrogen-like effects of 7,12-Dimethylbenz (a) anthracene on the female rat hypothalamo-pituitary axis". Journal of Steroid Biochemistry 36 (1990), pp. 485–491.

[113] Patrick, S. M., Bornman, M. S., Joubert, A. M., Pitts, N., Naidoo, V., and Jager, C. de. "Effects of environmental endocrine disruptors, including insecticides used for malaria vector control on reproductive parameters of male rats". Reproductive Toxicology 61 (2016), pp. 19–27.

[114] Pawlowski, S., Van Aerle, R., Tyler, C. R., and Braunbeck, T. "Effects of 17α-ethinylestradiol in a fathead minnow (Pimephales promelas) gonadal recrudescence assay". Ecotoxicology and Environmental Safety 57 (2004), pp. 330–345.

[115] Petersen, J., Paschke, A., Gunold, R., and Schüürmann, G. "Calibration of Chemcatcher® passive sampler for selected highly hydrophobic organic substances under fresh and sea water conditions". Environmental Science: Water Research & Technology 1 (2015), pp. 218–226.

[116] Pianosi, F., Beven, K., Freer, J., Hall, J. W., Rougier, J., Stephenson, D. B., and Wagener, T. "Sensitivity analysis of environmental models: A systematic review with practical workflow". Environmental Modelling & Software 79 (2016), pp. 214–232.

[117] Pies, C., Yang, Y., and Hofmann, T. "Distribution of polycyclic aromatic hydrocarbons (PAHs) in floodplain soils of the Mosel and Saar River". Journal of Soils and Sediments 7 (2007), pp. 216–222.

[118] Pignatello, J. J. and Xing, B. "Mechanisms of slow sorption of organic chemicals to natural particles". Environmental Science & Technology 30 (1996), pp. 1–11.

[119] Posada-Ureta, O., Olivares, M., Delgado, A., Prieto, A., Vallejo, A., Irazola, M., Paschke, A., and Etxebarria, N. "Applicability of polydimethylsiloxane (PDMS) and polyethersulfone (PES) as passive samplers of more hydrophobic organic compounds in intertidal estuarine environments". Science of The Total Environment 578 (2017), pp. 392–398.

[120] Posada-Ureta, O., Olivares, M., Zatón, L., Delgado, A., Prieto, A., Vallejo, A., Paschke, A., and Etxebarria, N. "Uptake calibration of polymer-based passive

samplers for monitoring priority and emerging organic non-polar pollutants in WWTP effluents". Analytical and Bioanalytical Chemistry 408 (2016), pp. 3165–3175.

[121] Poulier, G., Lissalde, S., Charriau, A., Buzier, R., Delmas, F., Gery, K., Moreira, A., Guibaud, G., and Mazzella, N. "Can POCIS be used in Water Framework Directive (2000/60/EC) monitoring networks? A study focusing on pesticides in a French agricultural watershed". Science of the Total Environment 497 (2014), pp. 282–292.

[122] Prieto, A., Rodil, R., Quintana, J. B., Cela, R., Möder, M., and Rodríguez, I. "Evaluation of polyethersulfone performance for the microextraction of polar chlorinated herbicides from environmental water samples". Talanta 122 (2014), pp. 264–271.

[123] Prieto, A., Rodil, R., Quintana, J. B., Rodríguez, I., Cela, R., and Möder, M. "Evaluation of low-cost disposable polymeric materials for sorptive extraction of organic pollutants in water samples". Analytica chimica acta 716 (2012), pp. 119–127.

[124] Prokeš, R., Vrana, B., and Klánová, J. "Levels and distribution of dissolved hydrophobic organic contaminants in the Morava river in Zlin district, Czech Republic as derived from their accumulation in silicone rubber passive samplers". Environmental Pollution 166 (2012), pp. 157–166.

[125] Reichenberg, F. and Mayer, P. "Two complementary sides of bioavailability: Accessibility and chemical activity of organic contaminants in sediments and soils". Environmental Toxicology and Chemistry 25 (2006), pp. 1239–1245.

[126] Rochman, C. M., Hoh, E., Hentschel, B. T., and Kaye, S. "Long-term field measurement of sorption of organic contaminants to five types of plastic pellets: Implications for plastic marine debris". Environmental Science & Technology 47 (2013), pp. 1646–1654.

[127] Rodriguez-Mozaz, S., Marco, M.-P., Alda, M. J. L. de, and Barceló, D. "Biosensors for environmental monitoring of endocrine disruptors: A review article". Analytical and Bioanalytical Chemistry 378 (2004), pp. 588–598.

[128] Roll, I. B. and Halden, R. U. "Critical review of factors governing data quality of integrative samplers employed in environmental water monitoring". Water Research 94 (2016), pp. 200–207.

[129] Ros, O., Aguirre, J., Prieto, A., Olivares, M., Etxebarria, N., and Vallejo, A. "Simultaneous enzymatic hydrolysis and extraction of endocrine-disrupting chemicals in fish bile using polyethersulfone polymer". Analytical and Bioanalytical Chemistry 407 (2015), pp. 7413–7423.

[130] Rusina, T. P., Smedes, F., and Klanova, J. "Diffusion coefficients of polychlorinated biphenyls and polycyclic aromatic hydrocarbons in polydimethylsiloxane and low-density polyethylene polymers". Journal of Applied Polymer Science 116 (2010), pp. 1803–1810.

[131] Rusina, T. P., Smedes, F., Klanova, J., Booij, K., and Holoubek, I. "Polymer selection for passive sampling: A comparison of critical properties". Chemosphere 68 (2007), pp. 1344–1351.

[132] Rusina, T. P., Smedes, F., Koblizkova, M., and Klanova, J. "Calibration of silicone rubber passive samplers: Experimental and modeled relations between sampling rate and compound properties". Environmental Science & Technology 44 (2010), pp. 362–367.

[133] Santodonato, J. "Review of the estrogenic and antiestrogenic activity of polycyclic aromatic hydrocarbons: Relationship to carcinogenicity". Chemosphere 34 (1997), pp. 835–848.

[134] Saquing, J. M., Saquing, C. D., Knappe, D. R. U., and Barlaz, M. A. "Impact of plastics on fate and transport of organic contaminants in landfills". Environmental Science & Technology 44 (2010), pp. 6396–6402.

[135] Schlezinger, J. J., Liu, D., Farago, M., Seldin, D. C., Belguise, K., Sonenshein, G. E., and Sherr, D. H. "A role for the aryl hydrocarbon receptor in mammary gland tumorigenesis". Biological Chemistry 387 (2006), pp. 1175–1187.

[136] Schreiber, T., Gassmann, K., Götz, C., Hübenthal, U., Moors, M., Krause, G., Merk, H. F., Nguyen, N.-H., Scanlan, T. S., Abel, J., Rose, C. R., and Fritsche, E. "Polybrominated diphenyl ethers induce developmental neurotoxicity in a human in vitro model: Evidence for endocrine disruption". Environmental Health Perspectives 118 (2010), p. 572.

[137] Schug, T. T., Blawas, A. M., Gray, K., Heindel, J. J., and Lawler, C. P. "Elucidating the links between endocrine disruptors and neurodevelopment". Endocrinology 156 (2015), pp. 1941–1951.

[138] Schult, K. A. and Paul, D. R. "Water sorption and transport in a series of polysulfones". Journal of Polymer Science Part B: Polymer Physics 34 (1996), pp. 2805–2817.

[139] Schult, K. A. and Paul, D. R. "Water sorption and transport in blends of polyethyloxazoline and polyethersulfone". Journal of Polymer Science Part B: Polymer Physics 35 (1997), pp. 993–1007.

[140] Schwarzenbach, R. P., Gschwend, P. M., and Imboden, D. M. Environmental organic chemistry. John Wiley & Sons, 2003.

[141] Shanle, E. K. and Xu, W. "Endocrine disrupting chemicals targeting estrogen receptor signaling: Identification and mechanisms of action". Chemical Research in Toxicology 24 (2010), pp. 6–19.

[142] Shi, X., Tal, G., Hankins, N. P., and Gitis, V. "Fouling and cleaning of ultrafiltration membranes: A review". Journal of Water Process Engineering 1 (2014), pp. 121–138.

[143] Skakkebaek, N. E., Rajpert-De Meyts, E., and Main, K. M. "Testicular dysgenesis syndrome: An increasingly common developmental disorder with environmental aspects: Opinion". Human Reproduction 16 (2001), pp. 972–978.

[144] Skinner, M. K., Manikkam, M., Tracey, R., Guerrero-Bosagna, C., Haque, M., and Nilsson, E. E. "Ancestral dichlorodiphenyltrichloroethane (DDT) exposure promotes epigenetic transgenerational inheritance of obesity". BMC medicine 11 (2013), p. 1.

[145] Smedes, F., Bakker, D., and de Weert, J. The use of passive sampling in WFD monitoring. The possibilities of silicone rubber as a passive sampler. Report. Deltares, 2010, pp. 59–59.

[146] Smedes, F. and Booij, K. Guidelines for passive sampling of hydrophobic contaminants in water using silicone rubber samplers. ICES Techniques in Marine Environmental Sciences. 2012, p. 20.

[147] Smedes, F., Geertsma, R. W., van der Zande, T., and Booij, K. "Polymer-water partition coefficients of hydrophobic compounds for passive sampling: Application of cosolvent models for validation". Environmental Science & Technology 43 (2009), pp. 7047–7054.

[148] Sohoni, P. and Sumpter, J. P. "Several environmental oestrogens are also anti-androgens". Journal of Endocrinology 158 (1998), pp. 327–339.

[149] SRC. FatePointers Search Module. 2015. URL: `http://esc.syrres.com/fatepointer/search.asp` (visited on 11/05/2015).

[150] Ssebugere, P., Kiremire, B. T., Henkelmann, B., Bernhöft, S., Kasozi, G. N., Wasswa, J., and Schramm, K.-W. "PCDD/Fs and dioxin-like PCBs in fish species from Lake Victoria, East Africa". Chemosphere 92 (2013), pp. 317–321.

[151] Ssebugere, P., Kiremire, B. T., Henkelmann, B., Bernhöft, S., Wasswa, J., Kasozi, G. N., and Schramm, K.-W. "PCDD/Fs and dioxin-like PCBs in surface sediments from Lake Victoria, East Africa". Science of the Total Environment 454 (2013), pp. 528–533.

[152] Stachel, B., Christoph, E.-H., Götz, R., Herrmann, T., Krüger, F., T., K., Lay, J., Löffler, J., Päpke, O., Reincke, H., Schröter-Kermani, C. ., Schwartz, R., Steeg, E., Stehr, D., Uhlig, S., and Umlauf, G. "Dioxins and dioxin-like

{PCBs} in different fish from the river Elbe and its tributaries, Germany". Journal of Hazardous Materials 148 (2007), pp. 199–209.

[153] Staples, C. A., Peterson, D. R., Parkerton, T. F., and Adams, W. J. "The environmental fate of phthalate esters: A literature review". Chemosphere 35 (1997), pp. 667–749.

[154] Sun, H., Qi, Y., Zhang, D., Li, Q. X., and Wang, J. "Concentrations, distribution, sources and risk assessment of organohalogenated contaminants in soils from Kenya, Eastern Africa". Environmental Pollution 209 (2016), pp. 177–185.

[155] Swan, S. H., Main, K. M., Liu, F., Stewart, S. L., Kruse, R. L., Calafat, A. M., Mao, C. S., Redmon, J. B., Ternand, C. L., Sullivan, S., and Lynn, T. J. "Decrease in anogenital distance among male infants with prenatal phthalate exposure". Environmental Health Perspectives 113 (2005), pp. 1056–1061.

[156] Tabb, M. M. and Blumberg, B. "New modes of action for endocrine-disrupting chemicals". Molecular Endocrinology 20 (2006), pp. 475–482.

[157] Takeuchi, S., Shiraishi, F., Kitamura, S., Kuroki, H., Jin, K., and Kojima, H. "Characterization of steroid hormone receptor activities in 100 hydroxylated polychlorinated biphenyls, including congeners identified in humans". Toxicology 289 (2011), pp. 112–121.

[158] Teuten, E. L., Saquing, J. M., Knappe, D. R. U., Barlaz, M. A., Jonsson, S., Björn, A., Rowland, S. J., Thompson, R. C., Galloway, T. S., Yamashita, R., Ochi, D., Watanuki, Y., Moore, C., Viet, P. H., Tana, T. S., Prudente, M., Boonyatumanond, R., Zakaria, M. P., Akkhavong, K., Ogata, Y., Hirai, H., Iwasa, S., Mizukawa, K., Hagino, Y., Imamura, A., Saha, M., and Takada, H. "Transport and release of chemicals from plastics to the environment and to wildlife". Philosophical Transactions of the Royal Society B 364 (2009), pp. 2027–2045.

[159] Tran, A. T., Hyne, R. V., and Doble, P. "Calibration of a passive sampling device for time-integrated sampling of hydrophilic herbicides in aquatic en-

vironments". Environmental Toxicology and Chemistry 26 (2007), pp. 435–443.

[160] UNEP. A snapshot of the world's water quality: Towards a global assessment. Report. Nairobi, Kenya, (2016), p. 162.

[161] UNEP. Phasing out DDT. (2016). URL: http://www.unep.org/chemicalsandwaste/POPs/ChemicalsManagementandReduction/PhasingoutDDT/tabid/1061105/Default.aspx (visited on 09/25/2016).

[162] Vallejo, A., Prieto, A., Moeder, M., Usobiaga, A., Zuloaga, O., Etxebarria, N., and Paschke, A. "Calibration and field test of the Polar Organic Chemical Integrative Samplers for the determination of 15 endocrine disrupting compounds in wastewater and river water with special focus on performance reference compounds (PRC)". Water Research 47 (2013), pp. 2851–2862.

[163] Ventrice, P., Ventrice, D., Russo, E., and De Sarro, G. "Phthalates: European regulation, chemistry, pharmacokinetic and related toxicity". Environmental Toxicology and Pharmacology 36 (2013), pp. 88–96.

[164] Vermeirssen, E. L., Bramaz, N., Hollender, J., Singer, H., and Escher, B. I. "Passive sampling combined with ecotoxicological and chemical analysis of pharmaceuticals and biocides–evaluation of three Chemcatcher™ configurations". Water Research 43 (2009), pp. 903–914.

[165] Vermeirssen, L. M. E., Dietschweiler, C., Escher, B. I., van der Voet, J., and Hollender, J. "Transfer kinetics of polar organic compounds over polyethersulfone membranes in the passive samplers POCIS and Chemcatcher". Environmental Science & Technology 46 (2012), pp. 6759–6766.

[166] Vrana, B., Allan, I. J., Greenwood, R., Mills, G. A., Dominiak, E., Svensson, K., Knutsson, J., and Morrison, G. "Passive sampling techniques for monitoring pollutants in water". Trends in Analytical Chemistry 24 (2005), pp. 845–868.

[167] Vrana, B., Mills, G. A., Leonards, P. E. G., Kotterman, M., Weideborg, M., Hajslova, J., Kocourek, V., Tomaniova, M., Pulkrabova, J., Suchanova, M.,

Hajkova, K., Herve, S., Ahkola, H., and Greenwood, R. “Field performance of the Chemcatcher passive sampler for monitoring hydrophobic organic pollutants in surface water”. Journal of Environmental Monitoring 12 (2010), pp. 863–872.

[168] Vrana, B., Paschke, A., and Popp, P. “Calibration and field performance of membrane-enclosed sorptive coating for integrative passive sampling of persistent organic pollutants in water”. Environmental Pollution 144 (2006), pp. 296–307.

[169] Vrana, B., Paschke, A., and Popp, P. “Polyaromatic hydrocarbon concentrations and patterns in sediments and surface water of the Mansfeld region, Saxony-Anhalt, Germany”. Journal of Environmental Monitoring 3 (2001), pp. 602–609.

[170] Vrana, B., Paschke, A., Popp, P., and Schüürmann, G. “Use of semipermeable membrane devices (SPMDs)”. Environmental Science and Pollution Research 8 (2001), pp. 27–34.

[171] Wandiga, S. O., Yugi, P. O., Barasa, M. W., Jumba, I. O., and Lalah, J. O. “The distribution of organochlorine pesticides in marine samples along the Indian Ocean coast of Kenya”. Environmental Technology 23 (2002), pp. 1235–1246.

[172] Wang, I.-J., Karmaus, W. J., Chen, S.-L., Holloway, J. W., and Ewart, S. “Effects of phthalate exposure on asthma may be mediated through alterations in DNA methylation”. Clinical Epigenetics 7 (2015), p. 1.

[173] Weber, W. J. and Morris, J. C. “Kinetics of Adsorption on Carbon from Solution”. Journal of the Sanitary Engineering Division 89 (1963), pp. 31–60.

[174] White, R., Jobling, S., Hoare, S. A., Sumpter, J. P., and Parker, M. G. “Environmentally persistent alkylphenolic compounds are estrogenic”. Endocrinology 135 (1994), pp. 175–182.

[175] WHO-UNEP. State-of-the-science of endocrine disrupting chemicals. Report. Nairobi & Geneva, (2012), p. 289.

[176] Worch, E. “Eine neue Gleichung zur Berechnung von Diffusionskoeffizienten gelöster Stoffe”. Vom Wasser 81 (1993), pp. 289–297.

[177] World Bank. Africa Stockpiles Programme - Project 1. (2012). URL: http://www.worldbank.org/projects/P075776/africa-stockpiles-programme-project-1?lang=en (visited on 10/01/2016).

[178] Wu, F.-C., Tseng, R.-L., and Juang, R.-S. “Initial behavior of intraparticle diffusion model used in the description of adsorption kinetics”. Chemical Engineering Journal 153 (1–8), p. 2009.

[179] Xing, B. and Pignatello, J. J. “Dual-mode sorption of low-polarity compounds in glassy poly (vinyl chloride) and soil organic matter”. Environmental Science & Technology 31 (1997), pp. 792–799.

[180] Yates, K., Davies, I., Webster, L., Pollard, P., Lawton, L., and Moffat, C. “Passive sampling: Partition coefficients for a silicone rubber reference phase”. Journal of Environmental Monitoring 9 (2007), pp. 1116–1121.

[181] Ye, T., Kang, M., Huang, Q., Fang, C., Chen, Y., Shen, H., and Dong, S. “Exposure to DEHP and MEHP from hatching to adulthood causes reproductive dysfunction and endocrine disruption in marine medaka (Oryzias melastigma)”. Aquatic Toxicology 146 (2014), pp. 115–126.

[182] Zama, A. M. and Uzumcu, M. “Fetal and neonatal exposure to the endocrine disruptor methoxychlor causes epigenetic alterations in adult ovarian genes”. Endocrinology 150 (2009), pp. 4681–4691.

[183] Zhao, C., Xue, J., Ran, F., and Sun, S. “Modification of polyethersulfone membranes–A review of methods”. Progress in Materials Science 58 (2013), pp. 76–150.

[184] Zolfaghari, M., Drogui, P., Seyhi, B., Brar, S. K., Buelna, G., and Dubé, R. “Occurrence, fate and effects of Di (2-ethylhexyl) phthalate in wastewater treatment plants: A review”. Environmental Pollution 194 (2014), pp. 281–293.

Appendices

A Structures of the target compounds

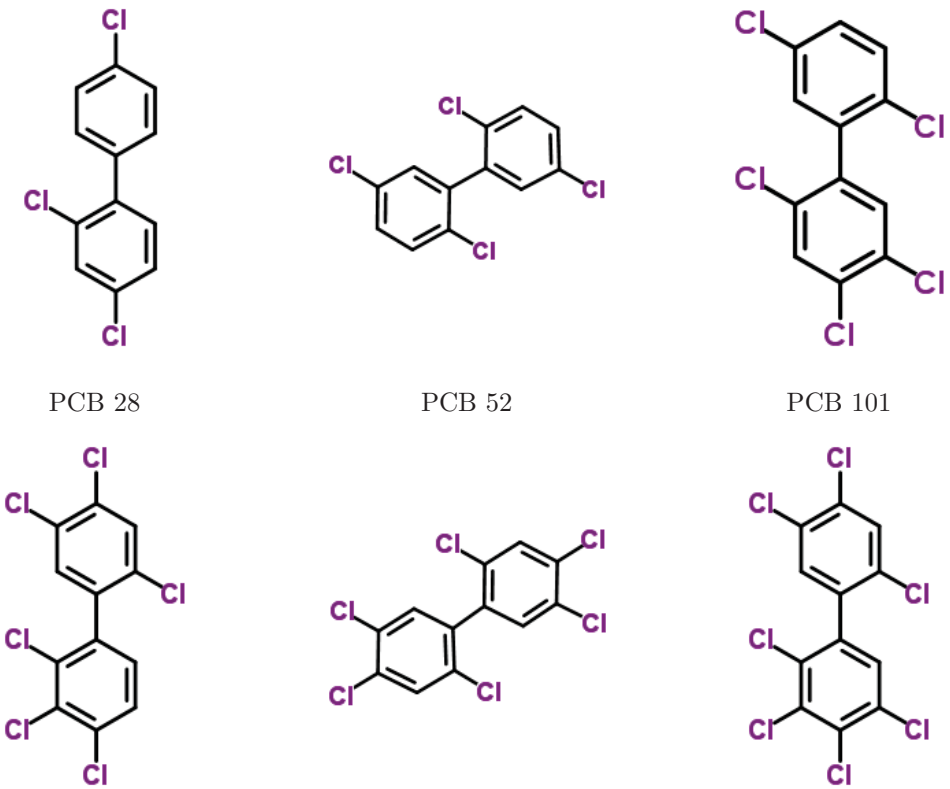

Figure A.1: Structures of PCBs .

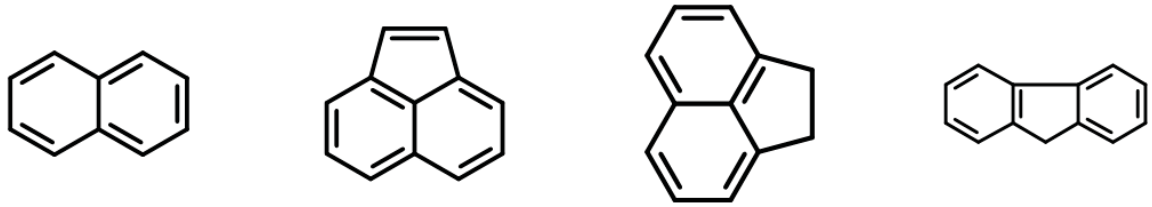

Naphthalene Acenaphthylene Acenaphthene Fluorene

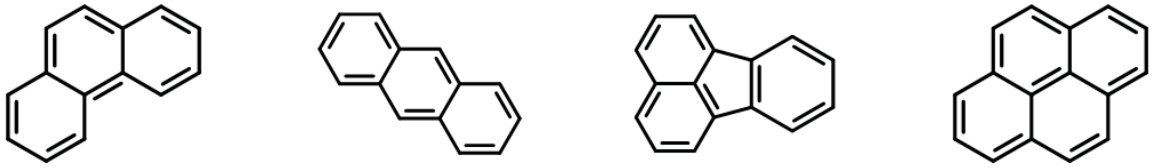

Phenanthrene Anthracene Fluoranthene Pyrene

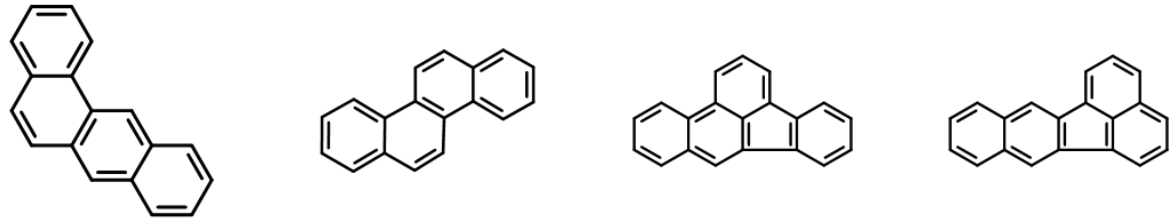

Benz(a)anthracene Chrysene Benzo(b)fluoranthene Benzo(k)fluoranthene

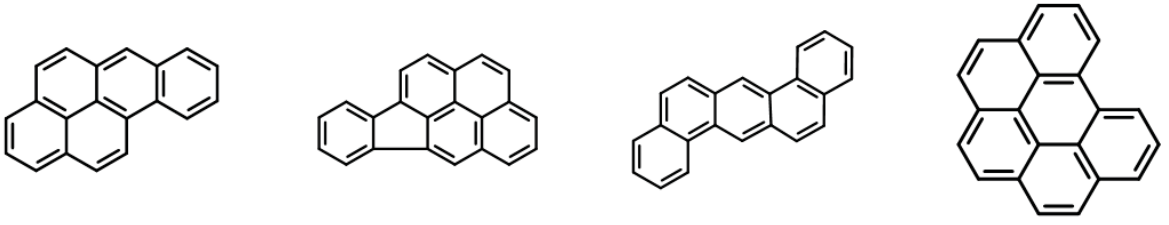

Benzo(a)pyrene Indeno(1,2,3-cd)pyrene Dibenz(a,h)anthracene Benzo(ghi)perylene

Figure A.2: Structures of PAHs.

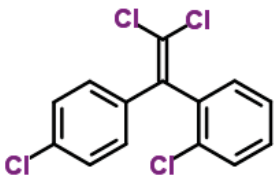

O,P' DDE

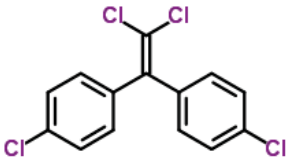

P,P' DDE

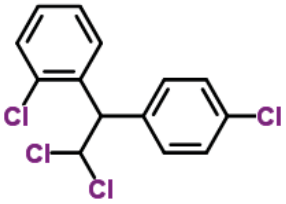

O,P' DDD

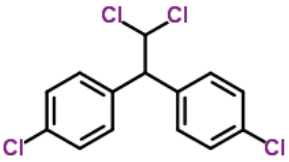

P,P' DDD

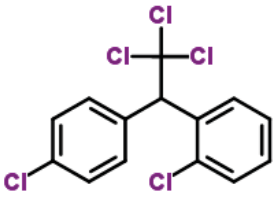

O,P' DDT

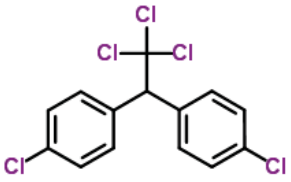

P,P' DDT

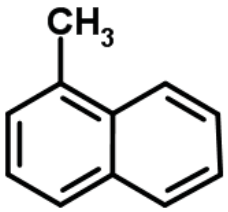

1-Methylnaphthalene

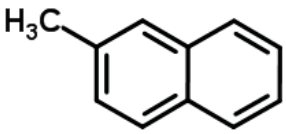

2-Methylnaphthalene

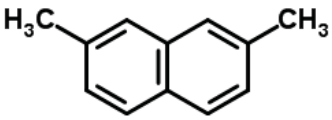

2,7-Dimethylnaphthalene

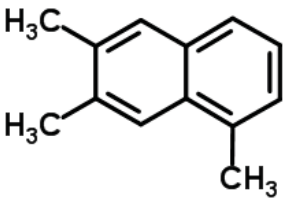

1,6,7-Trimethylnaphthalene

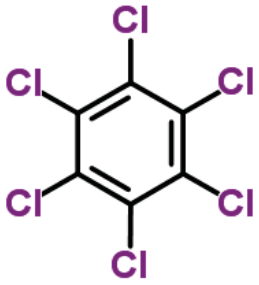

Hexachlorobenzene

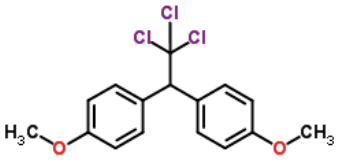

Methoxychlor

Figure A.3: Structures of DDXs, alkylated naphthalenes, hexachlorobenzene and methoxychlor.

B Derivation of equations

Derivation of equation 2.13

To derive equation 2.13, the starting point is equation 2.12 and follows the procedure outlined below.

$$\frac{dC_{\mathrm{p}}}{dt} = \frac{k_{\mathrm{o}}A}{m}\left(C_{\mathrm{w}} - \frac{C_{\mathrm{p}}}{K_{\mathrm{pw}}}\right)$$

Removing the denominator from the term in brackets gives:

$$\frac{dC_{\mathrm{p}}}{dt} = \frac{k_{\mathrm{o}}A}{m} \cdot \frac{1}{K_{\mathrm{pw}}}\left(C_{\mathrm{w}}K_{\mathrm{pw}} - C_{\mathrm{p}}\right)$$

Let $k_{\mathrm{ex}} = \frac{k_{\mathrm{o}}A}{K_{\mathrm{pw}}m}$, and consider a case where water concentrations, C_{w}, decrease linearly with time such that $C_{\mathrm{w}} = \mathrm{a} - \mathrm{b}t$, where a and b are constants. Substituting these in the equation above gives:

$$\frac{dC_{\mathrm{p}}}{dt} = k_{\mathrm{ex}}\left[K_{\mathrm{pw}}\left(\mathrm{a} - \mathrm{b}t\right) - C_{\mathrm{p}}\right]$$

$$\frac{dC_{\mathrm{p}}}{dt} = k_{\mathrm{ex}}K_{\mathrm{pw}}\mathrm{a} - k_{\mathrm{ex}}K_{\mathrm{pw}}\mathrm{b}t - k_{\mathrm{ex}}C_{\mathrm{p}}$$

Let the term on the right–hand–side of the equation be z. Then,

$$\frac{dC_{\mathrm{p}}}{dt} = z = k_{\mathrm{ex}}K_{\mathrm{pw}}\mathrm{a} - k_{\mathrm{ex}}K_{\mathrm{pw}}\mathrm{b}t - k_{\mathrm{ex}}C_{\mathrm{p}}$$

and,

$$\frac{dz}{dt} = -k_{\mathrm{ex}}K_{\mathrm{pw}}\mathrm{b} - k_{\mathrm{ex}}\frac{dC_{\mathrm{p}}}{dt}$$

$$\Rightarrow \frac{dz}{dt} = -k_{\mathrm{ex}}K_{\mathrm{pw}}\mathrm{b} - k_{\mathrm{ex}}z$$

$$\int \frac{dz}{-k_{\mathrm{ex}}K_{\mathrm{pw}}\mathrm{b} - k_{\mathrm{ex}}z} = \int dt$$

$$-\frac{1}{k_{ex}}\ln\left(-k_{ex}K_{pw}b-k_{ex}z\right)\Big|_{z_1}^{z_2}=t\Big|_0^t$$

$$\ln\left[\frac{-k_{ex}K_{pw}b-k_{ex}z_2}{-k_{ex}K_{pw}b-k_{ex}z_1}\right]=-k_{ex}t$$

$$\Rightarrow \frac{-k_{ex}K_{pw}b-k_{ex}z_2}{-k_{ex}K_{pw}b-k_{ex}z_1}=e^{-k_{ex}t}$$

When $t=t, z=z_2=k_{ex}K_{pw}a-k_{ex}K_{pw}bt-k_{ex}C_p$. At the initial conditions, $C_p=0$ at $t=0$ and $z=z_1=k_{ex}K_{pw}a$. Substituting these expressions in the equation above gives:

$$\frac{-k_{ex}K_{pw}b-k_{ex}^2K_{pw}a+k_{ex}^2K_{pw}bt+k_{ex}^2C_p}{-k_{ex}K_{pw}b-k_{ex}^2K_{pw}a}=e^{-k_{ex}t}$$

$$k_{ex}^2C_p=-k_{ex}^2K_{pw}a\,e^{-k_{ex}t}+k_{ex}^2K_{pw}a-k_{ex}K_{pw}b\,e^{-k_{ex}t}+k_{ex}K_{pw}b-k_{ex}^2K_{pw}bt$$

$$C_p=\frac{k_{ex}^2K_{pw}a}{k_{ex}^2}\left(1-e^{-k_{ex}t}\right)+\frac{k_{ex}K_{pw}b}{k_{ex}^2}\left(1-k_{ex}t-e^{-k_{ex}t}\right)$$

$$C_p=K_{pw}a\left(1-e^{-k_{ex}t}\right)+\frac{K_{pw}b}{k_{ex}}\left(1-k_{ex}t-e^{-k_{ex}t}\right)$$

Assuming that C_w does not change with time, $b=0$ in $C_w=a-bt$ implying $C_w=a$. The second term on the right of the equation above will effectively be zero and the equation will reduce to:

$$C_p=K_{pw}C_w\left(1-e^{-k_{ex}t}\right)$$

which is equation 2.13.

Derivation of equation 2.22

Equation 2.17 can be re–written as:

$$N_t=C_wK_{pw}m\left[1-e^{-\frac{R_St}{K_{pw}m}}\right]$$

where at equilibrium, $C_wK_{pw}m=N_t$ according to equation 2.19. If this is represented as N_∞, and factoring in initial concentrations, N_0, the equation above can be re-

written as [132]:

$$N_t = N_0 + (N_\infty - N_0)\left[1 - e^{-\frac{R_s t}{K_{pw} m}}\right]$$

For PRCs, N_t represents the remaining amount at time t following deployment, N_0 the initial amount before deployment, which in this case would be the maximum amount, and N_∞ the amount at infinity following full dissipation and which would effectively be equivalent to zero. Therefore, the equation above reduces to:

$$N_{t,PRC} = N_0\left[\exp\left(-R_s \cdot \frac{t}{K_{pw} m}\right)\right]$$

where $N_{t,PRC}$ (ng) is the amount of PRCs remaining at time t.

For PAHs and PCBs, R_s can be related to molar mass (M) as $R_s = M^{-0.47}B$, where B is a proportionality constant that depends on the hydrodynamic conditions and is linearly proportional to the surface area of the PSD [146]. Substituting this relation in the equation above gives:

$$N_{t,PRC} = N_0\left[\exp\left(-\frac{B}{M^{0.47}} \cdot \frac{t}{K_{pw} m}\right)\right]$$

Therefore the fractions of remaining PRCs (f) after time t can be given as:

$$\frac{N_{t,PRC}}{N_0} = \exp\left(-\frac{B}{M^{0.47}} \cdot \frac{t}{K_{pw} m}\right)$$

which is equation 2.22.

Fugacity calculations

Fugacity (f in Pa) varies linearly with concentration (C in mol/m^3) and is given as:

$$C = Z \cdot f$$

where Z in the fugacity capacity given in $\mathrm{mol\,m^3/Pa}$. Z values are calculated from the fundamental fugacity equation given as:

$$f = C \cdot v \cdot \gamma \cdot f_{\mathrm{R}}$$

where v ($\mathrm{mol/m^3}$) is the molar volume derived from phase density, γ is the activity coefficient of the chemical, and f_{R} is the reference fugacity (Pa).

Fugacity capacity in water Z_{w} is calculated as:

$$Z_{\mathrm{w}} = \frac{C_{\mathrm{w}}}{f_{\mathrm{w}}} = \frac{1}{v_{\mathrm{w}}\gamma_{\mathrm{w}}f_{\mathrm{R}}} = \left(\frac{P_{\mathrm{L}}^{0}}{S_{\mathrm{w}}}\right)_{-1} = \frac{1}{H}$$

where P_{L}^{0} is the liquid state vapor pressure of the organic chemical, S_{w} is solubility and H is the Henry's law constant.

$$C_{\mathrm{w}}v_{\mathrm{w}}\gamma_{\mathrm{w}}f_{\mathrm{R}} = C_{\mathrm{s}}v_{\mathrm{s}}\gamma_{\mathrm{s}}f_{\mathrm{R}}$$

Therefore:

$$C_{\mathrm{s}} = C_{\mathrm{w}}\frac{v_{\mathrm{w}}\gamma_{\mathrm{w}}}{v_{\mathrm{s}}\gamma_{\mathrm{s}}} = Z_{\mathrm{w}}f_{\mathrm{w}}\frac{v_{\mathrm{w}}\gamma_{\mathrm{w}}}{v_{\mathrm{s}}\gamma_{\mathrm{s}}} = f_{\mathrm{w}}Z_{\mathrm{w}}K_{\mathrm{d}}^{'} = f_{\mathrm{w}}\frac{\rho_{\mathrm{s}}K_{\mathrm{d}}}{H}$$

But

$$C_{\mathrm{s}} = Z_{\mathrm{s}}f_{\mathrm{s}}$$

and at equilibrium,

$$f_{\mathrm{w}} = f_{\mathrm{s}}$$

Hence,

$$Z_{\mathrm{s}} = \frac{f_{\mathrm{w}}}{f_{\mathrm{s}}} \cdot \frac{\rho_{\mathrm{s}}K_{\mathrm{d}}}{H} = \frac{\rho_{\mathrm{s}}K_{\mathrm{d}}}{H}$$

But $K_{\mathrm{d}} = K_{\mathrm{oc}}f_{\mathrm{oc}}$. Thus:

$$Z_{\mathrm{s}} = \frac{\rho_{\mathrm{s}}K_{\mathrm{oc}}f_{\mathrm{oc}}}{H}$$

Since $f_w = f_s$, it follows that:

$$\frac{f_w}{f_s} = \frac{C_s Z_w}{C_w Z_s} = \frac{C_s}{C_w \rho_s K_{oc} f_{oc}}$$

C Instrumental analytical methods and data for the target compounds

PES and SR extracts were analyzed on a 6890 Agilent gas chromatograph (GC) coupled to a 5973N Agilent mass selective detector (MSD) and a Gerstel multipurpose sampler. Analytes were separated on a DB-5MS capillary column (60 m × 0.25 mm × 0.25 µm) (Chrompack). The GC was operated in splitless mode with an injection volume of 2.0 µL. Helium flowing at 1.1 mL/s was used as the carrier gas. The oven temperature programme was: initially at 60 °C held for 1 min, then increased to 180 °C at a rate of 10 °C/min, then to 220 °C at 2 °C/min and finally to 280 °C at 10 °C/min held for 30 min. Total runtime was 44 min. Electron ionization was used for spectra acquisition at 70 eV ionization energy. The MSD transfer line, ion source and quadrupole temperatures were set at 300 °C, 230 °C and 150 °C respectively. Mass spectra were acquired in both scan (m/z 35 to 700) and selected ion monitoring (SIM) modes. External calibration was used for analyte quantitation.

Analytes sorbed onto Twisters were desorbed by thermal desorption on a GC (6890N, Agilent) coupled to a MSD (5973, Agilent), a thermal desorption unit (Gerstel) and a HP-5MS (5 % Phenylmethylsiloxane column; 60 m×0.25 mm×0.25 µm) (Chrompack). Oven temperature programme was: 60 °C held for 5 min then increased at a rate of 15 °C/min to 180 °C then at 10 °C/min to 220 °C then finally at 15 °C/min to 300 °C held for 30 min. Helium was used as the carrier gas. Chromatograms were obtained SIM mode.

Table C.1: List of target analytes and analytical data used in the calibration experiment

CAS	Compound name	Cal. range[a] (ng)	Cal. levels[b]	R^2	LOQ[c] (ng)
91-20-3	Naphthalene	0.08...0.50	8	0.9971	0.01
208-96-8	Acenaphthylene	0.08...1.00	9	0.9997	0.02
83-32-9	Acenaphthene	0.08...0.35	7	0.9989	0.02
85-01-8	Phenanthrene	0.03...1.00	10	0.9954	0.01
120-12-7	Anthracene	0.08...0.50	9	0.9907	0.02
206-44-0	Fluoranthene	0.12...1.00	8	0.9959	0.01
129-00-0	Pyrene	0.12...1.00	8	0.9950	0.01
56-55-3	Benzo(a)anthracene	0.08...1.00	8	0.9980	0.02
218-01-9	Chrysene	0.10...1.00	7	0.9955	0.02
205-99-2	Benzo[b]fluoranthene	0.10...1.00	7	0.9990	0.03
207-08-9	Benzo[k]fluoranthene	0.10...1.00	7	0.9986	0.03
50-32-8	Benzo[a]pyrene	0.08...1.00	7	0.9995	0.03
193-39-5	Indeno[1,2,3-cd]pyrene	0.10...0.35	7	0.9964	0.04
53-70-3	Dibenz[a,h]anthracene	0.02...0.12	7	0.9913	0.04
191-24-2	Benzo[g,h,i]perylene	0.02...0.20	9	0.9933	0.04
91-57-6	2-methylnaphthalene	0.10...0.50	7	0.9956	0.01
582-16-1	2,7-Dimethylphthalate	0.08...1.00	9	0.9989	0.01
7012-37-5	PCB 28	0.12...1.00	8	0.9987	0.04
35693-99-3	PCB 52	0.04...0.50	9	0.9952	0.02
37680-73-2	PCB 101	0.12...1.00	8	0.9984	0.04
35065-28-2	PCB 138	0.10...1.00	8	0.9988	0.06
35065-27-1	PCB 153	0.10...1.00	7	0.9994	0.06
35065-29-3	PCB 180	0.10...1.00	7	0.9990	0.06
3424-82-6	o,p´ DDE	0.10...1.00	8	0.9983	0.04
72-55-9	p,p´ DDE	0.14...1.00	7	0.9990	0.04
53-19-0	o,p´ DDD	0.12...1.00	8	0.9978	0.04
72-54-8	p,p´ DDD	0.06...0.35	7	0.9953	0.02
789-02-6	o,p´ DDT	0.08...0.35	7	0.9949	0.02
50-29-3	p,p´ DDT	0.10...1.00	7	0.9988	0.04
118-74-1	Hexachlorobenzene	0.08...1.00	10	0.9982	0.02
72-43-5	Methoxychlor	0.12...1.00	7	0.9990	0.10
85-68-7	Butyl benzyl phthalate (BBP)	0.08...1.00	7	0.9949	0.02

[a] Calibration range; [b] calibration levels; [c] limit of quantitation was taken as the lowest concentration from the calibration data that could be quantified.

Table C.2: Analytical data used in calculation of concentrations from field-deployed sorbents

CAS	Compound name	Cal. range[a] (ng)	Cal. levels[b]	R^2	LOQ[c] (ng)
91-20-3	Naphthalene	0.15...4.00	8	0.9987	0.02
208-96-8	Acenaphthylene	0.02...1.50	7	0.9994	0.02
83-32-9	Acenaphthene	0.02...1.50	7	0.9995	0.02
86-73-7	Fluorene	0.05...1.50	7	0.9995	0.02
85-01-8	Phenanthrene	0.15...4.00	7	0.9997	0.02
120-12-7	Anthracene	0.05...1.50	7	0.9993	0.02
206-44-0	Fluoranthene	0.10...2.50	7	0.9990	0.02
129-00-0	Pyrene	0.05...2.50	8	0.9993	0.02
56-55-3	Benz[a]anthracene	0.05...2.50	7	0.9995	0.02
218-01-9	Chrysene	0.05...2.50	7	0.9992	0.02
205-99-2	Benzo[b+k]fluoranthene	0.05...2.50	8	0.9990	0.05
192-97-2	Benzo[e]pyrene	0.10...2.50	7	0.9995	0.05
50-32-8	Benzo[a]pyrene	0.10...2.50	7	0.9995	0.05
198-55-0	Perylene	0.10...2.50	7	0.9995	0.05
193-39-5	Indeno[1,2,3-cd]pyrene	0.15...2.50	7	0.9955	0.10
53-70-3	Dibenz[a,h]anthracene	0.15...2.50	7	0.9943	0.10
191-24-2	Benzo[ghi]perylene	0.50...4.00	7	0.9903	0.20
90-12-0	1-Methylnaphthalene	0.15...4.00	8	0.9987	0.02
91-57-6	2-Methylnaphthalene	0.15...4.00	8	0.9989	0.02
582-16-1	2,7-Dimethylnaphthalene	0.05...2.50	8	0.9996	0.02
2245-38-7	1,6,7-Trimethylnaphthalene	0.15...4.00	7	0.9998	0.02

[a] Calibration range; [b] calibration levels; [c] limit of quantitation was taken as the lowest concentration from the calibration data that could be quantified.

D Sorbed concentrations from the calibration experiment experiment

Table D.1: Concentrations of HOCs that were sorbed onto PES during the calibration experiment

Compound name	Sorbed concentrations (µg/g PES)					
	day 2	day 4	day 7	day 10	day 12	day 14
Naphthalene	3.02 ± 0.28	6.43 ± 2.20	6.67 ± 0.31	7.99 ± 0.50	9.12 ± 0.42	7.68 ± 1.06
Acenaphthylene	3.43 ± 0.26	6.20 ± 1.03	8.02 ± 0.49	10.90 ± 0.67	11.72 ± 0.17	12.24 ± 1.75
Acenaphthene	3.01 ± 0.09	5.63 ± 0.87	6.95 ± 0.15	9.29 ± 0.28	9.81 ± 0.23	10.02 ± 1.69
Phenanthrene	7.72 ± 0.46	13.06 ± 2.27	17.47 ± 1.56	27.26 ± 0.22	26.17 ± 0.44	27.71 ± 3.07
Anthracene	3.89 ± 0.32	5.37 ± 0.77	6.85 ± 0.56	10.08 ± 0.47	9.87 ± 0.16	10.65 ± 0.93
Fluoranthene	6.24 ± 0.48	11.79 ± 1.29	15.39 ± 1.26	24.61 ± 0.42	23.47 ± 1.14	22.80 ± 2.17
Pyrene	4.77 ± 0.34	8.75 ± 0.81	10.72 ± 0.91	16.90 ± 0.29	16.19 ± 0.63	15.22 ± 1.37
Benz[a]anthracene	8.02 ± 0.13	10.29 ± 0.11	11.19 ± 1.43	17.76 ± 1.01	16.38 ± 0.76	14.03 ± 1.31
Chrysene	4.46 ± 0.08	5.79 ± 0.06	8.37 ± 0.84	13.43 ± 0.37	12.78 ± 0.59	11.62 ± 1.37
Benzo[b]fluoranthene	10.28 ± 0.48	12.39 ± 0.18	19.11 ± 2.31	30.07 ± 1.66	28.88 ± 3.67	21.37 ± 0.66
Benzo[k]fluoranthene	5.90 ± 0.00	6.27 ± 0.17	9.31 ± 0.70	14.11 ± 1.43	14.67 ± 2.58	12.09 ± 0.59
Benzo[a]pyrene	2.81 ± 0.11	3.20 ± 0.00	4.30 ± 0.52	5.98 ± 0.38	6.12 ± 0.88	4.85 ± 0.18
Indeno[1,2,3-cd]pyrene	3.27 ± 0.02	3.97 ± 0.09	5.98 ± 0.75	7.68 ± 0.88	8.48 ± 1.70	6.23 ± 0.12
Benzo[ghi]perylene	0.07 ± 0.00	0.49 ± 0.07	2.05 ± 0.51	3.14 ± 0.36	3.92 ± 0.77	3.07 ± 0.10
2-Methylnaphthalene	3.01 ± 0.12	5.84 ± 1.40	7.82 ± 0.26	10.90 ± 0.54	11.85 ± 0.42	12.56 ± 2.42
2,7-Dimethylnaphthalene	2.71 ± 0.25	4.96 ± 1.13	7.14 ± 0.24	10.44 ± 0.55	11.11 ± 0.30	11.96 ± 2.09
PCB 28	4.53 ± 0.26	6.94 ± 1.19	9.55 ± 0.72	13.25 ± 0.67	13.72 ± 0.60	15.85 ± 1.99
PCB 52	0.86 ± 0.30	3.22 ± 0.90	5.26 ± 0.68	7.46 ± 0.31	8.70 ± 0.70	9.44 ± 0.93
PCB 101	4.46 ± 0.21	6.97 ± 1.20	9.91 ± 1.01	12.82 ± 0.15	14.01 ± 0.98	14.91 ± 0.96

Continued on next page

Table D.1 Continued from previous page

Compound name	Sorbed concentrations (µg/g PES)					
	day 2	day 4	day 7	day 10	day 12	day 14
PCB 138	3.63 ± 0.15	6.17 ± 0.98	8.69 ± 0.49	9.09 ± 1.00	12.73 ± 0.67	12.56 ± 0.65
PCB 153	3.29 ± 0.13	5.63 ± 0.90	7.60 ± 0.62	10.22 ± 0.06	11.21 ± 0.88	11.32 ± 0.71
PCB 180	3.15 ± 0.08	6.22 ± 1.01	8.07 ± 0.46	8.38 ± 0.31	11.75 ± 0.64	12.05 ± 0.90
o,p´-DDE	4.29 ± 0.31	6.97 ± 1.05	9.77 ± 1.15	12.33 ± 0.34	13.95 ± 1.52	14.29 ± 0.77
p,p´-DDE	4.91 ± 0.33	7.87 ± 1.25	11.17 ± 1.30	14.34 ± 0.28	16.17 ± 1.41	16.72 ± 0.93
o,p´-DDD	4.46 ± 0.44	7.34 ± 0.89	9.69 ± 1.25	11.80 ± 0.28	14.23 ± 1.94	14.07 ± 0.39
p,p´-DDD	2.27 ± 0.17	3.94 ± 0.62	5.41 ± 0.83	6.37 ± 0.25	8.53 ± 1.85	7.78 ± 0.13
o,p´-DDT	2.80 ± 0.23	4.69 ± 0.79	5.96 ± 0.85	7.51 ± 0.42	9.41 ± 1.29	8.86 ± 0.22
p,p´-DDT	4.86 ± 0.20	8.43 ± 1.25	12.47 ± 1.11	13.66 ± 0.31	18.72 ± 2.97	17.37 ± 0.02
Hexachlorobenzene	2.81 ± 0.16	5.28 ± 0.83	6.67 ± 0.17	9.45 ± 1.48	9.66 ± 0.35	10.33 ± 1.82
Methoxychlor	4.85 ± 0.24	8.50 ± 1.44	11.22 ± 1.34	9.83 ± 0.32	13.97 ± 1.67	13.49 ± 0.57
BBP	1.70 ± 0.23	3.33 ± 0.11	3.47 ± 0.86	4.17 ± 0.35	4.54 ± 0.24	3.92 ± 0.21

Errors represent the standard deviation from the mean (n=2 and n=4 for day 7).

E Analytical method and other data for the elimination experiment

Table E.1: Instrumental method used in analysis of data from the elimination experiment

Item	Details/Specification
Instrument	Agilent GC 6890N with MSD 5973N
Column	HP-5MSUI; 60 m×0.25 mm×0.25 µm

Continued on next page

Table E.1 Continued from previous page

Item	Details/Specification
Carrier gas	Helium
Flow rate	1 mL/s
Injection volume	2 µL in splitless mode
Injector temperature	250 °C
Temperature programme	60 °C held for 1 min, then increased to 180 °C at a rate of 15 °C/min, then to 220 °C at 5 °C/min and finally to 300 °C at 20 °C/min held for 19 min
Solvent delay	8 min
Scan parameter	m/z 50 to 550
Data acquisition mode	Scan and SIM using target ions

Table E.2: Amount of analytes remaining over time during the elimination experiment

Compound name	Amount of analytes remaining at the sampling time (h):																
	0.2[a]	1	2	4	5.5	6	12.5	18	24	48	72	96	120	144	168	240	360
Naphthalene	1.98	2.36	2.12	2.02	2.00	2.26	1.84	1.95	1.94	2.02	1.98	2.50	2.08±0.01	2.41	1.82	2.17±0.03	2.25±0.04
1,2,3-Trichlorobenzene	2.08	1.87	1.72	2.12	2.05	2.45	1.97	2.03	2.04	2.20	2.25	2.38	2.21±0.22	2.04	1.76	2.06±0.25	2.18±0.11
1,2,3,4-Tetrachlorobenzene	4.22	4.87	4.69	4.27	3.64	4.43	3.78	3.74	3.68	4.18	4.18	4.01	3.81±0.52	4.00	4.85	3.94±0.39	4.19±0.04
Acenaphthene	3.67	3.56	3.56	3.66	3.06	3.79	3.15	3.18	3.18	3.45	3.05	3.55	3.46±0.31	3.64	3.65	3.47±0.23	3.71±0.28
Pentachlorobenzene	4.24	4.34	4.51	4.60	4.36	5.09	4.33	4.40	4.38	4.93	4.06	3.69	4.16±0.23	3.77	3.72	4.48±0.09	4.17±0.29
Fluorene	3.33	3.11	3.43	3.08	3.69	3.88	3.61	3.77	3.67	3.44	3.48	3.21	3.48±0.22	3.25	3.49	3.94±0.22	3.63±0.27
alpha-HCH	3.06	3.71	3.13	2.89	3.11	3.50	3.19	3.42	3.09	3.67	2.95	2.77	2.69±0.33	2.83	2.10	3.42±0.25	2.87±0.17

Continued on next page

Table E.2 Continued from previous page

Compound name	Amount of analytes remaining at the sampling time (h)																
	0.2[a]	1	2	4	5.5	6	12.5	18	24	48	72	96	120	144	168	240	360
Hexachlorobenzene	4.62	4.60	4.77	5.07	4.57	5.03	4.62	4.88	4.49	5.12	4.38	4.26	4.60±0.09	4.81	4.67	5.00±0.41	4.86±0.09
gamma-HCH	2.44	2.75	2.34	2.44	2.46	2.67	2.48	2.71	2.42	2.90	2.40	2.30	2.22±0.10	2.35	1.97	2.69±0.12	2.35±0.04
Phenanthrene	4.22	4.26	4.43	4.17	4.16	4.50	4.14	4.38	4.03	4.70	4.15	4.33	4.35±0.33	4.32	4.44	4.40±0.33	4.48±0.37
Anthracene	4.38	4.20	4.48	4.37	4.73	4.87	4.83	4.83	3.91	4.28	4.51	4.24	4.50±0.07	4.24	4.29	4.33±0.21	4.66±0.13
PCB 28	4.81	4.77	4.81	5.08	4.72	4.97	4.66	4.91	4.52	5.24	4.42	4.80	4.44±0.38	4.45	5.19	5.03±0.43	4.73±0.27
Heptachlor	1.25	1.01	1.11	1.10	1.19	1.17	1.05	1.17	1.25	1.16	1.19	1.09	1.12±0.15	1.13	0.88	1.41±0.06	1.14±0.03
PCB 52	4.83	5.37	5.29	5.36	4.72	4.94	4.66	4.92	4.52	5.32	4.43	4.37	4.25±0.08	4.36	4.23	5.01±0.36	5.14±0.28
Chlorpyrifos	5.61	5.42	5.34	5.83	5.45	6.40	6.24	5.70	5.95	6.39	6.18	6.04	5.94±0.14	6.20	6.07	6.10±0.02	5.72±0.18
Aldrin	1.37	1.29	1.48	1.19	1.49	1.59	1.43	1.43	1.38	1.32	1.44	1.16	1.41±0.03	1.20	1.31	1.35±0.12	1.37±0.15
Fluoranthene	5.56	5.38	5.21	5.48	5.51	5.81	5.57	5.95	5.36	5.50	5.38	5.35	5.36±0.02	5.29	5.66	5.64±0.10	5.30±0.10
o,p'-DDE	4.52	4.17	4.51	4.27	4.41	4.50	4.37	4.69	4.22	4.91	4.79	4.73	4.48±0.09	4.22	4.33	4.64±0.20	4.61±0.21
Pyrene	4.76	4.60	4.56	4.70	4.70	4.88	4.74	5.00	4.54	4.92	4.57	4.55	4.41±0.24	4.53	4.79	4.80±0.05	4.54±0.09
Endosulfan	1.36	1.30	1.30	1.30	1.37	1.43	1.31	1.41	1.19	1.36	1.19	1.27	1.25±0.01	1.26	1.20	1.34±0.02	1.31±0.07
p,p'-DDE	4.79	4.67	4.39	4.81	4.79	4.90	4.72	5.08	4.54	5.14	4.60	4.53	4.42±0.19	4.54	4.85	5.05±0.24	4.86±0.23
o,p'-DDD	4.23	4.25	3.98	4.34	4.32	4.35	4.29	4.46	4.13	4.62	4.10	4.10	4.02±0.13	4.22	4.51	4.56±0.24	4.28±0.04
Dieldrin	1.09	1.05	1.01	1.10	1.12	1.18	1.07	1.12	1.02	1.07	0.97	0.97	1.03±0.08	1.06	1.01	1.04±0.02	1.04±0.07
p,p'-DDD	5.46	5.84	5.47	6.04	5.49	5.87	5.76	6.03	5.54	6.20	5.59	5.58	5.52±0.28	5.73	6.32	6.24±0.19	5.88±0.07
o,p'-DDT	3.57	3.86	3.86	3.84	3.29	4.11	4.04	4.00	3.38	3.84	3.46	3.33	3.33±0.01	3.43	3.34	3.85±0.05	3.52±0.13
PCB 153	5.51	5.65	5.23	5.69	5.45	5.64	5.54	5.81	5.16	6.12	5.20	5.20	5.18±0.01	5.18	5.74	5.78±0.34	5.70±0.17
Butyl benzyl phthalate	8.54	8.14	8.01	8.33	8.03	8.72	8.58	8.39	7.95	8.28	8.10	8.41	8.11±0.20	8.58	8.26	8.53±0.04	8.32±0.04
p,p'-DDT	2.71	3.28	3.38	2.93	2.37	3.55	3.45	3.36	2.36	3.29	2.51	2.36	2.48±0.02	2.49	2.25	2.83±0.09	2.84±0.15

Continued on next page

Table E.2 Continued from previous page

Compound name	Amount of analytes remaining at the sampling time (h)																
	0.2[a]	1	2	4	5.5	6	12.5	18	24	48	72	96	120	144	168	240	360
PCB 138	5.04	5.18	4.87	5.25	4.90	5.21	5.10	5.28	4.72	5.74	4.76	4.74	4.79±0.04	4.78	5.31	5.28±0.28	5.01±0.05
Benz[a]anthracene	5.51	6.31	5.95	6.27	5.71	6.67	6.57	6.54	5.41	6.60	5.82	5.73	5.43±0.42	5.79	6.43	6.10±0.15	5.40±0.37
PCB 180	5.07	5.43	5.08	5.42	4.96	5.31	5.33	5.40	4.73	5.82	4.82	4.76	4.67±0.25	4.83	5.48	5.31±0.36	5.00±0.17
Benzo[a]pyrene	8.03	7.44	7.59	8.58	7.79	7.45	7.70	8.23	7.84	8.45	7.39	7.57	8.19±0.19	7.77	8.91	7.80±0.49	7.87±0.21
Dibenz[a,h]anthracene	5.23	5.28	5.17	5.68	5.33	5.11	5.39	5.64	4.80	5.57	5.32	5.37	5.48±0.70	5.54	5.46	5.44±0.31	5.48±0.05

[a] Average ($n = 3$) of initial values (C_0) at 0.1 h, 0.2 h, and 0.3 h. Calibration values used ranged from 0.1 ng–5.0 ng over 7–11 levels. R^2 ranged from 0.97 to 0.99. Errors represent standard deviation from the mean ($n = 2$).

F Determination of R_s and K_{pw}

Raw data from the calibration experiment that were used in calculations are given in section K. Apparent log K_{pw} were calculated as the logarithm to base 10 of the ratio of the highest measured PES concentration and the average water concentration. For instance, log K_{pw} for pyrene was calculated as:

$$\begin{aligned} \log K_{pw} &= \log_{10}\left(\frac{16899\ \text{ng/g}}{0.0032\ \text{ng/mL}}\right) \\ &= 6.72\ \text{mL/g or L/kg} \end{aligned} \tag{F.1}$$

log K_{pw} was similarly calculated from the individual measurements and used to determine the standard deviation. R_s were calculated by linear regression using all the measured PES concentrations that approached linearity in the uptake curve, average water concentrations listed in section K and equation 2.18. Examples of the linear regressions are given in figure F.1. The product of slopes as in figure F.1 and sampler mass yielded sampling rates.

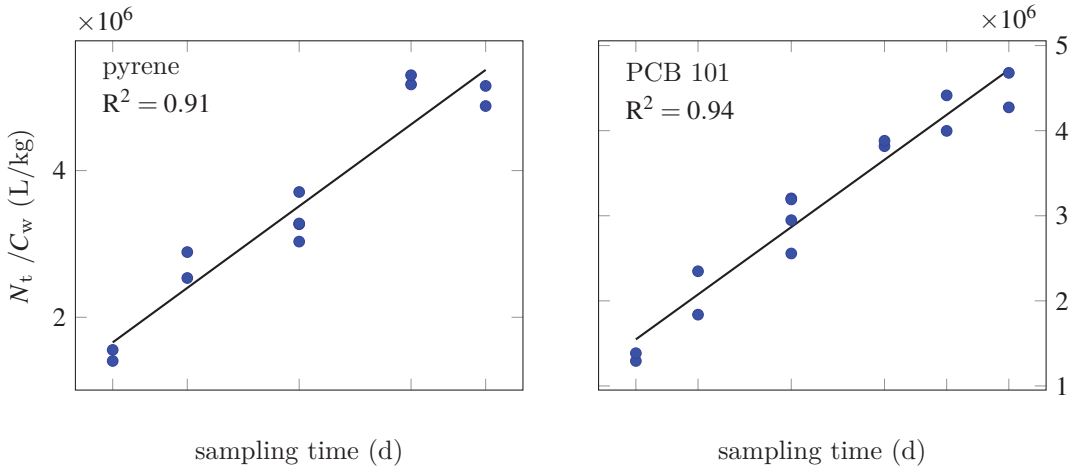

Figure F.1: Plots of N_t /C_w against time. • represents data points and —— is the regression line.

G Determination of K_{hdw}

Table G.1: Abraham's descriptors for the HOCs and n–hexadecane, and predicted log K_{hdw}

Compound name	E	S	A	B	V	L	c	Log K_{hdw}
n-hexadecane	0.67	-1.62	-3.59	-4.87	4.43	0.00	0.09	-
Naphthalene	1.34	0.92	0.00	0.20	1.09	5.16	-	3.33
Acenaphthylene	1.75	1.14	0.00	0.26	1.22	6.18	-	3.54
Acenaphthene	1.60	1.05	0.00	0.22	1.26	6.47	-	3.97
Phenanthrene	2.06	1.29	0.00	0.29	1.45	7.63	-	4.41
Anthracene	2.29	1.34	0.00	0.28	1.45	7.57	-	4.53
Fluoranthene	2.38	1.55	0.00	0.24	1.59	8.83	-	5.03
Pyrene	2.81	1.71	0.00	0.28	1.59	8.83	-	4.86
Benz[a]anthracene	2.99	1.70	0.00	0.35	1.82	10.29	-	5.71
Chrysene	3.03	1.73	0.00	0.36	1.82	10.33	-	5.64
Benzo[b]fluoranthene	3.19	1.82	0.00	0.40	1.95	11.63	-	5.99
Benzo[k]fluoranthene	3.19	1.91	0.00	0.33	1.95	11.61	-	6.18
Benzo[a]pyrene	3.63	1.96	0.00	0.37	1.95	11.74	-	6.20
Indeno[1,2,3-cd]pyrene	3.61	1.93	0.00	0.42	2.08	12.70	-	6.57
Benzo[ghi]perylene	4.07	1.90	0.00	0.45	2.08	13.45	-	6.78
2-Methylnaphthalene	1.30	0.81	0.00	0.25	1.23	5.62	-	3.86
2,7-Dimethylnaphthalene	1.35	0.82	0.00	0.25	1.37	6.15	-	4.50
PCB 28	1.76	1.33	0.00	0.15	1.69	7.90	-	5.88
PCB 52	1.90	1.48	0.00	0.15	1.81	8.14	-	6.27
PCB 101	2.04	1.61	0.00	0.13	1.94	8.87	-	6.79
PCB 138	2.18	1.74	0.00	0.11	2.06	9.77	-	7.32
PCB 153	2.18	1.74	0.00	0.11	2.06	9.59	-	7.32
PCB180	2.29	1.87	0.00	0.09	2.18	10.42	-	7.82
o,p'-DDE	1.90	1.50	0.00	0.18	2.05	8.91	-	7.15
p,p'-DDE	1.80	1.40	0.06	0.14	2.05	9.73	-	7.23
o,p'-DDD	1.80	1.73	0.10	0.26	2.10	9.57	-	6.15
p,p'-DDD	1.76	1.71	0.02	0.22	2.10	9.86	-	6.64
o,p-DDT	1.85	1.70	0.00	0.25	2.22	9.56	-	7.18
p,p'-DDT	1.81	1.76	0.00	0.16	2.22	10.02	-	7.50
Hexachlorobenzene	1.49	0.75	0.00	0.09	1.45	6.99	-	5.86
Methoxychlor	1.59	2.09	0.00	0.73	2.37	10.84	-	4.72

Continued on next page

Table G.1 Continued from previous page

Compound name	E	S	A	B	V	L	c	Log K_{hdw}
Butyl benzyl phthalate	1.30	1.51	0.00	1.13	2.46	10.82	-	3.91

All solute descriptors were obtained from the Abraham Absolv database (UFZ-LSER database v3.1).

H PRC application in PES membrane

H.1 Fractions of remaining PRCs in spiked PES strips following field exposure

Fractions of remaining PRCs were calculated as a ratio of GC–MS responses of field–exposed and undeployed PES strips. The instrumental responses were not recalculated to absolute amounts/concentrations using for instance external calibration, assuming that the GC–MS response is directly proportional to the calculated amount.

Table H.1: Fractions of remaining PRCs from spiked PES strips that were deployed in the Saale river, Germany during 30 days

Name of PRC	PES strip A	PES strip B	PES strip C	CV (%)
Acenaphthene-d10	0.65	0.63	0.59	4
Fluorene-d10	0.66	0.64	0.61	4
Phenanthrene-d10	0.80	0.76	0.74	4
Pyrene-d10	0.85	0.79	0.79	5
Benzo(a)anthracene-d12	0.65	0.57	0.55	9
Chrysene-d12	0.83	0.77	0.76	5
PCB 29	0.86	0.84	0.78	5
PCB 77	0.91	0.84	0.79	7
PCB 81	0.92	0.84	0.80	7

CV represents the coefficient of variation calculated as a ratio of the standard deviation to the average value of the measurements (n=3) expressed as a percentage.

H.2 Further examples of anisotropy exhibited in the uptake of a compound versus release of an analogous PRC

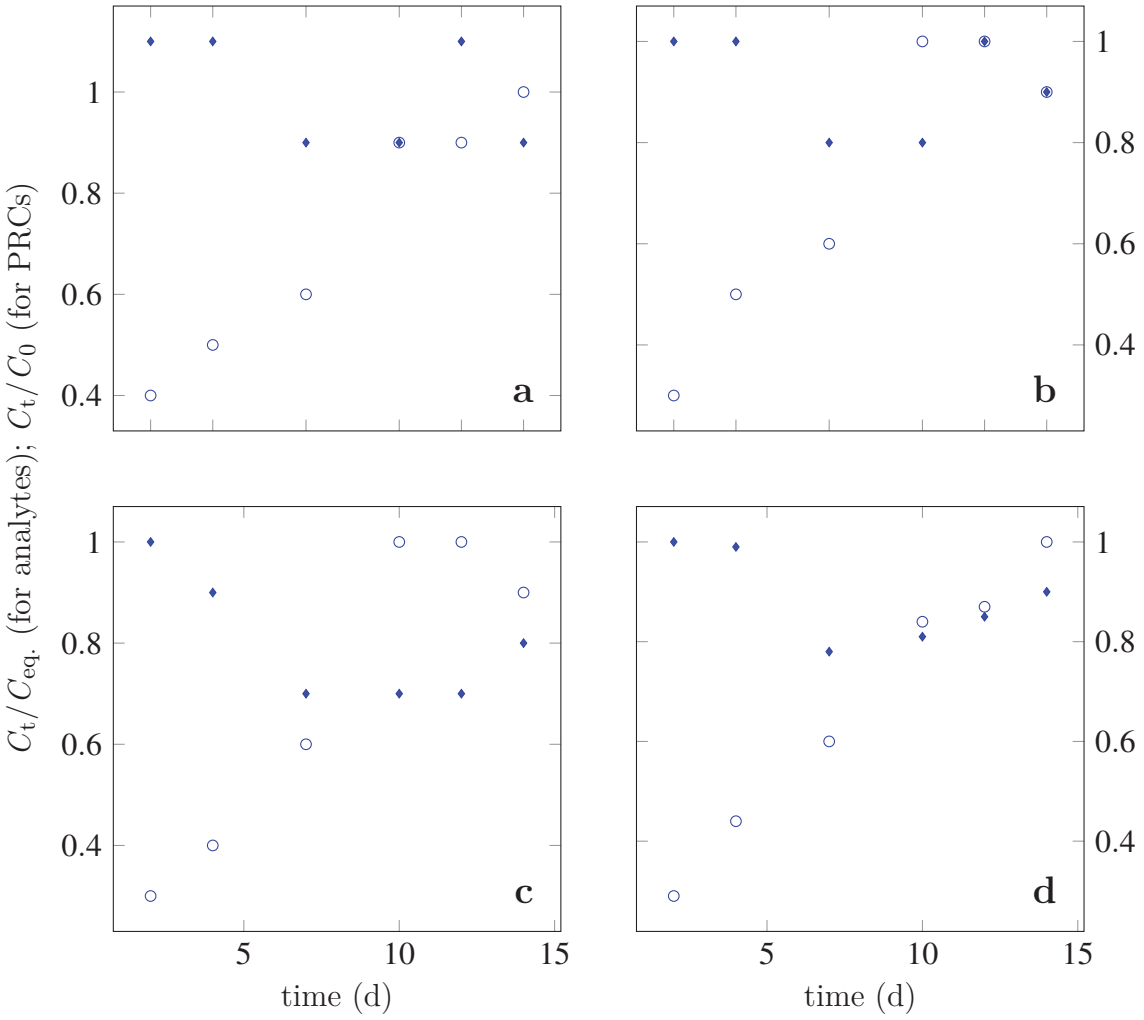

Figure H.1: A plot of the (a) uptake of anthracene (○) versus release of anthracene-d10 (♦), (b) uptake of pyrene (○) versus release of pyrene-d10 (♦), (c) uptake of chrysene (○) versus release of chrysene-d12 (♦) and (d) uptake of PCB 28 (○) versus release of PCB 29 (♦) by PES .

I Field deployment of PES and SR

I.1 Estimation of sampling rates of PAHs by SR from fractions of remaining PRCs.

Table I.1: Nonlinear least squares estimation of $R_{s,\,(300)}$ of the hypothetical compound from PRC data

PRC raw data	Sampler ID =	Sosiani ST1 (1)	
	Exposure duration (d) =	30	
	Sampler mass (g) =	10.16	
PRC	N_0 (av.)	N_t	
Acenaphthene-d10	22645	1319	
Fluorene-d10	83092	9674	
Phenanthren-d10	40140	7127	
Anthracene-d10	22337	1749	
Pyrene-d10	51184	10156	
Chrysene-d12	11926	5478	
Benz[a]anthracene-d12	33913	12559	
Perylene-d12	3557	1097	
PCB 29	20518	17185	
PCB 54	6151	5421	
PCB 81	18704	15357	
PCB 77	16579	14216	
PRC fraction in sampler	Sampler ID =	Sosiani ST1 (1)	
PRC	Molar mass (g/mol)	N_t/N_0 (exp.)	log K_{pw}
Acenaphthene-d10	164.3	0.058	3.58
Fluorene-d10	176.3	0.116	3.65
Phenanthren-d10	188.3	0.178	4.06
Anthracene-d10	188.3	0.078	4.19
Pyrene-d10	212.3	0.198	4.64
Chrysene-d12	240.4	0.459	5.22
Benz[a]anthracene-d12	240.4	0.370	5.40
Perylene-d12	264.4	0.308	5.49
PCB 29	257.5	0.838	5.43

Continued on next page

Table I.1 Continued from previous page

PCB 54	292.0	0.881	5.66
PCB 81	292.0	0.821	6.10
PCB 77	292.0	0.857	6.10
Model calculation	Sampler ID =	Sosiani ST1 (1)	
PRC	Molar mass (g/mol)	N_t/N_0 (model.)	K_{pw}
Acenaphthene-d10	164.3	0.000	3802
Fluorene-d10	176.3	0.000	4467
Phenanthren-d10	188.3	0.000	11482
Anthracene-d10	188.3	0.000	15488
Pyrene-d10	212.3	0.023	43652
Chrysene-d12	240.4	0.392	165959
Benz[a]anthracene-d12	240.4	0.537	249678
Perylene-d12	264.4	0.618	309030
PCB 29	257.5	0.572	269153
PCB 54	292.0	0.733	457088
PCB 81	292.0	0.893	1258925
PCB 77	292.0	0.893	1258925
Solver estimate	Sampler ID =	Sosiani ST1 (1)	
	Sampler B =	692	
	Sampler SSD =	3.13E-01	
	Total SSD =	9.30E-01	
	Residual variance =	3.13E-02	
	R_s (300) (L/d) =	47.4	

The table is an example for estimation of $R_{s,\,(300)}$ for one sampler, Sosiani ST1(1). Triplicate samplers were used, that is, also ST1(2) and ST1(3). PRC analysis data was entered in the first box where N_0(av.) represented an average of GC-MS responses from duplicate unexposed samplers and N_t the response from the exposed sampler ST1(1). GC-MS responses were used in lieu of absolute values to save time and costs incurred in calibration, assuming proportionality between the responses and absolute values determined by calibration. In the second box, fractions of remaining PRCs, that is $\frac{N_t}{N_0}$ were calculated and this represented the experimental model. Theoretical fractions of remaining PRCs in the third box were determined using equation 2.22. Excel's solver was then used to solve equation 2.22 by considering f as a continuous $K_{pw}M^{0.47}$ with B as an adjustable parameter. In solver, the GRG solving method was used to minimize the value 9.30E-01 (total SSD) by changing B of all triplicate samplers. Total sum of squared differences (SSD) was a summation of the individual SSD for each sampler determined using the SUMXMY2 function and the array of values in the third (model calculation) and second (PRC fraction in sampler) boxes.

Table I.2: Example of auxiliary data used in fitting fractions of remaining PRCs as shown in figure 4.10

Sampler ID = Log ($K_{pw}M^{0.47}$)	Sosiani ST1 (1) f(curve)	Log K_{pw}	Molar mass	Sosiani ST1 (1) f(exp.)
3.96	0.000	3.00	112	
4.19	0.000	3.20	125	
4.40	0.000	3.40	137	
4.62	0.000	3.58	164	0.058
4.71	0.000	3.65	176	0.116
4.84	0.000	3.80	163	
5.06	0.000	4.00	176	
5.13	0.000	4.06	188	0.178
5.26	0.000	4.19	188	0.078
5.48	0.001	4.40	201	
5.73	0.023	4.64	212	0.198
5.70	0.016	4.60	214	
5.91	0.080	4.80	227	
6.12	0.211	5.00	239	
6.33	0.383	5.20	252	
6.34	0.392	5.22	240	0.459
6.52	0.537	5.40	240	0.370
6.56	0.572	5.43	258	0.838
6.63	0.618	5.49	264	0.308
6.75	0.694	5.60	278	
6.82	0.733	5.66	292	0.881
6.96	0.798	5.80	290	
7.17	0.870	6.00	303	
7.26	0.893	6.10	292	0.821
7.26	0.893	6.10	292	0.857
7.37	0.917	6.20	316	
7.58	0.948	6.40	329	
7.79	0.967	6.60	341	
8.00	0.980	6.80	354	
8.21	0.987	7.00	367	
8.41	0.992	7.20	380	

Continued on next page

Table I.2 Continued from previous page

Sampler ID = Log ($K_{pw}M^{0.47}$)	Sosiani (1) f(curve)	Log K_{pw}	Molar mass	Sosiani ST1 (1) f(exp.)
8.62	0.995	7.40	392	
8.83	0.997	7.60	405	
9.03	0.998	7.80	418	
9.24	0.999	8.00	431	
10.27	1.000	9.00	494	

Figure 4.10 is a plot of theoretical (f curve) and experimental (f exp.) fractions of remaining PRCs against log $K_{pw}M^{0.47}$. Theoretical values for the curve (f curve) in the figure were calculated using equation 2.22 over hypothetical log K_{pw} ranges from 3.00–9.00. The values f(exp.) representing the experimental data points were extracted from table I.1.

Table I.3: Example for calculation of freely dissolved concentrations of PAHs in Sosiani river measured using SR

		Exposure duration (d) =		30	
		Sampler mass (kg) =		0.01016	
		$R_{s,\,(300)}$ (L/d) =		47.4	
Compound name	Molar mass (L/kg)	K_{pw} (L/kg)	N_t (ng)	R_s (L/d)	C_w^{TWA} (ng/L)
Naphthalene	128.2	1.07E+03	198.6	70.7	18.24
Acenaphtylene	152.2	1.82E+03	118.4	65.2	6.40
Acenaphthene	154.2	8.32E+03	81.0	64.8	0.96
Fluorene	166.2	6.17E+03	408.3	62.6	6.52
Phenanthrene	178.2	1.29E+04	1159.5	60.6	8.86
Anthracene	178.2	1.62E+04	131.2	60.6	0.80
Fluoranthene	202.3	4.17E+04	800.4	57.1	1.92
Pyrene	202.3	4.79E+04	856.7	57.1	1.82
Benzo[a]anthracene	228.3	2.09E+05	103.5	53.9	0.09
Chrysene	228.3	1.78E+05	221.4	53.9	0.21
Benzo[b&k]fluoranthene	252.3	5.50E+05	94.4	51.4	0.07
Benzo[e]pyrene	252.3	4.39E+05	63.7	51.4	0.05
Benz[a]pyrene	252.3	4.90E+05	26.8	51.4	0.02

Continued on next page

Table I.3 Continued from previous page

Compound name	Molar mass (L/kg)	Exposure duration (d) = 30 Sampler mass (kg) = 0.01016 $R_{s,\ (300)}$ (L/d) = 47.4 K_{pw} (L/kg)	N_t (ng)	R_s (L/d)	C_w^{TWA} (ng/L)
Perylene	252.3	4.39E+05	0.0	51.4	0.00
Indeno[1,2,3-cd]pyrene	276.3	1.15E+06	0.0	49.3	0.00
Dibenzo[a,h]anthracene	278.3	1.74E+06	0.0	49.1	0.00
Benzo[g,h,i]perylene	276.3	1.05E+06	0.0	49.3	0.00
1-methylnaphthalene	142.2	2.43E+03	108.7	67.4	4.41
2-methylnaphthalene	142.2	2.43E+03	125.3	67.4	5.08
2,7-dimethylnaphthalene	156.2	4.70E+03	167.9	64.4	3.51
1,6,7-trimethylnaphthalene	170.3	9.12E+03	350.8	61.9	3.79

N_t were sorbed amounts determined by instrumental analysis of SR extracts. Then the site- and compound-specific sampling rates were calculated from the $R_{s,\ (300)}$ of the hypothetical compound using equation 4.3. Finally, freely dissolved concentrations (C^{TWA}) were calculated using equation 2.17. Similar calculations were made for all triplicates then an average was used for reporting.

I.2 Sampling site and pictures of exposed PES and SR

The diagram below shows a map of the study site and pictures of PES and SR strips after retrieval.

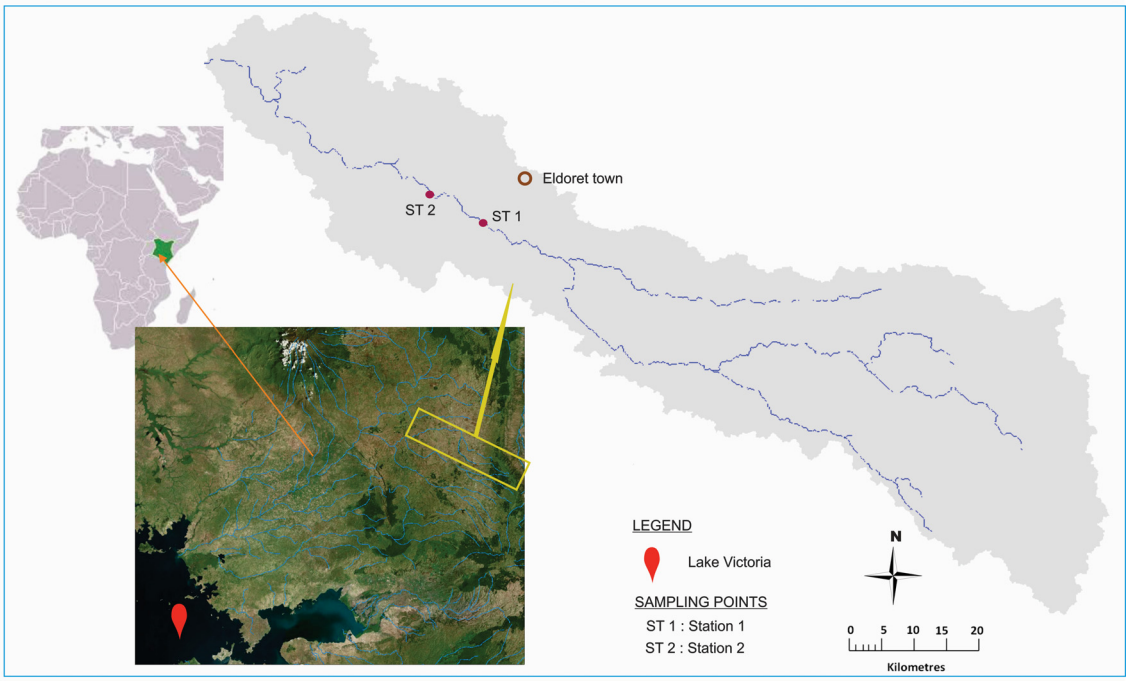

(a)

(b)

(c)

Figure I.1: (a) map showing sampling stations along Sosiani river and pictures of (b) PES and (c) SR after retrieval from the river.

I.3 Raw field data

Table I.4: GC–MS responses of extracts from field–deployed PES and SR and calculated sorbed concentrations

Compound name	GC–MS responses				Sorbed concentrations (ng/130 cm^2 PES and ng/300 cm^2 SR)							
	PES		SR		PES				SR			
	ST1	ST2	ST1	ST2	ST1	CV	ST2	CV	ST1	CV	ST2	CV
Naphthalene	45402	93777	14207	31958	221	29	795.4	13	175.6	27	391.3	71
Acenaphthylene	12871	28317	9463	12708	149.3	5	335	12	111.5	5	149.5	24
Acenaphthene	2535	3943	4171	4552	40.2	2	67	8	70.9	13	78	29
Fluorene	15446	28991	24208	29918	250.9	4	484	13	395.9	3	491	12
Phenanthrene	59961	115342	107124	131918	614.2	4	1261.1	13	1125.5	3	1411	4
Anthracene	3702	7652	9003	12425	43.4	3	90.8	4	107.1	20	148.1	1
Fluoranthene	28873	47199	75853	120896	317.5	6	521.8	11	784.6	4	1236.1	2
Pyrene	34263	49189	82589	150650	372	4	534.6	10	836.2	3	1504	2
Benzo[a]anthracene	2219	2755	6844	13130	37.1	5	44.2	6	97.9	9	182	2
Chrysene	6806	9535	18277	31395	81.1	3	112.8	9	214.6	6	367.3	1
Benzo[b+k]fluoranthene	2030	2010	6530	10253	38.6	5	38.4	5	90.6	4	131.9	5
Benzo[e]pyrene	1020	1034	3848	5551	<LOQ	nil	<LOQ	nil	60.4	5	80.7	3
Benzo[a]pyrene	418	441	1054	1913	<LOQ	nil	<LOQ	nil	27.1	7	37.3	12
Perylene	0	0	649	1969	n.d	nil	<LOQ	nil	<LOQ	nil	<LOQ	nil
Indeno[1,2,3]pyrene	0	0	426	597	n.d	nil	n.d	nil	<LOQ	nil	<LOQ	nil
Dibenz[a,h]anthracene	0	0	0	0	n.d	nil	n.d	nil	n.d	nil	n.d	nil
Benzo[ghi]perylene	0	0	800	950	n.d	nil	n.d	nil	<LOQ	nil	<LOQ	nil
1-Methylnaphthalene	12181	20130	4321	6698	169.9	2	318.3	13	86.4	22	132.1	54

Continued on next page

Table I.4 Continued from previous page

Compound name	GC–MS responses				Sorbed concentrations (ng/130 cm^2 PES and ng/300 cm^2 SR)							
	PES		SR		PES				SR			
	ST1	ST2	ST1	ST2	ST1	CV	ST2	CV	ST1	CV	ST2	CV
2-Methylnaphthalene	14994	20570	4629	7143	205.3	4	318.1	16	100.4	22	152.8	54
2,7-Dimethylnaphthalene	10268	12715	6828	7408	218.2	0	269.8	14	147.2	12	159.3	44
1,6,7-Trimethylnaphthalene	7630	9721	18444	24446	156.1	2	199.6	12	378.7	6	505.1	31

LOQ, limit of quantitation; n.d, not determined; ST1, sampling station 1; ST2, sampling station 2.

I.4 Aqueous concentrations of PAHs determined using PES and SR

Table I.5: Aqueous concentrations of PAHs from two stations along Sosiani river measured using PES and SR. Errors represent the standard deviation from the mean ($n = 3$).

Compound name	Calibration data				Aqueous concentrations (ng/L)			
	points(levels)	R^2	SL_{SR}	SL_{PES}	PES		SR	
	(ng)		(ng)	(ng)	station 1	station 2	station 1	station 2
Naphthalene	0.15-4.00(8)	0.9987	4.70E-02	0.06	5.62 ± 1.65	20.22 ± 2.55	16.13 ± 4.30	25.95 ± 9.38
Acenaphthylene	0.02-1.50(7)	0.9994	2.70E-02	0.13	3.29 ± 0.16	7.38 ± 0.90	6.03 ± 0.32	8.09 ± 1.94
Acenaphthene	0.02-1.50(7)	0.9995	6.00E-03	0.14	0.93 ± 0.02	1.56 ± 0.12	0.84 ± 0.11	0.92 ± 0.27
Fluorene	0.05-1.50(7)	0.9995	1.00E-02	0.05	3.54 ± 0.16	6.82 ± 0.86	6.32 ± 0.18	7.84 ± 0.96
Phenanthrene	0.15-4.00(7)	0.9997	3.90E-03	0.03	7.21 ± 0.30	14.81 ± 1.91	8.60 ± 0.29	10.80 ± 0.41
Anthracene	0.05-1.50(7)	0.9993	3.10E-03	0.03	0.39 ± 0.01	0.82 ± 0.03	0.65 ± 0.13	0.91 ± 0.01

Continued on next page

Table I.5 Continued from previous page

Compound name	Calibration data				Aqueous concentrations (ng/L)			
	points(levels)	R^2	SL_{SR}	SL_{PES}	PES		SR	
	(ng)		(ng)	(ng)	station 1	station 2	station 1	station 2
Fluoranthene	0.10-2.50(7)	0.9990	1.20E-03	0.02	2.91 ± 0.16	4.78 ± 0.53	1.89 ± 0.07	3.51 ± 0.14
Pyrene	0.05-2.50(8)	0.9993	1.10E-03	0.02	4.24 ± 0.19	6.09 ± 0.64	1.77 ± 0.06	3.92 ± 0.16
Benz[a]anthracene	0.05-2.50(7)	0.9995	4.20E-04	0.03	0.23 ± 0.01	0.28 ± 0.02	0.09 ± 0.01	0.30 ± 0.02
Chrysene	0.05-2.50(7)	0.9992	4.40E-04	0.02	0.45 ± 0.01	0.62 ± 0.06	0.20 ± 0.01	0.62 ± 0.04
Benzo[b+k]fluoranthene	0.05-2.50(8)	0.9990	3.45E-04	0.04	0.24 ± 0.01	0.24 ± 0.01	0.07 ± 0.01	0.21 ± 0.02
Chrysene	0.10-2.50(7)	0.9995	3.50E-04	0.07	< SL	< SL	0.05 ± 0.01	0.13 ± 0.01
Benzo[a]pyrene	0.10-2.50(7)	0.9995	3.50E-04	0.07	< SL	< SL	0.02 ± 0.00	0.06 ± 0.01
Perylene	0.10-2.50(7)	0.9995	3.50E-04	0.07	n.d	n.d	< SL	< SL
Indeno[1,2,3-cd]pyrene	0.15-2.50(7)	0.9955	3.30E-04	0.10	n.d	n.d	< SL	< SL
Dibenz[a,h]anthracene	0.15-2.50(7)	0.9943	3.30E-04	-	n.d	n.d	n.d.	n.d.
Benzo[ghi]perylene	0.50-4.00(7)	0.9903	3.30E-04	0.27	n.d	n.d	< SL	< SL
1-Methylnaphthalene	0.15-4.00(8)	0.9987	2.10E-02	0.03	2.31 ± 0.04	4.33 ± 0.55	3.50 ± 0.79	5.35 ± 2.88
2-Methylnaphthalene	0.15-4.00(8)	0.9989	2.10E-02	0.03	2.79 ± 0.12	4.33 ± 0.69	4.07 ± 0.88	6.20 ± 3.36
2,7-Dimethylnaphthalene	0.05-2.50(8)	0.9996	1.10E-02	0.02	2.33 ± 0.01	2.88 ± 0.39	3.08 ± 0.38	3.33 ± 1.47
1,6,7-Trimethylnaphthalene	0.15-4.00(7)	0.9998	1.77E-02	0.03	1.87 ± 0.04	2.39 ± 0.29	4.09 ± 0.27	5.45 ± 1.71

n.d., not detected; SL is the TWA sampling limit (see below for explanation).

200 mL of water was spiked with different concentrations (0.5 ng to 10 ng) of the analytes mixture then a PES strip was inserted and the mixture left to extract during one week. The strips were removed and extracted, and the extracts were analyzed by GC–MS to determine the lowest concentration that could be sensed by the sampler.

Water concentration that was detectable by the samplers (SL_{SR} and SL_{PES}) was calculated by inserting the instrumental quantification limit (per sampler unit) instead of analyte mass N_t into equation 2.17 for SR and equation 2.18 for PES as [145]:

$$SL_{SR} = \frac{QL_{sampler}}{K_{pw} m_p \left(1 - \exp\left(-\frac{R_s \cdot t}{K_{pw} m_p}\right)\right)} \tag{I.1}$$

$$SL_{PES} = \frac{QL_{sampler}}{R_s t} \tag{I.2}$$

where QL_{water} is the quantitation limit in the sampler. For SR, R_s were PRC–derived field values, K_{pw} values were obtained from Smedes et al. [147] except those of DDT and its metabolites, hexachlorobenzene and methoxychlor which were estimated by interpolation from the log K_{pw}–log K_{ow} relationship of the other compounds. For PES, R_s were determined in the calibration experiment.

I.5 Equations used to estimate diffusivity in water

Othmer and Thakar [106]:

$$D_{\mathrm{w}} = \frac{14.0 \times 10^{-5}}{\mu^{1.1} V^{0.6}} \tag{I.3}$$

Hayduk and Laudie [58]:

$$D_{\mathrm{w}} = \frac{13.26 \times 10^{-5}}{\mu^{1.14} V^{0.589}} \tag{I.4}$$

Schwarzenbach et al. [140]:

$$D_{\mathrm{w}} = \frac{2.7 \times 10^{-8}}{M^{0.71}} \tag{I.5}$$

Worch [176]:

$$D_{\mathrm{w}} = \frac{3.595 \times 10^{-14} T}{\eta M^{0.53}} \tag{I.6}$$

Chang and Wilke [29]:

$$D_{\mathrm{w}} = \frac{7.4 \times 10^{-10} (2.6 M_{\mathrm{w}})^{0.5} T}{\eta V^{0.6}} \tag{I.7}$$

Hayduk and Minhas [57]:

$$D_{\mathrm{w}} = 1.25 \times 10^{-8} (V^{-0.19} - 0.292) T^{1.52} \eta^{(\frac{9.58}{V} - 1.12)} \tag{I.8}$$

Where M and M_{w} in (g/mol) are the molecular weights of the compound and solvent (water) respectively, V (cm^3/mol) is molecular volume, T (K) the temperature and μ or η is dynamic viscosity of the solvent in centiPoise for equations I.3, I.4 and I.8, Poise for equation I.7 and Pa s for equation I.6. As suggested by some authors, an exponent value of 1.14 on μ in equation I.4 was used in place of 1.4 as given by the original authors [58]. D_{w} is the diffusion coefficient in water in (cm^2/s) in equations I.3, I.4 I.7 and I.8 or (m^2/s) in equations I.5 and I.6. For purposes of uniformity to enable comparison, D_{w}s from equations I.3, I.4 and I.7 were recalculated to m^2/s. Molecular volumes were obtained from Huckins et al. [61] and μ or η from Schwarzenbach et al. [140]. 24 °C, that is field temperature was used in calculation. Calculated values given in table I.6.

Table I.6: Molecular diffusivity of PAHs in water estimated using various equations

Compound name	Diffusivity, D_w (m^2/s), of PAHs in water					
	Othmer-Thakar	Hayduk-Laudie	Wilke-Chang	Schwarzenbach	Worch	Hayduk-Minhas
Naphthalene	7.75E-10	7.78E-10	8.25E-10	8.61E-10	8.95E-10	7.53E-10
Acenaphtylene	7.23E-10	7.27E-10	7.70E-10	7.62E-10	8.17E-10	6.87E-10
Acenaphthene	7.04E-10	7.09E-10	7.50E-10	7.55E-10	8.11E-10	6.62E-10
Fluorene	6.70E-10	6.75E-10	7.13E-10	7.16E-10	7.80E-10	6.16E-10
Phenanthrene	6.48E-10	6.53E-10	6.89E-10	6.81E-10	7.52E-10	5.85E-10
Anthracene	6.52E-10	6.57E-10	6.94E-10	6.81E-10	7.52E-10	5.90E-10
Fluoranthene	6.15E-10	6.20E-10	6.55E-10	6.22E-10	7.03E-10	5.37E-10
Pyrene	6.20E-10	6.25E-10	6.60E-10	6.22E-10	7.03E-10	5.45E-10
Benzo[a]anthracene	5.68E-10	5.73E-10	6.04E-10	5.71E-10	6.59E-10	4.66E-10
Chrysene	5.63E-10	5.69E-10	6.00E-10	5.71E-10	6.59E-10	4.60E-10
Benzo[b+k]fluoranthene	5.41E-10	5.47E-10	5.76E-10	5.32E-10	6.25E-10	4.24E-10
Benzo[e]pyrene	5.48E-10	5.54E-10	5.83E-10	5.32E-10	6.25E-10	4.35E-10
Benz[a]pyrene	5.48E-10	5.54E-10	5.83E-10	5.32E-10	6.25E-10	4.35E-10
Perylene	5.48E-10	5.54E-10	5.83E-10	5.32E-10	6.25E-10	4.35E-10
Indeno[1,2,3-cd]pyrene	5.24E-10	5.30E-10	5.58E-10	4.99E-10	5.96E-10	3.97E-10
Dibenzo[a,h]anthracene	5.06E-10	5.12E-10	5.39E-10	4.96E-10	5.93E-10	3.68E-10
Benzo[g,h,i]perylene	5.31E-10	5.37E-10	5.65E-10	4.99E-10	5.96E-10	4.08E-10
1-methylnaphthalene	7.12E-10	7.17E-10	7.58E-10	7.99E-10	8.47E-10	6.73E-10
2-methylnaphthalene	7.12E-10	7.17E-10	7.58E-10	7.99E-10	8.47E-10	6.73E-10
2,7-Dimethylnaphthalene	6.62E-10	6.67E-10	7.04E-10	7.48E-10	8.06E-10	6.04E-10

J Sediment sampling and analysis

(a)

(b)

Figure J.1: (a) Stainless steel can and scoop used in sampling sediments and (b) samples sediments.

J.1 Determination of sediment characteristics

To determine organic matter, 10 g of sediments, in triplicate, were placed in a 1000 mL beaker and weighed. 100 mL hydrogen peroxide (15%) was added and the mixture swirled gently, then the beaker was covered with a watchglass and left overnight at room temperature. Thereafter the beaker was placed on a sandbath and heated at 90 °C until froth was formed and the sediments became lighter in color. Then the beaker and its contents were heated at 105 °C in an oven to constant weight followed by cooling in a desiccator and reweighing. The difference in weight defined the organic matter content. Total organic carbon (TOC) was calculated as:

$$\text{TOC} = \frac{\text{average of triple measurements}}{\text{measured dry matter}} \times 100 \tag{J.1}$$

Sediments were placed in a mixing cylinder then 25 mL of 0.4 N sodium diphosphate solution was added and the solution made up to the 1000 mL mark using distilled water. Controls were similarly prepared but without sediments. The solution was poured into a series of pre–weighed sieves arranged sequentially on a stand according

to mesh sizes (0.63 mm, 0.2 mm and 0.063 mm), covered and left for about 20 min. Thereafter, the residue–containing sieves were dried at 105 °C in an oven to constant weight and weighed again. Differences in weights of the sieves yielded silt, clay and sand fractions. Average of duplicate measurements were normalized to 100 g and corrected for the organics lost during heating to yield a value f_{raw} which was then used to determine the percentage of the fraction in sediment as:

$$\text{fraction}\ (\%) = \frac{f_{raw} \times 100}{\text{blank value}} \tag{J.2}$$

Sediment characteristics were determined by sedimentation method. Sediments were placed in a mixing cylinder, 0.4 N sodium diphosphate solution added and the solution made up to the 1000 mL mark using distilled water. Controls were similarly prepared but without sediments. Weighing glasses were dried, marked and weighed to one decimal place then they were placed in the selected positions in the sediment. Then the Köhn apparatus was turned on and run. Thereafter the weighing glasses were removed and dried at 105 °C in an oven to constant weight followed by cooling in a desiccator and reweighing. Differences in weights yielded the fractions of silt, clay and sand.

J.2 Non-depletion of analytes by PES from porewater

A suitable size of PES strips used was selected to ensure that the amount of compound extracted by the strips was kept substantially low. This was estimated using the equation [97]:

$$\frac{V_{\mathrm{p}} \times K_{\mathrm{pw}}}{V_{\mathrm{w}} + V_{\mathrm{matrix}} \times K_{\mathrm{matrix,w}}} <<< 1 \tag{J.3}$$

where V_{p}, V_{w} and V_{matrix} are the volumes of polymer, solution and entire sample matrix (sediments and water). $K_{\mathrm{matrix,w}}$ is the sediment–water partition coefficient where sediments are represented essentially by the organic carbon fraction. Given

that volume is proportional to mass (m) the equation above can be rewritten as:

$$\frac{m_{\mathrm{p}} \times K_{\mathrm{pw}}}{m_{\mathrm{w}} + m_{\mathrm{matrix}} \times K_{\mathrm{oc,w}}} <<< 1 \tag{J.4}$$

For this initial calculation, secondary $K_{\mathrm{oc,w}}$ values that were estimated using equation 2.29 were used [13].

J.3 Concentrations of PAHs sorbed onto PES from sediment porewater

Table J.1: Concentrations of PAHs sorbed onto PES from sediment porewater in monitoring station 1.

Compound name	Average PAH concentrations (ng/gPES)[a] and coefficients of variation						
	air-dried			wet			
	30 d	54 d	CV[b]	30 d	54 d	CV[b]	overall CV[c]
Naphthalene	16263	13868	18	2184	2132	20	83
Acenaphthylene	1158	1132	4	1026	1053	3	6
Acenaphthene	2605	2263	8	2211	1842	11	13
Fluorene	2500	2474	4	1789	1711	13	20
Phenanthrene	3237	3079	6	2079	2079	20	25
Anthracene	2421	2237	7	2447	2211	12	9
Fluoranthene	2763	2737	2	2658	2816	6	4
Pyrene	2368	2421	2	2395	2632	7	6
Benzo(a)anthracene	2789	2789	0	2789	2816	1	1
Chrysene	1921	1921	2	1895	1974	3	3

Continued on next page

Table J.1 Continued from previous page

Compound name	Average PAH concentrations (ng/gPES)[a] and coefficients of variation						
	air-dried			wet			
	30 d	54 d	CV[b]	30 d	54 d	CV[b]	overall CV[c]
Benzo(b+k)fluoranthene	2684	2684	0	2658	2684	1	1
Benzo(e)pyrene	<LOQ	<LOQ	-	<LOQ	<LOQ	-	-
Benzo(a)pyrene	<LOQ	<LOQ	-	<LOQ	<LOQ	-	-
Perylene	n.d.	n.d.	-	n.d.	n.d.	-	-
Indeno(1,2,3)pyrene	n.d.	n.d.	-	n.d.	n.d.	-	-
Dibenz(a,h)anthracene	n.d.	n.d.	-	n.d.	n.d.	-	-
Benzo(g,h,i)perylene	n.d.	n.d.	-	n.d.	n.d.	-	-
1-methylnaphthalene	3684	3632	4	1237	1237	5	53
2-methylnaphthalene	4789	4605	8	1658	1500	9	54
2,7-Dimethylnaphthalene	2289	2395	3	1816	1842	4	14
1,6,7-Trimethylnaphthalene	3053	3079	1	2895	2974	3	3

[a]averages were calculated from duplicate measurements; [b]coefficients of variation (%) calculated using all the raw data within each category; [c]calculated using all the raw data from the air-dried and wet sediments.

Table J.2: Concentrations of PAHs sorbed onto PES from sediment porewater in monitoring station 2.

Compound name	Average PAH concentrations (ng/gPES)[a] and coefficients of variation						
	air-dried			wet			
	30 d	54 d	CV[b]	30 d	54 d	CV[b]	overall CV[c]
Naphthalene	22421	26737	15	1632	1921	16	94

Continued on next page

Table J.2 Continued from previous page

Compound name	Average PAH concentrations (ng/gPES)[a] and coefficients of variation						
	air-dried			wet			
	30 d	54 d	CV[b]	30 d	54 d	CV[b]	overall CV[c]
Acenaphthylene	1000	1053	3	947	947	0	5
Acenaphthene	2474	2132	9	2158	1842	9	11
Fluorene	2237	2447	7	1421	1474	2	26
Phenanthrene	2342	2658	9	1184	1237	4	38
Anthracene	2184	2184	1	2105	2105	0	2
Fluoranthene	2237	2237	1	2105	2079	1	4
Pyrene	1737	1789	2	1684	1737	2	2
Benzo(a)anthracene	2737	2763	1	2737	2737	0	1
Chrysene	1789	1816	1	1789	1789	0	1
Benzo(b+k)fluoranthene	2632	2632	0	2632	2632	0	0
Benzo(e)pyrene	<LOQ	<LOQ	-	<LOQ	<LOQ	-	-
Benzo(a)pyrene	<LOQ	<LOQ	-	<LOQ	<LOQ	-	-
Perylene	n.d.	n.d.	-	n.d.	n.d.	-	-
Indeno(1,2,3)pyrene	n.d.	n.d.	-	n.d.	n.d.	-	-
Dibenz(a,h)anthracene	n.d.	n.d.	-	n.d.	n.d.	-	-
Benzo(g,h,i)perylene	n.d.	n.d.	-	n.d.	n.d.	-	-
1-methylnaphthalene	4132	4816	14	1026	1053	5	68
2-methylnaphthalene	6053	7158	14	1342	1342	5	72
2,7-Dimethylnaphthalene	2053	2132	4	1579	1579	0	15
1,6,7-Trimethylnaphthalene	2789	2868	2	2737	2737	0	2

[a]averages were calculated from duplicate measurements; [b]coefficients of variation (%) calculated using all the raw data within each category; [c]calculated using all the raw data from the air-dried and wet sediments.

K Raw data

Table K.1: Raw calibration and field data

Compound name	GC–MS responses														
PES extracts															
	-	-	-	-	-	-	-	-	-	-	-	-	-	-	-
Name	D2.1	D2.2	D4.1	D4.2	D7.1	D7.2	D7.3	D7.4	D10.1	D10.2	D12.1	D12.2	D14.1	D14.2	Av.Blank
Naphthalene	17844	17028	21241	27636	24036	25455	24941	25334	26918	28359	30561	29350	28532	25467	11240
Acenaphthylene	2696	3062	4895	6328	7061	7664	6932	7950	9774	10705	11161	10930	12770	10329	0
Acenaphthene	2098	2196	3702	4650	5082	5241	5138	5346	6862	7165	7539	7290	8506	6654	0
Phenanthrene	5774	6212	8514	10686	14039	12631	11606	12081	19105	19317	18261	18686	20985	18044	766
Anthracene	2428	2804	3406	4318	5743	5095	4625	4957	7551	8110	7550	7744	8860	7753	0
Fluoranthene	6257	6954	11375	13244	17275	14202	16201	16375	25187	25798	25144	23491	25209	22054	195
Pyrene	5254	5760	9055	10243	12996	10723	11519	11552	17924	18346	17856	16935	17396	15371	535
Benzo(a)anthracene	4392	4480	5566	5489	6875	5272	6065	5633	8783	9471	8720	8203	7776	6885	573
Chrysene	3906	4016	5162	5245	8764	7230	7542	6991	12144	12634	12165	11378	11595	9771	0
Benzo(b)fluoranthene	4166	4519	5505	5370	10694	8079	8343	8593	13999	15220	15337	12646	10338	9856	0
Benzo(k)fluoranthene	4805	4804	5036	5261	8875	7617	7425	7851	11427	13288	14548	11196	10888	10118	0
Benzo(a)pyrene	840	916	1081	1078	2034	1512	1453	1553	2358	2633	2888	2250	1984	1854	0
Indeno(1,2,3)pyrene	718	709	915	957	1895	1420	1373	1593	1914	2307	2745	1985	1677	1625	0
Dibenz(a,h)anthracene	194	182	183	246	464	375	328	337	489	565	623	497	442	366	0
Benzo(g,h,i)perylene	415	368	468	489	913	829	671	763	963	1066	1282	1060	1014	985	0

Continued on next page

Table K.1 Continued from previous page

Compound name	GC–MS responses														
2-Methylnaphthalene	4224	4411	6293	8422	9290	9737	9220	9748	12401	13220	14159	13517	16447	12756	1073
2,7-Dimethylnaphthalene	2145	2434	3491	4821	5930	6105	5703	6124	8382	9029	9436	9085	11194	8739	0
PCB 28	1611	1836	2670	3681	5095	5131	4488	4274	6687	7260	7005	7516	9392	7696	0
PCB 52	1088	1290	1998	2595	3469	3512	3219	2819	4184	4390	4635	5099	5521	4902	0
PCB 101	1288	1429	2129	2917	4241	4222	3845	3240	5189	5287	5467	6112	6521	5894	0
PCB 138	628	712	1396	1936	2657	2856	2709	2392	3086	2532	4048	4420	4345	3987	0
PCB 153	621	700	1374	1907	2573	2665	2554	2086	3551	3587	3723	4248	4243	3821	0
PCB 180	480	517	1289	1772	2039	2081	2382	2124	2333	2187	3244	3551	3713	3282	0
o,p´ DDE	1401	1637	2558	3351	4900	4971	4292	3646	5693	5953	6114	7267	7164	6583	0
p,p´ DDE	987	1152	1807	2434	3613	3661	3213	2664	4342	4484	4708	5412	5490	5024	0
o,p´ DDD	899	1170	2022	2577	3652	3840	3238	2595	4176	4350	4726	5935	5380	5135	2
p,p´ DDD	528	643	1175	1598	2330	2468	1997	1571	2471	2638	2963	4215	3184	3274	0
o,p´ DDT	688	845	1413	1950	2551	2691	2155	1778	2899	3184	3519	4400	3622	3770	0
p,p´ DDT	555	612	1133	1495	2275	2357	2083	1847	2339	2430	2989	3848	3145	3141	0
Hexachlorobenzene	1064	1191	2171	2820	3320	3348	3252	3138	4218	5379	4778	5054	5997	4574	0
Methoxychlor	374	425	800	1110	1497	1583	1239	1156	1191	1122	1607	1966	1652	1774	0
BBP	1740	2085	3718	3550	3370	2835	3975	4959	4271	4791	5103	4741	4100	4419	120
Water concentrations															
	-	-	-	-	-	-	-	-	-	-	-	Sediment			
	-	-	-												
Name	Pr.0	Pr.1	Pr.2	Pr.3	Pr.4	Pr.5	Pr.6	Pr.7	Pr.8	Pr.9	Pr.10	Name	Blank	ST1.av.	ST2.av.
Naphthalene	44354	47503	45699	41683	42793	30630	40815	43981	46491	47039	67261	-	169375	243444	252251
Acenaphthylene	37945	44550	66536	52703	80421	22635	18393	25696	56891	27717	34115	-	0	4366	1131
Acenaphthene	40711	32682	67775	60149	83697	27434	25512	32792	67209	40203	46624	-	0	3926	2082
Phenanthrene	356141	272388	218185	177660	246808	220886	256592	215190	168657	233966	251750	-	9080	81648	48185

Continued on next page

Table K.1 Continued from previous page

Compound name	GC–MS responses														
Antracene	67254	47263	79238	46767	95379	30238	30094	28766	49629	36816	52365	-	0	9083	4998
Fluroranthene	373200	257123	444412	402051	619811	245885	249923	231936	403714	285036	260976	-	905	57704	24626
Pyrene	405536	246500	480326	429721	615851	182755	253357	258157	435386	327949	316198	-	0	59044	21616
Benzo[a]anthracene	75176	55986	93822	72980	117682	39219	27970	46647	106683	86089	72556	-	0	14875	6672
Chrysene	198090	111856	417546	359203	409888	106170	94439	104742	330018	193181	166248	-	0	27334	10402
Benzo[b]fluoranthene	364355	293570	592842	593464	625765	308080	283779	292879	493839	431660	330580	-	0	23517	10723
Benzo[k]fluoranthene	447951	392027	692298	643823	730390	352131	313004	333263	491379	495029	426242	[a]	0	12570	4885
Benzo[a]pyrene	85119	86723	132708	118555	176798	70262	91726	81578	131183	129246	109604	-	0	10146	5082
Indeno[1,2,3]pyrene	122783	155126	348210	446376	453760	218506	201366	232562	347215	334417	267058	-	0	1671	1036
Dibenz[a,h]anthracene	43184	49138	112628	146286	123554	62734	65277	74609	111961	100184	78930	-	0	0	0
Benzo[g,h,i]perylene	50118	60975	119534	175249	158015	74389	70221	73846	116623	111825	86932	-	0	1934	1134
2-methylnaphthalene	28412	26194	45119	37549	42222	21722	21291	23225	39811	31420	31227	-	5977	28252	24900
2,7-Dimethylnaphthalene	36406	29682	89466	71087	95018	22793	19091	24708	74096	36900	31803	-	966	11284	6366
PCB 28	145704	84851	233350	205210	208374	70099	58334	73244	200131	120087	86620	[b]	2445	14564	12528
PCB 52	150300	97258	248261	230213	237345	78982	65144	80785	219368	122364	98535	[c]	0	6999	1474
PCB 101	121352	114690	263238	247748	237459	97043	76951	91575	213025	133195	101306	[d]	1226	16101	9836
PCB 138	70180	95529	232069	240946	229772	103349	92193	101437	208119	147228	115104	[e]	0	3637	1793
PCB 153	69419	92032	239326	249746	238487	99218	91682	97988	215342	142661	112639	DBP	1170951	5755458	1696676
PCB180	103053	294482	343294	244990	230982	113701	108068	110856	208639	150851	126738	DEHP	35317	4076917	583083
o,p´-DDE	184533	172067	395649	357767	343233	137270	114393	136995	311337	198215	151027	-	-	-	-
p,p´-DDE	116751	110055	266631	258665	240307	101343	90244	100155	215724	142743	110759	-	-	-	-
o,p´-DDD	325441	214788	412432	407693	430546	199939	170288	211624	373200	276424	252811	-	-	-	-
p,p´-DDD	296363	189219	377589	371131	418334	154233	131953	190196	347160	252711	240936	-	-	-	-
o,p´-DDT	64617	86224	174573	188184	165054	119749	94937	83797	190211	121279	72827	-	-	-	-
p,p´-DDT	34514	33831	99663	110694	90587	53324	36123	46067	115699	66205	43034	-	-	-	-

Continued on next page

Table K.1 Continued from previous page

Compound name	GC–MS responses														
Hexachlorobenzene	92307	73601	258914	233933	248160	55037	46358	62920	242836	105051	77710	-	-	-	-
Methoxychlor	0	57054	55145	22705	33021	0	60753	0	22759	31074	32478	-	-	-	-
BBP	2784883	1695960	559960	684575	1226356	1795438	2000177	1560879	693568	1530273	1874068	BBP	34703	5106	2231
Field data	SR	-	-	-	-	-	-				PES				
	-	-	-	-	-	-	-								
Name	Blank	ST1A	ST1B	ST1C	ST2A	ST2B	ST2C	Blank	ST1A	ST1B	ST1C	ST2A	ST2B	ST2C	-
Naphthalene	21370	16098	16748	9776	33805	8353	53717	26793	39130	47935	49142	85020	94398	101912	-
Acenaphthylene	0	10049	9151	9190	13808	9248	15069	0	12191	13037	13384	24464	29656	30832	-
Acenaphthene	0	4708	3760	4045	4933	3179	5545	0	2546	2580	2480	3660	3949	4220	-
Fluorene	1704	24953	23612	24058	30844	25930	32980	2231	15768	14701	15868	24914	30581	31477	-
Phenanthrene	9393	110080	103540	107753	129142	129338	137275	7376	60404	57618	61861	100078	118636	127313	-
Anthracene	0	11011	7919	8078	12427	12320	12529	0	3783	3580	3742	7756	7908	7292	-
Fluoranthene	2733	77426	72164	77969	117963	122676	122048	0	30237	27161	29222	41261	49274	51063	-
Pyrene	2251	84682	79282	83802	148062	152865	151024	0	34575	32637	35577	43297	51724	52545	-
Benzo(a)anthracene	0	7262	6118	7152	12988	13498	12903	0	2231	2088	2339	2532	2954	2780	-
Chrysene	0	18857	17090	18883	31110	31871	31203	0	6667	6733	7019	8493	9920	10191	-
Benzo(b&k)fluoranthene	0	6872	6179	6539	10097	10935	9728	0	1811	2154	2124	1841	2149	2039	-
Benzo(e)pyrene	0	4126	3605	3813	5370	5747	5537	0	958	1069	1032	927	1138	1037	-
Benzo(a)pyrene	0	1026	911	1224	1637	2322	1779	0	434	388	431	420	449	454	-
Perylene	0	667	625	656	2178	2073	1657	0	0	0	0	425	415	419	-
Indeno(1,2,3)pyrene	0	429	409	439	406	661	725	0	0	0	0	0	0	0	-
Dibenz(a,h)anthracene	0	0	0	0	0	0	0	0	0	0	0	0	0	0	-
Benzo(g,h,i)perylene	0	815	775	811	952	995	904	0	129	130	140	0	0	0	-
2-Methylnaphthalene	0	5826	3906	4155	8275	2719	10435	4844	14507	15103	15371	17717	21559	22434	-
1-Methylnaphthalene	0	5483	3687	3793	7546	2653	9894	3088	12143	12056	12344	17668	20921	21800	-

Continued on next page

Table K.1 Continued from previous page

Compound name	GC–MS responses														
2,7-Dimethylnaphthalene	0	7817	6156	6512	8150	3772	10301	1414	10292	10240	10273	10701	13730	13714	-
1,6,7-Trimethylnaphthalene	0	17120	18916	19297	27358	15891	30088	0	7476	7635	7779	8387	10476	10301	-
DBP	1949826	1331822	1599659	1359400	1978646	2114074	3638388	278822	339624	344218	367557	458423	461656	535297	-
BBP	5712	17234	14702	17469	33889	35718	34972	0	3503	3788	4285	6186	7776	7729	-
DEHP	315379	1812489	1620115	1698827	2030800	2379764	2462408	41660	570494	596532	691637	650449	708103	771930	-

Table K.2: Raw GC–MS calibration data

Compound name	*Calibration points* (*ng/m*L, **ng/L**) and GC–MS responses													
Compound name	10	15	20	25	40	50	60	70	80	90	100	175	250	500
Naphthalene	1630	2140	2635	3180	4565	5710	6486	7843	8660	9591	10774	18320	30076	42930
Acenaphthylene	759	982	1125	1398	2041	2607	2937	3753	4142	4644	5261	9657	17766	28936
Acenaphthene	658	856	1000	1207	1728	2172	2842	3084	3475	3901	4344	7976	14150	19715
Fluorene	634	764	847	1043	1452	1879	2057	2642	2846	3195	3649	6748	12132	17614
Phenanthrene	717	877	998	1204	1477	2160	2243	3052	3206	3564	4308	8380	14511	20182
Anthracene	657	950	1068	1199	1749	2069	2264	2967	3336	3598	4048	7617	12368	17594
Fluoranthene	840	1019	1137	1382	1627	2332	2446	3330	3519	3737	4510	9138	15349	28965
Pyrene	788	1025	1094	1330	1642	2278	2333	3405	3457	3748	4643	9239	15680	29256
Benz[a]anthracene	386	398	404	522	666	852	955	1538	1458	1467	2071	4766	8846	13699
Chrysene	916	1105	1099	1470	1553	2403	2633	3818	3841	3855	5365	10854	19131	27476
Benzo[b]fluoranthene	366	344	294	389	499	660	814	1414	1321	1350	1897	4533	8788	14483
Benzo[k]fluoranthene	994	1141	1089	1369	1577	2159	2244	3511	3615	3670	4673	9551	17814	26693

Continued on next page

Table K.2 Continued from previous page

Compound name	*Calibration points* (*ng/m*L, **ng/L**) and GC–MS responses													-
Benzo[a]pyrene	503	510	543	661	819	980	1204	1667	1665	1817	2427	4584	8528	14726
Indeno[1,2,3-cd]pyrene	280	344	312	418	531	594	769	1048	1233	1321	1623	2967	5097	9776
Benzo[ghi]perylene	463	567	605	699	902	956	1148	1203	1644	1267	1570	3236	5838	10968
2-Methylnaphthalene	635	873	1066	1349	2052	2453	3143	3703	4050	4513	4956	8904	15230	21715
2,7-Dimethylnaphthalene	632	823	982	1181	1847	2320	2987	3664	3920	4482	4913	9277	16259	24651
Butyl benzyl phthalate	8848	8102	7375	8223	1597	8378	2408	3215	3114	3230	11458	8481	15546	29969
Compound name	500	250	175	100	90	80	70	60	50	40	30	20	10	-
PCB 28	17011	8076	4988	2425	2337	1703	1584	1451	1108	853	696	469	-	-
PCB 52	14986	7994	5450	3327	3249	2706	2578	2468	2116	1927	1764	1493	195	-
PCB 101	13131	6382	3885	1942	1862	1350	1261	1177	917	718	587	385	-	-
PCB 138	10899	5171	3086	1463	1461	974	938	841	285	528	441	280	-	-
PCB 153	11805	5592	3338	1617	1536	1071	961	835	665	623	519	321	-	-
PCB180	9541	4398	2614	1265	1258	813	803	731	579	452	378	238	-	-
o,p'-DDE	15233	7379	4473	2184	2132	1513	1413	1302	1032	804	653	422	-	-
p,p'-DDE	9904	4703	2882	1371	1358	938	907	817	657	512	404	277	-	-
o,p'-DDD	12257	5692	3336	1588	1565	1011	1002	891	713	540	437	270	-	-
p,p'-DDD	18128	8054	4554	2123	2086	1198	1353	1153	954	612	515	354	148	-
o,p-DDT	18096	8054	4521	2123	2086	1198	1353	1153	920	612	546	340	148	-
p,p'-DDT	5731	2579	1483	689	685	416	455	374	285	206	175	98	-	-
Hexachlorobenzene	16036	8160	5037	2686	2603	1995	1831	1714	1312	1049	862	560	248	-
Methoxychlor	4232	1897	1180	530	504	201	336	250	201	107	97	0	-	-
Compound name	10	25	50	75	100	250	500	750	1000	1250	1500	2000	-	-

Continued on next page

Table K.2 Continued from previous page

Compound name	*Calibration points* (*ng/m*L, **ng/L**) and GC–MS responses													
Naphthalene	1463	1905	4675	5990	8022	20141	39396	61266	82951	95984	129899	165113	-	-
Acenaphthylene	1419	2142	5132	6755	8076	21292	40989	63507	86644	100377	135950	173320	-	-
Acenaphthene	946	1331	3579	4470	5746	13144	25533	39817	54504	62799	84707	108606	-	-
Fluorene	2171	2161	4111	5039	6872	15446	29282	44825	61532	70920	96137	122258	-	-
Phenanthrene	1901	2188	5340	5968	8160	19901	39639	61671	84711	97397	132691	170360	-	-
Anthracene	1929	2326	4856	6488	8094	20522	40773	63305	86828	100664	137993	176101	-	-
Fluoranthene	1859	3693	5471	6366	9073	22372	44810	70259	96118	111250	152602	195034	-	-
Pyrene	1639	2151	5177	6582	8864	22910	45656	71371	97946	113609	155672	199249	-	-
Benz[a]anthracene	1619	1905	4078	4910	6493	17200	37348	56691	83101	92385	129348	168326	-	-
Chrysene	1822	1902	5413	6284	8546	20753	42024	66510	91918	106295	146294	187653	-	-
Benzo[b]fluoranthene	1800	1485	3973	5084	7042	19870	41995	68340	96648	110312	153332	204716	-	-
Benzo[k]fluoranthene	1663	2052	5370	6530	7793	23342	46875	76823	106483	124485	173558	215316	-	-
Benzo[a]pyrene	1209	1474	3482	4931	7219	18291	41382	62777	88679	103139	146053	189770	-	-
Indeno[1,2,3-cd]pyrene	780	714	1926	2479	3249	10317	23690	40243	57868	67856	99349	131128	-	-
Dibenz(a,h)anthracene	474	643	1568	1969	2754	8456	19062	32562	48246	56749	83922	111631	-	-
Benzo(g,h,i)perylene	811	1053	2634	3435	4495	13126	28826	47639	68460	80032	114840	150074	-	-
2-Methylnaphthalene	832	1093	2685	3431	4620	11760	22907	35525	48464	56295	75786	97058	-	-
1-Methylnaphthalene	919	1187	2928	3737	5054	12779	24885	38678	52436	60433	82515	104940	-	-
2,7-Dimethylnaphthalene	813	1045	2562	3306	4423	12395	23106	35317	47668	54810	73903	94065	-	-
1,6,7-Trimethylnaphthalene	833	1094	3347	4076	5281	12261	23278	35750	48634	56203	75929	96525	-	-
Butyl benzyl phthalate	2975	4193	9445	12731	16885	47178	102071	157615	226596	264660	362453	468565	-	-
Compound name	**0.5**	**1**	**2.5**	**5**	**7.5**	**10**	**12.5**	**15**	**20**	**22.5**	**25**	**30**	-	-

Continued on next page

Table K.2 Continued from previous page

Compound name	*Calibration points* (*ng/m*L, **ng/L**) and GC–MS responses												-	-
Naphthalene	38837	38735	41583	63925	72102	76006	82912	83546	95204	107421	113801	133903	-	-
Acenaphthylene	21945	18658	32448	73917	87657	104413	201482	133613	160978	175647	198194	329248	-	-
Acenaphthene	22069	20121	33939	77860	96444	113413	194604	145757	173284	195803	212991	326276	-	-
Phenanthrene	123751	111500	131202	292035	344880	466397	493724	530613	702205	785427	798216	1561812	-	-
Antracene	91533	65504	101514	233553	297678	409107	452692	471546	563705	610419	700987	1314113	-	-
Fluroranthene	175201	174879	252883	453953	603881	863869	1413309	1050700	1320298	1446243	1537186	2705413	-	-
Pyrene	169734	171065	275137	522076	740194	1028628	1620826	1253741	1568874	1698241	1811574	3074935	-	-
Benzo[a]anthracene	60650	60502	124542	311397	496241	750333	995320	922279	1178182	1138282	1341778	2091263	-	-
Chrysene	178810	172938	236533	572321	785009	958499	1536749	1202021	1575999	1608072	1760654	2363617	-	-
Benzo[b]fluoranthene	122300	138083	281334	612626	1140634	1464133	1884013	1869860	2592631	2587553	2862268	4040371	-	-
Benzo[k]fluoranthene	257410	269260	347720	807811	1406111	1838811	2111920	2346458	2436529	2840832	3058133	3907413	-	-
Benzo[a]pyrene	196259	197908	144806	476319	934782	1666990	1824035	2179274	2657472	2696654	2442671	4054512	-	-
Indeno[1,2,3]pyrene	166547	206593	377875	786410	699878	1667895	1830301	1909496	2354046	2579477	2884280	3700539	-	-
Dibenz[a,h]anthracene	55701	56997	122988	298140	433724	542479	599859	599990	749799	808414	923618	1255123	-	-
Benzo[g,h,i]perylene	54223	57747	117970	245626	403289	522617	557030	568217	774870	817041	919012	1086003	-	-
2-Methylnaphthalene	21254	21598	29517	58041	68226	76207	124291	96728	114368	131814	139264	197899	-	-
2,7-Dimethylnaphthalene	33574	32978	57344	119503	156184	194096	312523	236884	288423	331726	346941	523820	-	-
PCB 28	73359	83919	151775	271667	453727	571123	716315	732833	944096	982773	983341	1304629	-	-
PCB 52	65185	75918	133171	241562	403834	482828	618956	652510	846455	855742	828446	1123069	-	-
PCB 101	67532	78609	139417	253824	425062	521287	638035	693051	867882	945149	917092	1165591	-	-
PCB 138	70806	82355	141294	263549	443726	540264	617438	702803	826253	926269	979171	1175931	-	-
PCB 153	72824	84717	143873	267510	453527	547992	622729	709545	840787	954122	985432	1210833	-	-

Continued on next page

Table K.2 Continued from previous page

Compound name	*Calibration points* (*ng/m*L, **ng/L**) and GC–MS responses												-	-
PCB180	78041	93789	154785	308697	504283	594005	669047	768396	818507	1028450	1104954	1302816	-	-
o,p´-DDE	90258	106949	188334	341118	578821	715487	859925	959590	1202642	1261210	1252638	1598016	-	-
p,p´-DDE	69843	80357	145086	265277	435854	531955	624842	703520	884516	950160	945318	1187988	-	-
o,p´-DDD	102434	110072	201443	396310	616186	759382	959183	1001699	1272863	1331240	1410222	1845885	-	-
p,p´-DDD	99157	103559	191240	384656	596226	740846	952501	950685	1231818	1226369	1368091	1861822	-	-
o,p´-DDT	11911	20065	42766	112969	216369	191258	417826	346535	436032	736803	634363	863344	-	-
p,p´-DDT	0	0	14789	45574	89325	74637	227889	168776	213333	444041	360371	512951	-	-
Hexachlorobenzene	60643	70774	123161	220557	379184	472416	574336	581436	740353	773026	785136	994249	-	-
Methoxychlor	12299	7035	5380	11746	24203	0	54139	46076	67598	67162	77664	158039	-	-
Butyl benzyl phthalate	798176	441648	553949	1639758	1549139	1348295	3588275	1617523	2142385	2383078	2367390	6732264	-	-

L Sediment–water flux modeling

L.1 Model input and output parameters

Table L.1: Sediment model input data for phenanthrene and fluoranthene

Parameter	Phenanthrene	Fluoranthene	Reference/source
Chemical properties			
Molar mass (g/mol)	178.2	202.3	EPISUITE 4.1
Data temperature (°C)	25	25	EPISUITE 4.1
Water solubility (g/m^3)	1.15	0.26	EPISUITE 4.1
Vapour pressure (Pa)	1.61E-02	1.23E-03	EPISUITE 4.1
Degradation half-life (h)	1.42E+03	3.84E+03	Mackay et al. [91]
Log K_{ow}	4.57	5.22	Smedes et al. [147]
K_{mmw} (L/kg)	0.130	0.788	Mader et al. [92]
Concentrations			
Total C_w (g/m^3)	8.25E-05	3.82E-06	experimental
C_s (µg/g)	7.19E-02	9.18E-03	experimental
Environmental properties			
Dimensions			
Area (squarem)	1000	1000	default
Water depth (m)	0.8	0.8	field value
Sediment depth (m)	0.03	0.03	field value
Volume fraction of porewater in sediment	0.8	0.8	default
C_{TSS} (g/m^3)	568	568	experimental
Densities (kg/m^3)			
Air	1.185	1.185	default
Water	1000	1000	default
Organic matter	1000	1000	default
Mineral matter	2500	2500	default
Organic carbon			
Log K_{oc}	7.21	6.29	experimental
Mass fraction of organic carbon			
Suspended particles	0.02	0.02	experimental

Continued on next page

Table L.1 Continued from previous page

Parameter	Phenanthrene	Fluoranthene	Reference/source
Sediment solids	0.01	0.01	experimental
Organic matter	0.03	0.03	estimated [66]
Transport			
Diffusion path length in sediment (metre)	0.015	0.015	default
Molecular diffusivity in water (m^2/h)	6.81E-10	2.24E-06	estimated [140]
Transfer rates (g/(m^2 d))			
Sediment deposition	3	3	default
Sediment resuspension	1	1	default
Burial	1.5	1.5	default

Table L.2: Model output for phenanthrene: Z values, concentrations, fugacities, transfer rates and half–life

Water	Z values	Concentration		Amount		
	(mol/(m^3 Pa))	(mol/m^3)	(µg/g)	(mol)	(g)	(% in system)
Bulk water	4.84E-01	4.63E-07	8.25E-05	3.71E-04	6.60E-02	9.42E+00
Water	4.01E-01	3.84E-07	6.84E-05	3.07E-04	5.47E-02	7.80E+00
Total suspended particles	1.57E+02	1.50E-04	2.50E-02	6.37E-05	1.14E-02	1.62E+00
Organic matter	1.65E+02	1.58E-04	2.81E-02	6.37E-05	1.14E-02	1.62E+00
Mineral matter	1.30E-01	1.25E-07	8.89E-06	2.52E-09	4.49E-07	6.40E-05

Sediment	Z values	Concentration		Amount		
	(mol/(m^3 Pa))	(mol/m^3)	(µg/g)	(mol)	(g)	(% in system)
Bulk sediment	2.34E+01	1.19E-04	1.94E-02	3.56E-03	6.35E-01	9.06E+01
Porewater	4.01E-01	2.04E-06	3.63E-04	4.89E-05	8.71E-03	1.24E+00
Total sediment solids	1.15E+02	5.86E-04	7.19E-02	3.52E-03	6.26E-01	8.93E+01
Organic matter	1.65E+02	8.38E-04	1.49E-01	3.51E-03	6.26E-01	8.93E+01
Mineral matter	1.30E-01	6.62E-07	4.72E-05	1.20E-06	2.13E-04	3.04E-02

Fugacity	(Pa)	Half life	(h)	(yr)
F_w	9.57E-01	Water-sediment transfer	14633	1.67
F_s	5.08E-00	Sediment-water transfer	1.46E+05	16.7
Sediment to water ratio	5.31	Sediment burial and reaction	1.41E+03	0.2
Fugacity predictions at steady state		Sediment losses and transfer	1401	0.16
Sediment to water ratio at steady state	5.29E-02			
Water fugacity (given sediment fugacity as above)	9.62E-05			

Continued on next page

Table L.2 Continued from previous page

Sediment fugacity (given water fugacity as above)	5.06E-08				
Transfer rates	D value	G value		Flux	
	(mol/(Pa h))	(m^3/h)	(mol/h)	(kg/yr)	(%)[a]
Diffusion (water-sediment)	1.30E-05		1.25E-11	1.95E-08	0
Diffusion (sediment-water)	1.30E-05		6.62E-11	1.03E-07	0
Deposition	1.83E-02	1.17E-04	1.75E-08	2.74E-05	100
Resuspension	3.31E-03	2.87E-05	1.68E-08	2.63E-05	96
Burial	4.96E-03	4.31E-05	2.52E-08	3.94E-05	144
Reaction	0.3385		1.72E-06	2.69E-03	9805
Water-sediment transfer	1.83E-02		1.75E-08	2.74E-05	100
Sediment-water transfer	3.32E-03		1.69E-08	2.64E-05	96
Sediment burial and reaction	3.43E-01		1.75E-06	2.73E-03	9949

[a] % of net water–sediment transfer

Table L.3: Model output for pyrene: Z values, concentrations, fugacities, transfer rates and half–life

Water	Z values	Concentration		Amount		
	(mol/(m^3 Pa))	(mol/m^3)	(µg/g)	(mol)	(g)	(% in system)
Bulk water	2.05E+00	6.30E-08	1.27E-05	5.04E-05	1.02E-02	1.79E+00
Water	1.11E+00	3.42E-08	6.91E-06	2.73E-05	5.52E-03	9.67E-01
Total suspended particles	1.77E+03	5.45E-05	1.03E-02	2.31E-05	4.68E-03	8.18E-01
Organic matter	1.86E+03	5.72E-05	1.16E-02	2.31E-05	4.68E-03	8.18E-01

Continued on next page

Table L.3 Continued from previous page

Mineral matter	2.73E+00	8.39E-08	6.79E-06	1.69E-09	3.43E-07	6.00E-05
Sediment	Z values	Concentration			Amount	
	(mol/(m^3 Pa))	(mol/m^3)	(µg/g)	(mol)	(g)	(% in system)
Bulk sediment	2.62E+02	9.25E-05	1.72E-02	2.77E-03	5.61E-01	9.82E+01
Porewater	1.11E+00	3.93E-07	7.95E-05	9.44E-06	1.91E-03	3.34E-01
Total sediment solids	1.30E+03	4.61E-04	6.42E-02	2.76E-03	5.59E-01	9.79E+01
Organic matter	1.86E+03	6.59E-04	1.33E-01	2.76E-03	5.59E-01	9.78E+01
Mineral matter	2.73E+00	9.66E-07	7.82E-05	1.75E-06	3.53E-04	6.18E-02
Fugacity		(Pa)	Half life		(h)	(yr)
F_w		3.07E-02	Water-sediment transfer		5494	0.63
F_s		3.53E-01	Sediment-water transfer		1.45E+05	16.6
Sediment to water ratio		11.51	Sediment burial and reaction		1.01E+02	0
Fugacity predictions at steady state			Sediment losses and transfer		101	0.01
Sediment to water ratio at steady state		3.85E-03				
Water fugacity (given sediment fugacity as above)		9.19E-05				
Sediment fugacity (given water fugacity as above)		1.18E-10				
Transfer rates	D value	G value		Flux		
	(mol/(Pa h))	(m^3/h)	(mol/h)	(kg/yr)	(%)[a]	
Diffusion (water-sediment)	3.30E-05		1.01E-12	1.80E-09	0	
Diffusion (sediment-water)	3.30E-05		1.17E-11	2.07E-08	0	
Deposition	2.07E-01	1.17E-04	6.36E-09	1.13E-05	100	

Continued on next page

Table L.3 Continued from previous page

Resuspension	3.74E-02	2.87E-05	1.32E-08	2.34E-05	208
Burial	5.61E-02	4.31E-05	1.98E-08	3.52E-05	312
Reaction	53.7605		1.90E-05	3.37E-02	298826
Water-sediment transfer	2.07E-01		6.36E-09	1.13E-05	100
Sediment-water transfer	3.74E-02		1.32E-08	2.35E-05	208
Sediment burial and reaction	5.38E+01		1.90E-05	3.37E-02	299138

[a] % of net water–sediment transfer

L.2 Sediment Model code

The following is the code for Sediment Model version 2.00 as provided by the Centre for Environmental Modelling and Chemistry [27]. The code was re-written in excel to enable alterations where necessary.

Key: Air(1), Water(2), Organic Matter(3), Mineral Matter(4)

CHEMICAL PROPERTIES
TSD = TSH / 24 'Sedt. reaction half-life (h)
RSH = Log(2) / TSH 'Sedt. rate constant (/h)
RSD = RSH * 24 'Sedt. rate constant (/day)
H = P * W / S 'Henry's Law constant
TK = TC + 273.15 'Data Tempertature (K)
WS = S / W 'Water solubility (mol/m3)
FOMP = FOCP / FOCM 'Organic matter from organic carbon in suspend solids
FOMS = FOCS / FOCM 'Organic matter from organic carbon in bottom solids
PARTITION COEFFICIENTS
KOW = 10^{LKOW} 'Octanol-water
KOC = 0.41 * KOW 'Organic carbon
KOM = FOCM * KOC 'Organic matter
KAW = H / GASCNST / TK 'Air Water
KMMW = KPM * DEN(4) / 1000 'Mineral-water (dimensionless)
KOMW = KOM * DEN(3) / 1000 'Organic matter (dimensionless)
VOLUME FRACTIONS
VFW(3) = CSP * FOMP / 1000 / DEN(3) 'Organic matter in water
VFW(4) = CSP * (1 - FOMP) / 1000 / DEN(4) 'Mineral matter in water
VFW(2) = 1 - VFW(3) - VFW(4) 'Water in water
VFS(4) = (1 - VFS(2)) / (1 + (DEN(4) / DEN(3)) * FOMS / (1 - FOMS)) 'Mineral matter in sedt.
VFS(3) = 1 - VFS(2) - VFS(4) 'Organic matter in sedt.
VWT = A * YW 'Total water volume
VST = A * YS 'Total sedt. volume
For i = 2 To 4

VW(i) = VWT * VFW(i) 'Volume in water (m3)

VS(i) = VST * VFS(i) 'Volume in sedt. (m3)

Next i

MASS

MSTS = 0

MSTW = 0

For i = 2 To 4

MSW(i) = VW(i) * DEN(i) 'Mass of water sub-compartment (kg)

MSS(i) = VS(i) * DEN(i) 'Mass of sedt. sub-compartment(kg)

MSTS = MSTS + MSS(i) 'Total mass of sedt. (kg)

MSTW = MSTW + MSW(i) 'Total mass of water (kg)

Next i

DENSITY

DENTW = MSTW / VWT 'Total water

DENTS = MSTS / VST 'Total sedt.

DENS = (DEN(3) * VS(3) + DEN(4) * VS(4)) / (VS(3) + VS(4)) 'Suspended solids

DENP = (DEN(3) * VW(3) + DEN(4) * VW(4)) / (VW(3) + VW(4)) 'Bottom solids Z VALUES

Z(1) = 1 / GASCNST / TK 'Air

Z(2) = 1 / H 'Water

Z(3) = Z(2) * KOMW 'Organic matter

Z(4) = Z(2) * KMMW 'Mineral matter

ZWPT = (Z(3) * VW(3) + Z(4) * VW(4)) / (VW(3) + VW(4)) 'Suspended solids

ZSST = (Z(3) * VS(3) + Z(4) * VS(4)) / (VS(3) + VS(4)) 'Bottom solids

ZWT = VFW(2) * Z(2) + VFW(3) * Z(3) + VFW(4) * Z(4) 'Total water

ZST = VFS(2) * Z(2) + VFS(3) * Z(3) + VFS(4) * Z(4) 'Total Sedt.

CONCENTRATIONS

CGSS = CSUG * DENS / 1000 'Sedt. Solids concentration (g/m3)

CWT = CWTG / W 'Total water concentration (mol/m3)

FUGACITIES

FW = CWT / ZWT 'Water fugacity

FWU = FW * 10^6 '(uPa)

FS = CGSS / W / ZSST 'Sedt. fugacity

FSU = FS * 10^6 '(uPa)

CONCENTRATIONS

CST = FS * ZST 'Total Sedt. concentration mol/m3)

```
For i = 2 To 4
CW(i) = FW * Z(i) 'Concentration in water (mol/m3)
CWG(i) = CW(i) * W '(g/m3)
CWGM(i) = CWG(i) * 1000 / DEN(i) '(ug/g)
CS(i) = FS * Z(i) 'Concentration in sedt. (mol/m3)
CSG(i) = CS(i) * W '(g/m3)
CSGM(i) = CSG(i) * 1000 / DEN(i) '(ug/g)
Next i
AMOUNTS
MWT = CWT * VWT 'Total water amount (mol)
MST = CST * VST 'Total sedt. amount (mol)
MT = MWT + MST 'Total amount in system (mol)
MWTG = MWT * W 'Amount(g)
MSTG = MST * W 'Amount(g)
MTG = MWTG + MSTG 'Total amount in system (g)
For i = 2 To 4
MW(i) = CW(i) * VW(i) 'Amount in sedt.(mol)
MWG(i) = MW(i) * W '(g)
PCTW(i) = 100 * MW(i) / MT '(%)
MS(i) = CS(i) * VS(i) 'Amount in sedt. (mol)
MSG(i) = MS(i) * W '(g)
PCTS(i) = 100 * MS(i) / MT '(%)
Next i
PCTWT = 100 * MWT / MT
PCTST = 100 * MST / MT
PCTT = 100 * MT / MT ' Total percent amount
CONCENTRATIONS
CSGMT = MSTG / MSTS * 1000 '(ug/g)
CWGMT = MWTG / MSTW * 1000 '(ug/g)
CSGT = MSTG / VST 'Total sedt. concentration (g/m3)
CWPT = FW * ZWPT 'Suspended Solid concentration (mol/m3)
CWPTG = CWPT * W '(g/m3)
CWPTU = CWPTG * 1000 / DENP '(ug/g)
CSPT = FS * ZSST 'Bottom solid concentration (mol/m3)
CSPTG = CSPT * W '(g/m3)
```

CSPTU = CSPTG * 1000 / DENS '(ug/g)

AMOUNTS IN SOLID FRACTIONS

MWPT = MW(3) + MW(4) ' mol

MSPT = MS(3) + MS(4) ' mol

MWPTG = MWPT * W ' g

MSPTG = MSPT * W ' g

PCTWPT = PCTW(3) + PCTW(4) ' %

PCTSPT = PCTS(3) + PCTS(4) ' %

Amount in sub-compartments as % of total in Water and as % of total in Sediment

PercentSumInWater = 0

PercentSumInSed = 0

For i = 2 To 4

PercentInWater(i) = 100 * MW(i) / MWT

PercentInSed(i) = 100 * MS(i) / MST

PercentSumInWater = PercentSumInWater + PercentInWater(i)

PercentSumInSed = PercentSumInSed + PercentInSed(i)

Next i

BIOTIC CONCENTRATIONS

BCFW = LW * KOW 'Bioconcentration factor of water organisms

CBW = CW(2) * BCFW 'Biotic concentration of water organisms (mol/m3)

CBWG = CBW * W '(ug/g)

BCFS = LS * KOW 'Bioconcentration factor of sedt. organisms

CBS = CS(2) * BCFS 'Biotic concentration of sedt. organisms (mol/m3)

CBSG = CBS * W '(ug/g)

G VALUES

GD = GDN * A / 24 / 1000 / DENP 'Deposition (m3/h)

GR = GRN * A / 24 / 1000 / DENS 'Resuspension (m3/h)

GB = GBN * A / 24 / 1000 / DENS 'Burial (m3/h)

D VALUES

DD = GD * ZWPT 'Deposition (mol/Pa h)

DR = GR * ZSST 'Resuspension (mol/Pa h)

DB = GB * ZSST 'Burial (mol/Pa h)

DS = VST * ZST * 0.693 / TSH 'Reaction (mol/Pa h)

MolcDiffYcm2s = BW * 10000 / 3600 'Molecular diffusivity in cm2/s from m2/h

BWE = BW * VFS(2)$^{1.5}$ 'Effective diffusivity of chemical (m2/h)

KMW = BWE / YD 'Sedt. water transfer MTC (m/h)

DW = KMW * A * Z(2) 'Diffusion (mol/Pa h)

DND = DD + DW 'Water sedt. transfer

DNU = DR + DW 'Sedt. water transfer

DSL = DB + DS 'Sedt. losses

FLUXES

ND = DD * FW 'Deposition (mol/h)

NR = DR * FS 'Resuspension (mol/h)

NB = DB * FS 'Burial (mol/h)

NS = DS * FS 'Reaction (mol/h)

NWD = DW * FW 'Downward difference in water (mol/h)

NWU = DW * FS 'Upward difference in water (mol/h)

NWUD = NWU - NWD 'Water diffusion (mol/h)

NUP = NR + NWU 'Sedt. water transfer (mol/h)

NDN = ND + NWD 'Water sedt. transfer (mol/h)

NLS = NS + NB 'Sedt. loss (mol/h)

RATES

NND = ND * 8.76 * W 'Deposition (kg/year)

NNR = NR * 8.76 * W 'Resuspension (kg/year)

NNB = NB * 8.76 * W 'Burial (kg/year)

NNS = NS * 8.76 * W 'Reaction (kg/year)

NNWD = NWD * 8.76 * W 'Downward difference in water (kg/year)

NNWU = NWU * 8.76 * W 'Upward difference in water (kg/year)

NNUP = NUP * 8.76 * W 'Sedt. water transfer (kg/year)

NNDN = NDN * 8.76 * W 'Water sedt. transfer (kg/year)

NNLS = NLS * 8.76 * W 'Sedt. losses (kg/year)

RATES AS A % OF NET WATER-SEDT. TRANSFER

NDR = ND / NDN * 100 'Deposition

NRR = NR / NDN * 100 'Resuspension

NBR = NB / NDN * 100 'Burial

NSR = NS / NDN * 100 'Reaction

NWDR = NWD / NDN * 100 'Downward difference in water

NWUR = NWU / NDN * 100 'Upward difference in water

NUPR = NUP / NDN * 100 'Sedt. water transfer

NDNR = NDN / NDN * 100 'Water sedt. transfer

NLSR = NLS / NDN * 100 'Sedt. losses

HALF-LIVES (h)

HLS = 0.693 * FS * VST * ZST / (NUP + NLS) 'Sedt. losses and transfer

HLSW = 0.693 * FS * VST * ZST / NUP 'Sedt. transfer to water

HLSL = 0.693 * FS * VST * ZST / NLS 'Sedt. burial and reaction

HLW = 0.693 * FW * VWT * ZWT / NDN 'Water transfer to sedt.

HALF-LIFE (YRS)

HLSY = HLS / 8760 'Sedt. losses and transfer

HLSWY = HLSW / 8760 'Sedt. transfer to water

HLSLY = HLSL / 8760 'Sedt. burial and reaction

HLWY = HLW / 8760 'Water transfer to sedt.

FUGACITIES

FRAT = FS / FW 'Ratio of prevailing fugacities (sedt./water)

FRSS = DND / (DNU + DSL) 'Ratio of Steady-State fugacities (sedt./water)

FWSS = FS / FRSS 'Water w.r.t. prevailing sedt. fugacity

FSSS = FW * FRSS 'Sedt. w.r.t. prevailing water fugacity